A Detailed Study of Desalination Exergy Models and their Application to a Semiconductor Ultra-Pure Water Plant

By

Lorna Fitzsimons B.Eng.

A Thesis Submitted in Fulfilment of the Requirements for the Degree of Doctor of Philosophy (PhD)

Supervisors

Dr. Brian Corcoran & Dr. Paul Young

School of Mechanical and Manufacturing Engineering

Dublin City University

May 2011

DECLARATION

I hereby certify that this material, which I now submit for assessment on the programme of study leading to the award of PhD is entirely my own work, that I have exercised reasonable care to ensure that the work is original, and does not to the best of my knowledge breach any law of copyright, and has not been taken from the work of others save and to the extent that such work has been cited and acknowledged within the text of my work.

Signed: _____ (Candidate) ID No.: _____ Date: _____

ACKNOWLEDGEMENTS

I would like to gratefully acknowledge the support, feedback, and encouragement that I received from my supervisors Dr. Brian Corcoran and Dr. Paul Young. As my primary supervisor Dr. Corcoran has ensured that I remained focused but also gave me the scope to explore peripheral research areas in greater depth. Dr. Corcoran's approach to research and people management has helped make this PhD research a rewarding and enjoyable experience. I would also like to thank him for passing additional work and projects my way, which financially, were a major help to the completion of this thesis. I would like to acknowledge the help of my secondary supervisor Dr. Young, and specifically thank him for his attention to detail, his great help in getting me established with the industry partner, and his impressive software skills, which came to my aid on several occasions.

I would like to acknowledge the help of Dr. Greg Foley from the School of Biotechnology and thank him for taking the time to meet with me and discuss the joys of chemical thermodynamics. Dr. Foley is not well at present and I would like to wish him a speedy recovery.

I would like to acknowledge the help of Naomi Brammer and thank her for discussing her work with me and for helping me locate various references. I hope our discussions were mutually beneficial.

I would like to gratefully acknowledge the help I received from personnel at Intel, Leixlip. In particular, thank you to Kevin Geoghegan my industry partner mentor, but also Luke Fenner, Malcolm Mclagan, Sean Dowd, and Joe Mitchell.

I would also like to thank the UPW engineering and technical personnel Tom Doyle, Alan Gannon and Pat Reynolds. Special thanks must go to Pat Wilson and David Griffin for helping me with the UPW plant data collection.

I would like to acknowledge the support of the Irish Research Council for Science Engineering and Technology (IRCSET) for funding this research, without their financial support, this research would not have been possible.

I would like to acknowledge the love, support, and encouragement I received from my husband John Hayes, my best friend and the love of my life. Thank you Anna for putting up with an often distracted and stressed mother, I love you very much and am very proud of the young woman you are becoming.

I would like to acknowledge the love, support, and encouragement of all my family and my parents Margaret and Jack Fitzsimons in particular. Thank you for all the practical help, particularly my Dad for the greatly appreciated and numerous babysitting and collecting duties you have performed.

I would like to acknowledge the support of my friends, particularly Ruth Pritchard, whose encouragement and faith in me ensured that I persevered through the more difficult periods in this research.

I would like to acknowledge the support and encouragement of my research colleagues and friends in DCU, particularly Katharina Posten, Neill Byrne, Fiachra Collins and Mustafa Ramzi Salman. Thank you for all the fun and laughs too.

Finally, thank you to all the staff in the School of Mechanical and Manufacturing Engineering for making DCU a great place to study.

TABLE OF CONTENTS

ABSTRACT

A Detailed Study of Desalination Exergy Models and their Application to a Semiconductor Ultra-Pure Water Plant

By

Lorna Fitzsimons

Ultra-Pure Water (UPW) is a high energy raw material used in the semiconductor manufacturing industry. However, to date, the production of UPW has received little focus in terms of energy consumption mitigation. Exergy analysis is perhaps the most powerful tool available in the search for industrial energy efficiency. The objective of this research was to develop an approach for the exergy analysis of Semiconductor UPW plants in an effort to characterise energy consumption. However, following an extensive literature review, it became evident that several desalination exergy models were in current use, and it was unclear which model was the most appropriate, presenting a serious challenge to researchers seeking to apply exergy analysis to water purification processes. A detailed study and comparison of two predominant desalination exergy models was undertaken to determine the most appropriate model for UPW and other water purification applications. Neither of these models was deemed suitable due to inappropriate underlying model assumptions. Two potentially suitable exergy calculation models were identified from the broader literature and developed further for UPW applications. A novel method (based on Szargut's chemical exergy reference environment) was developed to calculate the chemical exergy of electrolytic solutions at non-standard dead state temperatures. It was found that, in general, the chemical exergy of ionic species was sensitive to changes in dead state temperature. The exergy models were applied to a UPW plant in an effort to compare the models and characterise the plant. In general, the exergy destruction rates were similar for the three models, the hot water heat exchanger being the main exception (and also a key source of exergy destruction). Chemical exergy proved vital for the calculation of several process exergetic efficiency values and the assessment of plant exergy losses. Following a detailed assessment of the UPW plant exergy analysis results, the most appropriate model was identified.

NOMENCLATURE

Acronyms

ASTM	American Society for Testing and Materials
BOD	Biological Oxygen Demand
COD	Chemical Oxygen Demand
CSR	Corporate Social Responsibility
EDI	Electro-Deionisation
gfd	Gallons per square foot per day
HVAC	Heating, Ventilation and Air Conditioning
IP	Intellectual Property
ISMI	International SEMATECH Manufacturing Technology Initiative
ITRS	International Technology Roadmap for Semiconductors
IX	Ion exchange
LCA	Life-Cycle Analysis
MCr	Membrane Crystallisation
MD	Membrane Distillation
MED	Multi-Effect Distillation
MEE	Multi-Effect Evaporation
MF	Microfiltration
MSF	Multi-Stage Flash
MUA	Make-up Air
NIST	National Institute of Standards and Technology
NF	Nanofiltration

P&ID	Piping and Instrumentation Diagram
ppb	Parts per billion
ppm	Parts per million
ppt	Parts per trillion
psig	Pounds per square inch gauge
RO	Reverse Osmosis
SCADA	Supervisory Control and Data Acquisition
SEMATECH	Semiconductor Manufacturing Technology
TDS	Total Dissolved Solids
TEE	Total Energy Equivalence
TOC	Total Organic Carbon
UPW	Ultra-Pure Water
UV	Ultra-Violet
VSD	Variable Speed Drive
VLSI	Very Large Scale Integration

Symbols

a	Activity
A	Membrane permeability coefficient
B	Membrane permeability coefficient for the salt
c	Specific heat capacity (kJ/kg.K)

c	Regarding the Szargut lithosphere exergy values refers to the fraction of the element under consideration appearing in the form of reference species
$\overline{c}_P$	Molar heat capacity at constant pressure (kJ/mol.K)
$\Delta_R \overline{c}_P$	Change in specific heat capacity of the reaction (kJ/mol.K)
cr	Substance in crystalline structure
C	Concentration (mg/l or g/l when specified)
C	Heat capacity (kJ/K or J/K when specified)
CF	Conductivity factor
D	Exergy destruction
e	Specific exergy (kJ/kg)
$\overline{e}$	*Molar chemical exergy (kJ/mol)*
$\dot{E}$	Exergy rate (kW or kJ/hr when specified)
EC	Electrical conductivity ($\mu S / cm$)
F	Fuel exergy
g	Substance in gaseous or vapour state
g	Gravitational acceleration (m/s^2)
$\overline{g}$	Molar Gibbs energy (kJ/mol)
G	Gibbs energy (kJ)
$\Delta_R \overline{g}$	*Gibbs energy of the reaction (kJ/mol)*
$\Delta_F \overline{g}$	*Gibbs energy of formation (kJ/mol)*
h	Specific enthalpy (kJ/kg)

$\Delta_F \overline{h}$	Enthalpy of formation (kJ/mol)
I	The ionic strength of an electrolyte solution (mol/kg)
j	The number of reference ions or molecules derived from one molecule of the element under consideration
J	Flux (m^3/m^2/unit time)
l	Regarding the Szargut lithosphere exergy values refers to number of atoms in the element under consideration in the molecule of the reference species
L	Exergy loss
$\dot{m}$	Mass flow rate (kg/s or kg/hr when specified)
mf	Mass fraction
M	Molality (moles of solute per kg of solvent)
M	Refers to the relevant cation (meaning should be clear from the context)
MW	Molar mass (kg/kmol)
n	Regarding the Szargut lithosphere exergy values refers to the mean molar concentration of the element in the earth's crust (mol/kg)
N	Number of moles (mol or kmol when specified)
$\dot{N}$	Molar flow rate (mol/s)
N	Number of moles per mass unit of the solution (mol/kg) (used only when specifically referring to Model A)
P	Absolute pressure (Pa or bar when specified)

P	Product exergy
Q	Volumetric flow rate (m^3/s or m^3/hr when specified)
$\dot{Q}$	Rate of heat transfer (kW)
R	Universal gas constant (kJ/kmol.K), when accompanied by the subscript *im* refers to the specific gas constant of the ideal mixture
s	Specific entropy (kJ/kg)
$\overline{s}$	Molar entropy (kJ/kmol.K)
$\dot{s}$	Rate of entropy, refers specifically to $\dot{s}_{gen}$ the rate of entropy generation (kW/K)
$\Delta_R \overline{s}$	Molar entropy of the reaction (kJ/mol.K)
S	Conductivity (siemens)
T	Absolute Temperature (K)
u	Specific internal energy (kJ/kg)
v	Specific volume (m^3/kg) (meaning should be clear from the context)
v	Stoichiometric coefficient (meaning should be clear from the context)
V	Velocity (m/s)
$\overline{w}$	Molar work input (kJ/mol)
W	Work input (kJ)
$\dot{W}$	Rate of work transfer (kW)
$\dot{X}$	Rate of exergy destruction, refers specifically to $\dot{X}_{des}$ (kW or kJ per unit time when specified)

X	Refers to the relevant anion
x	Mole fraction
z	Ionic valence
z	Height or elevation (meaning should be clear from the context)

Greek Symbols

α	Parameter for Debye-Huckel model, dependent on ion size
β	Number of ions/particles generated from dissociation
Δ	Refers to a difference or a change in values
$\in$	The dielectric constant of water
Π	Osmotic pressure of the feed water (Pa)
ρ	Density (kg/m^3)
γ	Activity coefficient
μ	Chemical potential (kJ/mol)
ϕ	Relative humidity
Ω	Resistance (ohms)

Subscripts and superscripts

On occasion, the chemical formula of a substance is used as a subscript. In these cases, the subscript refers specifically to the substance denoted by the chemical formula. The valence of ionic species is often denoted by plus or minus signs, the number of the plus or minus signs refers to the valence of the ion, e.g. Ca^{++} signifies the calcium ion with a valence of two. Other subscripts and superscripts are explained as follows.

aq	Denotes aqueous species
Ch	Chemical
cold	Refers to heat exchanger cold stream
compound	Denotes relevant compound under consideration
des	Destruction (refers specifically to $\dot{X}_{des}$ the rate of exergy destruction)
Desired output	Refers to the desired exergy output of the process under consideration
Dry air	Refers to dry air mole fractions
DS	Refers to dead state
e	Denotes element *e*
F	The feedwater stream
gen	Generation, refers specifically to the rate of entropy generation $\dot{s}_{gen}$
H	Henryan (refers to activity coefficient)
hot	Refers to heat exchanger hot stream
i	Denotes the relevant chemical species
ig	Ideal gas
im	Ideal mixture
min	Minimum
n	Denotes relevant process stage
°	Standard values, e.g. temperature, pressure and molality
0	Denotes the dead state
p	Denotes the products of a chemical reaction

Ph	Physical
P	The permeate stream (should be clear from the context)
P	Pressure
PS	Refers to relevant process stage
pure	Refers specifically to mixture or solutions constituents in their pure form
r	Denotes the reactants of a chemical reaction
ref	At the reference value
R	The retentate stream
R	Raoultian (refers to activity coefficient), the meaning should be clear from the context
RDS	Refers to the restricted dead state
s	Salt
sat	Refers to saturation pressure
sol	The solvent (in this research water)
T	Thermal
Tr	Trans-membrane pressure
used	Refers to exergy used in a process to achieve desired exergy output
v	Constant volume, refers to specific heat capacity for a constant volume process
w	Water

TABLE OF FIGURES

TABLE OF TABLES

PUBLICATIONS RESULTING FROM THIS RESEARCH

Conference papers/presentations:

Fitzsimons, L., Corcoran, B., Young, P. and Foley, G., "*A Comparison of Prevalent Desalination Exergy Models*", HEFAT 2010, 19-21 July 2010, 7th International Conference on Heat Transfer, Fluid Mechanics and Thermodynamics, Antalya, Turkey.

Fitzsimons, L., Corcoran, B., Young, P. and Foley, G., "*Desalination Exergy Models: Mathematical and Seawater Model Comparison*", Fifth International Ege Energy Symposium and Exhibition (IEESE-5) 2010, 27-30 June 2010, Denizli, Turkey.

Fitzsimons, L., Corcoran, B. and Young, P., "*Review of Strategic Semiconductor Cleanroom Energy Reduction Efforts"*, International Manufacturing Conference 2009 (IMC 26), 2-4 September 2009, Trinity College Dublin, Ireland. (Awarded a special commendation)

Fitzsimons, L., Posten, K., Corcoran, B. and Young, P., "*Energy Reduction in Semiconductor Manufacturing*", Presentation at the Intel European Research and Innovation Conference 2008, Leixlip, Ireland.

Abstracts/ Posters:

Fitzsimons, L., Corcoran, B., Young, P. and Foley, G., "*Exergy - the true measure of energy efficiency"*, Extended abstract and poster for the Intel European Research and Innovation Conference 2010, 12-14 October 2010, Leixlip, Ireland.

Fitzsimons, L., Corcoran, B. and Young, P., "*UPW energy optimisation– exergy, a novel approach*"**,** Extended abstract and poster for the Intel European Research and Innovation Conference 2009, Leixlip, Ireland.

Fitzsimons, L., Corcoran, B. and Young, P., "*The Use of Exergy Analysis for UPW Energy optimisation"*, Abstract and poster for the IRCSET Symposium 2009, Dublin, Ireland.

Fitzsimons, L., Corcoran, B. and Young, P., "*Energy Reduction in UPW*", Extended abstract for the Intel European Research and Innovation Conference 2008, Leixlip, Ireland.

1 Introduction

Energy and water are two key inputs of the highly complex semiconductor manufacturing process, and both are used intensively [1-4]. Despite their status as important raw materials, the goals of energy efficiency and water conservation are relatively new in the semiconductor manufacturing industry. Recent fluctuations in the cost of energy, the depletion of fossil fuels, the current water scarcity crisis [5-7], and the wide acceptance that carbon footprint mitigation is necessary to reduce the impact of climate change, have led to a greater focus on the effective and efficient use of these resources. The conservation of both has been highlighted as difficult challenges in the International Technology Roadmap for Semiconductors (ITRS) [8].

Alongside environmental concerns, there is a strong business case for sustainable manufacturing and the conservation of resources, and the traditionally held corporate view that an ultimate trade-off between the environment and the economy exists [9, 10] is changing. Corporate environmental responsibility awareness has increased; at the time of writing, the top five companies in Fortune 500 [11], Exxon-Mobil, Wal-Mart, Chevron, ConocoPhillips and General Electric all report on Corporate Social Responsibility (CSR), including environmental sustainability, in some form or other. According to an earlier 2002 KPMG report, the main reasons given for such corporate responsibility reporting were, "*enhanced reputation, competitive advantage and cost savings* [12]*"*. Whether this reporting is only paying lip service to stakeholder pressure, or not, is open to debate, but at least companies are acknowledging stakeholder concerns regarding the need for sustainable

development. The efficient use of resources plays a vital role in sustainable manufacturing, and the ability to optimise resource inputs, such as energy and water, should be perceived as a technological asset. There is also the growing acceptance of the incontrovertible fact that the economy can only exist and thrive in the long-term if the environment can sustain the economy; the "*economy, after all, is embedded in the environment* [13]". The criticality of a healthy natural environment is also illustrated when one considers that this environment "*serves as both the source of raw materials as well as the sink for the wastes of industrial processes* [14]".

Since the industrial revolution, humankind's consumption of natural resources has "*put him in the position of a fantastic spendthrift [15]"*. In 1971 Georgescu-Roegen [15] stated that the rate of natural resource depletion was linked to our ability to sustain a growing global population. At the time of writing his seminal work, the world's population was between three and four billion, now the population has risen to almost seven billion (predicted to reach nine billion by 2045) [16]. Hence, the efficient use of resources, although correlated to industrial cost bases, transcends various industrial sectors and becomes an important human issue.

In general, the manufacture of newer high technology products such as carbon nanotubes and silicon wafers have high specific electrical energy requirements, largely due to the high purity input materials, high dimensional accuracy and low production rate [17]. Although energy intensive, the semiconductor manufacturing industry has been relatively slow to adopt resource and energy efficiency, this is primarily a function of semiconductor

manufacturing industry economics and manufacturing process complexity. Compressed product life cycles, driven by Moore's law, characterise semiconductor manufacturing economics. For new technologies, the main objective is to maximise yield quickly, and therefore profit; in these efforts, energy efficiency often plays a minor role. Typically, in order to speed up new process production, tried and tested methods are used even though they may not be energy efficient. The production ramp-up for new device technologies is highly challenging, and in this respect the sheer complexity of the semiconductor manufacturing process plays a vital role in cyclical design inefficiency, or what Lovins [13, 18] terms, the "*infectious repititis"* of the semiconductor industry design strategy. When technologies mature, a change from high profit margins to commodity occurs [19], and operating cost reduction, and hence energy efficiency becomes more important to the industry. At this stage, energy efficiencies can be achieved by retrofitting facilities systems such as boilers, chilled water systems, air handling systems; the literature on these efforts has been reviewed previously by the author, see Appendix A.

Ultra-Pure water (UPW) is used in large quantities in the semiconductor industry; it is used primarily for wet cleaning operations, where, due to its physical properties such as high dielectric constant and high dipole moment, it is a highly effective solvent. Typically, the physical properties of UPW are combined with mechanical processes such as megasonic and quick dump rinsing to strip the wafer of impurities. According to Peters [3], two to three million gallons of UPW per day is used in a typical 200 mm fab (semiconductor fabrication plant). UPW is also used in other industries, such as the power and

pharmaceutical industries, but the purity of UPW used in semiconductor manufacturing applications far exceeds that of its other uses [20].

UPW production has been selected as the target for semiconductor manufacturing energy reduction in this research. One of the principal reasons for selecting UPW as the focus of this research thesis is its high energy intensity; according to two benchmarking studies [21, 22], UPW has the highest energy intensity of all the utilities used in semiconductor manufacturing. Both the quantity and the quality of UPW used in the semiconductor manufacturing processes are expected to increase in line with Moore's Law [23, 24]. As the quality of UPW increases to stricter purity levels, the energy used to produce UPW is also expected to increase and become a "*key issue of concern* [25]". Semiconductor manufacturing industry research to date has advocated a 'Reduce, Reuse, Recycle' strategy. However, in light of expected increases in both quality as well as quantity, and the resulting increased energy demands, research into the energy characterisation and optimisation of UPW production is required in conjunction with the 'Reduce, Reuse, Recycle' strategy. The current conservation strategy is not sufficient in itself. However, little, if any, academic research exists on UPW energy reduction, and this research seeks to address this gap in the academic literature. The reasons for choosing UPW as the focus of this research can be summarised as follows;

- High energy intensity;
- Little focus to date;
- Expected increases in both quantity and quality of UPW used – limitations of the 'Reduce, Recycle, Reuse' approach in addressing the expected quality increases;

- Applicability of UPW to other industries.

Having chosen UPW as a focus for this energy reduction research, the next step was to determine which method to use in order to characterise the use of energy in UPW production. Looking further afield to the desalination industry, it became evident that energy reduction research was already a well established research area. The objective then was to assess the methods used in the desalination industry, and to determine if any of these methods were transferrable to UPW. Having reviewed the desalination literature, exergy analysis was chosen as the key research methodology.

Exergy, a thermodynamic property, combines the First and Second Laws of Thermodynamics to establish that energy should not only be thought of in terms of quantity, but also in terms of quality. Exergy refers to the quality of energy and the potential ability of energy to do work; this potential ability is destroyed in systems due to irreversibilities, and this lost potential can be quantified using an exergy balance, which calculates the system exergy destruction, or the lost potential to do work. The First Law of thermodynamics shows that energy is always conserved, in real systems, exergy is never conserved.

The relevant UPW and exergy research literature is reviewed in Chapter 2. The main sections of the literature review include a brief, general introduction to energy use within semiconductor manufacturing, an overview of UPW which attempts to answer the following questions;

- UPW, what are the industrial applications?
- What is UPW and how is it defined?
- How pure is the UPW used in semiconductor manufacturing?
- Why is it used in semiconductor manufacturing?
- How is UPW produced?

The literature review then considers general energy reduction efforts carried out in the desalination industry with a focus on Reverse Osmosis (RO) and other shared technologies, and finally, exergy is introduced. Previous exergy research in the desalination industry is reviewed, and as a result of this literature review, a basic methodology for the characterisation of energy use in UPW production is proposed.

Following the literature review, an initial comparison of two prevalent desalination exergy models (termed the Drioli aqueous solution model and Cerci ideal mixture model) is presented in Chapter 3. These two exergy models were compared by applying them to a dataset in literature. The outcome of this preliminary analysis work leads to the formulation of the research hypothesis and research objectives in Chapter 4, and the development of the research plan. In Chapter 5, a detailed comparison of the current desalination exergy models is undertaken.

Chapter 6 details the author's development of Model C. In essence, Model C is a novel approach which facilitates the accurate application of the electrolytic solution exergy model to water purification systems. A second potentially suitable model for UPW applications, the Szargut model, is detailed in Chapter 7. Commonly, standard chemical exergy values

are used to undertake exergy analyses. Importantly, in Chapter 7, a method is developed by the author to calculate the chemical exergy of ionic species, and hence electrolytic solutions, at non-standard states (Model D). The change in chemical exergy of ionic species as a function of changing dead state temperature is also investigated.

An exergy analysis of a semiconductor UPW plant is undertaken in Chapter 8 using the Cerci ideal mixture model, the developed Model C, and the developed Model D. The models are compared and the plant is characterised in terms of exergy flows, exergy destruction and process rational exergetic efficiency. Certain other relevant issues arising from this research are also addressed, for example, the relevance of chemical exergy at low ionic concentrations and a comparison between the use of the ideal mixture model and the electrolytic solution model at relevant UPW plant concentrations. Finally, the conclusions of this research and recommendations for further work are presented in Chapter 9.

2 Literature review

The objective of this chapter is to assess the published research on the energy characterisation/optimisation of semiconductor UPW plants. The published literature in this area is very rare. Consequently, it became necessary to review the desalination industry literature in order to select a suitable approach. As will become evident, this research spans several disciplines and draws on elements from UPW and RO technology, but also from desalination research, thermodynamics and exergy analysis in particular. The literature review in this chapter identifies the gaps in the literature and acts as a research focus; however, due to the cross-discipline nature of the research there is ongoing, timely incorporation of research findings from other academic fields throughout this thesis.

2.1 Energy use in semiconductor manufacturing

Energy is used in the semiconductor manufacturing industry via the electrical power consumption to run the fab and all associated subsystems, and in the combustion of fossil fuels for the plant boilers. The proportional breakdown of the electrical energy used in the fab is shown in Figure 2-1; the electrical energy is split between the processing tools (35%) and the facilities systems (65%) [26]. The facilities systems generate the utilities required to maintain the exacting purity, humidity, and temperature specifications of the cleanroom environment but also the high purity utilities used to supply the processing equipment, for example make-up air (MUA) and UPW. This breakdown shown in Figure 2-1 is based on the average electrical use of 12 fabs [26].

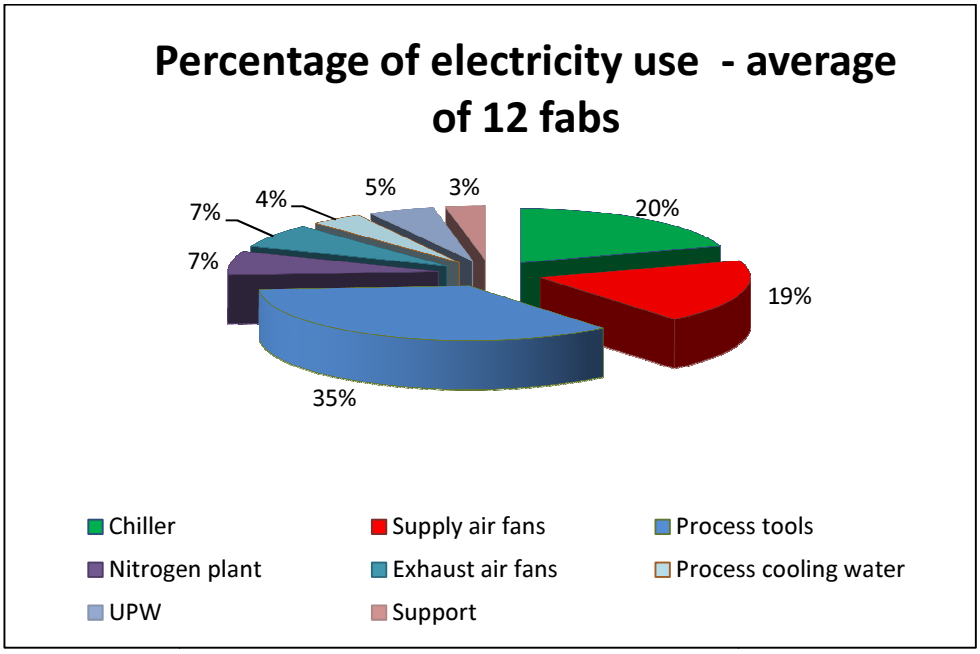

Figure 2-1: Percentage electrical energy breakdown, adapted from [26]

Alongside studies assessing the proportional energy use in fabs, industry consortia such as International Semiconductor Manufacturing Initiative (ISMI), have also carried out benchmarking studies between different fabs in order to quantify the energy required to process wafers; generally, the metrics used are kWh per unit of production or kWh per unit area of silicon. Both metrics are used to address an inherent difficulty in benchmarking different fabs; this difficulty arises because the energy required to process wafers is a function of several factors, for example;

- The chip complexity and number of layers;
- The quantity of wafers processed;
- The process maturity and operational expertise;
- The fab location and climatic factors;

- The wafer and device dimensions.

In the literature, an average figure of 1.5 kWh/cm^2 has been chosen as representative for the electrical energy required per square centimetre of silicon wafer processed and 1 MJ/cm^2 has been selected for fossil fuels [1]. Energy reduction targets set by the ITRS 2007 report, aim to reduce the energy intensity of semiconductor manufacturing from 1.9 kWh/cm^2 for 2009 to 1.2 kWh/cm^2 by 2016 [27].

Other energy benchmarking studies have been carried out on the various fab facilities systems that produce the utilities used in the manufacturing process, and to maintain the cleanroom environmental conditions [21, 22]. In these two studies, the energy required to produce one unit of the utility in question was calculated for a specific fab model. The energy intensities of the utilities are shown, using a logarithmic scale, in Figure 2-2. Again, as in the case of benchmarking overall fab energy use, the difficulty of comparing different operational criteria remains; however, the benchmarking exercise does facilitate comparison between the energy impacts of the various utilities used in the semiconductor manufacturing process. One utility stands out in Figure 2-2, UPW has an "*energy conversion factor*" of 10.2 kWh/m^3 [22]. This value is similar to the "*energy index*" value of 9.55 kWh/m^3, calculated for UPW in the Taiwan benchmarking study [21]. Although the energy intensities are given two different names, and are based on two different fab models, both benchmarking exercises serve the same purpose, i.e. to quantify the energy intensity of the fab utilities. When coupled with utility usage rates, the key fab energy drivers can be identified.

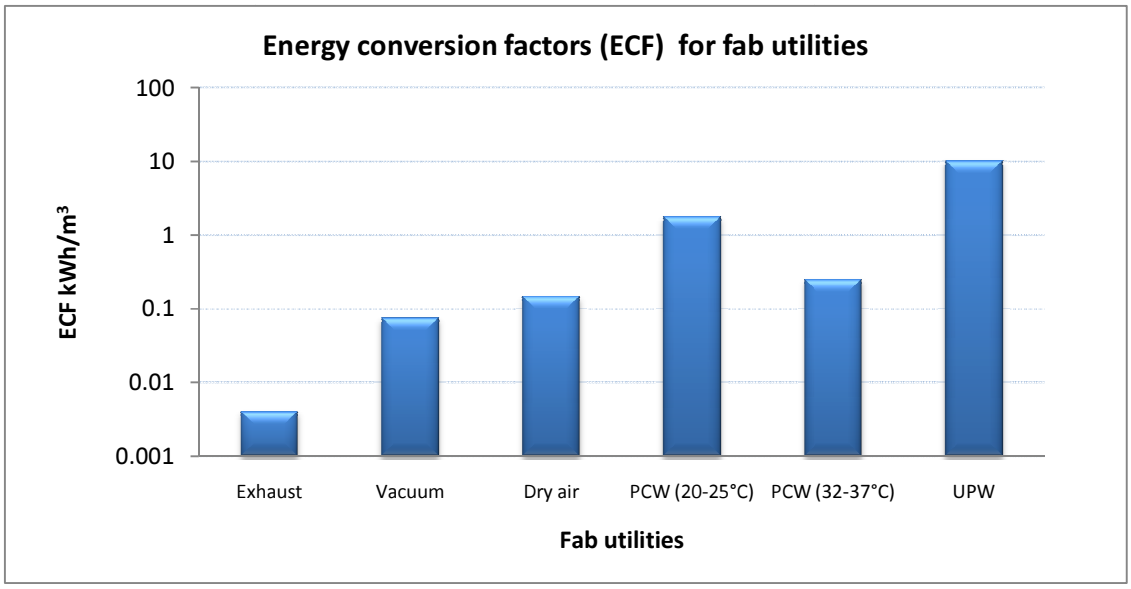

Figure 2-2: Energy conversion factors of fab utilities used in SEMI S23 (logarithmic scale), adapted from [22]

It is important to state at the outset, that semiconductor manufacturing energy reduction research, reported in the academic literature, is relatively rare. There are several reports on energy reduction projects undertaken by the semiconductor manufacturing industry, including the reduction of air change rates in the cleanroom HVAC system; improved boiler efficiency; the use of heat recovery; and the use of dual temperature chiller loops among others [28-35]. On a more strategic level, there have been initiatives taken to benchmark, manage and improve the use of energy in the industry. These approaches have been previously reviewed by the author [36]. The cited publication assessed efforts such as whole system optimisation, matching needs to capacity in order to avoid over-sized facilities energy demands [37-39], and the development of the Total Energy Equivalence (TEE) method and TEE reporting tool [40, 41]. The author concluded that energy efficient design has the most leverage at the design phase and that the lack of suitable inbuilt

measurement equipment was a significant challenge to effective energy management in the semiconductor manufacturing industry. Following an extensive literature review, it is evident that very few, if any, of these energy reduction efforts, have focused on reducing the energy impact of UPW production.

2.2 UPW

UPW is used in the semiconductor industry for the wet cleaning of the silicon wafer. It is used at several different stages during the manufacturing process to rinse the wafer, and also, to clean tool parts such as chemical mechanical planarisation equipment. The engineering properties of water such as high dipole moment, hydrogen bonding, and a high dielectric constant (important for ensuring and maintaining the separation of ions in solution), make UPW an excellent solvent [42, 43]. These properties, coupled with mechanical cleaning processes such as quick dump rinsing and megasonic cleaning, prove highly effective at stripping the wafer of impurities. The primary semiconductor manufacturing process technologies that use UPW are the wet benches and chemical mechanical planarisation tools.

According to *Ullmann's Encyclopedia of Industrial Chemistry* [44], UPW is defined as,

> *"…having electrolytic conductivity less than 0.1 µS/cm. For comparison, the theoretical conductivity of pure water is 0.054 µS/cm at 25 °C. To be classified as ultrapure water, the ionic concentration must be less than 20 µg/L…"*.

Ultra-Pure water (UPW), as the name suggests, is extremely pure water, but even under the general term of UPW, different standards and purity priorities exist for different UPW

using industries. There are several industrial applications for UPW including the power generation, pharmaceutical and semiconductor industries [44]. The purity specifications for different industries vary depending on requirements, the main priorities of the pharmaceutical industry are "*reproducibility, reliability and documentation*", the power industries require low conductivity and silica levels, and the semiconductor industry requires minimal impurity levels [45]. Of the industries using UPW, the semiconductor industry has the most stringent specifications [19, 46]. Meltzer states, "*it would be fair to say that the sophistication of semiconductor pure water preparation far exceeds that practiced in pharmaceutical settings* [20]".

Water purification plants were introduced into the semiconductor manufacturing process in the 1960s. With the onset of Very Large Scale Integration (VSLI) in the 1970s, the semiconductor industry began to focus on water purity standards. Initially, the main industry concern for water purity was resistivity (or conductivity), and as the integrated circuit geometry shrank in size, the specifications for water purity became stricter. In the 1960s the resistivity specifications were between 10 and 16 MΩ.cm [47]. Current UPW resistivity specifications are in the range of 18.2 MΩ.cm at 25°C, theoretically pure water has a resistivity of 18.25 MΩ.cm at 25°C [47]. Aside from resistivity, other important UPW purity requirement metrics include maximum allowable values for impurities such as;

- Silicon Dioxide;
- Number of particles;
- Particle size;
- Bacteria;

- Dissolved gases;
- Total Organic Carbon. [20, 48]

Conductivity is directly related to an important water quality metric - Total Dissolved Solids (TDS). TDS is a measure of all the minerals dissolved in water and is used later to calculate mass and mole fractions for process water. The relationship between TDS and conductivity can be estimated by multiplying the conductivity (μS/cm) of the water by a factor of 0.64 [48], a second method of calculating the TDS of a natural water sample is given as the product of the conductivity by a factor in the range of 0.55 to 0.7 [20]. Meltzer [20] does not state how to choose the appropriate factor in this range, and this is considered in more detail later in the thesis. Although theoretically pure water is an ideal, the high purity of UPW used in the semiconductor industry approaches this ideal very closely.

The water purity objectives for different UPW applications have already been discussed, however, there are also varying UPW purity standards within semiconductor manufacturing applications for different product technologies. Purity standards vary depending on the line width of devices, which is a measure of the microelectronic device dimensions; as line width decreases, the UPW purity standards increase. An example of standards for varying line widths is shown in Table 2-1 where Type E-1.1 is the purity standard for water used in producing devices with a line width between 0.25 and 0.5 μm and Type E-1.2 relates to devices with a line width of between 0.18 and 0.25 μm [48]. Table 2-1 is adapted from ASTM 5127-99: Standard Guide for Ultra Pure Water used in the electronics and semiconductor industry [48]. The permitted ion and metal quantities are expressed in parts

per trillion (ppt). This table highlights the increasingly stringent requirements as line width decreases. For example, the permitted quantities of several ions and metals, such as calcium, magnesium, iron and copper, have decreased by a factor of 10 as line widths have decreased by a maximum factor of 2.7.

As purity standards increase, the energy required to purify water, to these ever more exacting standards, increases. One research study [25] empirically investigated the impact of increased water purity standards on energy consumption. The research showed that for a reverse osmosis (RO) process, twice as much primary energy was required (kJ/gallon of UPW) to purify water from 0.01 ppm to parts per billion values (one order of magnitude), than was required to increase the water purity from 80-480 ppm to 0.01 ppm (four to five orders of magnitude). As UPW purity standards increase further, the energy required to produce this purer water is expected to increase, and become a "*key issue of concern* [25]".

The question arises as to how these specifications are determined, and whether these purity requirements are necessary? This question is important from the energy perspective, due to the increased energy demands with increasing water purity, and requires investigation. The purity standards required by the industry are often only limited by the resolution of the current measurement technology [48]. In 1993 Meltzer considered whether these measurement detection limited purity standards were enough, and stated that they "*…do not necessarily reflect bounds that are sufficient; rather they are the best levels currently possible and thus they must be tolerated* [20]." This statement appears to infer that these standards are not adequate. Later in the same chapter, however, Meltzer argues that whether or not greater purity standards are necessary from the point of view of their application, the

fact that higher purity standards are achievable and measurable drives tighter specifications. So, on the one hand, the standards may not be strict enough, on the other hand, the standards are driven purely by current technology achievements. There is obvious doubt regarding the necessary purity levels. This case of technology driving standards is not a sound scientific basis for selecting purity standards. The issue of setting purity specifications requires further research if a fundamental issue of the energy impact of UPW is to be addressed.

Table 2-1: Semiconductor UPW standards - adapted from ASTM 5127-99: Standard Guide for Ultra Pure Water used in the electronics and semiconductor industry in [48]

	Type E-1.1	***Type E-1.2***
Resistivity, 25°C (MΩ.cm)	*18.2*	*18.2*
Ions and metals (ppt)		
Ammonium	*100*	*50*
Chloride	*50*	*20*
Fluoride	*50*	*30*
Nitrate	*50*	*20*
Sulphate	*50*	*20*
Aluminium	*20*	*5*
Boron	*20*	*5*
Calcium	*20*	*2*
Chromium	*20*	*2*
Copper	*20*	*2*
Iron	*20*	*2*
Magnesium	*20*	*2*
Sodium	*20*	*5*
Potassium	*20*	*5*
Zinc	*20*	*2*
Total (ppt)	***500***	***172***

2.2.1 UPW conservation

The conservation of UPW is acknowledged as an important issue by both Semiconductor Manufacturing Technology (SEMATECH) and the ITRS, a 'Reduce, Reuse, Recycle' strategy has been adopted by SEMATECH. In the literature, the benefits and risks associated with recycling UPW, and other various reduction and reclamation strategies have been studied [49]. According to this study the benefits of these strategies include;

- Improved feedwater quality, and as a result, improved product water quality;
- Reduced UPW facility maintenance such as reduced membrane cleaning;
- Reduced ion exchange regeneration, thereby lowering ion exchange regeneration chemical usage;
- Reduced feedwater and waste water treatment costs (due to lower volume requirements of feedwater and less wastewater to process);
- Improved RO retentate quality for other reuse purposes.

There are risks, however, and these include;

- The build-up of recalcitrant compounds;
- The introduction of compounds into the UPW system, for example, species that the system was not designed to remove (e.g. the wet bench waste streams);
- Risk of biofouling.

This study also discusses some methods of UPW use reduction in processes, including;

- The use of quick spray rinsing instead of overflow and quick dump method;
- Improved rinse tank geometries;
- Megasonic cleaning;

- Idle flow rate reductions;
- Analytical monitoring of rinse-water quality.

Other recommendations advocate the use of hot UPW over cold UPW as a conservation method, i.e. hot UPW is more effective than cold and therefore less UPW is required for cleaning processes. From the energy perspective, however, the use of hot UPW adds an extra energy burden that should be evaluated with respect to the quantity of ambient UPW conserved (the ambient temperature depends on the specific plant). Another issue is that the outflow from certain process streams is not suitable for recycling, due to the presence of unwanted organic compounds. Therefore, stream separation for the different rinse waters is required to segregate the recyclable streams from the others. However, this has an associated capital expenditure for extra plumbing. In summary, there is great potential for the Recycle, Reduce, Reuse strategy but the risks and the benefits need to be assessed carefully, particularly with respect to UPW recycling. UPW use optimisation appears to offer some easy wins, namely spray rinsing and improved bath geometries, and reduced idling flows. Again, risks remain, such as the potential for increased biofouling. Some of these conservation efforts were undertaken and reported in the literature [50], including the reduction of UPW idling flows, leak repairs, the replacement of faulty resistivity probes and reducing the number of quick dump rinses. These UPW reduction efforts resulted in a saving of approximately 18.5 million U.S. gallons per year without impacting wafer quality, showing again that easy wins do exist. As always though, the impact of any changes on quality (i.e. water purity) requires careful assessment.

Despite the industry acknowledgement that water conservation is vital, it is expected that UPW requirements, in terms of quantity, quality and number of applications in the manufacturing process, will increase with shrinking geometries for next generation devices in line with Moore's Law [23, 24]. Regarding UPW, the main focus to date has been on the conservation of water through the Reduce, Reuse and Recycle strategy. However, the present energy requirements of UPW, and the predicted growth of future energy requirements with increased UPW purity, point towards the necessity of energy characterisation and optimisation.

2.2.2 The production of UPW

UPW is generated using a series of purification technologies such as reverse osmosis (RO), ion exchange (IX), ultra-violet (UV) radiation, electro-deionisation (EDI), various levels of filtration, and degasification. A typical UPW plant schematic is shown in Figure 2-3 [51]; the first two unit processes in the diagram show the initial purification technologies used to produce city water, which then acts as the feed water to the UPW plant. This city water will generally undergo three purification stages, each stage containing a number of sequential unit processes. The three loops typically comprise a pre-treatment or make-up loop, a primary loop and a final polishing loop.

RO is the engine of the UPW system, and there is often a first and second pass RO with multiple stages in each pass. The distinction between two-pass and two-stage RO can be explained as follows; in two-pass RO, the product water or permeate from the first pass acts as the feed water for the second pass, however, in two-stage RO, the retentate from the first stage is used as the feed water for the second stage (both are shown in Figure 2-4).

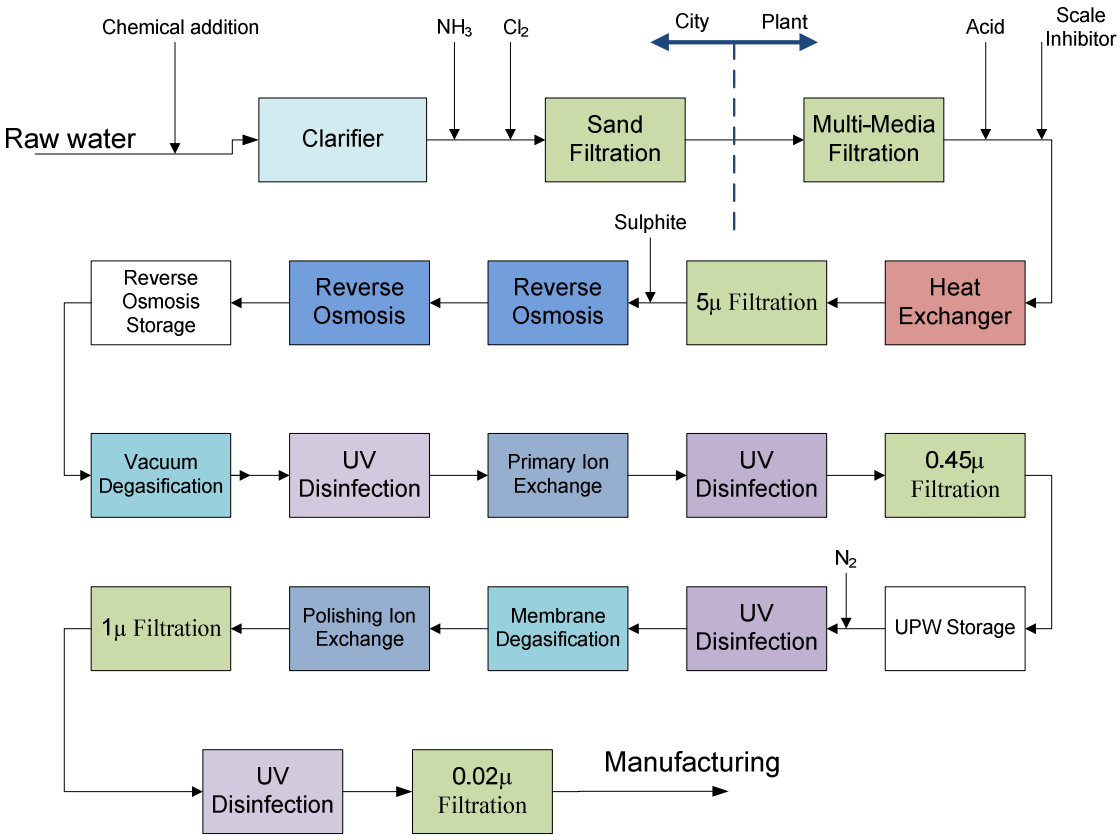

Figure 2-3: Typical UPW plant technologies, adapted from [51]

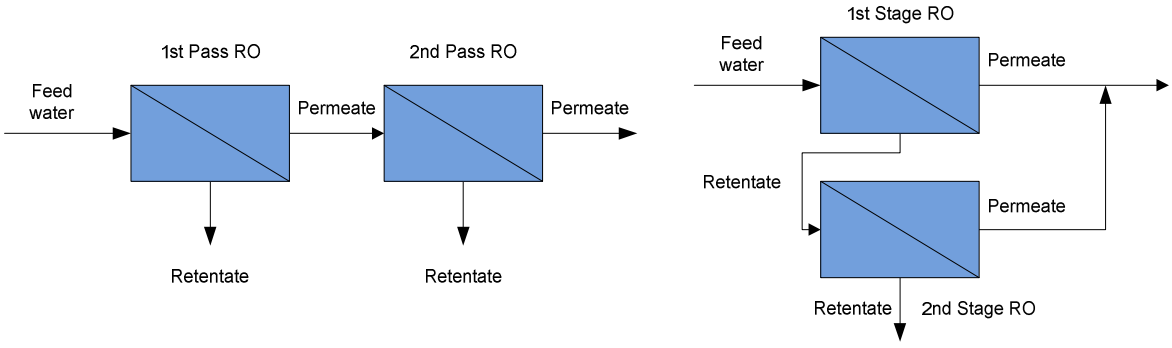

Figure 2-4: Two-Pass and Two-Stage RO

According to Dey and Thomas [48], almost 80% of the energy used in UPW systems is pumping energy to overcome osmotic pressure in the RO membranes and pressure losses due to filtration processes. Meltzer [20], however, differentiates between the pumping energy required to overcome osmotic pressure and the pressure to achieve adequate permeate flux across the membranes. According to Meltzer, osmotic pressure needs play only a minor role in pumping energy requirements, this is due to the low TDS of the incoming feedwater, for example, feedwater with a TDS of 200 ppm only requires 2 psig (pounds per square inch gauge) which is approximately equal to 0.14 bar. This calculation is based on a 'rule of thumb' also discussed in Dey and Thomas [48], which states that for quick calculations, for water rich in divalent ions, the osmotic pressure is equal to 1 psig for every 100 ppm of TDS (1.2 psig for water rich in NaCl). However, given the low values for osmotic pressure seen in high purity plants, typical operating pressures are reported to be in the range of 200-400 psig (approximately 14 to 28 bar). According to these figures, at least one hundred times the pumping energy required to overcome the osmotic pressure is generally used. What is the excess pumping energy used for? It is used to ensure adequate flux hence inferring that it is the membrane's resistance to flow which drives this energy excess.

2.3 The RO process

In RO systems, the feed water, which is a mixture of pure water and impurities, is pressurised using a high pressure pump. The feedwater flows tangentially to the membrane surface, the permeate passes through the membrane (and in reality a small proportion of ionic impurities), see Figure 2-5. The retentate or concentrate refers to the liquid that cannot pass through the membrane; the retentate flow is controlled by the concentrate valve. A

number of these membranes are contained in a pressure vessel and a number of these pressure vessels are contained in an array. Several arrays make up the RO process, see Figure 2-6.

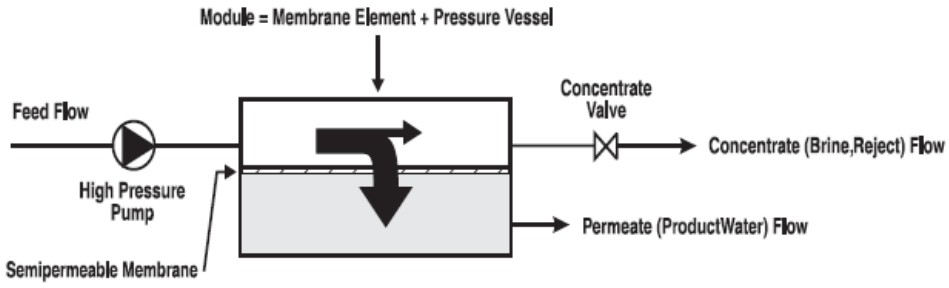

Figure 2-5: RO cross-flow filtration [52]

Figure 2-6: RO arrays in a UPW plant [53]

2.3.1 Osmosis and reverse osmosis

Osmosis is a natural phenomenon occurring when "*pure water flows from a dilute saline solution through a membrane into a higher concentration saline solution*" [48]. The osmosis process is shown in Figure 2-7, the height of the concentrated liquid increases as pure water passes across the membrane, this occurs until the increased pressure in the high column of liquid exerts a force which counteracts the passage of the pure water through the membrane and no further transport of pure water takes place, this point of equilibrium is called osmotic pressure [52]. If however, a pressure is exerted on the concentrated side, which exceeds the osmotic pressure, the phenomenon of osmosis is reversed; Figure 2-8 shows how pure water now flows from the more concentrated side of the membrane to the less concentrated side.

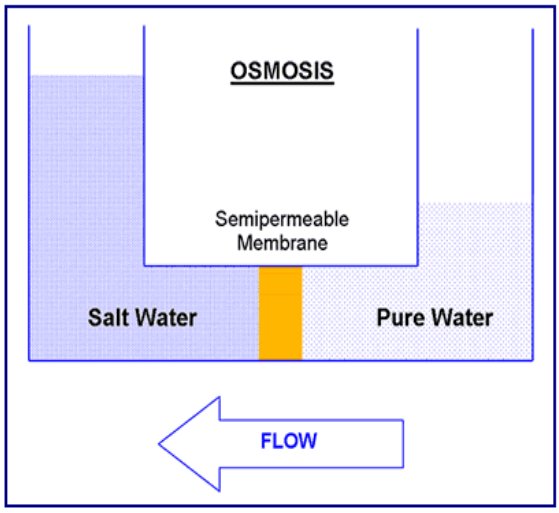

Figure 2-7: Osmosis [54]

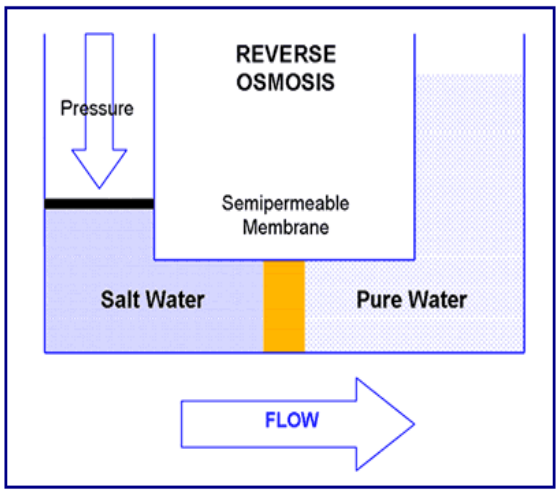

Figure 2-8: Reverse Osmosis [54]

On a more scientific level, it is the difference in chemical potential between the fluids that drives the osmosis process, always in the direction of lower chemical potential [55]. The chemical potential of a pure substance is always greater than the chemical potential of that substance existing in a mixture due to the entropy of mixing. Osmosis occurs because the chemical potential of pure water is higher than the chemical potential of water in aqueous solution with other species; to attain equilibrium, pure water will cross the semi-permeable membrane into the aqueous solution until the passage is halted due to increased pressure which exerts a force on the solution side of the membrane.

2.3.2 RO separation models and performance metrics

There are two main models which attempt to characterise the RO separation process, one is the porous model of the membrane. The porous model of the membrane assumes that the flow through the membrane "*occurs through the pores, which have a characteristic size distribution* [48]". The alternative model that is widely accepted for RO systems is the

solution-diffusion model. This model assumes that each component of the high-pressure solution "*diffuses through the membrane in response to the concentration and pressure difference*" (originally from [56] in [48]).

The performance of an RO unit depends on many factors, including most importantly, suitable feed water pre-treatment. To assure final product water quality, UPW plants are designed to complement the incoming feed water characteristics to the RO unit so that performance capabilities are not compromised. This pre-treatment is essential to minimise fouling and scaling effects. Once the feed water is suitably pre-treated, the performance is generally measured in terms of several important metrics, (1) the permeate water flux, (2) the percentage salt rejection, and (3) the percentage recovery. The permeate water flux can be defined as the quantity of permeate water attained per unit area of membrane per unit time ($m^3/m^2/s$); in imperial units, this is commonly referred to as gfd (gallons per square foot per day). The water flux J_w through the membrane is represented in its most simple form by (2.1).

$$J_w = A(P_{Tr} - \Pi_F) \tag{2.1}$$

In (2.1) A is the membrane permeability coefficient (experimentally calculated for various membranes, it characterises the membrane's resistance to flow), P_{Tr} is the trans-membrane pressure, and Π_F is the osmotic pressure of the feed water. As (2.1) illustrates, for a given membrane, the permeate flux is proportional to the difference between the trans-membrane pressure and the osmotic pressure of the feed water. The osmotic pressures dealt with in UPW plants are not significant when compared to seawater, and therefore, the permeate flux is primarily a function of the trans-membrane pressure. So, because the energy

required for the RO process is electrical pump energy, there is a necessary trade-off between the operating pressure of the pump and the permeate flux rate; the lower the operating pressure, the lower the permeate flux. Hence, the efficiency of the pump is very important to energy efficient RO. Therefore, in order to maintain the same permeate flux rate at a lower operating pressure, raising the membrane permeability coefficient *A* is necessary.

The salt flux through the membrane is given by (2.2).

$$J_s = B(C_F - C_P) \tag{2.2}$$

Equation (2.2) shows that the flow of salt across the membrane is independent of pressure but is a function of the difference in concentration across the membrane where *B* is the membrane permeability coefficient for the salt, C_F is the concentration of the salt in the feed and C_P is the concentration of the salt in the permeate. The second important performance metric, and particularly important for UPW applications, is the percentage salt rejection, see (2.3).

$$\% \text{ salt rejection} = \left(1 - \frac{C_P}{C_F}\right) \times 100 \tag{2.3}$$

The percentage salt rejection metric is a measure of the permeate water quality and is defined as unity minus the salt passage, where the salt passage is defined as the concentration of the permeate divided by the concentration of the feed water. The recovery metric is defined according to (2.4) as the volumetric flow rate of the permeate water divided by the flow rate of the feed water.

$$\% \text{ Recovery} = \frac{Q_P}{Q_F} \times 100 \qquad (2.4)$$

The recovery is controlled by the concentrate valve, if the recovery is too high, the flow rate tangential to the membrane surface is not sufficient to prevent concentration polarisation, as a consequence, salt rejection increases and permeate flow decreases. [43, 52]

Other main factors affecting performance include operating parameters such as temperature, pressure, recovery and feedwater concentration. These factors are shown in Figure 2-9 where the direction of each arrow (within each of the four plots) indicates the relationship between the relevant performance metric and the independent variables. The feed concentration is controlled as much as possible by suitable pre-treatment. Therefore, regarding RO operating parameters, and specifically RO system performance, the areas of influence include pressure, temperature and recovery rates. As Figure 2-9 illustrates, increased pressure, is beneficial to both permeate flux and salt rejection. Higher operating temperatures increase the permeate flux but have a detrimental effect on salt rejection. The operation of RO systems at higher recoveries has a negative effect on both the percentage salt rejection and the permeate flux, this negative effect increases dramatically after a certain percentage recovery. Feed concentration increases have a negative effect on both percentage salt rejection and permeate flux, although salt rejection performance decreases steadily initially and then experiences a more dramatic decline in performance; permeate flux falls off sharply initially and then more steadily. Figure 2-9 shows the complexity involved in parameter set-up, and importantly, how this set-up often entails a trade-off between permeate flux and percentage salt rejection. Also, two of these parameters,

temperature and pressure are explicitly related to plant energy consumption. The temperature affects the viscosity of the water, reduced viscosity means greater permeate flux. However, in order to increase the temperature of the water, energy must be expended, again involving a trade-off between the energy required to heat the water and the increased permeate flux as a result of this increased permeate flow rate, but also with an added caveat that increased temperature also increases salt passage. Pressure increases appear to be a win-win situation with respect to permeate flux and salt rejection, but increased pressure also has an associated energy cost. The influence of pressure on permeate flux can be seen clearly from (2.1), what is not obvious is the non-linear mathematical relationship between salt rejection and pressure. The reason the percentage salt rejection increases with increased pressure is that increased pressure causes increased permeate flux, however, due to the fact that salt flux is independent of pressure, see (2.2), the salt flux does not change and becomes more diluted leading to higher percentage salt rejection [57].

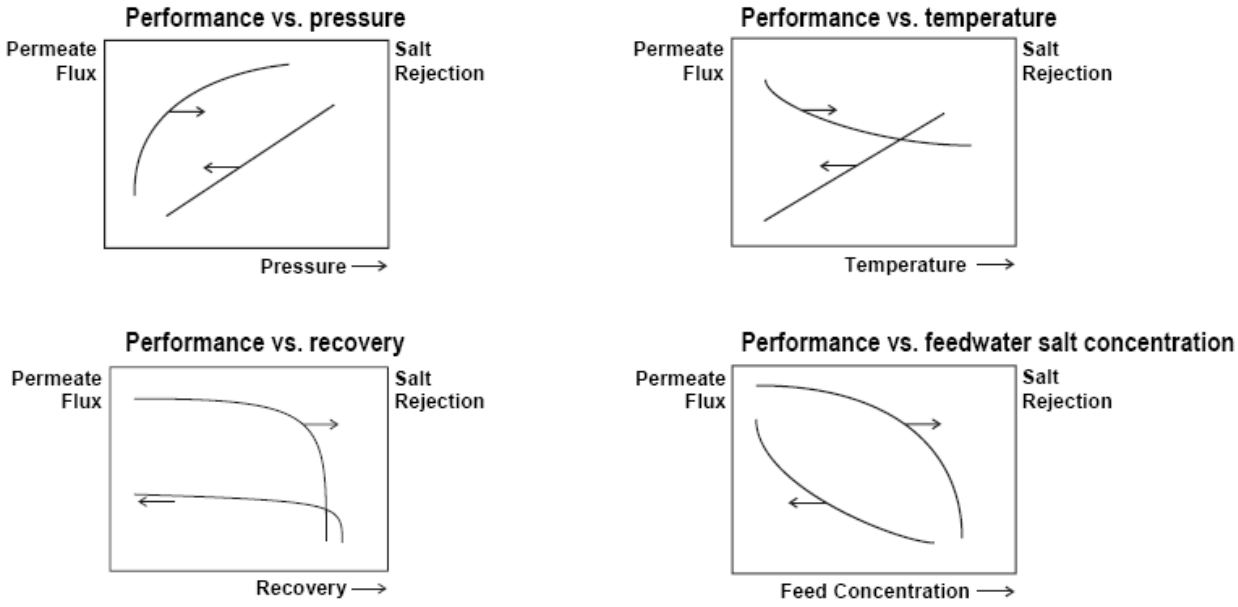

Figure 2-9: RO performance parameters [52]

2.4 Energy reduction in the desalination industry

Energy reduction efforts reviewed in the semiconductor manufacturing industry literature did not include research on the energy optimisation of UPW plants. To assess the work previously carried out in the field of energy reduction in water purification processes, it has been necessary to turn to desalination energy research. The published literature shows that the reduction of energy has become a very important issue and hence energy research in desalination is already well established.

The most significant factor that has a bearing on energy consumption is the choice of purification process. RO requires a lower energy input than thermal processes [5, 58] such as multi-effect distillation (MED) or multi-stage flash distillation (MSF). The operational

energy requirements for different desalination methods, collated from recent publications in the literature, are shown in Table 2-2.

Table 2-2: Desalination energy requirements

Technology	*Energy requirements (kWh/m^3)*	*Reference*
Brackish water RO (core process)	1	[59]
Seawater RO with Energy recovery (core process)	2.2 to 2.7	[59]
Seawater RO (all auxiliary requirements)	5 to 7	[60]
MSF (all auxiliary requirements)	38.5 to 125	[60]
MSF	20	[61, 62]
MED (all auxiliary requirements)	32 to 122.5	[59, 60]

RO requires the lowest energy input of common desalination systems [63]. This is possibly one of the main reasons for the use of membrane processes in comparison to thermal distillation processes. RO is particularly cost effective for high energy cost regions like Europe [63, 64]. The Arabian Gulf States are the major exception due to the low energy costs and the high salinity of the local seawater [7, 64], for example, Kuwait uses only MSF for desalination [61]. Although RO is considered a relatively low energy desalination process compared to thermal distillation processes, great strides have been made in lowering the energy footprint of the reverse osmosis process. RO processes in the 1970s produced product water with an energy intensity of approximately 20 kWh/m^3, a value

which had reduced to less than 2 kWh/m^3 by 2004, see Figure 2-10. According to reports cited in references [6, 64], a recent value of 1.58 kWh/m^3 has been achieved under ideal conditions (new membrane, low water flux at 42% recovery). However, this low specific energy value was obtained at the expense of permeate quality [64].

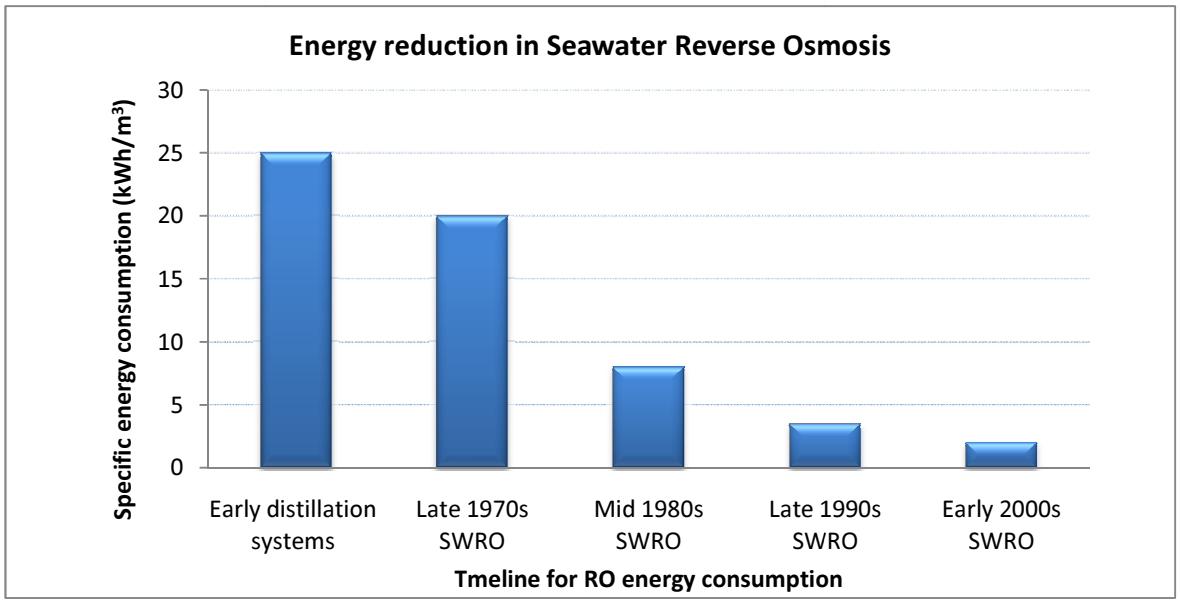

Figure 2-10: Decreasing energy consumption for RO processes, adapted from [65]

RO desalination processes have significantly reduced process energy consumption. The main energy reduction improvements have come about as a result of several factors, which are not mutually exclusive;

- Improved membranes, lower specific energy requirements as a result of higher flux [65, 66];
- Pump and motor efficiency improvements, and the use of VSDs [63, 65];
- Studies in RO system optimisation [67-74];

- The implementation of energy recovery devices to harness the wasted throttling valve energy, such as pressure exchangers, turbo-chargers, and Pelton and Francis turbines [59, 64, 65, 75, 76].

Other research approaches seeking to reduce the energy impact of RO desalination processes include;

- Pre-treatment and post-treatment of RO with the integration of other technologies such as membrane distillation (MD) and nanofiltration (NF) [5, 58, 77, 78];
- Better membrane management strategies [79];
- The coupling of reverse osmosis with sustainable technologies such as solar/wind/wave power [80-85];
- Membrane fouling studies [86];
- The use of life-cycle analysis to benchmark and improve RO plant life-cycle impact, including energy impact [87-90];
- The use of exergy analysis and/or thermo-economics for the characterisation and optimisation of RO plants (references discussed in separate section).

Not all of these technologies are suitable for the semiconductor UPW process, for example, wave power and wind power. It is not clear yet whether the use of energy recovery devices is economically or technically feasible in UPW plants. Moftah [76] researched the issue for brackish water plants, either as a means to increase feed pressure, inter-stage pressure in multi-stage RO systems, or inter-pass feed pressure. According to this cited study, the pressure energy available for recovery is proportional to the difference between the final

RO stage retentate pressure and atmospheric pressure. This recoverable energy is then used as a form of overall energy cost avoidance. The economics of such a system are highly sensitive to energy prices and are particularly attractive in high energy cost regions, like Ireland.

However, there are more complicated factors affecting energy recovery and these include TDS, temperature, membrane type, number of membrane elements in pressure vessel, fouling factor, recovery, and concentrate flowrate [76]. The applicability of a suitable energy recovery device, most likely the turbine-pump combination or piston pressure exchanger still requires detailed investigation.

Life-cycle analysis (LCA) is a cradle-to-grave approach, which measures the environmental impact, including energy, of various stages in a product's life, e.g. product manufacture, use and disposal. The energy required to manufacture and use a product is considered and mitigating alternatives are suggested. Due to the fact that the main source of energy for RO systems is electricity, an example of mitigation methods would be RO energy optimisation, the sourcing of greener electricity, and the use of waste heat [88-90]. The approach does consider the environmental impact of various desalination systems; however, it does not easily facilitate process system energy characterisation, the focus of this research. Essentially, LCA is a very useful indicator of plant environmental impact, i.e. it identifies *what* the main negative environmental impacts are (energy in the case of water production), but it does not tell one *how* to approach energy consumption mitigation. The methodology

that shows the most promise and offers the most insight into process characterisation, through the quantification of system irreversibilities, is exergy analysis.

2.5 Exergy analysis

Exergy analysis has been identified as a key tool for the assessment of thermal and energy processes by many energy researchers [91-96]. The history of exergy is based in the development of classical thermodynamics in the 19th century. Sciubba and Wall [97] traced the history of exergy from Carnot, Clausius and Gibbs to the "*availability*"' or Second Law analysis of Keenan in 1932, and the coining of the term "*exergy*" by Rant in 1954, and finally on to the applications of exergy analysis up until 2004. Sciubba and Wall's key review paper contains 2600 references relating to exergy in fields such as cryogenics, power cycles, chemical processes, industrial and agricultural applications, and desalination. As well as looking at the historical development of exergy, the authors also looked to the future of exergy analysis and the areas ripe for further investigation. Some of these identified areas included the use of exergy analysis in the field of thermo-fluid dynamics applications, the extension of exergy analysis in the life-cycle analysis approach, and the inclusion of environmental concerns into thermoeconomics. It should be stated that Tsatsaronis [98] and Yantovski [99] both commented on some alleged errors and omissions of this review paper, to which the authors of the review paper then responded [100, 101]. Notwithstanding this argument and counter-argument, the paper does provide a key resource for exergy researchers.

A second recent review paper reports that exergy analysis has been applied to renewable technologies such as solar power applications, wind energy systems, geothermal systems and biomass in the quest for sustainable development [102]. From the energy perspective, the application of exergy analysis has also been extended to assess the energy utilisation efficiencies of various countries including the U.S., Canada, Japan, and the U.K. [103, 104]. Therefore, it is evident that exergy analysis is widely used and accepted by many leading energy experts as providing a powerful basis for the characterisation and optimisation of thermal or energy systems.

The property exergy is used in an exergy balance to quantify inherent process irreversibilities. An exergy analysis is undertaken by;

- Calculating the rate of exergy destruction using an exergy balance;
- Using the exergy balance and exergy destruction rates to calculate the exergetic efficiency of, (1) individual components within processes, (2) processes, and (3) overall process plant efficiency.

Although the rate of exergy destruction, initially, may not be significant as a stand-alone quantity, it does provide a critical benchmarking tool, both for the components within a multi-component process and between similar processes. The rate of exergy destruction is also an ideal platform for assessing possible process plant improvements and optimisation.

Exergy analysis has been chosen as the means of characterising the energy footprint of a typical UPW plant. Exergy, a thermodynamic property, is a theoretical measure of the maximum available (or potential) work that a system can do as it comes into equilibrium

with its environment. As a corollary, therefore, it is also a theoretical measure of the necessary minimum work input to bring a system from its relevant reference environment to a desired thermodynamic state. The exergy at any point in a system is measured with reference to the 'dead state', i.e. the state of the system's environment. In this thesis, the environment is defined as a large system where the intensive properties are not affected by the plant processes under consideration. Common forms of exergy include kinetic exergy, potential exergy, thermo-mechanical exergy and chemical exergy. When equilibrium between the system under consideration and its environment is reached the opportunity to do useful work no longer exists and the value of exergy is zero.

Exergy analysis incorporates both the First and Second Laws of thermodynamics, and considers the *quality* and the *quantity* of energy in systems. An example of the difference between the concept of energy quality and energy quantity is the throttling process; using the First law, the throttling process occurs without thermodynamic loss, however, an exergy analysis quantitatively accounts for this source of energy waste [95]. In his PhD thesis, O'Toole [105] carried out an exergy analysis of a paint drying oven to identify system components responsible for energy inefficiencies and compared it with an energy analysis of the same process. Components responsible for energetic and exergetic losses were placed in a hierarchy of importance and the results obtained showed that the exergy analysis and the energy analysis identified a different order of components in the hierarchy. The problem with solely using an energy balance to assess systems is that there is a possibility of incorrectly identifying the most important source of thermodynamic loss and hence allocating improvement resources to the wrong process.

The First Law energy balance can be considered as the law of *conservation of energy*, according to Kotas [92], the "*exergy balance may be looked upon as a statement of the law of degradation of energy*". The fact that energy in the scientific sense cannot be created or destroyed implies that it is an ever-available source of doing work or causing change, what one really means by the term energy is a true measure of its potential to cause change, this is elegantly proposed as a paradox by Gaggioli and Petit [106],

> "*When does the layman ascribe "energy" to a material? When it has a potential to cause change for him. But that which is called energy by the scientist is not this potential; our energy cannot be produced or destroyed. Therefore, if it were truly a resource it would be nondepletable. We cannot resolve this paradox by stating that "it is conserved, but it is degradable." Because, if energy loses potential to cause change for us then energy cannot be a measure of that potential. The only true resolution of the paradox is to realize that it is availability – potential energy – which is the rational measure of this potential to cause change for us.*
>
> *It is potential energy that is needed to make processes go; in doing so, it is literally used up – not degraded, not converted, but used up (consumed)."*

This availability or potential energy described by Gaggioli and Petit is the property exergy.

As stated previously, the use of the exergy property to assess process irreversibilities typically takes the form of an exergy balance. The exergy balance equations are now introduced (however, for the purpose of simplicity, chemical exergy is not discussed presently but is considered in greater depth later in this chapter). When effects such as

nuclear, magnetic, electrical, and surface tension are absent, the general exergy balance equation for a control volume operating under steady state conditions is given by (2.5).

$$\sum_j \left(1-\frac{T_0}{T_j}\right)\dot{Q}_j - \dot{W} + \sum_{in} \dot{m}e - \sum_{out} \dot{m}e - \dot{X}_{des} = 0$$

where e the specific exergy is calculated as follows (2.5)

$$e = (h-h_0) - T_0(s-s_0) + \frac{V^2 - V_0^2}{2} + g(z-z_0)$$

The first term in (2.5) relates to the rates of exergy transfer associated with any heat transfers $\dot{Q}_j$ which may take place at various locations j on the system boundary where the instantaneous temperature is T_j. The second term relates to the rates of exergy transfer associated with work transfer. The third and fourth terms relate to the relevant transfers of specific exergy e into and out of the system by mass flow $\dot{m}$, and $\dot{X}_{des}$ refers to the rate of exergy destruction. Regarding the calculation of specific exergy e, h is the specific enthalpy at the relevant process stage under consideration, h_0 is the specific enthalpy at the dead state, T_0 is the temperature at the dead state, s is the specific entropy at the relevant process stage and s_0 is the specific entropy at the dead state. The remaining terms refer to kinetic and potential exergy where V is the velocity at the process stage, V_0 is the velocity at the dead state, g is the gravitational acceleration, z is the elevation at the process stage and z_0 is the elevation at the dead state. When no heat transfer takes place across the system boundary, no work interactions occur and changes in the velocity and elevation can be disregarded, (2.5) simplifies to (2.6).

$$\sum_{in} \dot{m}e - \sum_{out} \dot{m}e - \dot{X}_{des} = 0$$

where e is calculated as follows (2.6)

$$e = (h - h_0) - T_0(s - s_0)$$

Using thermodynamic property relationships, the exergy rate $\dot{E}$ can be calculated using (2.7), where c is the specific heat capacity, v is the specific volume and P is absolute pressure.

$$\dot{E} = \dot{m}\left[\int_{T_0}^{T} c dT + v(P - P_0) - T_0 \int_{T_0}^{T} \frac{c}{T} dT \right] \quad (2.7)$$

If the flowing fluid under consideration is a liquid and can be assumed incompressible, and the specific heat capacity is assumed constant, the exergy rate can be calculated using (2.8), where ρ is the density.

$$\dot{E} = \dot{m}\left[c(T - T_0) - cT_0 \ln\left(\frac{T}{T_0}\right) + \frac{P - P_0}{\rho} \right] \quad (2.8)$$

As (2.8) shows, the exergy rate consists of a thermal and a mechanical (or pressure) contribution, this combined exergy rate is generally termed thermo-mechanical or physical exergy [92-95, 107, 108].

The exergy balance identifies processes or process components responsible for the greatest exergy destruction. A complementary approach is to calculate the exergetic efficiency of processes and process components. There are several versions of exergetic efficiency discussed in the literature, for example, the simple exergetic efficiency and the rational

exergetic efficiency. The simple exergetic efficiency is a ratio of the exergy output to the exergy input of the system (the sum of the exergy streams out divided by the sum of the exergy streams in). The rational exergetic efficiency takes account of the objective of the system under consideration. For example, consider a heat exchanger, one common purpose of a heat exchanger is to increase the exergy of the cold stream at the expense of the hot stream, and therefore, the rational exergetic efficiency is the ratio of the increase of the exergy of the cold stream $\Delta\dot{E}_{cold}$ to the decrease of the exergy of the hot stream $\Delta\dot{E}_{hot}$, see (2.9) [95, 109].

$$\text{Exergetic efficiency of heat exchangers} = \frac{\Delta\dot{E}_{cold}}{\Delta\dot{E}_{hot}} \tag{2.9}$$

Kotas [92] defined rational efficiency as the ratio of the desired exergy output $\dot{E}_{Desired\ output}$ to the exergy used $\dot{E}_{Used}$. The desired exergy output "*is the sum of all exergy transfers from the system, which must regarded as constituting the desired output, plus any by-product, which is produced by the system. The desired output is determined by examining the function of the system.* $\dot{E}_{Used}$ *is the required exergy input for the process to be performed* [sic] [110]". Using the approach of Kotas [92], the definition of the rational exergetic efficiency of a heat exchanger can be further refined as the change in thermal exergy of the cold stream $\Delta\dot{E}^{T}_{cold}$ divided by the decrease in thermal exergy of the hot stream $\Delta\dot{E}^{T}_{hot}$ plus the change in both pressure ($\Delta\dot{E}^{P}_{cold}$ and $\Delta\dot{E}^{P}_{hot}$) and chemical exergy ($\Delta\dot{E}^{Ch}_{cold}$ and $\Delta\dot{E}^{Ch}_{hot}$) of the hot and cold streams. Thus, the desired exergy output, the exergy used, and the rational exergetic efficiency of a heat exchanger can be calculated according to (2.10), (2.11) and (2.12) respectively.

$$\dot{E}_{Desired\ output} = \Delta\dot{E}^{T}_{Cold} \tag{2.10}$$

$$\dot{E}_{Used} = \Delta\dot{E}^{T}_{Hot} + \Delta\dot{E}^{P}_{Cold} + \Delta\dot{E}^{P}_{Hot} + \Delta\dot{E}^{Ch}_{Cold} + \Delta\dot{E}^{Ch}_{Hot} \tag{2.11}$$

$$\text{Exergetic efficiency of heat exchangers} = \frac{\Delta\dot{E}^{T}_{Cold}}{\Delta\dot{E}^{T}_{Hot} + \Delta\dot{E}^{P}_{Cold} + \Delta\dot{E}^{P}_{Hot} + \Delta\dot{E}^{Ch}_{Cold} + \Delta\dot{E}^{Ch}_{Hot}} \tag{2.12}$$

Note that (2.11) and (2.12) include chemical exergy for completeness although these terms typically cancel in heat exchanger analyses.

The exergetic efficiency can also be thought of in terms of product exergy (P) and fuel exergy (F). The product exergy is the sum of the fuel exergy, the exergy destruction (D) and the exergy losses (L), see (2.13). Exergy losses can be defined as exergy streams that add no further exergy value to the process. [111]

$$P = F - D - L \tag{2.13}$$

The exergetic efficiency can then be calculated using (2.14).

$$\text{Exergetic efficiency} = \frac{P}{F} = 1 - \frac{D + L}{F} \tag{2.14}$$

This development of exergy losses takes stock of the fact that not all exergy streams are valuable; this is best explained by comparing the case of the exergetic efficiency that does not consider exergy losses with a case that does take account of the exergy losses. Excluding exergy losses, the product exergy is defined according to (2.15).

$$P = F - D \tag{2.15}$$

The exergetic efficiency is then given by (2.16) in a similar manner to the previous analysis of (2.14).

$$\text{Exergetic efficiency} = \frac{P}{F} = 1 - \frac{D}{F} \tag{2.16}$$

Comparing (2.14) and (2.16), it is clear that the simple exergetic efficiency does not take into account the fact that some 'exergy out' streams go to waste (exergy losses), thereby over-estimating the exergetic efficiency.

Rational exergetic efficiency considers the purpose of the system, and the use of exergy losses considers that some exergy streams go to waste. Ideally, the purpose of the system should be assessed and defined, all waste streams should be identified and, either used for some other useful purpose, or discounted from exergetic efficiency calculations.

For systems changing in composition, there is also a chemical exergy term which must be taken into consideration and this term is added to the physical exergy to give total exergy. However, before discussing chemical exergy in detail, the rational exergetic efficiency of a process, where the sole function is to change the chemical exergy, is defined. Based on the preceding discussion of Kotas rational exergetic efficiency definitions, the desired exergy output, the exergy used and the exergetic efficiency of a separation process like RO can be calculated using (2.17), (2.18) and (2.19) respectively.

$$\dot{E}_{Desired\ output} = \left| \dot{E}_F^{Ch} - (\dot{E}_P^{Ch} + \dot{E}_R^{Ch}) \right| \tag{2.17}$$

$$\dot{E}_{Used} = \dot{E}_F^{Ph} - (\dot{E}_P^{Ph} + \dot{E}_R^{Ph}) + \dot{W} \tag{2.18}$$

$$\text{Exergetic efficiency of the RO process} = \frac{\left| \dot{E}_F^{Ch} - (\dot{E}_P^{Ch} + \dot{E}_R^{Ch}) \right|}{\dot{E}_F^{Ph} - (\dot{E}_P^{Ph} + \dot{E}_R^{Ph})} \tag{2.19}$$

In the preceding equations, the subscripts *F*, *P* and *R* refer to the feedwater, the permeate and the retentate respectively, and the superscripts *Ch* and *Ph* refer to chemical and physical. Note that the work term is omitted from the exergetic efficiency in the case of RO; in this thesis, the RO pump and the RO module are considered separately and the electrical work is attributed to the pump.

Chemical exergy can be thought of as the theoretical maximum potential work that a system can do as it changes reversibly from thermo-mechanical or physical equilibrium to total equilibrium or the dead state. Thermo-mechanical equilibrium has been termed the "*restricted dead state* [94, 95]" in contrast to the dead state. Therefore, chemical exergy represents the maximum theoretical work that process waste products could do as they are allowed to dissipate and interact with their environment at environmental temperature and pressure. The chemical exergy term can be split into a reactive chemical exergy term and a nonreactive chemical exergy term [112, 113]. The reactive term relates to electrostatic bond energy and the non-reactive term relates to the concentration of the species in the system under consideration relative to the concentration of that species in the reference environment [114]. The latter non-reactive term considers the mixing of system species at different concentrations from that of the reference environment, some authors consider the mixing chemical exergy terms as physical exergy [115]. Alternatively, total system exergy can be thought of as the combination of thermo-mechanical exergy, chemical exergy and a separate mixing exergy term [112]. In this document, chemical exergy is defined as exergy which is not physical (or thermo-mechanical).

Regarding the calculation of chemical exergy, and in an effort to consider and quantify the natural capital of the earth's resources, several researchers have modelled the earth (atmosphere, lithosphere and hydrosphere) as a standard reference environment or standard reference state. The reference environment is classified into three categories, (1) gaseous reference substances (atmosphere), (2) solid reference substances (lithosphere) and (3) reference substances dissolved in seawater (hydrosphere). The standard reference environment has been used as the basis for computing the standard chemical exergy of elements and compounds [116-119]. Suitable reference species from the three environmental categories are ascribed to each element (based on different criteria) and the chemical exergy is calculated according to the reference environment category.

Different chemical exergy values of elements and compounds arise from the fact that the natural capital of the earth is made up of different substances of "*a particular composition which differentiates them from the surrounding environment, and a distribution which places them in a specific concentration* [117]". However, while there is debate in the literature on the most appropriate way to model a standard reference environment, there is general consensus on what conditions a suitable reference environment should satisfy;

- Thermodynamic equilibrium conditions;
- Similarity to the natural environment (Earth similarity criterion);
- Practicality from a technical perspective;
- Should consider economics in the allocation of standard exergy values. [120, 121]

The natural environment is not in equilibrium, however, as pressure, composition, and temperature change with regards to location and time, and therefore, satisfying the

reference environment conditions is not an easy task [120]. As a consequence, significant compromises have to be made [95]. Several models of reference environments have been developed [93, 103, 106, 118, 119, 122-124]. These various models can be considered as either partial or comprehensive reference environments [117]. The intricacies of all these models are beyond the scope of this thesis, and therefore, only a brief overview of some key contributions is given, rather than an exhaustive list.

The comprehensive reference environments can be divided up into four criteria;

- Szargut's criterion;
- Chemical equilibrium criterion;
- Chemical stability criterion;
- Abundance criterion. [117]

Ahrendts [122] imposed a chemical equilibrium criterion on the environment based on interactions between the atmosphere, the hydrosphere and the lithosphere. He considered various depths of the earth's crust and found that the modelled environment was very different from the real environment at depths other than one metre [95, 103, 122]. Kameyama et al. established a criterion of chemical stability and used Clarke numbers (estimating the abundance of elements in the earth's crust) as an indicator of economic value [123]. This model was deemed unsuitable by both Van Gool and Szargut for several reasons, (1) the fact that economic value does not form part of traditional thermodynamic theory, and (2) on the basis that the use of the Clarke number for estimating material abundance has little correlation to economic market values of metals [103]. Szargut et al. disputed the Kameyama et al. model on the grounds that some of the compounds selected

as reference species for chemical elements, were not suitable for elements such as fluorine, bromine, chlorine and iodine, because they were unlikely to form in the environment [117, 118]. On the whole, according to Szargut et al. [117], the chemical equilibrium and the chemical stability criteria contravene the Earth similarity criterion and are therefore not suitable methods for natural capital evaluation.

Van Gool [103] attempted to bridge some of the gaps arising from, what he considered, curiosities between exergy thermodynamic theory and regular thermodynamic theory. Van Gool's attempts to reconcile exergy theory and traditional thermodynamic theory included the abandonment of the use of the Abundance criterion, and the use of only well defined thermodynamic data in the reference system development.

Several of these exergy environmental reference state models were compared by Munoz and Michaelides [120] by calculating the chemical exergy rates and the exergetic efficiency for a cogeneration plant, a coal-fired plant and a geothermal plant. The cited authors found that several reference environment models gave very similar results (including models by Szargut et al., Ahrendts, and Kameyama et al.), the only major difference between these models was the relatively high chemical exergy values of water in the Szargut et al. model. Other findings included the observation that the Van Gool model led to high chemical exergy values for air. The authors found that although the chemical exergy rates may differ, it is the calculation of exergy destruction that is important for assessing system irreversibilities, and in that case, the standard reference environments cancel out. Consequently, the choice of reference environment becomes largely irrelevant.

Other authors base chemical exergy calculations on specific characteristics of the process under consideration rather than standard chemical exergy environments [106, 124, 125]. The debate continues regarding the most appropriate approach. Szargut et al. [117] called for consensus on reference environments in a 2005 conference paper and the adoption of an international legal reference environment. In this paper, several of the aforementioned reference environments were reviewed, and more recent geochemical data [126] and other recent accurate data [121] were included in order to revise and update the tables of standard chemical exergies. The authors advocated the selection of one reference environment, that proposed by Szargut and his colleagues.

The Szargut criterion model acknowledges that thermodynamic equilibrium does not exist [93, 117], and that reference species should be chosen to reflect the most probable interaction between the substance under consideration and the environment [117]. Szargut's criterion facilitates selection of the most appropriate reference substance for a particular element from a potential group of stable and naturally occurring abundant reference substances. Essentially, Szargut's criterion dictates that if the stability of the considered reference substances is within a certain threshold, with respect to the Gibbs energy of formation (considered separately for various elements due to geological uncertainties), then the most abundant reference substance will be chosen. If however, the substance exceeds the chosen stability threshold, then the most stable reference substance from the group will be chosen as long as the choice does not contravene the Earth similarity criterion. This should become clearer with some examples taken from Szargut et al.; in this example

consideration is given to the most suitable reference substance for the element Sb using Szargut's criterion [117],

> *"…in the case of Sb, the substance Sb_2S_3 is more abundant than Sb_2O_5, nevertheless, according to Szargut's criterion, Sb_2O_5, which is much more stable, will be taken as a reference substance."*

Another point of note is that nitrates such as $Ca(NO_3)_2$ and $NaNO_3$ are not chosen as reference substances for various elements, because even though they are the most stable, they are not abundant in the natural environment, and therefore, contravene the Earth similarity criterion.

Once the specific reference substance has been chosen according to Szargut's criterion, a reference reaction can be formulated for the element. Only the element in question, the specific reference substance and other reference species make up the reference reaction. Again, for the purposes of clarity, an example of the reference reaction for the element calcium is shown below, this example is taken from [93].

$$Ca + \frac{1}{2}O_2 + CO_2 \rightarrow CaCO_3 \tag{2.20}$$

The element under consideration is allowed to react with the chosen reference substances, in this case, the reference species of O_2 has been chosen for oxygen, CO_2 for carbon and the specific reference species $CaCO_3$ for calcium. The standard molar chemical exergy of a compound or element (calcium in this example) can then be calculated using an exergy balance for the reference reaction, see (2.21).

$$\bar{e}_{Ca}^{\circ Ch} = -\Delta_R \bar{g}^{\circ} + \sum_p v\bar{e}^{\circ Ch} - \sum_r v\bar{e}^{\circ Ch} \qquad (2.21)$$

In (2.21) $\Delta_R \bar{g}^{\circ}$ is the standard molar Gibbs energy of the reaction, i.e. the difference in molar Gibbs energy between the products and the reactants at the standard temperature and pressure, v is the stoichiometric coefficient in the balanced reference reaction, $\bar{e}^{\circ Ch}$ is the molar standard chemical exergy (calcium carbonate in the case of the product, carbon dioxide and oxygen in the case of the reactants). The subscripts *p* and *r* signify the products and the reactants of the reference reaction respectively, and the superscript *Ch* denotes chemical. The over-bar denotes molar properties. Naturally, by definition, the use of the reference reaction method to calculate chemical exergy assumes that the standard chemical exergy of the other reference substances in the reference reaction is known. At the fundamental level, the methods for calculating the standard chemical exergies of the reference species and elements (each with a reference datum level in one of the following, atmosphere, lithosphere or hydrosphere) are discussed in greater detail in Chapter 7.

The chemical exergy of reference species (including elements and compounds) which use the atmosphere as a reference datum level is calculated as a function of dead state temperature and the ratio of their respective mean partial pressures in the environment to the standard atmospheric pressure, i.e. their standard mole fraction in the environment, assuming the ideal gas model. Elements and compounds that can be modelled in this manner include oxygen, nitrogen, carbon dioxide, water vapour and helium. The periodic table of elements and their respective datum reference levels are shown in Figure 2-11, which is based on data in [117] and on a graphical representation in [121].

The chemical exergy of solid reference species using the lithosphere as the datum level substance is also a function of the reference temperature and the mole fraction of the species under consideration in the environment. However, it is difficult to estimate the mole fraction of solid reference species in the earth's crust with any degree of certainty, a method has been developed in [118]. Values have been updated as new geochemical or geological data has come to light; research in this particular area has been carried out by Ranz [126] and Grigor'ev (private communication detailed in [117]).

The method to determine the standard chemical exergy of elements which use seawater as the datum level substance (hydrosphere) was originally developed by Morris [119]. However, in contrast to the lithosphere datum, more accurate data are available on the composition of substances which use the seawater datum and thus calculations of chemical exergy are more exact [117]. The chemical exergy of an element with a seawater reference datum level is a function of the Gibbs energy of the formation of the reference ion or unionised reference species, the valence of the reference ion, the standard chemical exergy of hydrogen gas, the standard molarity and activity coefficient of the reference species in seawater, the standard temperature and the pH of seawater [119]. Certain substances whose chemical exergy was originally calculated based on the seawater datum in [119], e.g. elements from the second column of the periodic table such as calcium and magnesium (existing as positive divalent ions in seawater) were changed to a lithosphere datum level in later publications [117]. The reason for this change of datum level was that the chemical exergy values for these 'column 2' elements calculated using the seawater datum, when later used to calculate the values of chemical exergy of certain compounds common in the

Earth's crust which contained these elements, resulted in negative values of chemical exergy, hence the datum level was changed to the lithosphere [117].

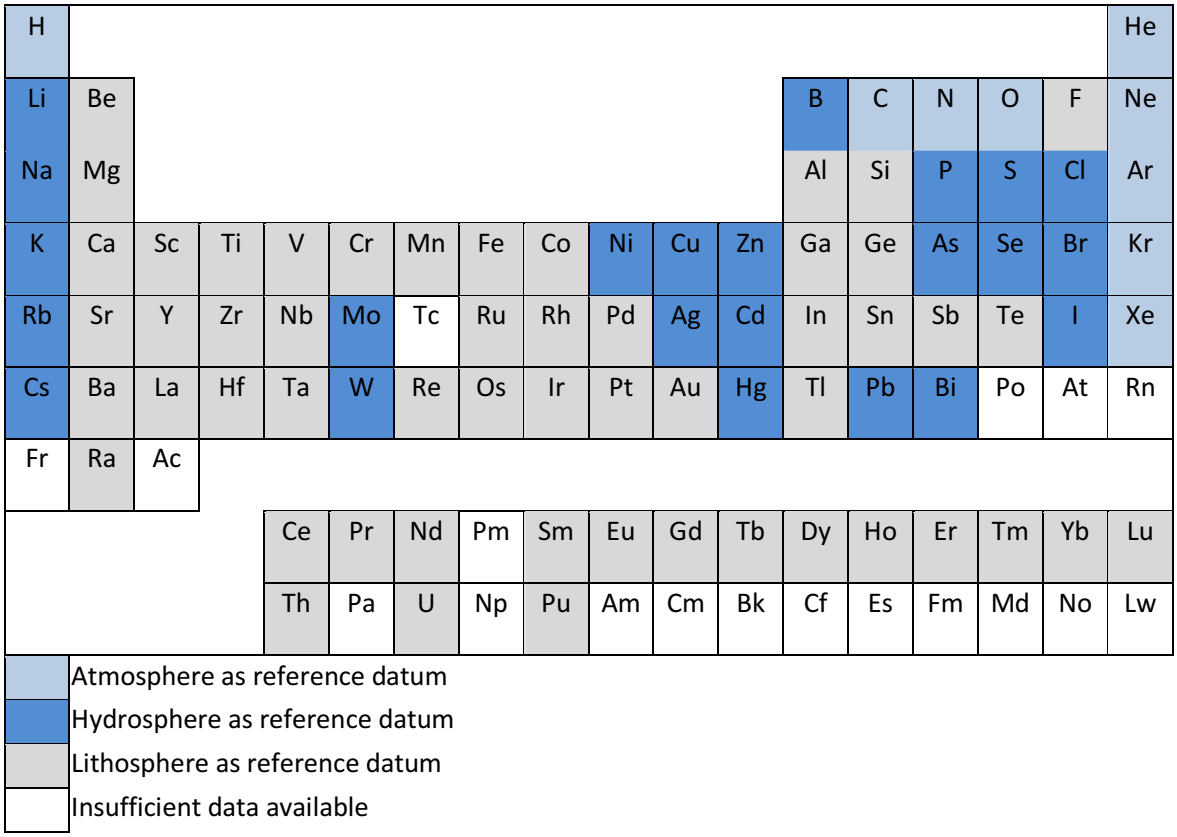

Figure 2-11: The periodic table of elements their reference datum levels, based on data in [117]

Rivero and Garfias [121] later proposed some variations to the elemental reference datum levels illustrated in Figure 2-11, based on certain anomalies they found when the seawater salinity was increased, for example, in the case of the Red Sea. Rivero and Garfias proposed solid reference datum levels for certain elements, however, Szargut et al. maintained their choice of seawater reference datum for elements such as zinc, silver, copper, nickel and lead, on the basis that, (1) increased salinities in the seas seldom arise,

and (2) the deviations were not large and could be accepted considering the previously mentioned inaccuracies associated with the lithosphere as a reference datum level. It is evident that there is still some debate on the choice of reference datum levels for various elements. However, the arguments put forward by Szargut et al. regarding the choice of reference datum, particularly with respect to the lithosphere inaccuracies, are valid and the Szargut model outlined in [117] is adopted as the standard reference environment in this thesis when applicable.

In summary, regarding the importance of exergy analysis, Bejan et al. [95] state that the rational exergetic efficiency is,

> "*…generally more meaningful, objective and useful than any other efficiency based on the first or second law of thermodynamics, including the thermal efficiency of a power plant, the isentropic efficiency of a compressor or turbine, and the effectiveness of a heat exchanger*".

With respect to exergy destruction (termed exergy losses by Szargut), Szargut [93] states that exergy destruction must only be accepted if it is,

> "*…indispensible for the reduction of investment expenditures. Exergy losses without any economic justification should be treated as the result of an engineer's error*".

The fundamental difference between the traditional energy balance of the First Law and the exergy balance incorporating the Second Law is that energy is conserved, exergy is not. Although exergy analysis offers a more comprehensive picture of energy flows, it is still

not as widely used as traditional methods [110]. However, looking at the quantity of recent exergy papers, this appears to be changing and exergy analysis is becoming more widely used for various applications. Monographs on exergy can be found in the thermodynamics literature by Ahern [91], Kotas [92], Szargut et al. [93, 116] and Dincer and Rosen [127]. Chapters on exergy analysis are included in Bejan, Tsatsaronis and Moran [95], Bejan [94], and thermodynamics text books by Moran and Shapiro [109] and Cengel and Boles [128].

2.6 Exergy analysis of reverse osmosis plants

Exergy analysis has been applied by several research groups, to various types of desalination plants including Multi-Stage Flash (MSF), Multi-Effect Evaporation (MEE), Multi-Effect Distillation (MED), Vapour Compression Distillation, Co-generation plants (combining power generation and distillation), Humidification-Dehumidification desalination cycles and RO systems [5, 7, 58, 61, 62, 77, 78, 80, 111, 129-151]. Exergy analysis has also been used as a modelling output in a software package for the design and simulation of various desalination processes [152-154]. As the main focus of this thesis is the energy characterisation and optimisation of a UPW plant, a detailed review of the exergy analysis of thermally driven distillation plants is not given; these technologies are not shared with UPW, and have a much larger energy and exergy destruction footprint than membrane processes. For example, one study [131] compared the exergy destruction of various seawater desalination techniques; as shown in Table 2-3, the exergy destruction of RO is almost a third lower than vapour compression distillation or multi-effect evaporation.

Table 2-3: Exergy destruction in desalination systems, adapted from [131]

Desalination system	***Exergy destruction***	
	(kWh/ton)	***(J/mol)***
RO	0.98	63.8
Electro-dialysis	12.87	834
Vapour compression	2.77	179
Multi-effect evaporation	2.83	183
Multi-stage flash	4.89	316.5

The main focus of this section is therefore to present an in-depth review of the exergy analysis of desalination processes common to UPW, particularly RO. There are several different approaches to the exergy analysis of RO taken in the literature, which can be broken down into different categories although there is often some crossover in theme;

- A focus on the exergy model itself and the thermodynamics of desalination;
- The development of computer models to calculate exergy and exergy destruction;
- The use of exergy analysis to assess the exergy destruction in different system configurations;
- The development of a computer model combining the transport model equations with exergy to predict the exergy destruction when changing operating parameters such as pressure;
- Thermoeconomics - a focus on system design which uses exergy as a factor in the trade-off between the cost of producing the system and the cost of operating the system.

One important issue that comes to attention in the literature is the number of different models and approaches that have been used by various research groups. Table 2-4 shows

exergy models which have been used for desalination purposes and the literature reviewed indicates that the model differences typically relate to the chemical exergy terms. One body of research has used what is termed in this thesis, the Drioli aqueous solution model [5, 7, 58, 77, 78]. Another approach has used a different model, termed the Cerci ideal mixture model [134, 136-138, 141, 146, 147]. In the author's opinion, the sheer amount of different exergy models in the literature presents a difficult challenge to the increased utilisation of exergy analysis as a tool for desalination energy optimisation. In a recent paper, Tsatsaronis [113] advocated the need for symbol and nomenclature uniformity in exergy analysis, although this consensus is desirable, the difference in exergy calculation models evident in Table 2-4 is a more pressing issue.

Table 2-4: Desalination exergy model equations

Relevant Exergy or specific exergy equation variations	*Specific nomenclature*	*Source*
$e = h - h_0 - T_0(s - s_0) + R_w T_0 \left[\frac{\phi x_s x_{s0}}{x_s - x_{s0}} \ln \frac{x_s}{x_{s0}} - \phi x_{s0} \right]$	φ is a factor which accounts for the electrolytic nature of the salt, R_w is the gas constant for water	[129-131]
Exergy calculations based on Leyendekker, Thermodynamics of Seawater, Part 1, 1976	Not applicable	[111, 140]
$e = c_p \left(T - T_0 - T_0 \ln \frac{T}{T_0} \right) + \frac{P - P_0}{\rho} - N_{sol} R T_0 \ln x_{sol}$ where $N_{sol} = \left[1000 - \sum \frac{C_i}{\rho} \right] / MW_{sol}$ and $x_{sol} = N_{sol} / \left[N_{sol} + \sum \frac{\beta_i C_i}{\rho MW_i} \right]$	c_p is the specific heat capacity	[5, 7, 58, 77, 78]
Variations of the following equation $e = h - h_0 - T_0(s - s_0)$ where $h = mf_s h_s + mf_w h_w$ and $s = mf_s s_s + mf_w s_w - R_{im}(x_s \ln x_s + x_w \ln x_w)$	Not applicable, see main nomenclature	[134, 136, 137, 141, 146, 147, 154-156]
$e = c_{p\,w} \left(T - T_0 - T_0 \ln \frac{T}{T_0} \right) + v_w (P - P_0) + \sum x_i (\mu_i - \mu_{i0})$ where $\sum x_i (\mu_i - \mu_{i0}) = R T_0 \sum x_i \ln \frac{a_i}{a_{i0}}$	$c_{p\,w}$ is the specific heat capacity of pure water	[131, 157] The chemical exergy term is also proposed in [131].

Other variations in the application of exergy analysis to RO systems, and the obtained results, also exist. One approach that has not been considered in the model comparison, although it may be considered in the future for approximate calculations, is that of Spiegler and El-Sayed [131]. Although, essentially a thermoeconomics study, the exergy destruction calculations of this cited research are proposed in a different manner to other research groups; in this case, the rate of exergy destruction is calculated by multiplying the dead state temperature by a flow rate and a "*excess generalised driving force*" conjugated to that flow rate. Regarding RO, the driving force conjugated to the flow is defined as the excess pressure used in the process divided by the temperature of the water. This conjugated driving force is then multiplied by the molar volume of pure water to give the molar entropy creation rate, which in turn is multiplied by the dead state temperature (according to the Gouy-Stodola relationship). Utilising the molar volume of pure water entails one important assumption, i.e. that the membrane is perfectly semi-permeable and that only pure water is transported across the membrane. This assumption is not entirely valid due to the low salt passage in RO. However, there are benefits to this approach as it offers a simple method for calculating the rate of molar exergy destruction and enables ready comparison between different RO configurations. For RO molar exergy destruction calculations, all that is required is the excess pressure measurement and temperature of the water. The authors used this method to calculate the exergy destruction rates of different desalination methods by using relevant driving forces conjugated to the various relevant flows, e.g. in the case of electro-dialysis this is based on excess voltage conjugated to the electric current flow. The various exergy destruction rates were shown previously in Table 2-3.

Exergy research has been carried out by several groups using the Cerci ideal mixture model, introduced earlier in this section. Essentially, this model, developed by Cerci [134, 136], considers brackish water [136, 137, 141] or seawater [138] as an ideal mixture of pure water and solid NaCl(cr). The total enthalpy and entropy of the ideal mixture are calculated using the mass fractions of the ideal mixture constituents. The incoming water concentration in this ideal mixture model is treated as the dead state concentration. The choice of dead state definition in the Cerci ideal mixture model is contrary to the Drioli aqueous solution model which treats pure water as the dead state.

Cerci [136] calculated the exergetic efficiency of a brackish water reverse osmosis plant in California to be 4.3%. After proposing an alternate plant design (incorporating an energy recovery device) the exergetic efficiency increased to 4.9%. As a proportion of the overall system exergy destruction, the maximum component exergy destruction took place in the RO membranes (74.1%). Improvement suggestions for plant efficiency included membrane replacement (which was not considered an economic option by the plant management) and the use of an energy recovery device. One aspect of the exergy analysis that appeared to be lacking in the cited paper [136] was the calculation of pump exergy losses. Excluding pump exergy analysis assumes that the pumps are 100% efficient.

Pump exergy losses were considered in later research by Kahraman et al. [137]. Part of this work again considered the exergy analysis of a brackish water RO plant. However, possibly due to the pump inclusion, the results of this exergy analysis were somewhat different to the results obtained by Cerci [136]. In this case the proportional system exergy destruction

was reported as follows; 39.7% for the pump and motor units and 36.2% for the RO module. The overall system efficiency was reported as 8.4%.

Similar work to [136, 137] was carried out on a brackish water RO plant in Jordan [141]. The findings of this work (including pump exergy analyses) were an overall plant exergetic efficiency of 4.1% and the following proportional exergy destruction; Throttling valve 1, 26.4%, Throttling valve 2, 25.4%; Pumps, 19.6%; RO 1, 9%; RO 2, 12%. Suggested plant improvements included the use of energy recovery devices and the use of VSDs for high efficiency pumps and motors. [141]

Although similar in overall exergetic efficiency to Cerci [136], the distribution of exergy destruction in Aljundi [141] is quite different to the findings of Cerci [136] and Kahraman et al. [137], particularly with regards to the throttling valves. The lower contribution of RO exergy destruction was evident in [137]. One observation is that both analyses [137, 141] involve a two-stage RO module and that this, coupled with the pump exclusion of [136], may have caused some of the differences in exergy destruction distribution results.

Using the model developed by Cerci, Bouyazani et al. [146] studied configurations linking RO to a Rankine cycle, this thermal coupling was found to increase the permeate flux but to the detriment of permeate quality, the temperature-flux-salt rejection relationship was previously discussed and is shown in Figure 2-9. The cited authors found that there was an optimum temperature which resulted in the permeate salinity not exceeding 1000 ppm. This optimum operating temperature resulted in the maximum energetic and exergetic

performance. It should be stated that 1000 ppm salinity is high for potable water, let alone UPW applications. However, the analysis showed the trade-off between higher feed water temperatures, which results in greater permeate flux but also poses a risk to permeate quality. Following an extensive literature review, it appears that the reporting of these parametric optimisations or inclusion of exergy destruction or exergetic efficiency in the analysis has not been published for semiconductor UPW plants.

Work carried out by researchers using the Drioli aqueous solution model approach includes the analysis of various integrated membrane systems. Exergy analyses were used as a means to assess the energy impact of various process flows and how these flow configurations affect permeate quantity and quality, and brine concentration. Flow configurations involving RO pre-treatment and post-treatment were assessed, including the use of NF as an RO pre-treatment step and the use of MD, a thermal membrane distillation process, as a post-treatment step. NF improves the feed water to the RO module by reducing the osmotic pressure and thereby enabling operation at higher recovery factors, which consequently results in increased RO permeate [77]. The use of MD ensures a higher permeate recovery and a lower flow rate of more concentrated retentate. However, these integrated system benefits require a higher energy input. [58]

The preceding research approach was further developed to include microfiltration as a secondary pre-treatment process and membrane crystallisation (MCr) as a post-treatment step. MCr is a very interesting technology which operates on RO retentate, "*this innovative technology uses evaporative mass transfer of volatile solvents through microporous*

hydrophobic membranes in order to concentrate feed solutions above their saturation limit, thus attaining a superheated environment where crystals may nucleate and grow [77]*"*. Thus, rather than solely viewing the retentate as a waste stream requiring disposal, MCr facilitates the recovery of salts present in seawater, e.g. calcium sulphate, sodium chloride and magnesium sulphate. This is an important consideration as the disposal of retentate brine in seawater desalination may become an important issue, bearing in mind that not long ago the atmosphere was viewed as an interminable sink for production wastes such as carbon dioxide.

In the cited research [77], exergy analysis was used to assess the energy impact of the various process flows, and the introduction of energy recovery devices. The authors stress that energy, although important, is not the only determining factor for process flow selection, and factors such as increased permeate flows (increased universal recovery), permeate quality, salt recovery, or in essence, overall cost, must be considered [5, 77]. So, in other words, the specific exergy destruction is the important factor. Hence, the energy impact can be reduced in several ways, (1) increasing the amount of product for the same energy input, (2) obtaining the energy from a 'greener' source, (3) improving the energy efficiency of the process, and (4) different combinations of all three.

Other research, running in parallel with the integrated membrane technology research, centres on the development and optimisation of MD. According to one study, the cost of desalination using Memstill® will be reduced to \$0.26/m^3. This research is still at a relatively early stage and optimisation is ongoing into morphological parameters such as

porosity, tortuosity and thickness; physical properties such as thermal conductivity; and operating conditions such as temperatures and flow rates. From an energy perspective, MD is a thermal process and thus has a higher energy impact than RO. However, it is not limited by issues concerning RO, for example, concentration polarisation. [78]

The use of exergy analysis in the integrated membrane approach facilitated comparison between different integrated membrane plant configurations (leading to different exergy destruction distributions). However, it is not clear whether the use of NF as a pre-treatment for RO is viable in UPW applications. If the function of the NF modules is to reduce the osmotic pressure of the feed water to the RO modules, then it is uncertain whether NF pre-treatment will be of benefit to the already low osmotic pressures seen by UPW RO modules. The same applies to the post-treatment of RO where the suitability of the retentate concentration for either MD or MCr is again questionable. Both issues may warrant further investigation.

Romero-Ternero [111, 140] used specific seawater thermodynamics based on *Thermodynamics of Seawater* by Leyendekkers and the methodology of Valero and Lozano in their *Curso de termoeconomia* at the University of Zaragoza, as the basis for exergy calculations used in his research. An exergy analysis of a seawater RO plant (with energy recovery) in Tenerife was undertaken. Although this specific exergy calculation method, based on specific seawater characteristics cannot be applied directly to UPW, other elements of the exergy analysis can be used, notably the definition of system exergy losses, and the inclusion of these losses in exergy efficiency calculations.

One element of Romero-Ternero's work that is similar to the Cerci ideal mixture model approach is the dead state exergy concentration definition - given as incoming water salinity, as opposed to pure water in Drioli aqueous solution model. However, it differs from the preceding exergy analysis work reviewed to date, because each exergy stream in the analysis is defined as either a fuel (F), a product (P) or a loss (L) (see (2.13) and (2.14)).

Romero-Ternero also ascribes exergy costs to flows, where the exergy cost of any flow is the exergy cost to produce it, essentially a cumulative exergy calculation, an interesting approach which considers the exergy value added at each previous process stage. This would imply that the exergy further upstream in sequential processes is more valuable than the exergy of early process stages and that these exergy losses or exergy destruction should be minimised where possible. However, the inclusion of the exergy losses, leads to some anomalies in the author's opinion, which are now discussed. The plant analysis was broken down into a pre-treatment section, a core-process section and a distribution section. The results obtained included an exergy destruction breakdown as follows; 80% of the exergy destruction occurred in the core processes (RO, pump, valve, and turbine);

- RO module, 34.5%
- Pelton turbine, 23.7%
- High pressure pump and regulation valve, 21.5%.

However, the most interesting result is the overall exergetic efficiency of the plant 48.5%. This reported efficiency value is very high in comparison to the previously discussed results of Cerci and Kahraman et al. [136, 137]. What is particularly interesting is that the equation used by Romero-Ternero to calculate the exergetic efficiency should result in

lower exergetic efficiency due to the inclusion of exergy losses, see (2.14). The reason for this unusual result in the author's opinion, can in part, be ascribed to Romero-Ternero's treatment of the exergy losses in the RO module, i.e. the retentate has a negative exergy flow rate. According to Romero-Ternero, the negative quantity, obtained for the exergy losses in the RO retentate stream, relates to the "*potential use of rejected chemical exergy with respect to seawater. Commonly, this potential use is wasted in desalination facilities where rejected brine is merely returned to the sea. Then this loss of exergy represents the impact of waste on the surroundings* [111]." This negative value for RO retentate was explained in a different manner by Cerci [136], who explained the negative quantity of the retentate as the work input required to bring the retentate to the dead state (the dead state being at a lower salinity than the retentate). However, what is important is that when this negative quantity is used in the exergetic efficiency equation, it has the effect of increasing the overall plant exergetic efficiency, which is counter-intuitive. For example, the use of (2.14) to calculate the exergetic efficiency for the negative exergy losses reported in the cited paper (-436 kW) results in the aforementioned high exergetic efficiency of 48.5%. However, when the absolute value or the magnitude of the exergy losses rather than the negative value is used, which is more intuitive, an exergetic efficiency of 21.2% is obtained. The approach taken by Cerci to calculate the exergetic efficiency involved, what he termed, taking the *difference* between the exergy rate of the retentate stream and the exergy rate of the permeate stream – this *difference* was termed "*net salinity discharge*". This value was then divided by the total exergy into the plant. However, the exergy of the retentate is a negative quantity, so in reality Cerci summed the two (although he describes it as a *difference*); as in the case of Romero-Ternero, this negative value of exergy for the

retentate should be classified as a magnitude. According to Van Gool [103], in order to calculate the exergetic efficiency, both the exergy inputs and outputs should be positive. However, despite the author's reservations about the exergetic efficiency results, the method of breaking down the exergy streams into product, fuel and losses offers valuable insight into process analysis. So too does the consideration of cumulative exergy as a means to focus attention on upstream exergy destruction and losses.

Recently, Abdulrahim and Alasfour [158] performed a multi-objective optimisation of a hybrid MSF-RO plant, unfortunately for this RO exergy model review, the paper focused on the optimisation procedure, and as a result, the exergy model used to calculate the exergy destruction in the RO membranes was not described. Tchanche et al. [159] undertook an exergy analysis of micro-organic Rankine power cycles for a small scale solar driven RO desalination system. The exergy analysis focused on the Rankine cycle and did not include the RO process. A similar analysis, but this time for a combined solar organic Rankine cycle with RO desalination process, was carried out by Nafey and Sharaf [160], again the chemical exergy term of the desalination process was not discussed. However, in other desalination research work, Nafey has adopted variations of the Cerci model, see references in Table 2-4. Gasmi et al. [161] performed a study of an industrial RO desalination unit and although the feedwater salinity is characterised in the cited reference, the chemical exergy model is not explicitly stated.

The previous section has attempted to outline some of the differences in the approach to exergy analyses used in RO applications. It is evident that there are a number of methods

and models. However, following an extensive review of the literature, there appears to be no research comparing these different desalination exergy models. Therefore, it is unclear whether the choice of model is important, whether these exergy models give similar results when applied to water purification, or indeed, whether these models are all valid.

The extension of exergy analysis, referred to as thermoeconomics, exergoeconomics or entropy generation minimisation has also been used to optimise desalination system performance, the thermoeconomics approach combines thermodynamics and economics and aims to optimise overall system cost. Capital and exergy costs are allocated to system processes and the objective is to optimise overall system cost. Thermoeconomic analyses have been performed by several researchers for desalination systems [61, 62, 80, 130-132, 139, 140, 142, 145, 148, 162].

2.6.1 RO exergy simulation models

A significant challenge in RO exergy analysis is the simulation and modelling of proposed improvements to mitigate exergy destruction and increase system efficiency. The reason for this complexity is that the factors which influence the plant energy consumption also have a large bearing on water quality performance. This pertains to UPW where purity specifications are critical. The relationship between temperature, pressure, recovery and TDS/feed concentration on RO performance metrics was illustrated previously in Figure 2-9, and thus, in order to simulate suggested process improvements, a model that combines exergy calculations and the transport equations for RO is desirable.

The transport equations for the calculation of permeate flux and percentage salt rejection (for specified water quality and permeate flux rates) can be modelled using membrane manufacturer's software like Filmtec membranes ROSA software from Dow [163], or IMSDesign® from Hydranautics [164]. ROSA software, shown in Figure 2-12, facilitates the calculation of a specific energy value for various membrane choices. For example, low pressure membranes require less feed pressure and thus have a lower specific energy. This is a direct result of their higher permeability factors. However, there is a caveat, i.e. the lower pressure membranes may not have the same salt rejection capabilities as their higher pressure counterparts for various feed water characteristics. For UPW, this is critical and requires careful evaluation. The ROSA software calculates the specific energy for different membrane types, but importantly, it also calculates the relevant ionic salt rejection for that membrane. However, it does not directly link the exergy calculations to the transport equations. One possible way to overcome this limitation would be to assess the low pressure membranes with respect to the permeate quality, and then use the relevant temperatures, pressures, and concentrations in a different exergy calculation program.

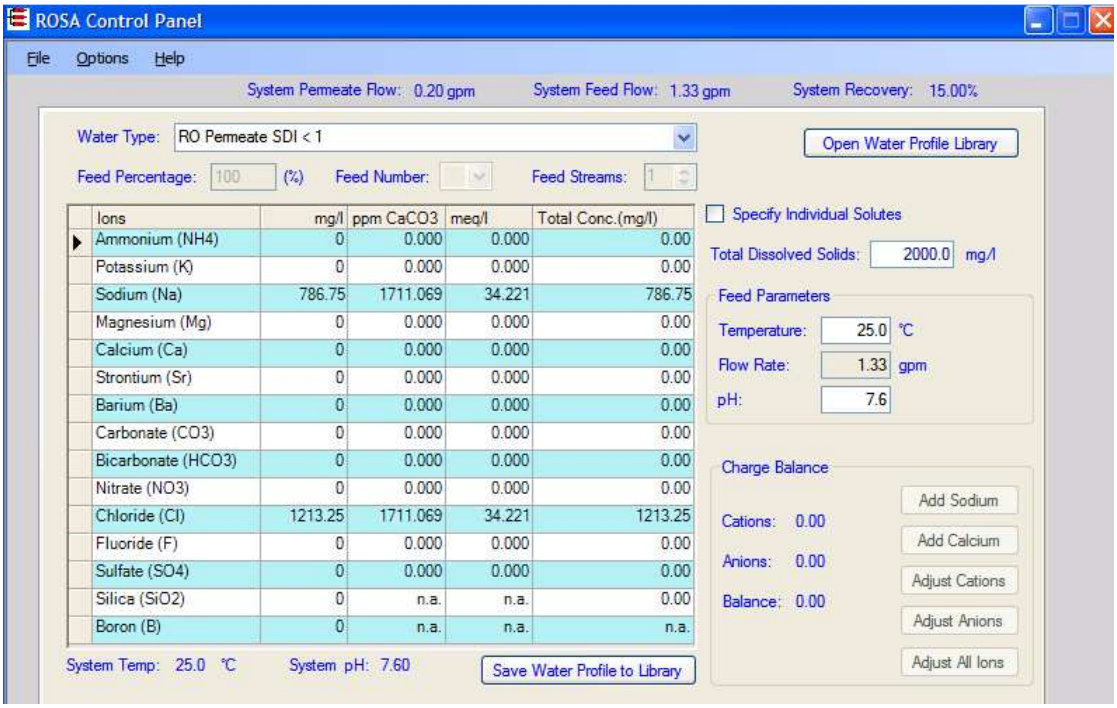

Ions	mg/l	ppm CaCO3	meq/l	Total Conc.(mg/l)
Ammonium (NH4)	0	0.000	0.000	0.00
Potassium (K)	0	0.000	0.000	0.00
Sodium (Na)	786.75	1711.069	34.221	786.75
Magnesium (Mg)	0	0.000	0.000	0.00
Calcium (Ca)	0	0.000	0.000	0.00
Strontium (Sr)	0	0.000	0.000	0.00
Barium (Ba)	0	0.000	0.000	0.00
Carbonate (CO3)	0	0.000	0.000	0.00
Bicarbonate (HCO3)	0	0.000	0.000	0.00
Nitrate (NO3)	0	0.000	0.000	0.00
Chloride (Cl)	1213.25	1711.069	34.221	1213.25
Fluoride (F)	0	0.000	0.000	0.00
Sulfate (SO4)	0	0.000	0.000	0.00
Silica (SiO2)	0	n.a.	n.a.	0.00
Boron (B)	0	n.a.	n.a.	n.a.

Figure 2-12: ROSA water specifications excerpt [163]

There are several publications relating to simulation/modelling programs, which aim to combine RO and exergy simulation. One program uses building blocks for simulation in an object oriented approach [152], and another develops process flow sheets from an icon library using Visual Basic language [153, 154]. Uche et al. [152] reported the development of a software program for the thermodynamic and thermoeconomic analysis of integrated power and desalination plants. The program enables the creation of flow sheets made up of process blocks that can be "*parametrically described by means of some properties* [152]". Description parameters include isentropic efficiency and specific energy. The software consists of process building blocks including RO, heat exchangers, valves, and pumps among others, and calculates heat and mass balances, including exergy balances. Capabilities extend to a comprehensive thermoeconomic analysis. Unfortunately, the case

study presented in the cited publication, considers a coupled power and MSF plant, and not RO. On this basis, it is difficult to assess the possible application of the *Building Blocks Software for Water and Energy Systems (BBWES)* to the high purity requirements of UPW RO systems.

A design and simulation package was developed by Nafey et al. [153, 154]. Figure 2-13 illustrates some of this tool's calculation capabilities. One of the cited publications does contain a case study for seawater RO [153]. Reported results were compared with ROSA and show good correlation: a 2% (>ROSA) difference was reported in the permeate salinity calculations and a 7% (<ROSA) was found in the feed pressure calculations. The main benefit of the package over ROSA is that it does contain exergy calculation capabilities (including recovery pressure energy). Also, importantly, the exergy calculations used in the package take account of exergy losses in efficiency calculations. The exergy calculation model for the simulation package [154] is based on the ideal mixture model by Cerci [134, 136]. There are two concerns, (1) whether the package is accurate for high purity applications (seawater feed salinity used in the analysis was 45,000 ppm with a 30% recovery), and (2) whether membrane substitution is straightforward, i.e. for the energy and exergy comparison of low pressure membranes.

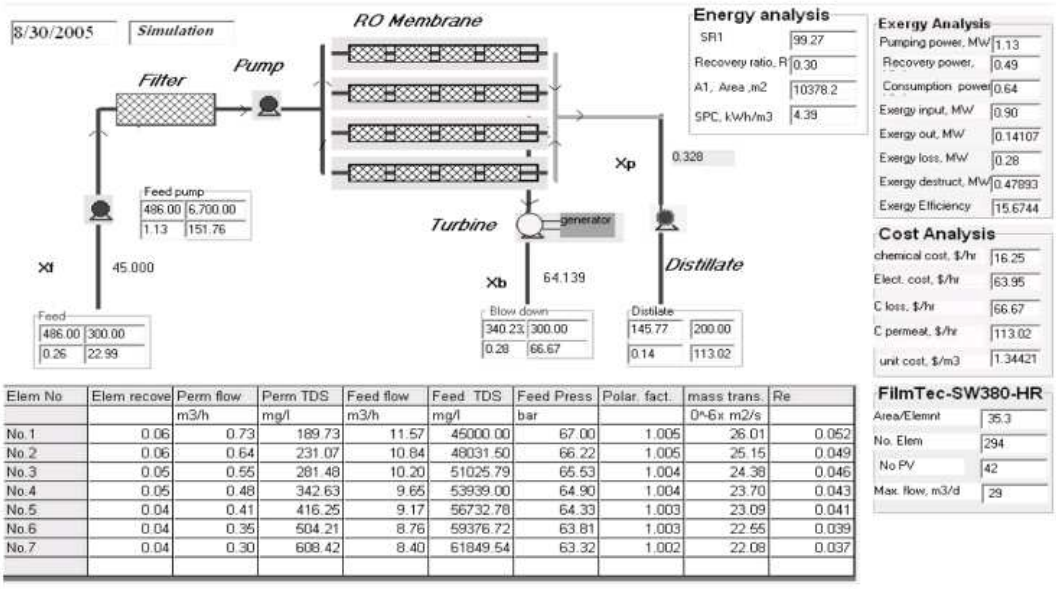

Elem No	Elem recove	Perm flow	Perm TDS	Feed flow	Feed TDS	Feed Press	Polar. fact.	mass trans.	Re
		m3/h	mg/l	m3/h	mg/l	bar		0^-6x m2/s	
No.1	0.06	0.73	189.73	11.57	45000.00	67.00	1.005	26.01	0.052
No.2	0.06	0.64	231.07	10.84	48031.50	66.22	1.005	25.15	0.049
No.3	0.05	0.55	281.48	10.20	51025.79	65.53	1.004	24.38	0.046
No.4	0.05	0.48	342.63	9.65	53939.00	64.90	1.004	23.70	0.043
No.5	0.04	0.41	416.25	9.17	56732.78	64.33	1.003	23.09	0.041
No.6	0.04	0.35	504.21	8.76	59376.72	63.81	1.003	22.55	0.039
No.7	0.04	0.30	608.42	8.40	61849.54	63.32	1.002	22.08	0.037

Fig. 11. Panel of the RO system flow sheet (VDS package).

Figure 2-13: RO simulation package excerpt [153]

Mehdizadeh [7] developed a mathematical model combining the Drioli aqueous solution model equations with a multi-solute RO analytical model in an effort to model the changes in exergy with respect to different plant operating conditions for both and RO and an integrated NF and RO plant. The reported method divides the membrane module into a number of completely mixed cells; it is an iterative approach similar to a finite element type analysis. The concentration of the first cell retentate and permeate is calculated, the first cell retentate acts as the feed to the second cell and so on. The advantage of this model is that the rejection rate for each solute is calculated, similar to ROSA, and it is combined with exergy calculations. The disadvantage is that the RO transport equations, described in the work, are difficult to follow and assess because, (1) the nomenclature is incomplete, and (2) the concentration equations are not clearly explained. According to the reported results,

the integrated NF/RO plant performed better than the RO plant, with higher permeate flux and lower exergy destruction. However, it should be noted that the plant feed water had high salinity (45,000 ppm). Considering just the RO process, it was found that the specific exergy destruction rate decreased, the recovery increased and the percentage salt rejection rate increased with increased operating pressures, all favourable outcomes due to higher operating pressures. It should also be noted, however, that the favourable outcomes resulted in an operating recovery of only 9%, low even by seawater standards. The model is interesting, if the equations can be assessed, and compared to ROSA, the exergy calculation capability makes the program an interesting alternative to the two previous simulation packages.

2.7 Discussion

This chapter has reviewed the literature on UPW production energy mitigation, which is rare. Questions have been posed regarding the necessity of such stringent UPW quality specifications and the suitability of energy recovery devices for UPW applications. These important questions merit further investigation. However, following an in-depth review of energy reduction in the desalination literature, exergy analysis has been chosen as the analytical tool to model and characterise UPW production processes.

To date, the application of exergy analysis to characterise a UPW production plant has not been reported in the literature. Before undertaking such an exergy analysis, the correct choice of exergy calculation model must be carefully considered. Based on the literature reviewed, it is evident that there is a variety of exergy models used in desalination exergy

applications. Due to the fact that the merits and limitations of these models have not been previously assessed in the literature, it is unclear whether any, or all, of these models are suitable for the exergy analysis of a semiconductor UPW plant. It is also interesting that the reference environment models for calculating intrinsic chemical exergy, proposed by several key exergy researchers, have not been considered in specific desalination exergy analyses.

A methodology for the characterisation of UPW plants using exergy analysis is proposed. The basis of this methodology is exergy analysis because, (1) it offers keen insight into the system exergy and energy flows, and (2) it provides a very suitable platform for process system benchmarking. The proposed methodology can be summarised as follows;

1. Choose analytical model – exergy analysis;
2. Measure the plant operating parameters of interest;
3. Apply exergy model;
4. Analyse results;
5. Assess potential improvement;
6. Model improvement opportunities/make recommendations to the system owner.

There is at least one major obstacle to the proposed methodology, i.e. which is the most appropriate model for the exergy analysis of a UPW plant? An initial investigation is outlined in the next chapter. Another important consideration is the choice of exergetic efficiency definition. Ideally, the exergetic efficiency should take account of the system

function. The selection of the most suitable exergy model will most likely involve the synthesis of other models and approaches, or possibly, the development of a new model.

3 Preliminary model comparison

This chapter outlines the comparison of two prevalent desalination exergy models using a dataset from the literature in an effort to determine the most appropriate model for UPW exergy analyses. The preliminary model comparison was presented at the HEFAT conference 2010 [165].

3.1 Exergy model comparison

According to the literature review, the recent exergy analyses of desalination plants are predominantly carried out using two key models. There are other models, which have been tabulated in Table 2-4. However, the model comparison in this chapter consists of the two current and predominant desalination exergy models. In order to differentiate them and to avoid the use of long-winded terms, the two models from now on are termed Model A, which refers to the Drioli aqueous solution model, and Model B, which refers to the Cerci ideal mixture model.

Other models in Table 2-4 have also been considered but have been disregarded for several reasons. Spiegler and El-Sayed [131, 166] proposed a model based on simplifications applicable to distillation processes such as recovery ratios approaching zero and salt free product water; this model has been used to carry out an MED exergy analysis [129]. These specific assumptions do not relate to reverse osmosis desalination, and thus, this model is not considered further. For the more general case Spiegler and El-Sayed [131] derived the same model as that used by Uche [157], an approach which uses the ratio of the activity of

various species to calculate the chemical exergy. However, Spiegler and El-Sayed deem this model unsuitable for seawater desalination on the grounds that "*most of the activities of salt species are either unknown, uncertain or difficult to evaluate…* [131]". This particular approach is readdressed later in this thesis but for the present, only Model A and Model B are considered.

3.2 Model A and Model B

There are some key differences between Model A and Model B, (1) the choice of the dead state definition, (2) the modelling of the aqueous solution, and (3) the equations used to calculate the specific exergy at the relevant process stages. Model A treats water as an ideal aqueous solution of ions (including chloride, sodium, sulphate, calcium and magnesium). For Model A, the dead state is defined as pure water at ambient temperature and atmospheric pressure. As a consequence of this dead state definition, the chemical exergy is at a minimum in the purest water state.

Model B treats water as an ideal mixture of sodium chloride(cr) and water; the dead state is defined as the salinity of the incoming water at ambient temperature and atmospheric pressure. Therefore, the chemical exergy calculated using this model is at a minimum at incoming water salinity before purification.

How does one select the most appropriate model and do these two models give different exergy analysis results? To investigate these questions, an initial model comparison was undertaken using a dataset from the literature [5]. Initial findings showed some interesting

differences between the models, which in this chapter, have been assessed at the basic level. A more detailed investigation is reported in Chapter 5. The model equations are now introduced.

3.2.1 Model A – the Drioli aqueous solution model

Model A, which has been applied by several researchers, treats the system under consideration as an ideal aqueous solution. In this particular model, the general exergy equation (2.7) is calculated using (3.1) when the intensive system measurements consist of temperature, pressure and concentration, and the incompressible fluid model is assumed. Equation (3.1) can be broken down into the sum of three terms, (1) a thermal exergy term, (2) a pressure exergy term, and (3) a chemical exergy term, see (3.3) to (3.5). The researchers using Model A refer to chemical exergy as concentration exergy. However, as discussed in the literature review, in this thesis non-physical exergy is referred to as chemical exergy. Importantly, the dead state is defined as pure water at ambient absolute temperature T_0, and atmospheric pressure P_0.

$$\dot{E} = \dot{m}\left[c(T - T_0) - cT_0 \ln\left(\frac{T}{T_0}\right) + \frac{P - P_0}{\rho} - N_{sol} R T_0 \ln x_{sol} \right] \tag{3.1}$$

The total exergy is the sum of thermal, pressure and chemical exergy, see (3.2).

$$\dot{E} = \dot{E}^T + \dot{E}^P + \dot{E}^{Ch} \tag{3.2}$$

The thermal exergy term $\dot{E}^T$ is calculated using (3.3) where $\dot{m}$ is the mass flow rate, c is the specific heat capacity, T is the temperature at the process stage under consideration and T_0 is the temperature at the dead state.

$$\dot{E}^T = \dot{m}\left[c(T - T_0) - cT_0 \ln\left(\frac{T}{T_0}\right)\right] \tag{3.3}$$

The pressure exergy term $\dot{E}^P$ is calculated according to (3.4) where P is the pressure at the process stage under consideration, P_0 is the pressure at the dead state and ρ is the density of the solution.

$$\dot{E}^P = \dot{m}\left(\frac{P - P_0}{\rho}\right) \tag{3.4}$$

And the chemical exergy term $\dot{E}^{Ch}$ is calculated using (3.5).

$$\dot{E}^{Ch} = -\dot{m}(N_{sol} R T_0 \ln x_{sol}) \tag{3.5}$$

N_{sol} is calculated using (3.6).

$$N_{sol} = \frac{\left(1000 - \sum \frac{C_i}{\rho}\right)}{MW_{sol}} \tag{3.6}$$

According to the authors [5], the units of N_{sol} are defined as the number of moles of the solvent per unit weight of the solution, C_i is the concentration of species i (defined by the authors as the weight concentration of the relevant species *i* per litre of solution) and MW_{sol} is the molar mass of the solvent (pure water in this case). The mole fraction of the solvent x_{sol} (number of moles of the solvent divided by the number of moles of the solution) is then calculated according to (3.7).

$$x_{sol} = \frac{N_{sol}}{\left[N_{sol} + \sum\left(\frac{\beta_i C_i}{\rho MW_i}\right)\right]} \tag{3.7}$$

In (3.7) β_i is the number of particles generated on dissociation and MW_i is the molar mass of species i.

The derivation of the Model A chemical exergy term by the relevant authors is not detailed in the published literature. Consequently, for the initial model comparison in this chapter, the results obtained by the authors in the cited reference [5] are used as the basis for the model comparison. A detailed assessment of the chemical exergy term by the author is undertaken in Chapter 5.

This aqueous solution model approach has been used by various research groups; however, there is a slight discrepancy in the literature between the terminologies used to describe the thermal and pressure exergy equations. Criscuoli and Drioli [58] and Mehdizadeh [7] define the thermal exergy term $\dot{E}^T$ as (3.8), which in this work and the majority of other publications is considered the general exergy equation.

$$\dot{E} = \dot{m}\left[(h - h_0) - T_0(s - s_0)\right] \tag{3.8}$$

In other work, including work carried out by the same research group, the thermal exergy term is defined as (3.3), for example, Molinari et al. [167], Drioli et al. [5], Macedonio et al. [77], Al-Obaidani et al. [78] and Macedonio and Drioli [168]. When considering Model A in this thesis the latter definition is used. The source of this discrepancy may arise from changing definitions in the literature, for example, thermal exergy is defined as the sum of physical and chemical exergy by Szargut et al. in [116]. However, in later work by Szargut [93], physical exergy is divided into two parts, (1) a temperature dependent part, and (2) a part that depends on pressure.

3.2.2 Model B – the Cerci ideal solution model

Model B, developed by Cerci for his PhD dissertation [134, 136] forms the basis of the exergy research carried out by several authors (Kahraman et al. [137, 138], Aljundi [141], Nafey et al. [154] and Bouzayani et al. [146, 147]).

In Model B the saline solution is treated as an ideal mixture of NaCl and pure water, seawater is dilute, a typical seawater salinity of 35,000 ppm equates to a mass fraction of 3.5%. According to Cerci, a dilute solution has a mass fraction of 5% or less: on this basis, he defines seawater as an ideal solution [136]. The total exergy of an ideal mixture can be found by calculating the enthalpy and entropy of the ideal mixture constituents and multiplying them by their respective mass fractions. One key assumption of the ideal mixture model is that the different mixture constituents do not interact at the molecular level, and therefore, the enthalpy of mixing is zero. As a result, the specific enthalpy of the mixture at a certain temperature and pressure is equal to the sum of the specific enthalpies of the mixture constituents multiplied by the mass fractions of the mixture constituents at the same temperature and pressure, see (3.9).

$$h_{im} = \sum mf_i h_i = (mf_s h_s) + (mf_w h_w) \tag{3.9}$$

In (3.9) mf denotes the mass fraction and the subscripts im, i, s and w denote ideal mixture, the species i under consideration, salt and water respectively.

Salt is treated as an incompressible solid (crystalline). Thus, the specific enthalpy of salt at a certain temperature is calculated by first assigning salt a reference enthalpy value at a reference temperature, for example, the enthalpy of salt is equal to zero at 0˚C. Then the

enthalpy of salt at the required temperature is calculated by adding the enthalpy of salt at the reference temperature and the product of the specific heat capacity of salt by the temperature difference between the temperature of interest and the reference temperature (where the enthalpy of salt is assigned a zero value), see (3.10).

$$h(T) = h(T_{ref}) + c_s \left(T - T_{ref} \right) \tag{3.10}$$

The specific entropy of an ideal mixture s_{im} is calculated in a similar way, see (3.11).

$$s_{im} = \sum mf_i s_i = (mf_s s_s) + (mf_w s_w) \tag{3.11}$$

However, the entropy of mixing of an ideal mixture is not zero due to the fact that mixing is an irreversible process, and therefore, the entropy of the ideal mixture, at a certain temperature and pressure, is greater than the sum of the entropies of the mixture constituents if they existed alone at the same temperature and pressure. The molar entropy of each constituent in an ideal mixture is given by (3.12), where R is the universal gas constant and x_i is the mole fraction of constituent i.

$$\overline{s}_i = \overline{s}_{i\ pure}(T, P) - R \ln x_i \tag{3.12}$$

The final term in (3.12) is always positive because the natural logarithm of the mole fraction of constituent i is always negative (except in the pure state when the mole fraction is equal to unity and the last term is zero). Hence, the molar entropy of the ideal mixture $\overline{s}_{im}$ can be calculated using (3.13).

$$\begin{aligned} \overline{s}_{im} &= (x_s \overline{s}_s) + (x_w \overline{s}_w) \\ &= x_s \left[\overline{s}_{s\ pure}(T, P) - R \ln x_s \right] + x_w \left[\overline{s}_{w\ pure}(T, P) - R \ln x_w \right] \\ &= x_s \overline{s}_{s\ pure}(T, P) + x_w \overline{s}_{w\ pure}(T, P) - R \left(x_s \ln x_s + x_w \ln x_w \right) \end{aligned} \tag{3.13}$$

Equation (3.13) calculates the molar entropy of the ideal mixture at constant temperature and pressure; in order to calculate the specific entropy the last equality term is divided by the molar mass of the ideal mixture. The molar mass of the mixture is the sum of the mole fraction of each constituent multiplied by the molar mass of the respective constituent, i.e. $\sum x_i MW_i$. Dividing the universal gas constant *R* by the molar mass of the mixture, results in the specific gas constant for the ideal mixture R_{im}. The specific entropy can then be calculated using (3.14).

$$s_{im} = mf_s s_{s\ pure}(T,P) + mf_w s_{w\ pure}(T,P) - R_{im}(x_s \ln x_s + x_w \ln x_w) \tag{3.14}$$

The specific entropy of salt, existing in the pure state as an incompressible solid, can be calculated using (3.15), analogous to the specific enthalpy of salt calculated previously.

$$s(T) = s(T_{ref}) + c_s \ln\left(\frac{T}{T_{ref}}\right) \tag{3.15}$$

Using this approach requires the use of both mass and mole fractions, conversion between these quantities can be calculated using (3.16) and (3.17) [128, 136].

$$x_s = \frac{MW_w}{MW_s\left[\frac{1}{mf_s} - 1\right] + MW_w} \tag{3.16}$$

$$x_w = \frac{MW_s}{MW_w\left[\frac{1}{mf_w} - 1\right] + MW_s} \tag{3.17}$$

In the two preceding equations x is the mole fraction, MW is the molar mass, mf is the mass fraction, and the subscripts s and w refer to salt and water respectively. Summing the entropy and enthalpy calculation terms, i.e. (3.9) and (3.14), and considering the enthalpy and the entropy at the dead state (given by the superscript *DS*), the equation to

calculate the total exergy rate (refer to (3.8)) at a specific process stage (superscript *PS*) is given by (3.18). Note that the subscripts *pure* and the references to the entropy being a function of temperature and pressure are dropped for succinctness.

$$\dot{E} = \dot{m}\left[\begin{array}{l}\left[(mf_s h_s)+(mf_w h_w)\right]^{PS} - \left[(mf_s h_s)+(mf_w h_w)\right]^{DS} \\ -T_0\left(\begin{array}{l}\left[mf_s s_s + mf_w s_w - R_{im}(x_s \ln x_s + x_w \ln x_w)\right]^{PS} \\ -\left[mf_s s_s + mf_w s_w - R_{im}(x_s \ln x_s + x_w \ln x_w)\right]^{DS}\end{array}\right)\end{array}\right] \quad (3.18)$$

3.2.3 Application of the two models to a dataset

The models described in the previous sections were compared using measurement data in the literature [5]. The published information included seawater composition, NF and RO rejection rates, temperatures, pressure and concentrations. The main process parameters are shown in Table 3-1.

Table 3-1: Process parameters for the dataset [5]

Process stage	***Mass flow rate (kg/hr)***	***Temperature (K)***	***Pressure (bar)***	***Concentration (mg/l)***
1	1050000	293	1	34654
2	1050000	293	2	34654
3	55000	293	1	34654
4	995000	293	1	34654
5	995000	293	11	34654
6	245000	293	10	61852
7	245000	293	1	61852
8	750000	293	1	25733
9	750000	293	69	25733
10	231000	293	68	82567
11	231000	293	1	82567
12	516000	293	1	270

The process stages included various pumps, microfiltration (MF), NF, throttling valves (TV) and RO; a process schematic is shown in Figure 3-1.

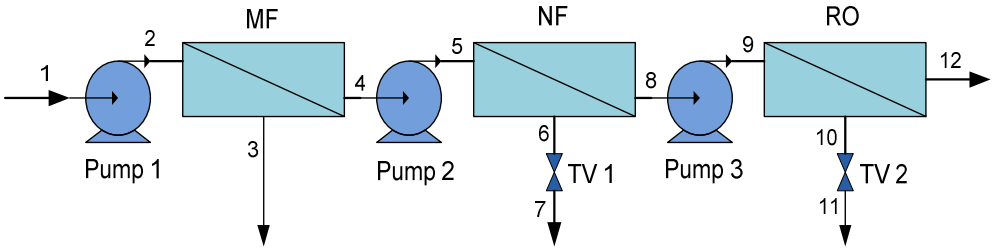

Figure 3-1: Desalination process stages from dataset, adapted from [5]

To facilitate this comparison, results and information from [5] were used to develop a series of MATLAB programmes to calculate the exergy rates according to the Model B approach. The X-Steam function, which is essentially a set of electronic steam tables available for download at the MATLAB central website [169], was used to calculate the water properties. The calculation sequence is shown in Figure 3-2.

To validate the author's use of the X-Steam function and the MATLAB calculation programmes, exergy rate values were calculated for an alternate dataset in the literature and were subsequently compared with exergy rate values obtained by Cerci for the same dataset [136]. Rather than the X-Steam function, Cerci used Engineering Equation Solver (EES) software [136], the results of the comparison are shown in Table 3-2, which shows negligible difference between the two approaches.

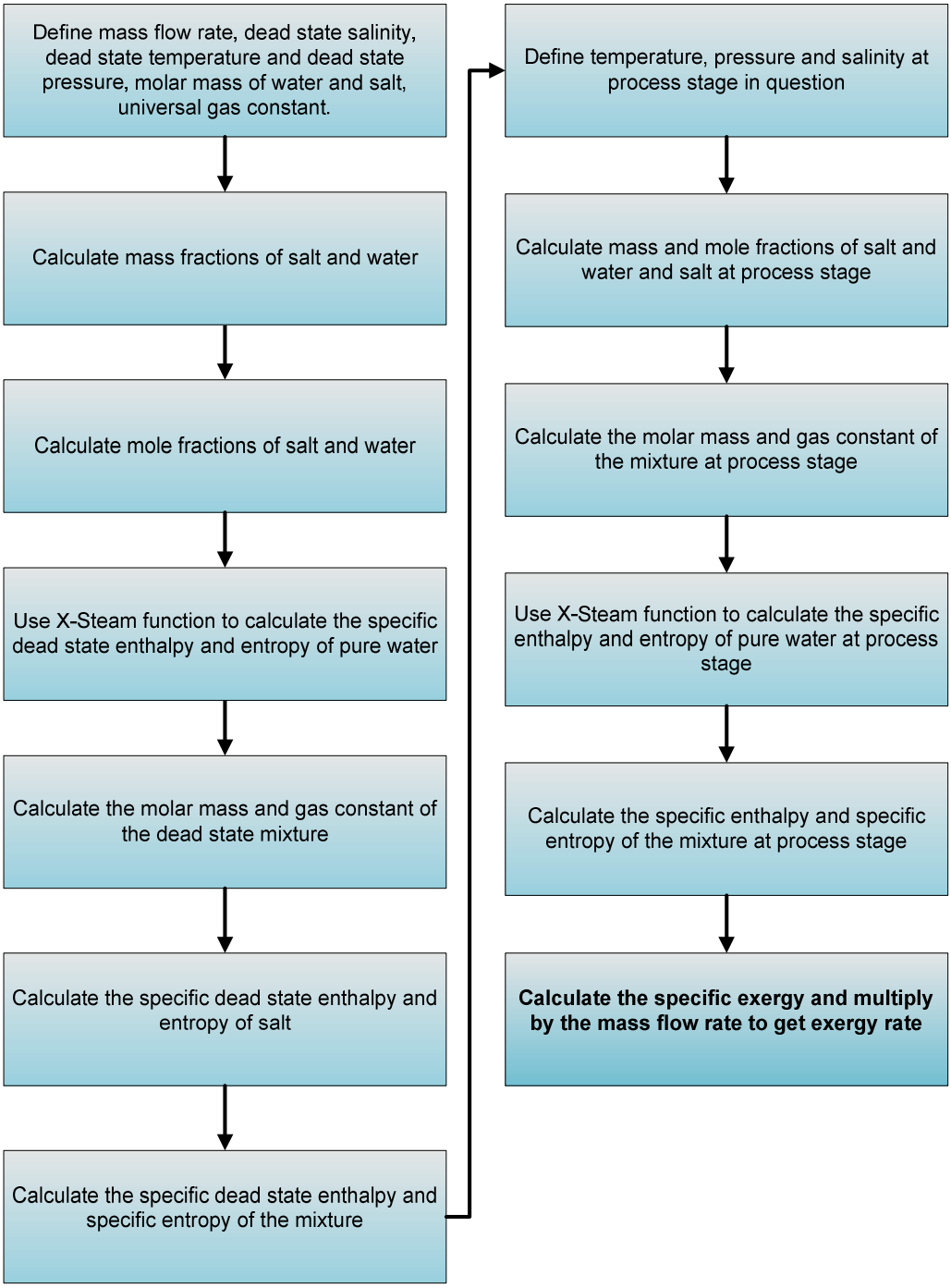

Figure 3-2: Model B exergy calculation sequence using X-Steam [169]

Table 3-2: MATLAB program comparison for original program validation

Stage	*MATLAB model exergy rates (kW)*	*Exergy rates from the literature (kW)* [136]
1	0	0
2	31.81	31.82
3	28.42	28.43
4	3.39	3.38
5	0	0
6	27.04	27.05
7	25.65	25.66
8	159.46	159.46
9	40.52	40.44
10	-3.73	-3.74
11	-18.17	-18.13
12	-24.79	-24.73
13	-32.09	-32
14	39.22	39.14
15	39.22	39.14

The concentration values of Model A (cited in Table 6 of reference [5]) were used as the basis for the salinity values for Model B. Salinity is defined differently to concentration, the concept of salinity was originally devised "*as a measure of the mass of dissolved salts in a given mass of seawater* [170]", or the mass fraction of sea salts. Generally in the literature, regarding Model B, salinity is equated to a mass fraction of NaCl; this was corroborated via email [171]. However, in order to use the concentration data in the cited dataset for the Model B analysis, the concentration values (mg/l) must be converted to mass fractions. To convert from mg/l to mass fraction requires the density. Equating the mass fraction (ppm) and concentration (mg/l) is common for dilute aqueous solutions, but doing so assumes that the density of the aqueous solution is equivalent to the density of water at 4°C (1000 kg/m^3). However, seawater at 20°C and a typical salinity mass fraction of 3.5% has a density of approximately 1025 kg/m^3 according to the UNESCO International Equation of

State of Seawater [172], which is a function of salinity, temperature and depth (or equivalent pressure). As the process water gets more concentrated, for example, the retentate streams of the NF and RO processes, the density increases. Consequently, due to increasing density, the direct conversion between mg/l and ppm becomes increasingly less accurate. Calculating an accurate density value for each stream is cumbersome. As an approximation, the International Equation of State of Seawater can be used to estimate density based on the dead state temperature and the relevant salinity. Salinity can be calculated as a function of the amount of chloride in the seawater [170]. However, due to the targeted ionic rejection of the NF and RO processes, the retentate and permeate streams are strictly no longer seawater. Therefore, calculating the salinity based solely on the chloride content is not feasible, one option is to use the total salts concentration rather than the more correct salinity input. This is a reasonable approximation based on the previously cited original purpose of the salinity concept. However, there is another issue which must be considered, i.e. calculating the density using the International Equation of State for Seawater requires an input of total salts (salinity) as a mass fraction not a concentration in mg/l but conversion from mg/l to mass fraction requires the density. To overcome this issue, the density was approximated as follows;

1. Equate concentration (mg/l) and mass fraction, use this value as an input to the International Equation of State for Seawater and calculate density;
2. Use the density value obtained to convert mg/l to mass fraction;
3. Use the mass fraction of the total salts as the salinity value for Model B – this value is then equated to the NaCl mass fraction (as per the literature).

The concentration values obtained from the cited reference [5] were converted from mg/l to a salinity value; the results are shown in Table 3-3. The second column in the table shows the concentration values in mg/l, the third column contains the estimated density values obtained using the International Equation of State of Seawater, and the final column shows the percentage difference in 'effective salinity' as a result of the mg/l to ppm conversion. As expected, the process retentate streams (stages 6 and 10 in Figure 3-1) exhibit the largest percentage differences due to the estimated density increases.

Table 3-3: Conversion from concentration values (mg/l) to salinity (ppm)

Stage	***Concentration (mg/l)***	***Estimated Density (kg/m^3)***	***Salinity (ppm)***	***% Diff. mg/l versus mf***
1	34654	1024.5	33825.3	2.4
6	61852	1045.4	59165.9	4.3
8	25733	1017.7	25285.4	1.7
10	82567	1061.6	77776.0	5.8
12	270	998.4	270.4	-0.2

Using the relevant density value gives a better salinity (ppm) estimate than solely equating mg/l with mass fractions. It is acknowledged that the International Equation of State for Seawater is only strictly valid for salinities between 0 and 42, and therefore, the densities calculated are approximations. To check the general validity of calculations, the density of an aqueous solution (a mixture of NaCl and $MgCl_2$) was estimated by interpolating (and weighting) relevant data on aqueous salt solutions in [173]. The results were compared with the International Equation of State for Seawater and showed very good correlation.

3.2.4 Model comparison Results

The exergy rates calculated at each process stage using Models A and B are shown in Table 3-4. It is evident that the exergy rates calculated by both models are very different; this is expected due to the different salinity dead state definitions and the resulting differences in chemical exergy. The negative exergy rate values in the last column of Table 3-4 have been explained in the literature in different ways, (1) as a measure of the work input required to bring the retentate salinities back to the original dead state salinity [136], and (2) as the "*potential use of rejected chemical exergy with respect to seawater* [111]*.*" However, where the models should not be expected to differ significantly is in the exergy change or exergy destruction in each of the process stages. The change in exergy was calculated for each process stage; the change in exergy (or the exergy destruction) $\Delta\dot{E}$ is defined in (2.6). A negative $\Delta\dot{E}$ value signifies that exergy has been destroyed and a positive value signifies that exergy has been added to the system (for example, via the three pumps). The fact that the pump exergy destruction has not been considered is an oversight and this was commented upon previously in the literature review. If the pump exergy destruction had been considered, the distinction between exergy change and exergy destruction would not exist. The comparison between the 'change in exergy rates' calculated by each of the models is shown in Table 3-5 and Figure 3-3. It is clear that there are some considerable differences between the $\Delta\dot{E}$ values calculated by Model A and Model B. For $\Delta\dot{E}$ due to the three pumps, the percentage difference is not large and varies between 2.5 and 3.2%. However, it is the two important separation processes that yield the significant differences, namely the NF and the RO processes, 23.6% and 29.8% respectively. The percentage difference in $\Delta\dot{E}$ between the models for the throttling valves, 6.1% and 7.7% respectively,

is most likely a direct result of the preceding NF and RO separation processes, although this is not fully discernable due to the integrated modelling approach of Model B.

Table 3-4: Comparison of exergy rates calculated using Model A and Model B

Stage	***Model A*** ***Exergy rate*** ***(kJ/hr)***	***Model B*** ***Exergy rate*** ***(kJ/hr)***
1	2808300	0
2	2913300	101625
3	148800	0
4	2659500	0
5	3654500	962822
6	1334700	-858894
7	1113400	-1066672
8	1541300	1226921
9	6638300	6199037
10	3048909	-238405
11	1502074	-1666071
12	11327	3926046

Table 3-5: Comparison between the change in exergy rates calculated using each model - Model A and Model B

Grouped Stage	***Processes***	***Model A*** $\Delta\dot{E}$ ***(kJ/hr)***	***Model B*** $\Delta\dot{E}$ **(*kJ/hr*)**	***% Diff.*** $\Delta\dot{E}$
1	*Pump 1*	105000	101625	3.2
	MF	-105000	-101625	3.2
2	*Pump 2*	995000	962822	3.2
	NF	-778500	-594795	23.6
	TV 1	-221300	-207778	6.1
3	*Pump 3*	5097000	4972116	2.5
	RO	-3578064	-2511396	29.8
	TV 2	-1546835	-1427666	7.7

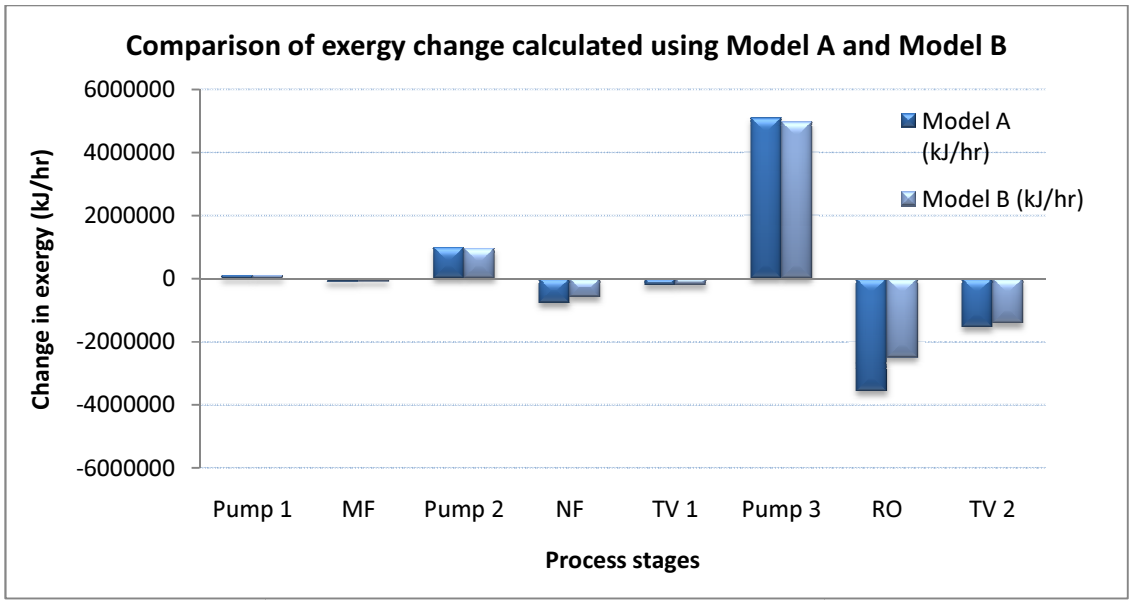

Figure 3-3: Comparison of exergy change calculated using Model A and Model B

Why do these models differ? There are three main possibilities that can be investigated, (1) the dead state definition, (2) the modelling of the aqueous streams and (3) the exergy model calculation equations. First, consider the dead state definition.

The influence of the dead state salinity was tested by amending the dead state definition in the series of MATLAB programs. For Model B the dead state was re-defined as pure water at ambient temperature and pressure (equivalent to Model A), and the MATLAB programs were rewritten accordingly. The results of this investigation are shown in Table 3-6 and Table 3-7.

Table 3-6: Comparison of exergy rates calculated using Model B for both the original dead state and the amended dead state (for comparison purposes Model A is also shown)

Stage	*Original DS Model B (kJ/hr)*	*Amended DS Model B (kJ/hr)*	*Model A (kJ/hr)*
1	0	-8111370	2808300
2	101625	-8009744	2913300
3	0	-424881	148800
4	0	-7686488	2659500
5	962822	-6723666	3654500
6	-858894	-2751547	1334700
7	-1066672	-2959324	1113400
8	1226921	-4566914	1541300
9	6199037	405202	6638300
10	-238405	-2022906	3048909
11	-1666071	-3450572	1502074
12	3926046	-60112	11327

Table 3-7: Comparison of the percentage exergy change calculated by Model A and Model B - the results are shown for both the Model A/Original dead state Model B comparison and the Model A/Amended dead state Model B comparison

Grouped Stage	*Process*	*Original DS %Diff. (kJ/hr)*	*Amended DS %Diff. (kJ/hr)*
1	Pump 1	3.2	3.2
	MF	3.2	3.2
2	Pump 2	3.2	3.2
	NF	23.6	23.6
	TV 1	6.1	6.1
3	Pump 3	2.5	2.5
	RO	29.8	30.5
	TV 2	7.7	7.7

The calculated exergy rates for Model B, using both the original salinity dead state definition (incoming seawater) and the amended salinity dead state definition (pure water),

are shown in Table 3-6, which also shows the exergy rates calculated using Model A. Originally, it was thought that the main reason why the exergy rates calculated using Model A and Model B were significantly different was a result of the different salinity dead states; Table 3-6 shows that this is not the case. When the salinity dead state was amended to pure water, all the previously positive Model B exergy rates (Table 3-4 column 3) changed to negative values, except State 9 which undergoes a large pressure exergy input due to the high pressure pump. Mathematically, due to the amended dead state, (3.18) simplifies to (3.19) shown below.

$$\dot{E} = \dot{m}\begin{bmatrix} \left\{\left[(mf_s h_s) + (mf_w h_w)\right]^{PS} - \left[(h_w)\right]^{DS}\right\} \\ -T_0\left\{\left[mf_s s_s + mf_w s_w - R_{im}(x_s \ln x_s + x_w \ln x_w)\right]^{PS} - \left[s_w\right]^{DS}\right\} \end{bmatrix} \qquad (3.19)$$

There are two causes of the negative exergy rates that come about as a result of the amended salinity dead state, one cause relates to changes in enthalpy and the other to changes in entropy;

1. At the majority of process stages $h - h_0 < 0$, this occurs because the enthalpy of water in the pure state is now greater than the enthalpy of the ideal mixture, see (3.18) and (3.19). The lower enthalpy of the ideal mixture is due to the presence of the salt (i.e. the heat capacity of salt in the ideal mixture lowers the overall enthalpy of the ideal mixture). There are two exceptions, process stages 9 and 10, where the high pumping pressure input counteracts the negative value of enthalpy differences. Process stage 10 is still at relatively high pressure, the pressure drop tangential to the RO membrane is 1 bar (from 69 bar at process stage 9 to 68 bar at process stage 10).

2. At all process stages $s - s_0 > 0$. Therefore, when multiplied by $(-T_0)$, the product is always negative. In the original dead state salinity definition $s - s_0 < 0$ except for cases where the salinity at the relevant process stage was greater than the dead state salinity (NF, RO, and their respective throttling valves), these exceptions contributed to negative exergy rates in the original dead state definition.

Table 3-7 column 3 shows the absolute percentage difference of exergy change calculated by the models (previously shown in the last column of Table 3-5). The last column of Table 3-7 reports the absolute percentage difference of exergy change, but this time using the amended dead state definition. These results indicate that the dead state definition has very little impact on the exergy change calculations with respect to the original model dead state definition. There is a slight change in the RO process, a 0.7% increase. However, this increase is relatively insignificant when compared with the magnitude of the exergy change calculation differences between the two models. Therefore, based on the preceding results, the salinity dead state definition does not have a significant impact on the $\Delta\dot{E}$ values calculated by the two models. However, it does have an impact on the exergy rates calculated using the Model B MATLAB programs.

3.3 Summary

In summary, this initial model comparison, based on process information obtained from a dataset in the literature, presented some interesting results which merit further investigation. The exergy rates calculated using Model A and Model B differed significantly; exergy rates calculated using Model A are positive, exergy rates calculated

using Model B can be positive or negative (depending on the stream concentration with respect to the salinity dead state). Although more aligned than the exergy rates, there are significant differences between the exergy destruction rates calculated for the NF and RO processes using Model A and Model B. The amended dead state did not have a significant effect on the exergy destruction rates calculated with Model B, however, it did have an important influence on the exergy rates calculated at each process stage.

Considering that the principal purpose of an exergy analysis is to identify system irreversibilities and to focus improvement efforts, this 29.8% deviation in RO exergy destruction between the two models is a matter of concern. Based on this preliminary investigation, it would suggest that either, one of the models is reasonably accurate and the other model is significantly over- or under-estimating the exergy destruction in the key separation processes or neither model is sufficiently accurate.

4 Research plan

The objective of this research is to develop an accurate approach to characterise and benchmark UPW production plants. There are two prevalent exergy calculation models used in the desalination literature, Model A and Model B, which differ on the basis of, (1) the specific exergy calculation equations, (2) the models chosen to represent feed water composition, and (3) the dead state definitions. These two models were compared using a dataset in the literature in Chapter 3. It was found that the exergy destruction rates calculated using the two models for the key separation processes differed significantly, a 23.6% difference for the NF process and a 29.8% difference for the RO process.

A preliminary investigation into the dead state definition showed that the choice of dead state salinity does not have an important effect on the exergy destruction rates calculated using the two models. However, the choice of dead state salinity does have a significant impact on the exergy rates calculated at the various process stages and dictates whether the exergy rate of the retentate is a positive or negative value.

Further investigation will be undertaken to establish the cause of these model differences; however, based on early findings, the author hypothesises that;

- A more accurate model exists than either Model A or Model B, and a new best approach is needed to deal with the exergy analysis of UPW systems.

The testing of this hypothesis will be carried out according to Figure 4-1.

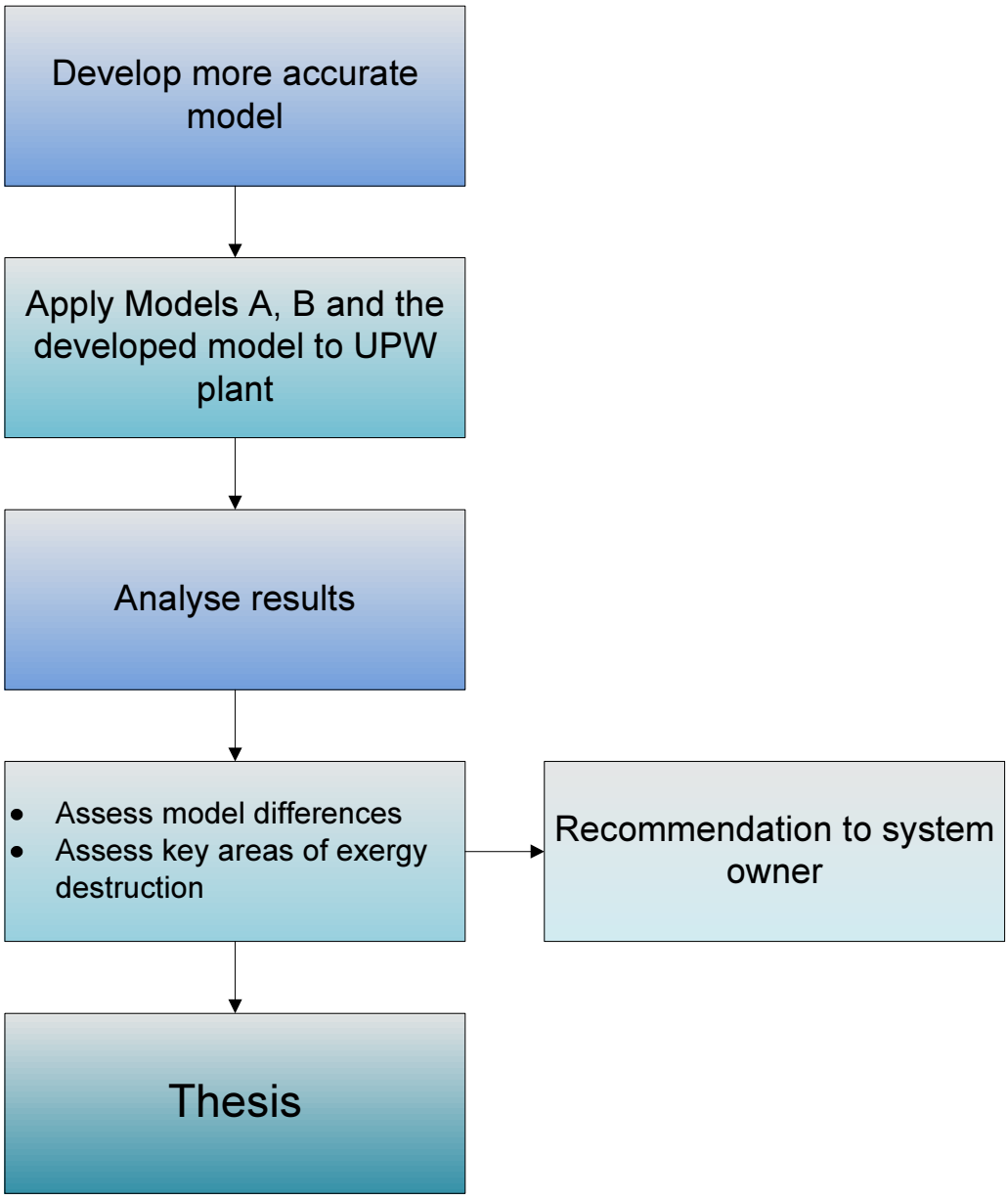

Figure 4-1: Planned work outline

4.1 Develop more accurate model

Table 2-4 collates various exergy models that have been applied to desalination systems. In the author's opinion, however, a more accurate model exists, and this more accurate model takes an intrinsic chemical exergy term into account, which the author believes may have been overlooked in Model A and Model B. This intrinsic chemical exergy term, often based on standard chemical exergy values, is included in the exergy model equations of key exergy authors [92, 93, 95] (although not specifically for desalination exergy calculations). Once the more accurate model has been determined, it will be applied to the UPW plant.

4.2 Apply Models to UPW plant

The models will be applied to a UPW plant; this serves three purposes, (1) it provides a means to compare the models, (2) it provides a means to validate the approach, and (3) it provides a means to characterise and benchmark the UPW plant. The developed model will be used to gauge the accuracy of both Model A and Model B. The factory SCADA system provides most of the flow rate, pressure, and temperature measurements required for this model analysis. Other measurements can be obtained from local instrumentation.

4.3 Analyse results

The results of the model comparison will be analysed. Based on the literature reviewed, it is expected that the main sources of exergy destruction will take place in the RO core processes. Although the developed model should be the most accurate model, it may not

necessarily be the best model for UPW exergy analysis. This will more than likely depend on several factors including;

- The computational complexity of each model and the consideration of possible trade-offs between complexity and accuracy;
- The level of information provided by the measurement instrumentation – for example, how conductivity is measured.

The last point is particularly relevant to UPW plants as conductivity measurement is vital to assure the permeate purity specifications. However, the granularity of the conductivity measurement may not suit the different models. For example, in the literature, the Model A concentrations have been calculated using theoretical rejection rates for NF and RO. One of the reasons for this is probably due to the nature of the multi-solute water model used. These factors should be weighed up when selecting the best exergy model for UPW plants.

Other areas for consideration include the salinity dead state definition and whether it is more appropriate or intuitive to define the dead state salinity as pure water or incoming water salinity. The results will be analysed. Improvement suggestions will be made, likely improvements may come from the use of low pressure membranes and high efficiency pumps. Recommendations, based on the exergy analysis, will be made to the system owner.

4.4 Thesis

The final stage is the thesis write-up.

4.5 Novelty of research

Based on the literature reviewed, no published research has addressed the issue of semiconductor UPW production exergy characterisation/optimisation. In the semiconductor industry the main UPW focus to date has been the Reduce, Reuse, Recycle strategy. The benefits and risks of this strategy have been outlined in the literature review. Although the issues of UPW conservation and energy conservation have been highlighted as important industry objectives, little regard has been given to reducing the energy required to produce UPW to the exacting semiconductor manufacturing industry standards. Energy reduction research in the desalination literature is well established, and having assessed various approaches, exergy analysis shows the most promise as a method to characterise UPW production energy. Thus, there are two novelty factors here, (1) the energy characterisation/optimisation of UPW has not been targeted previously, and (2) exergy analysis has not yet been applied to a UPW plant. Desalination plants, which have previously undergone exergy analyses in the literature, differ from UPW plants with regards to process intensity (i.e. recovery rates, number and various types of sequential processes) and criticality of application.

Another novel element of this research is the evaluation and comparison of desalination exergy models. Various models have been applied in the literature to desalination plants, however, a detailed assessment and comparison of these models has not been undertaken to date. Having reviewed the desalination exergy analyses in the literature, it is evident that several models have been used, and although certain publications (using one specific model) have referenced the work of other researchers (using a different exergy model), the

suitability of exergy model choice has not been questioned and no one model has been advocated in favour of others. In other words, recent desalination exergy analyses appear to have been carried out in isolation with regards to selecting the most appropriate exergy model. The comparison of two predominant exergy desalination models in Chapter 3 identified key model differences in the NF and RO separation processes. These findings would suggest that the model differences are related to the chemical exergy terms.

Munoz and Michaelides [120] did compare various exergy reference environment models for the analysis of several power plants. However, in that analysis, the cited authors were essentially comparing standard chemical exergy reference environments. Munoz and Michaelides commented that the use of different reference environment models cancel out when calculating process exergy destruction resulting in similar exergy destruction rates. The comparison of Model A and Model B undertaken in Chapter 3 found that this expected similarity in exergy destruction values did not occur due to the different model approaches. Hence, this proposed research also shows an element of novelty in the form of comparing, evaluating and synthesising the work of other researchers.

5 Model A and Model B: a detailed comparison

The purpose of this chapter is to further develop the work of Chapter 3, which identified significant differences in exergy rates and exergy destruction rates calculated with two prevalent exergy desalination models. The preliminary analysis in Chapter 3 considered the dead state definition as the possible cause of Model A and Model B differences. Here, following a re-assessment of the key exergy literature rather than just the desalination exergy literature, the two models are broken down and compared and contrasted on the basis of both physical exergy and chemical exergy. Model A does have one important advantage over the Model B approach in this respect, and that is the breakdown of exergy into the thermal, pressure and chemical exergy terms, thus facilitating a clearer understanding of the various system exergy flows.

This comparison is once again based on a dataset from the literature [5], the main process parameters are shown in Table 3-1. Part of this work was presented at the IEESE-05 Conference 2010 [174]. It should be stated that some of the research presented at the IEESE-05 conference was at an early stage, and this chapter presents a more comprehensive analysis.

5.1 Physical exergy comparison

Exergy is the theoretical maximum potential of developing work as a system comes into equilibrium with its environment,

"*When the pressure, temperature, composition, velocity or elevation of a system is different from the environment, there is an opportunity to develop work. As the system changes to that of the environment, the opportunity diminishes, ceasing to exist when the two, at rest relative to one another, are in equilibrium. This state of the system is called the dead state* [95]."

Generally, key exergy authors differentiate system exergy into two parts, the exergy that arises from, (1) a difference in the thermal and mechanical properties between the process stage state and the dead state, and (2) the exergy that arises from a difference in composition between the process stage and the dead state at the dead state temperature and pressure.

Physical exergy is concerned solely with thermo-mechanical equilibrium [92-95] or what has been termed, the restricted dead state [94], i.e. how the states of a system differ in thermal and mechanical equilibrium from the defined dead state "*without any change of the chemical composition of the considered substance*. [93]". Accordingly, in the desalination process under consideration (Figure 3-1), the physical exergy at each process stage can be described as the exergy that arises from the differences in thermo-mechanical properties between the process stage under consideration and the restricted dead state.

First, the physical exergy is calculated using Model A. Conveniently, this is the summation of (3.3) and (3.4) resulting in (5.1).

$$\dot{E}^{Ph} = \dot{m}\left[c(T - T_0) - cT_0 \ln\left(\frac{T}{T_0}\right) + \left(\frac{P - P_0}{\rho}\right)\right] \tag{5.1}$$

Again, this equation is derived under the assumptions of the incompressible fluid model and constant specific heat capacity. The desalination process shown in Figure 3-1 is regarded as isothermal, and as a result, the thermal component of exergy is negligible, leaving only the pressure exergy contribution.

The incompressible fluid model assumes that the density of a fluid is not a function of pressure and is constant. In seawater applications, the density does change at various process stages, not due to increasing pressure but to increasing or decreasing concentration, and this has an influence on the magnitude of physical exergy which decreases as the density increases, see (5.1).

Regarding Model A, and using process information data from the cited reference [5], the specific physical exergy (kJ/kg) can be calculated by dividing the pressure exergy (kJ/hr) by the mass flow rate (kg/hr), see Table 5-1. The density values can be calculated with further analysis of these published results and are shown in Table 5-2. The density is approximated by dividing the differential pressure term (P-P_0) in kilopascals by the specific exergy (kJ/kg), and where possible, the density values have been calculated from the process information given using this calculation. When the density values could not be determined from the differential pressure value, for example, for process stages at dead state pressure, equal density values were attributed to process stages with equal concentration values. To demonstrate; consider process stage 2 in Table 5-2, the density can be calculated from the differential pressure value and the specific exergy at process stage 2, this value is then used to determine the density values at process stages 1 to 5. The

density at process stage 8 (which is at the dead state pressure and thus cannot be determined on the basis of differential pressure) is determined from process stage 9 which is at the same concentration as process stage 8 and so forth.

Table 5-1: Model A physical exergy rates based on results in [5]

Process stage	*Physical exergy rate (kJ/hr)*	*Mass flow rate (kg/hr)*	*Specific physical exergy (kJ/kg)*
1	0	1050000	0
2	105000	1050000	0.100
3	0	55000	0
4	0	995000	0
5	995000	995000	1.000
6	221300	245000	0.903
7	0	245000	0
8	0	750000	0
9	5097000	750000	6.796
10	1546836	231000	6.696
11	0	231000	0
12	0	516000	0

Table 5-2: Model A density values

Process stage	*Model A Specific physical exergy (kJ/kg)*	*P-Po (Pa)*	*Calculated Density (kg/m^3)*
1	0.000	0	1000
2	0.100	100000	1000
3	0.000	0	1000
4	0.000	0	1000
5	1.000	1000000	1000
6	0.903	900000	996.4
7	0.000	0	996.4
8	0.000	0	1000.6
9	6.796	6800000	1000.6
10	6.696	6800000	1015.5
11	0.000	0	1015.5
12	0.000	0	

To facilitate previous model comparison work in Chapter 3 estimated density values at various concentration levels were calculated in order to convert given concentration values (mg/l) to salinity values in parts per million (ppm). The earlier density values of Table 3-3 differ from the density values calculated using process information in Table 5-2. The percentage difference in values between Table 5-2 and Table 3-3 is a maximum of 4.7% at process stage 6. The density values in Table 3-3 are used to compare the physical exergy calculated using Model A and Model B, rather than the values in Table 5-2, because they better reflect the changing densities as a result of concentration changes.

The next step in the physical exergy model comparison is to calculate specific physical exergy using Model B. It is more difficult to differentiate between the physical and chemical exergy parts of Model B as both are integrated due to changing mass fractions throughout the process stages, and importantly, the difference between the mass fraction at a particular process stage and the dead state salinity mass fraction. Based on the definition given at the start of this chapter, physical exergy analysis is not concerned with the changes in specific exergy due to the difference in mass fractions between the various process stages and the restricted dead state or the entropy of mixing term. Using this approach, the specific physical exergy e^{Ph} can be calculated using (5.2) below; this derivation is based on a simplification of (3.18).

$$\begin{aligned} e^{Ph} &= mf_w^{PS}(h_w^{PS} - h_w^{RDS}) + mf_s^{PS}(h_s^{PS} - h_s^{RDS}) \\ &-T_0[mf_w^{PS}(s_w^{PS} - s_w^{RDS}) + mf_s^{PS}(s_s^{PS} - s_s^{RDS})] \end{aligned} \tag{5.2}$$

The superscripts *PS* and *RDS* refer to the relevant process stage and the restricted dead state respectively. The mass fractions mf_w and mf_s can be calculated at the process stage under

consideration from given concentration values in [5], using the method outlined in Chapter 3. Based on (5.2) and using the XSteam function [169] to calculate the entropy and enthalpy of water, and the thermodynamic properties of solids to calculate the enthalpy and entropy of salt [136], the specific physical exergy at each process stage was calculated, the results are shown in Table 5-3.

Table 5-3: Model B specific physical exergy based on concentration values in [5]

Process Stage	***Conc. (mg/l)***	***Density (kg/m^3)***	***Salinity (ppm)***	***Specific physical exergy (kJ/kg)***
1	34654	1024.5	33825.3	0
2	34654	1024.5	33825.3	0.097
3	34654	1024.5	33825.3	0
4	34654	1024.5	33825.3	0
5	34654	1024.5	33825.3	0.968
6	61852	1045.4	59165.9	0.848
7	61852	1045.4	59165.9	0
8	25733	1017.7	25285.4	0
9	25733	1017.7	25285.4	6.629
10	82567	1061.6	77776	6.180
11	82567	1061.6	77776	0
12	270	998.4	270.4	0

The specific physical exergy results calculated using both Model A and Model B can now be compared and assessed. Table 5-4 shows that there is relatively little difference in the specific physical exergy calculated using each model, a 1.5% difference at process stage 6 and a maximum difference of 2.1% at process stage 10. It should be noted that the Model A values incorporate the amended density values, and that the Model B values are based solely on the physical specific exergy and do not consider the dead state definition salinity values when calculating the specific exergy at each process stage (according to the physical

exergy definition). Based on the process stages where the largest percentage differences occur, i.e. the most concentrated process stages 6 and 10, the differences in physical exergy are more than likely due to differences in the density calculations of Model A and the comparable mass fractions of Model B. The processes are isothermal, and consequently, the differences must relate to pressure exergy. The results presented in Table 5-4 would suggest that the significant exergy result differences found in Chapter 3 were not caused by the physical exergy calculation models outlined in this section.

Table 5-4: Comparison of specific physical exergy values calculated using Model A and Model B

Process stage	*Model A (kJ/kg) (amended density values)*	*Model B (kJ/kg)*
1	0	0
2	0.098	0.097
3	0	0
4	0	0
5	0.976	0.968
6	0.861	0.848
7	0	0
8	0	0
9	6.682	6.629
10	6.311	6.180
11	0	0
12	0	0

5.2 Chemical exergy

Chemical exergy is the maximum work potential of a system (due to differences in composition) as the system changes from thermo-mechanical equilibrium at the restricted dead state, to that of the dead state. According to Szargut [93],

"*Chemical exergy expresses the exergy content of the substance at environmental temperature and pressure*".

The molar chemical exergy of an ideal mixture/solution is given by (5.3) [92, 93, 95, 109].

$$\overline{e}^{Ch} = \sum_i x_i \overline{e}_i^{Ch} + RT_0 \sum_i x_i \ln x_i \tag{5.3}$$

In equation (5.3) $\overline{e}^{Ch}$ the molar chemical exergy of the ideal mixture/solution is a combination of two contributions, an intrinsic chemical exergy contribution from each of the mixture species *i* and a contribution from the entropy of mixing term, which has the effect of reducing the total system chemical exergy. There is consensus in key engineering exergy texts on what defines chemical exergy [92-95, 109]. However, due to the nature of the natural environment and the fact that it is not in equilibrium, several chemical exergy calculation models and standard chemical exergy tables exist [95], (standard typically refers to 298.15K and atmospheric pressure or 1 bar). Several of these chemical exergy models have been discussed in the literature review.

The chemical exergy term of Model A, see (3.5), is different from the widely accepted chemical exergy term in (5.3) with respect to both the sign of the natural logarithm and the intrinsic chemical exergy contribution term. Regarding Model A, the dead state of the aqueous solution is defined as pure water; accordingly, the chemical exergy calculated using (3.5) is positive when the mole fraction of water is less than unity and zero in the pure water state. Another point of note is that the lower the mole fraction of water in the aqueous solution the greater the contribution to chemical exergy.

The origin and suitability of the Model A chemical exergy term requires investigation. As discussed previously in Chapter 3, the derivation of the Model A chemical exergy term is not detailed by the relevant authors in the published literature. However, based on an examination of (3.5), it is evident that when the N_{sol} and $\dot{m}$ terms are excluded, the Model A chemical exergy simplifies to (5.4), which is identical to the equation defined by Szargut [93, 116] to calculate the molar chemical exergy of water obtained from seawater desalination.

$$\overline{e}_w^{Ch} = -RT_0 \ln x_w \tag{5.4}$$

The use of (5.4) and (3.5) to calculate the chemical exergy of desalination process streams requires consideration; the chemical exergy calculated should intuitively represent the potential work output as the system moves from thermo-mechanical equilibrium to the dead state. Generally, the dead state of the system in a desalination process occurs when the concentrated brine is allowed to mix with local seawater as the brine is returned to the sea, and therefore, the chemical exergy should reflect the maximum potential work that the brine could do if it was allowed to mix with local seawater. However, the chemical exergy calculated using (5.4) and (3.5) calculates the exergy of the brine based on the theoretical work potential of the brine mixing with one mole of pure water. A more realistic chemical exergy should not model the mixing of the brine with one mole of pure water but rather with local seawater (Model B). The differences underlying the separation models of Model A and Model are discussed in greater detail later in this chapter.

The chemical exergy calculated using Model A and Model B can be compared as follows; the specific chemical exergy of Model A can be calculated from values presented in the literature [5]. To do this, the chemical exergy rate (kJ/hr) is divided by the mass flow rate (kg/hr). Regarding Model B, the specific chemical exergy is coupled with the physical exergy. The specific chemical exergy can be calculated by subtracting the calculated Model B specific physical exergy from the total specific exergy calculated in Chapter 3, i.e. the specific exergy version of (3.18) minus (5.2), see (5.5).

$$e^{Ch} = \begin{bmatrix} h_w^{DS}(mf_w^{PS} - mf_w^{DS}) + h_s^{DS}(mf_s^{PS} - mf_s^{DS}) \\ -T_0 \begin{bmatrix} s_w^{DS}(mf_w^{PS} - mf_w^{DS}) + s_s^{DS}(mf_s^{PS} - mf_s^{DS}) \\ -R_{im}^{PS}(x_s^{PS}\ln x_s^{PS} + x_w^{PS}\ln x_w^{PS}) + R_{im}^{DS}(x_s^{DS}\ln x_s^{DS} + x_w^{DS}\ln x_w^{DS}) \end{bmatrix} \end{bmatrix} \quad (5.5)$$

The specific chemical exergy is therefore a function of, (1) the product of the dead state enthalpy and entropy of each constituent and the difference in the mass fractions of each constituent between the various process stages and the dead state, (2) the dead state temperature, and (3) the difference in the entropy of mixing terms between the process stage and the dead state.

The Model A and Model B comparison for specific chemical exergy is shown in Table 5-5. The values for specific chemical exergy are different due to the inherent model differences, and thus, there is little point in calculating a percentage difference value. It is noted that the magnitudes of specific chemical exergy appear to be similar for both models in process stages 6 to 11; however, as will become evident, this turns out to be coincidental. The choice of dead state reference for both models means that the chemical exergy is at a minimum, in terms of magnitude, at process stage 1 (and other stages of equal concentration) for Model B and a minimum at process stage 12 for Model A. The values of

chemical exergy are all positive for Model A and may be either positive or negative for Model B. Regarding Model B, the values are negative when the concentration of salts in the ideal solution at the process stage under consideration is greater than the incoming stream (seawater salinity). These values strongly suggest that the calculation of chemical exergy is the key source of the model differences.

Table 5-5: Comparison of specific chemical exergy for Model A and Model B

Process stage	***Model A (kJ/kg)***	***Model B (kJ/kg)***
1	2.67	0.00
2	2.67	0.00
3	2.71	0.00
4	2.67	0.00
5	2.67	0.00
6	4.54	-4.35
7	4.54	-4.35
8	2.06	1.64
9	2.06	1.64
10	6.50	-7.21
11	6.50	-7.21
12	0.02	7.61

5.3 Assessment of chemical exergy results

The preceding results lead to several other questions and areas of investigation. The results in Table 5-5 show that the chemical exergy values calculated using Model A and Model B are not readily comparable. Regarding the model differences, there are again three possible options where Model A and Model B differ, (1) the dead state, (2) the model of the aqueous solution and (3) the chemical exergy calculation model.

5.3.1 Dead state reference

First, the dead state is considered. Now that the physical and chemical exergy have been decoupled, it is worth investigating the possibility of amending the Model A dead state reference to that of Model B (local seawater salinity) and assessing the effect on chemical exergy results. In Chapter 3 the dead state of Model B was amended to the dead state of Model A, and it was found that this change in dead state reference resulted in negligible change in the exergy destruction rate calculated at the two dead states but did result in significant changes in the calculated exergy rates. Presently, it is solely the chemical exergy under consideration. Model A calculates the molar chemical exergy at each of the process stages according to (3.5), which in turn appears to be based on (5.4). The molar chemical exergy term of (5.4) relates to the minimum work input to separate one mole of pure water from seawater of water mole fraction x_w. Therefore, at process stage 1, the molar chemical exergy relates to the exergy to separate one mole of water from local seawater of mole fraction $x_{w\,1}$ (the subscript *w n* in $x_{w\,n}$ denotes the mole fraction of water at any process stage *n*). This incoming salinity can subsequently be used as the reference in all other process stage chemical exergy calculations. In addition to the amended dead state references, now consider the chemical exergy in terms of specific values rather than molar values. At process stage 1 the chemical exergy is zero; it is the specific chemical exergy to separate one kilogram of pure water from seawater of mole fraction $x_{w\,1}$ minus the specific chemical exergy to separate one kilogram of pure water from seawater of mole fraction $x_{w\,1}$. Consider the specific chemical exergy at the other process stages where changes in concentration occur, for example at process stage 6 the NF retentate (refer to Figure 3-1 below which has been shown below again for ease of reference).

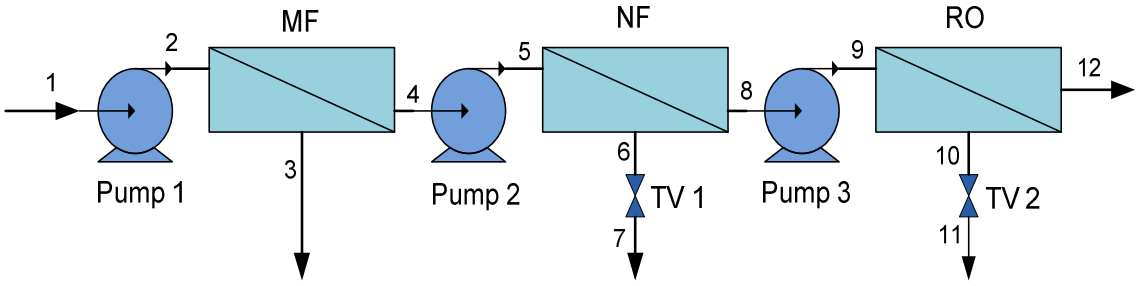

Figure 3-1: Desalination process stages from dataset, adapted from [5]

The specific chemical exergy is the minimum work input required to separate one kilogram of pure water from seawater of the NF retentate mole fraction $x_{w\,6}$ minus the specific chemical exergy required to separate one kilogram of pure water from seawater of incoming seawater mole fraction $x_{w\,1}$, and so forth for the various process stages. Mathematically, for each process stage, this is given in molar form by (5.6).

$$\bar{e}_n^{Ch} = -RT_0 \ln x_{w\,n} - (-RT_0 \ln x_{w\,1}) = RT_0 \ln \frac{x_{w\,1}}{x_{w\,n}} \tag{5.6}$$

Accordingly, if $x_{w\,1} > x_{w\,n}$, the molar chemical exergy is positive. In this case the mole fraction of the incoming water is greater than the mole fraction of water at the relevant process stage, and thus, the salinity of the incoming water is lower than the salinity of the relevant process stage. However, when $x_{w\,1} < x_{w\,n}$ the molar chemical exergy is negative and when $x_{w\,1} = x_{w\,n}$ the molar chemical exergy is zero. This is contrary to the negative chemical exergy values obtained for Model B in Table 5-5.

Referring back to the Model A chemical exergy, see (3.5) to (3.7), it is evident that $x_{w\,1}$ in (5.6) is unity, see (5.7) below.

$$\overline{e}^{Ch} = -RT_0 \ln x_w = RT_0 \ln \frac{1}{x_w} \tag{5.7}$$

Using a common, more appropriate, dead state reference, the chemical exergy values are easier to compare, these amended values are shown in Table 5-6. However, as Table 5-6 shows, the values of specific chemical exergy are still different. The incoming seawater chemical exergy is equivalent but the similarities end there. Even if the negative signs in Table 5-6 are deemed arbitrary, and the chemical exergy is considered as the departure from a composition reference, and therefore, only the magnitude of chemical exergy is of concern, the values are not similar. The amended exergy dead state reference results in different values of specific chemical exergy for Model A but it does not wholly account for the chemical exergy differences between the two models.

Table 5-6: Comparison of the specific chemical exergy calculated using Model A (both the original and amended dead states) and Model B

Process stage	***Original dead state Model (kJ/kg)***	***Amended dead state Model A (kJ/kg)***	***Model B (kJ/kg)***
1	2.67	0	0
6	4.54	1.87	-4.354
8	2.06	-0.61	1.636
10	6.50	3.83	-7.212
12	0.02	-2.65	7.609

5.3.2 Seawater aqueous solution model

The next point to investigate is the seawater model. This section considers several questions. First, does the Model A method for calculating the mole fraction of water result in a similar mole fraction to that obtained in Model B, and does this influence the molar chemical exergy calculation? Second, if the mole fractions differ and result in different values of molar chemical exergy, will equating the mole fractions reduce this difference?

The mole fraction of water was estimated for the concentration value at process stages 1 to 5 using the Model A calculation procedure for both chemical and total exergy outlined in Figure 5-1. Calculating the Model A mole fraction of water involves two-stages, first $\sum \beta_i c_i / \rho MW_i$ is calculated, see Table 5-7. This summed value is then used in (3.7) to calculate the mole fraction of the solvent x_{sol}, i.e. water according to the Model A terminology, (x_w and x_{sol} are used interchangeably here depending on whether a particular model or a general model is under consideration). The exact value of x_{sol} used in the dataset is not stated explicitly in the cited reference [5], however, it was estimated to be 0.99998 from the published chemical exergy rate results and other relevant process data using a commercial software model Excel™.

The mole fraction estimation method is now detailed. The value of the Model A mole fraction was calculated iteratively using a developed Excel™ model. First, the chemical exergy rate value was calculated using the density value for process stages 1 to 5 in Table 5-2. Using the relevant density value of 1000 kg/m^3, and assuming that the dissociation

values (β_i) were unity, resulted in a 0.8% difference between the published chemical exergy rate results and the results calculated by the author for process stage 1. According to the Excel™ model, a density value of 1009.75 kg/m^3 gave a very accurate approximation to the published results (although this density value is greater than that obtained in Table 5-2). Notwithstanding this discrepancy in the density values, the density value of 1009.75 kg/m^3 resulted in a mole fraction value of water of 0.99998 (using a density value of 1000 kg/m^3 also resulted in a mole fraction value of 0.99998). In fact, it was found that the mole fraction of water was not sensitive to density values using the Model A approach. This was tested for the process stage 1 concentration value over a density range of 1000 kg/m^3 to 1024.5 kg/m^3, resulting in a maximum 0.000044% difference between the mole fractions of water at density values of 1000 kg/m^3 and 1024.5 kg/m^3).

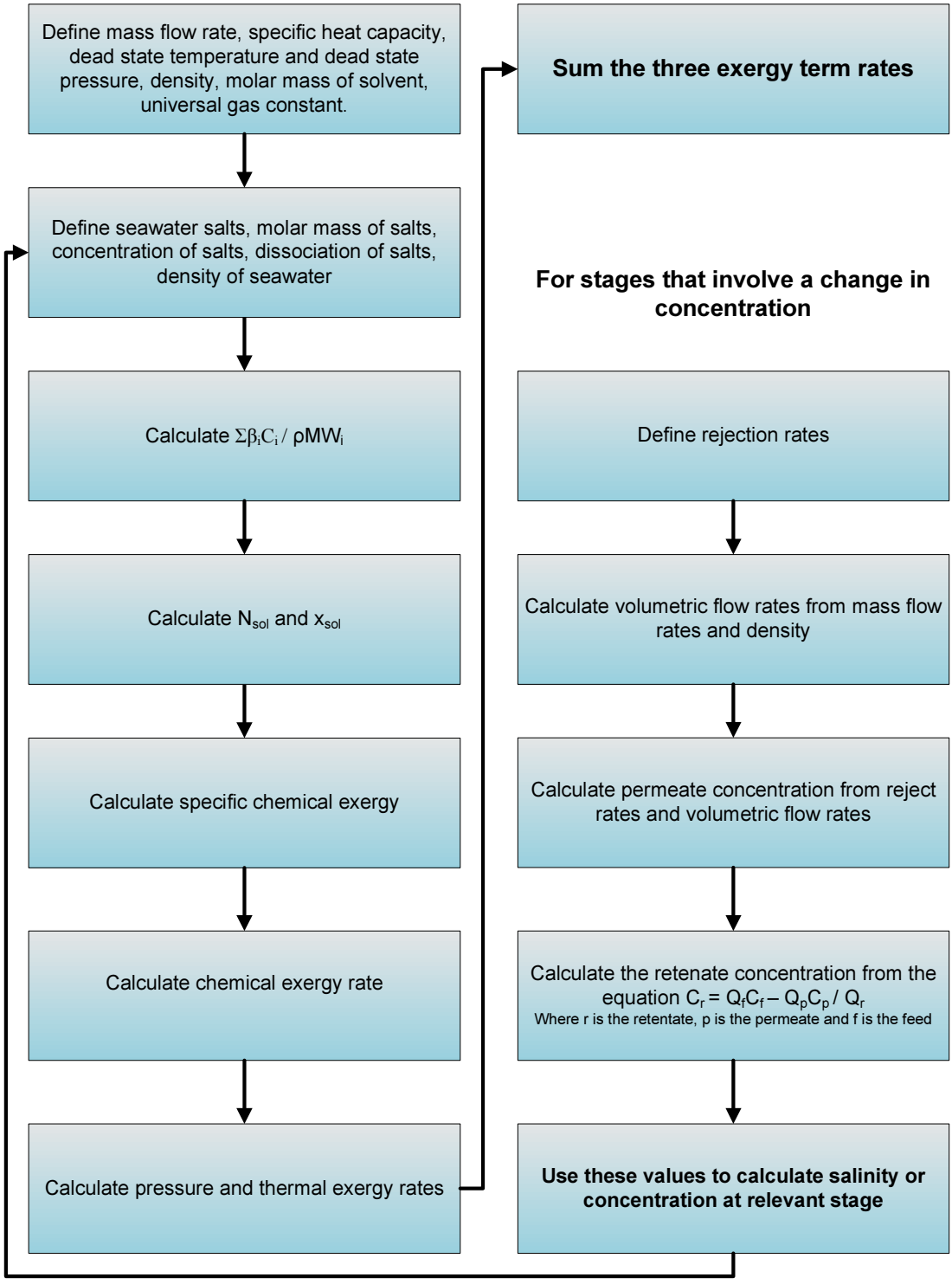

Figure 5-1: Model A calculation procedure

Table 5-7: Model A mole fraction calculation - stage 1

Species	β_i	C_i ***(g/l)***	ρ ***(g/l)***	MW_i ***(g/mol)***	$\beta_i C_i/\rho MW_i$ ***(mol/g)***
Cl^-	1	19.345	1000	35.5	0.00054493
Na^-	1	10.752	1000	23	0.00046748
$SO4^{--}$	1	2.701	1000	96	2.8135E-05
Mg^{++}	1	1.295	1000	24.3	5.3292E-05
Ca^{++}	1	0.416	1000	40	0.0000104
K^+	1	0	1000	39.1	0
$HCO3^-$	1	0.145	1000	61	2.377E-06
	Total (g/l)	**34.654**		$\sum \frac{\beta_i C_i}{\rho MW_i}$	**0.00110661**

The Model A approach resulted in a mole fraction for process stage 1 of 0.99998, this compares with 0.989 for the mole fraction calculated for the same process stages using Model B, a percentage difference of approximately 1%. However, although the percentage difference between the two mole fraction values is only 1%, when these two mole fraction values are used to calculate the molar chemical exergy ($-RT_0 \ln x_w$), the results are significantly different. A mole fraction of 0.989 equates to a molar chemical exergy of 26.95 kJ/kmol whereas a mole fraction of 0.99998 equates to a molar chemical exergy of 0.049 kJ/kmol due to the natural logarithm term. The reason for this difference in mole fraction values is due to the way each model calculates the mole fraction of the seawater constituents. In Model B, the salinity of seawater is used to calculate the mass fraction of water and from that value, the mole fraction of water can be calculated using equation (3.17). Essentially, the mole fraction is a function of the molar mass and mass fractions of salt and water, which can be obtained from the total concentration of salts. Regarding Model A, the mole fraction is obtained by first calculating the N_{sol} term, a function of

concentration, density and molar mass of the water, and then x_{sol}, a function of concentration, density, dissociation number and the molar mass of the various seawater constituents, see (3.5) to (3.7). The different mole fraction values obtained using the two approaches may be an important reason for the model differences.

It is interesting to note that, according to the authors' definitions of the terms in (3.6), the units in the equation do not appear to balance. On examination, the $\sum C_i / \rho$ term calculates the mass fractions of the solutes (i.e. unit weight of the solutes divided by unit weight of solution). However, the units reported by the authors [5] for the N_{sol} term in (3.6), i.e. number of moles of the solvent per unit weight of the solution, require that the units of the numerator are unit weight of pure water divided by unit weight of the solution, (i.e. units of the mass fraction of the solvent water). However, on closer inspection of the numerator in (3.6), the mass fraction of water is not 1000 minus the mass fractions of the solutes but unity minus the mass fractions of the solutes. It is not clear whether this is an oversight on the authors' behalf or if there is sound reasoning behind the N_{sol} term calculation. It is evident, however, that the mole fraction of water calculated using the Model A approach is greater than that of the Model B approach

The approaches used to calculate the mole fractions of the relevant species are different in Model A and Model B. The next step is to investigate whether the use of identical water mole fraction values will negate the chemical exergy differences shown previously in Table 5-6. To test this, the water mole fraction values at each process stage, calculated according to Model B, were substituted into the Model A molar chemical exergy equation. The results

are shown in Table 5-8, where the Model A molar chemical exergy is shown for both the original and amended dead states.

Table 5-8: Comparison of Model A molar chemical exergy calculated using Model B mole fractions, shown for both the original and amended dead states

Process stage	x_w *Model B mole fractions*	*Amended mole fractions Model A (kJ/kmol)*	*Amended mole fractions and dead state Model A (kJ/kmol)*
1	0.989	26.946	0.000
2	0.989	26.946	0.000
3	0.989	26.946	0.000
4	0.989	26.946	0.000
5	0.989	26.946	0.000
6	0.981	46.732	19.786
7	0.981	46.732	19.786
8	0.992	19.568	-7.379
9	0.992	19.568	-7.379
10	0.975	61.678	34.732
11	0.975	61.678	34.732
12	9.999E-01	0.195	-26.751

The Model A values (calculated using both the amended dead state and mole fractions) are compared with the molar chemical exergy values of Model B in Table 5-9. The molar chemical exergy for Model B was obtained by multiplying the specific chemical exergy values shown in Table 5-5 by the respective molar mass of the ideal mixture at the various process stages. Importantly, even though the mole fractions and dead state reference have been equated for Model A and Model B, the values are quite different for all stages except

those stages at incoming seawater salinity. Looking at Table 5-9, the magnitude of molar chemical exergy calculated using Model B is greater than that of Model A, generally, by a factor of four. The negative values for Model A and Model B have already been explained and are considered as a magnitude or a departure from a reference state.

Table 5-9: Comparison of molar chemical exergy values calculated using both Model A (with Model B mole fractions for water) and Model B

Process stage	*Model A -Amended dead state and mole fractions - molar chemical exergy (kJ/kmol)*	*Model B - molar chemical exergy (kJ/kmol)*
1	0.00	0.00
2	0.00	0.00
3	0.00	0.00
4	0.00	0.00
5	0.00	0.00
6	19.79	-81.78
7	19.79	-81.78
8	-7.38	30.00
9	-7.38	30.00
10	34.73	-137.22
11	34.73	-137.22
12	-26.75	137.10

The final area of consideration is to evaluate the underlying principles of the two chemical exergy calculation models used in Model A and Model B. This assessment is not straightforward because the Model A separation assumptions have not been detailed in the literature by the relevant authors. However, an evaluation in Cengel and Boles [128] concerning the limiting minimum work of separation for an ideal mixture can be adapted and applied to the two Models.

5.3.3 Calculation model principles

Based on the analysis to date, chemical exergy is the main source of the model differences. The defined dead states and the water mole fraction differences have been investigated and identified as sources of chemical exergy deviation between the models. Based on an equivalent dead state definition and water mole fraction, it was found that the molar chemical exergy was approximately four times greater when calculated using Model B in comparison to Model A. In this section, the principles behind the models are investigated in order to determine which of these models is the most applicable for desalination purposes.

Model A appears to specifically consider the molar chemical exergy as a function of the mole fraction of pure water in seawater; i.e. the other seawater constituents are implicit in this mole fraction. However, based on an analysis in Cengel and Boles [128], the Model A chemical exergy equation considers a particular case of separation when one mole of pure water is separated from a large quantity of seawater. Their analysis is reproduced, although adapted slightly, in Appendix C, and shows that the Model A chemical exergy term is still rooted in the entropy of mixing term of (3.13) and (3.18).

Essentially, the chemical exergy of Model A is determined from the minimum work input to separate one mole of water from seawater (treated as an ideal mixture of water and salt). This equates to the minimum work input to separate the mixture completely minus the minimum work input to separate the mixture if one mole of water is removed from a large number of moles of water in seawater ($N_w \gg 1$). Consider the difference between the two

principles. The minimum work input to completely separate an ideal mixture into its constituents at any process stage is given by (5.8), the entropy of mixing term [128].

$$\bar{w}_{\min} = -RT_0 \sum x_i \ln x_i \tag{5.8}$$

The minimum work input required to separate a process stream that does not involve complete separation is less than that of complete separation and can be calculated by subtracting the minimum work input to completely separate each of the outgoing streams from the minimum work input to completely separate the incoming ideal mixture [128]. This is illustrated in Figure 5-2 where seawater is separated into almost pure product water (relative to the incoming seawater) and brine.

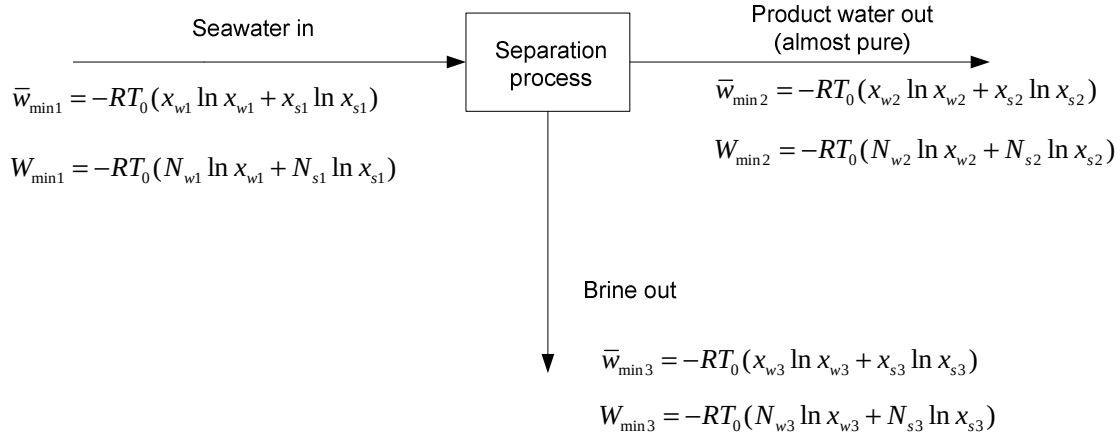

Figure 5-2: Minimum work of separation of seawater (based on analysis in [128]**)**

Looking at Figure 5-2, the minimum work for the separation of seawater (of mole fractions $x_{s\,1}$ and $x_{w\,1}$) into two process streams of mole fractions $x_{s\,2}$ and $x_{w\,2}$ and $x_{s\,3}$ and $x_{w\,3}$ respectively, is therefore given by (5.9).

$$W_{\min} = W_{\min\ 1} - (W_{\min\ 2} + W_{\min\ 3}) \tag{5.9}$$

The Model A exergy equation principle is illustrated in Figure 5-3 where one mole of pure water is extracted from a large quantity of incoming seawater, resulting in a practically identical outgoing brine composition with respect to the incoming seawater. In this case the minimum work input for separation is given by (5.10) because the minimum work of separation for the pure water is zero.

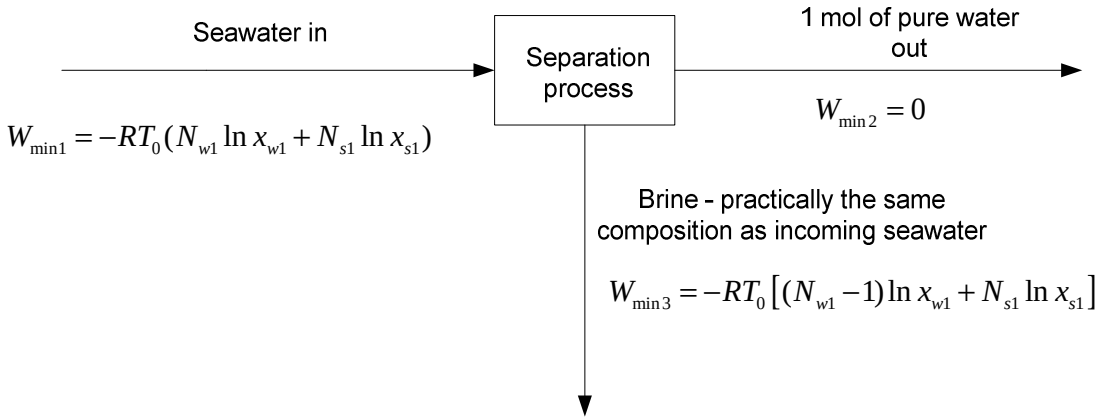

Figure 5-3: Minimum work of separation of seawater based on the extraction of one mole of pure water (based on analysis in [128]**)**

$$W_{\min} = W_{\min\ 1} - W_{\min\ 3} = -RT_0 \ln x_{w\ 1} \tag{5.10}$$

Then, according to the discussion in section 5.3.1 (specifically, the amended salinity dead state for Model A), the chemical exergy at any process stage is the chemical exergy at the relevant process stage minus the chemical exergy at the salinity dead state reference. The

most appropriate exergy reference state is the incoming local seawater salinity, as this is generally also the natural sink for the outgoing desalination plant process streams. Figure 5-4 shows the principle behind the Model A exergy calculation for outgoing brine (process stages 6 and 10) and incoming seawater or feedwater; the chemical exergy calculated for the lower process in Figure 5-4 is subtracted from the chemical exergy calculated for the top process in order to amend the salinity dead state. However, there is one very important consideration which becomes apparent when trying to re-set the dead state reference in light of the underlying Model A principles. This issue occurs because it has already been assumed in Model A that the brine is practically identical to the incoming seawater since only one mole of water has been extracted from the incoming seawater ideal mixture. Therefore, there is an implicit assumption that the brine has the same mole fraction of water as the incoming seawater, and consequently, there should be no difference in chemical exergy between the two process stages. This is a flaw in the Model A approach when used for plant analyses as opposed to the theoretical chemical exergy value of water obtained from desalination proposed in Szargut and Morris [93].

The Model B chemical exergy equation at any stage, when decoupled from the physical exergy equation, calculates the complete separation of the two mixture constituents at the process stage mole fractions minus the complete separation of the two constituents at the dead state mole fractions, see (5.5) for the entropy of mixing terms (note that (5.5) also takes the change in mass fractions at dead state enthalpy and entropy into account).

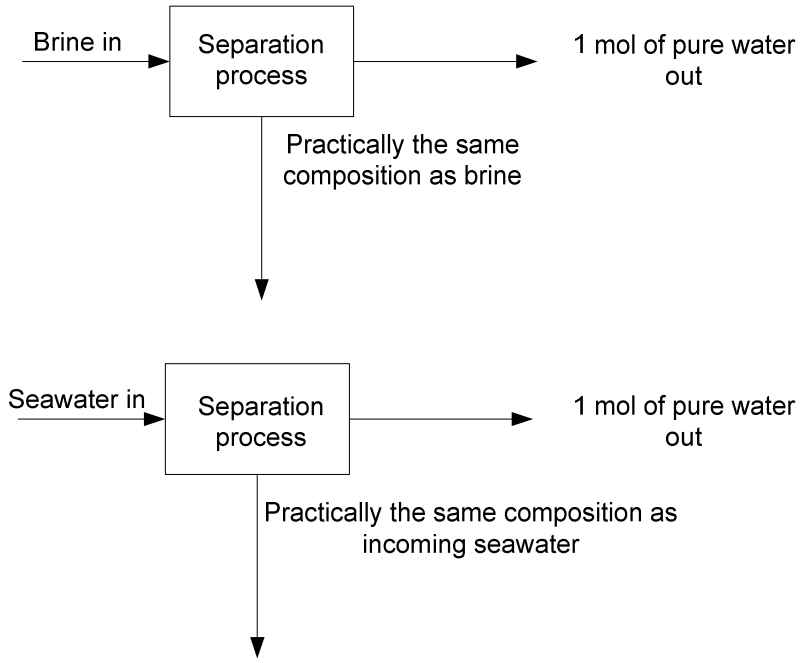

Figure 5-4: Model A molar chemical exergy of brine and incoming seawater stages

Of the two models, which is the most appropriate for desalination exergy analysis purposes? From the exergy analysis perspective, should the separation of water from seawater be analysed on the basis of the chemical exergy of water, which in turn is based on the extraction of one mole of water from a large quantity of water in an ideal mixture of salt and water according to Model A, or should it be based on Model B? This depends on the context. Theoretically, in seawater purification processes, the chemical exergy of water may be modelled as the extraction of a proportionately small quantity of water from a large ideal mixture reservoir. As a general model for calculating the chemical exergy of water which has been produced from desalination, the Model A molar chemical exergy term (5.4) may be appropriate and has been cited for this purpose in Szargut and Morris [93]. However, the use of Model A to carry out a plant analysis is not suitable. The principle

underlying Model A implicitly assumes that there is negligible change in brine composition, but at the various process stages, including two brine stages in the analysed dataset, the model is used to calculate the brine mole fraction and chemical exergy which is substantial in comparison with the seawater salinity (having previously assumed that there is negligible change). The suitability of Model B, regarding the modelling of aqueous streams as an ideal mixture of solid salt and water is considered further in the following chapters.

5.4 Summary

In summary, the differences between Model A and Model B are caused by, (1) the difference in the defined dead state, (2) the difference in the way in which the mole fraction of water is calculated, and (3) the differences in the underlying model assumptions, which lead to different chemical exergy equation terms. Noticeable differences in mole fraction calculations were identified in this chapter, however, even when the salinity dead state and mole fraction of water were equated, the molar chemical exergy calculated by Model A and Model B was shown to differ by a factor of four approximately. The separation principle underlying the Model A molar chemical exergy term was identified from an alternate source in the literature and it was found that the chemical exergy calculation term in Model A considers a special case of separation, i.e. the extraction of one mole of pure water from a large quantity of seawater. Based on the author's assessment of this assumption, it was determined that although the Model A molar chemical exergy term may be suitable as a theoretical method to calculate the exergy of water from desalination, Model A is not suitable for plant exergy analyses.

6 Model C

This chapter details the development of Model C. The major difference between Model C and Models A and B is that Model C does not treat ionic streams such as seawater and UPW incoming water as ideal mixtures/solutions but acknowledges that as electrolytic solutions, they do not behave ideally. The chemical exergy term detailed in this chapter is rooted in existing solution thermodynamics research. However, the approach developed in this chapter, which seeks to accurately apply the exergy terms to water purification processes is novel in its thorough and accurate determination of an appropriate aqueous solution model and the use of ionic strength calculations to determine the most appropriate activity coefficient calculation model.

6.1 Model C selection

Based on the results obtained in Chapter 5, the research hypothesis defined in Chapter 4 requires adjustment, i.e. Model A is not deemed appropriate for water purification exergy analyses, and thus, is not considered further for UPW plant exergy analyses. However, the need for an appropriate UPW exergy model remains. Following a refocused literature review of the broader chemical exergy and solution thermodynamics literature, two potentially suitable alternative approaches have been identified, (1) a chemical exergy model based on the Szargut reference environment, and (2) a chemical exergy model based on the solution thermodynamics literature.

Szargut developed standard chemical exergy tables, which provide a very sound basis for computing the chemical exergy of elements and compounds and thus evaluating the earth's natural capital. However, the use of standard chemical exergy tables, and indeed the overall Szargut model approach, has both advantages and disadvantages. First, although standard chemical exergy values are straightforward to use and greatly simplify the use of exergy analysis, they are only strictly valid for dead states at standard temperature and pressure. The limitations of the standard exergy tables particularly regarding standard temperature are problematic. Not all real life processes occur at standard values and it is often necessary to account for other thermodynamic states. Research has been, and is currently being, carried out to address this issue, and these developments are discussed in greater detail in Chapter 7. Without the use of the standard exergy tables, the fundamental calculation of chemical exergy values is quite complex. There are also uncertainties associated with the chemical exergy of species, whose chemical exergy uses the lithosphere as a reference datum level, as discussed previously in Chapter 2.

Second, and this can be seen as both an advantage or a disadvantage depending on one's viewpoint, the use of the standard chemical exergy approach takes a broader perspective of the natural environment, and importantly, considers possible interactions between process streams and this wider environment that may not necessarily be relevant to the process being analysed [93]. Some authors [125] advocate the need for practical limitations to be factored into the dead state definition. In the case of water purification, is this broader perspective necessary or valuable to understand and quantify process flows? This presents an interesting research question: how does the global perspective differ from the local

perspective for desalination or water purification exergy analyses? This question in essence considers whether it is more appropriate to reference the chemical exergy of every species in the process streams to the final, most likely, form of that species as it interacts with the environment or if it is more appropriate, as in the case of Model A and Model B, to just consider the difference in concentration between the process stream and the defined dead state. Model A and Model B adopt the latter approach albeit using a different underlying assumption regarding the separation of the streams. The use of the Szargut approach, and thus, the calculation of exergy in desalination or water purification applications from the global natural capital perspective, is rare in the literature. The Szargut model is discussed in greater detail with regards to the exergy analysis of electrolytic solutions for desalination purposes in Chapter 7.

The remainder of this chapter considers the development of Model C from the solution thermodynamics perspective, and this relates only to the difference in concentrations between the process stream and the dead state. In this respect, it is the same approach as Model A and Model B. Importantly however, the aqueous solution is not treated as an ideal mixture but as an electrolytic solution. The various approaches of the four considered models are compared in Figure 6-1 on the basis of several criteria such as the chemical exergy calculation approach, solution modelling and separation assumptions.

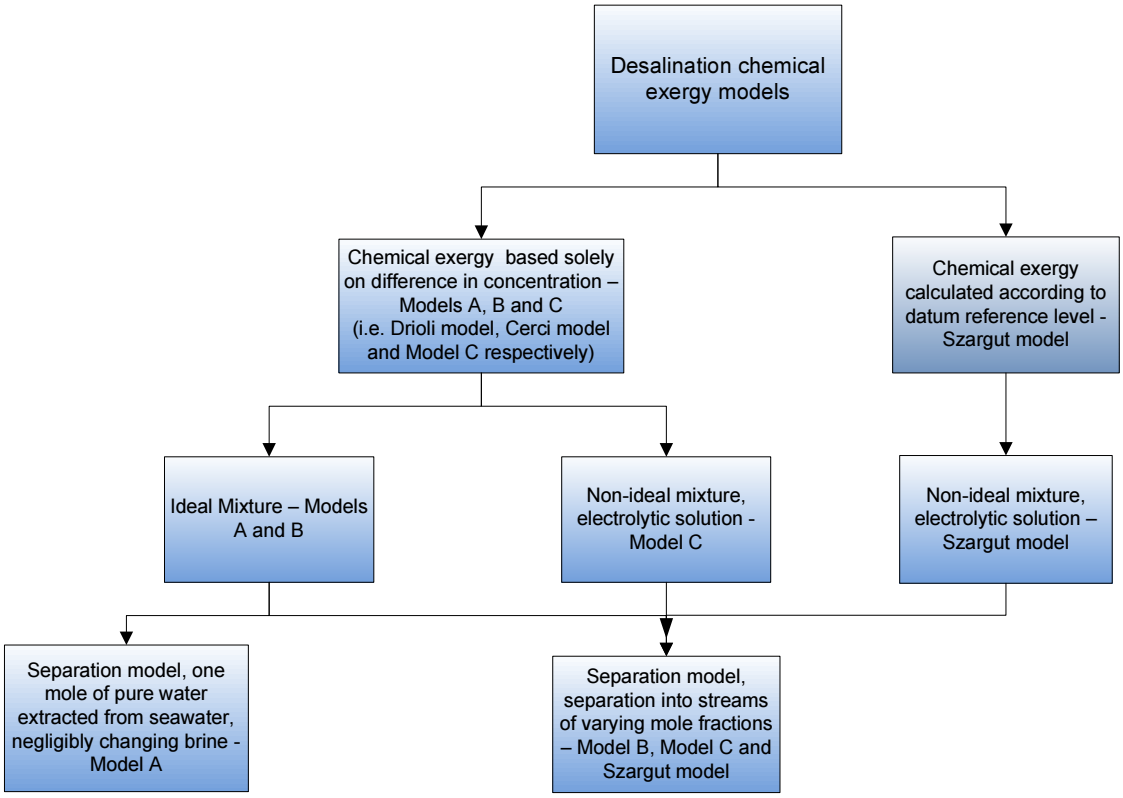

Figure 6-1: Breakdown of desalination exergy approaches

Careful consideration of the physical and chemical exergy definitions is also required. Importantly, the ability to differentiate clearly between chemical and physical exergy is necessary for understanding process flows and sites of exergy destruction. The physical exergy model is relatively straightforward: the assumptions of an incompressible fluid did not result in significant differences in physical exergy calculation according to the results obtained in Chapter 5. Constant specific heat capacity is often assumed thus facilitating the simple integration of (2.7). These assumptions are re-examined for the relevant applications later in this chapter. Therefore, for the development of Model C, the breakdown of total

exergy into physical and chemical exergy is preferred over the integrated approach of Model B, which is largely in agreement with key exergy monographs and publications reviewed previously. The choice of the most appropriate chemical exergy model is once again the main issue. How does one calculate the exergy of a system at a process stage which is at thermal and mechanical equilibrium but at different concentration to the dead state? This involves use of the chemical potential or partial molar Gibbs energy, which according to Pitzer and Brewer's revision of the classic text *Thermodynamics* by Lewis and Randall [175] has led to many misunderstandings,

> "*Of all the applications of thermodynamics to chemistry, none has in the past presented greater difficulties, or been the subject of more misunderstanding, than the one involved in the calculation of what has rather loosely been called the free energy of dilution, namely the difference in the chemical potential or partial molar free energy of a dissolved substance at two concentrations*".

The chemical exergy at constant temperature and pressure arises due to the difference in chemical potential between the state of thermo-mechanical equilibrium (restricted dead state) and the dead state. This difference in chemical potential is determined by the change in Gibbs energy as the concentration changes at constant temperature and pressure, see (6.1). The Gibbs energy is a function of temperature, pressure and concentration (number of moles), $G = f(T, P, N)$.

$$dG = \left(\frac{\partial G}{\partial T}_{P,N_j}\right) dT + \left(\frac{\partial G}{\partial P}_{T,N_j}\right) dP + \sum \left(\frac{\partial G}{\partial N_i}\right)_{P,T,N(i \neq j)} dN_i \qquad (6.1)$$

At constant temperature and pressure, the Gibbs energy is solely a function of the change in concentration of the relevant species. Utilising the TdS relations or Maxwell's equations, and the definition of chemical potential of constituent i as the change in molar Gibbs energy at constant temperature, pressure, composition of other mixture constituents j where $j \neq i$, $\mu_i = \frac{\partial G}{\partial N_i}(T, P, N_j \text{ constant})$, the change in Gibbs energy can be written as (6.2).

$$dG = -SdT + VdP + \sum_i \mu_i dN_i \tag{6.2}$$

At constant temperature and pressure (6.2) simplifies to (6.3).

$$dG = \sum_i \mu_i dN_i \tag{6.3}$$

Equations (6.1) to (6.3) define chemical potential, and it is this difference in chemical potential between the restricted dead state and the dead state that provides the driving force to perform chemical work, see Figure 6-2. Chemical work is analogous to the more common forms of work such as electrical and hydraulic work. Power or work can be thought of as the product of a relevant flowing current and a potential difference, i.e. electric power is the product of a potential difference and electric current, hydraulic power is the product of a potential difference arising from a pressure difference at two ends of a conduit and a volumetric flow rate [106]. Then chemical work is the product of the difference in chemical potentials at two states and the current, in this case the molar flow rate [106].

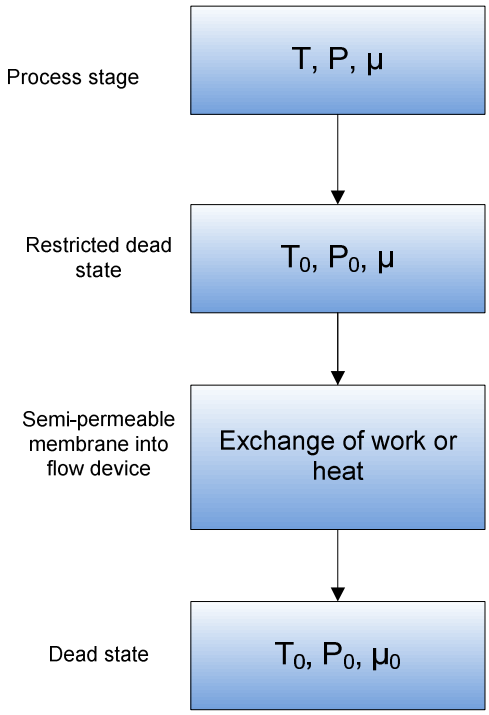

Figure 6-2: Restricted dead state to dead state via theoretical semi-permeable membrane

The chemical work potential of a substance as it comes into equilibrium with its environment can be derived theoretically by undertaking an energy and entropy balance of the mass interaction and mass transfer between the restricted dead state and the dead state through a semi-permeable membrane [125]. If $\dot{N}_i$ is the molar flow rate of constituent i and μ_i is the chemical potential of constituent i then an energy and entropy balance can be undertaken to derive the chemical exergy that results from the mass transfer that occurs between the restricted dead state and the dead state. First, consider the energy balance, see (6.4), noting that $\dot{Q}$ into the system is considered positive and $\dot{W}$ out of the system is positive.

$$\dot{Q} - \dot{W} = \sum_{DS} \dot{N}_i \overline{h}_i^{DS} - \sum_{RDS} \dot{N}_i \overline{h}_i^{RDS} \tag{6.4}$$

The entropy balance is given by (6.5) where $\dot{s}_{gen}$ is the rate of entropy generation.

$$\frac{\dot{Q}}{T_0} = \sum_{DS} \dot{N}_i \overline{s}_i^{DS} - \sum_{RDS} \dot{N}_i \overline{s}_i^{RDS} - \dot{s}_{gen} \tag{6.5}$$

Eliminating $\dot{Q}$ between (6.4) and (6.5) results in (6.6).

$$\dot{W} = \sum_{RDS} \dot{N}_i (\overline{h}_i^{RDS} - T_0 \overline{s}_i^{RDS}) - \sum_{DS} \dot{N}_i (\overline{h}_i^{DS} - T_0 \overline{s}_i^{DS}) - T_0 \dot{s}_{gen} \tag{6.6}$$

Noting that $(\overline{h}_i^{RDS} - T_0 \overline{s}_i^{RDS}) = \mu_i^{RDS}$ and $(\overline{h}_i^{DS} - T_0 \overline{s}_i^{DS}) = \mu_i^{DS}$, the maximum work obtainable from the transfer of mass from the restricted dead state to the dead state is given by (6.7).

$$\dot{E}^{Ch} = \sum \dot{N}_i (\mu_i^{RDS} - \mu_i^{DS}) \tag{6.7}$$

The preceding analysis was based on a derivation in the cited reference [125].

To calculate the chemical exergy of each constituent in a solution or mixture under consideration from (6.7), all that is needed is a means to evaluate the difference between the chemical potentials for each constituent. This is relatively straightforward for an ideal gas in an ideal gas mixture (a mixture of ideal gases behaves as an ideal gas). For example, consider the waste products of combustion, which can be modelled as an ideal gas mixture, the potential to do work exists due to the difference in partial pressures of the gases in the environment between the restricted dead state and the dead state. The change in chemical potential depends on both the change in enthalpy and the change in entropy between the restricted dead state and the dead state. By definition, there is no temperature difference between the restricted dead state and the dead state. For an ideal gas the change in enthalpy between two states is a function of temperature alone, and therefore, at constant

temperature, there is no change in enthalpy between the ideal gas at two states of differing partial pressures. The change in entropy for an ideal gas in an ideal gas mixture is a function of temperature and pressure. Thus, at constant temperature the change in entropy is solely a function of pressure, and can be derived from the TdS relations, see (6.8) where $dh = 0$.

$$Tds = dh - vdP \tag{6.8}$$

Using the ideal gas equation of state and Dalton's law of partial pressures, the change in entropy can be calculated as follows, where P_{i0}^{DS} and P_{i0}^{RDS} are the partial pressures of the ideal gas in the atmosphere at the dead state and the restricted dead state respectively.

$$s^{DS} - s^{RDS} = -\int_{RDS}^{DS} \frac{v}{T} dP = -\int_{RDS}^{DS} \frac{R}{P} dP = -R \ln \frac{P_{i0}^{DS}}{P_{i0}^{RDS}} = -R \ln \frac{x_i^{DS}}{x_i^{RDS}} \tag{6.9}$$

The molar chemical exergy of an ideal gas is obtained by multiplying the change in entropy by the dead state temperature T_0, see (6.10).

$$\overline{e}_{ig}^{Ch} = -RT_0 \ln \frac{x_i^{DS}}{x_i^{RDS}} \tag{6.10}$$

Hence, the molar chemical exergy of an ideal gas is a function of the dead state temperature and its concentration difference between two states.

Equation (6.10) moves ahead slightly in an effort to demonstrate how chemical exergy is calculated. In the general case the calculation of the chemical exergy of an ideal gas should really be thought of as a two-step process. First, the difference between the chemical potential of an ideal gas at each relevant concentration and the chemical potential of the

ideal gas in its pure state, or more correctly its *standard state*, can be calculated using (6.11).

$$\mu_i(T,P,x_i) = \mu_i(T,P,x_i=1) + RT\ln x_i \qquad (6.11)$$

The standard state for an ideal gas is defined as the gas existing in the pure state ($x_i = 1$) at standard pressure (1 bar) and standard temperature (298.15 K). Second, the chemical exergy resulting from the difference in concentration values between two states, for example, between the restricted dead state and the dead state, is calculated by subtracting the values for each state obtained in step 1. The chemical potential of the pure substance $\mu_i(T,P,x_i=1)$ in (6.11) cancels in (6.12).

$$\mu_i(T_0,P_0,x_i^{RDS}) - \mu_i(T_0,P_0,x_i^{DS}) = RT_0\ln x_i^{RDS} - RT_0\ln x_i^{DS} = RT_0\ln\frac{x_i^{RDS}}{x_i^{DS}} \qquad (6.12)$$

This chemical potential term is the unitary chemical potential and is defined as the standard state concentration for ideal gases, although the standard state concentration can change depending on the system of interest.

For the purposes of UPW plant analysis, the use of (6.10) presents a problem, the derivation was based on the ideal gas equation of state, and although this equation is relevant for flow streams which can be modelled as an ideal gas mixture, it does not apply to non-ideal gas systems. What is the alternative if the ideal system approach is not appropriate?

First, the various types of solutions must be considered: a solution is defined as "*a condensed phase (liquid or solid) containing several substances* [115]". There are several

classifications of solutions, perfect, ideal and non-ideal. One definition of a *perfect* solution is that it obeys (6.11) over the complete range of concentrations (Raoult's law). An *ideal* solution obeys Raoult's law for dilute concentrations only. However, there is a special class of ideal solution, the "*ideal dilute solution* [115]", where the change in chemical potential of the main solvent can be modelled according to (6.11), analogous to the "*extremely dilute solutions* [94]" referred to by Bejan. According to Pitzer and Brewer's revision of *Thermodynamics* [175], this approach is deemed valid for a liquid or a solid that may act as a solvent in infinitely dilute solutions.

Finally, for *non-ideal* solutions, an activity coefficient γ is required to adjust the mole fraction for the departure from ideal gas, perfect solution or ideal solution behaviour case, see (6.13).

$$\mu_i(T,P,x_i) = \mu_i(T,P,x_i=1) + RT\ln\gamma_i x_i = \mu_i(T,P,x_i=1) + RT\ln a_i \qquad (6.13)$$

The product of the activity coefficient and the mole fraction of constituent i is termed the activity a_i.

Based on the concept of the "*ideal dilute solution* [115]", one would expect that the difference in the chemical potential of water, as the main solvent in an ideal dilute solution, could be calculated according to Raoult's law. However, this simplification may not be valid for an aqueous solution of ions because an electrolytic solution behaves quite differently from a non-electrolytic solution and special consideration must be given to this deviation in behaviour.

An electrolyte can be defined as a substance that dissociates into ions in an aqueous solution. Arrhenius was the first to discover that certain solutes dissociate into electrically charged ions. The behaviour of these solutes at low concentrations was expected to follow ideal solution behaviour at low concentrations but it was observed that their behaviour was fundamentally dissimilar to non-electrolytic solutions due to long range electrostatic forces between the ions [175]. Based on these findings, electrolytes should not be modelled according to (6.10) but according to (6.13).

Hence, applying the same approach to calculate the difference in chemical potential between two concentration levels of an electrolyte in an aqueous solution as that used to derive (6.12), one would expect that the change in chemical potential could be calculated from (6.14).

$$\begin{aligned} &\mu_i(T_0, P_0, x_i^{RDS}) - \mu_i(T_0, P_0, x_i^{DS}) \\ &= RT_0 \ln x_i^{RDS}\gamma_i^{RDS} - RT_0 \ln x_i^{DS}\gamma_i^{DS} = RT_0 \ln \frac{a_i^{RDS}}{a_i^{DS}} \end{aligned} \tag{6.14}$$

There are two extra complications however, when dealing with electrolytic solution thermodynamics. The first is relatively straightforward: the definition of the mole fraction of an electrolyte can lead to ambiguities [176]. Take NaCl for example, the mole fraction of NaCl in an ideal mixture of NaCl and water was defined earlier for Model B using a variation of (6.15).

$$x_{NaCl} = \frac{N_{NaCl}}{N_{NaCl} + N_w} \tag{6.15}$$

However, NaCl is a strong electrolyte at the temperatures under consideration in this thesis (i.e. NaCl dissolved in water does not exist as NaCl molecules in water but as Na^+ and Cl^-

ions). Hence, the more traditional definition of the mole fraction for a strong electrolyte used in solution chemistry is (6.16) [176], where β is the number of ions generated on dissociation of the electrolyte (two for NaCl), N is the number of moles and the subscripts *NaCl* and *w* refer to the dissociated electrolyte NaCl and water respectively.

$$x_{NaCl} = \frac{\beta N_{NaCl}}{\beta N_{NaCl} + N_w} \tag{6.16}$$

The difference between the two approaches can be illustrated by considering a 1 M NaCl solution, i.e. one mole of NaCl in one kilogram of water (55.5 moles of water). In the first case, using (6.15), the mole fraction of NaCl is calculated to be 0.0177. Adopting the approach of (6.16) results in a mole fraction of 0.0348, almost twice that of the first case. Pitzer termed the latter approach the "*mole fraction on an ionized basis* [177]". In a similar manner, the mole fraction of water can be calculated using (6.17).

$$x_w = \frac{N_w}{\beta N_{NaCl} + N_w} \tag{6.17}$$

This approach is different to that used to determine the Model B mole fractions, see Chapter 3, section 3.2.

It is almost universal to use the molality scale when dealing with electrolytes due to the fact that molality is independent of the temperature and pressure of the solution, and also, equations tend to be simpler using the molality scale (concentrations in electrolytic solutions are generally dilute, leading to very small solute mole fraction values) [176]. Molality is defined as the number of moles of the solute in one kilogram of the solvent i.e. water. Conversion from solute concentration or mass fraction to molality is carried out as follows;

- To convert from the concentration of the solute (g/l, i.e. grams of solute per litre of solution) to the mass fraction of the solute (g/g, i.e. grams of solute per gram of solution) divide by the density of the solution;
- To convert from the mass fraction of the solute to molality divide the solute mass fraction by the product of the molar mass of the solute (g/mol) and the mass fraction of water (g/g, i.e. grams of water per gram of solution);
- Finally, multiply by one thousand to change from grams of water to kilograms.

It should be noted that the molality of the solute is undefined for the pure state of the solute [176]. The change in chemical potential of an electrolyte between one concentration and the concentration in the standard state, written in the molality scale, is shown in (6.18) where C_i is the concentration of species i, M_i is the molality and γ_i is the activity coefficient of species *i*, and C° is the standard state concentration of electrolyte species i.

$$\mu_i(T,P,C_i) = \mu_i(T,P,C^\circ) + RT\ln M_i\gamma_i = \mu_i(T,P,C^\circ) + RT\ln a_i \qquad (6.18)$$

Equation (6.18) leads to the second complication: the standard state is defined differently for the solutes in aqueous solutions (electrolytes and non-electrolytes) from that of the unitary chemical potential standard state applicable to ideal gases. The standard state is different for the solute and the solvent, i.e. it is asymmetrical for aqueous solutions. In order to mirror the simple relationship between the chemical potentials in (6.11) and (6.18) the value of $M_i\gamma_i$ in the standard state must be unity. To explain; if (6.11) is revisited, it is evident that the use of the pure state (i.e. $x_i = 1$) as the standard state simplifies matters greatly and that the final term is essentially $RT\ln\frac{x_i}{1}$. To maintain the same relationship in

(6.18) the standard state must be defined so that $(M_i\gamma_i)^\circ = 1$ and therefore $\frac{M_i\gamma_i}{(M_i\gamma_i)^\circ} = M_i\gamma_i$.

To facilitate this, the standard state is defined as a one molal solution and the activity coefficient is set to unity at one molal concentration. This specific activity coefficient is termed the Henryan activity coefficient, and this approach is universally used as the standard state for solutes [176]. The difference in chemical potential between the electrolyte (or solute) at the restricted dead state is therefore given by (6.19), where the activity coefficient γ_{Hi} is the Henryan activity coefficient.

$$\mu_i(T_0, P_0, M_i^{RDS}) - \mu_i(T_0, P_0, M_i^{DS}) = RT_0 \ln \frac{M_i^{RDS}\gamma_{Hi}^{RDS}}{M_i^{RDS}\gamma_{Hi}^{RDS}} = RT_0 \ln \frac{a_i^{RDS}}{a_i^{DS}} \qquad (6.19)$$

Presently, the solvent water is considered. The standard state for water is analogous to the ideal gas example, i.e. the standard state of water is defined as pure water, except in this case, the activity is used rather than the mole fraction to correct for the departure from ideal behaviour. Again, to replicate the chemical potential relationship of (6.11) and (6.18), the activity of pure water in the standard state is set equal to unity, $x_i\gamma_i = a_i$ therefore in the standard state when $x_i = 1$ the activity is equal to unity and thus $\gamma_i = 1$. The activity coefficient used when the standard state is the pure substance is termed the Raoultian activity coefficient. The difference in chemical potential resulting from the differences in the concentration of water between the restricted dead state and the dead state can be calculated using (6.20) where the activity coefficient γ_{Rw} is the Raoultian activity coefficient of water.

$$\mu_w(T_0, P_0, x_w^{RDS}) - \mu_w(T_0, P_0, x_w^{DS}) = RT_0 \ln \frac{x_w^{RDS} \gamma_{R\ w}^{\ RDS}}{x_w^{DS} \gamma_{R\ w}^{\ DS}} = RT_0 \ln \frac{a_w^{RDS}}{a_w^{DS}} \qquad (6.20)$$

The activity coefficient of water is not greatly different from unity even in concentrated electrolytic solutions [116, 176], for this reason the activity coefficient of water is assumed to be unity in this research. Thus, the exergy of water is a function of the mole fraction ratios. An alternative approach is to use the osmotic coefficient, see the cited reference [176]. The activity of water can change dramatically at high electrolytic solution concentrations, temperatures and pressures (solutions close to saturation, temperatures of 500 to 900°C and pressures up to 15,000 bar [176]). However, these parameters are not relevant to the concentrations, temperatures and pressures considered in this research.

Marin and Turegano [112] outlined a methodology for calculating the chemical exergy of aqueous electrolytic solutions whereby the chemical exergy of each species was calculated using activities rather than mole fractions according to (6.14) albeit based on a different derivation approach than that used here. Equation (6.14) has also been used for calculating the exergy of ionic species in river water [178, 179], seawater [157] and proposed for calculating the concentration exergy of a body of water [180]. However, in the author's opinion, the chemical exergy term proposed in [180] is confusing; the concentration exergy term in the main body of the journal article is changed from a ratio of activities to a ratio of concentrations in the appendix section. The concentration ratio is not necessarily equivalent to the activity ratio and the point of using the activity is that it accounts for a number of standard states and it maintains the relationship between the chemical potential "*for any component i in any system under any condition* [176]". Several attempts by email were

made to discuss this issue with the corresponding author of the cited reference [180], however, to date, no response has been forthcoming.

Equation (6.19) appears relatively straightforward; unfortunately, calculating activity coefficients of electrolytic solutions can be complex and is based on theories of the long-range and short-range forces which exist between ions. Probably the most famous of these theories is the Debye-Huckel theory [181, 182]. The ionic strength I and composition of the aqueous electrolyte solution determines the most appropriate activity coefficient calculation method. The ionic strength can be calculated using (6.21).

$$I = \frac{1}{2}\sum M_i z_i^2 \tag{6.21}$$

In (6.21) I is the ionic strength of the electrolytic solution, M_i is the molality of ionic constituent i and z_i is the valence of the ion. Some authors [43, 183, 184] use molarity in (6.21) instead of molality, the difference between the two approaches is assessed later in this chapter.

The applicability of several activity coefficient calculation models as a function of ionic strength has been discussed in Stumm and Morgan [184], their analysis is reproduced here;

1. The Debye-Huckel model (6.22) which is suitable for an approximate ionic strength $I < 10^{-2.3}\ \left(\approx 0.005\right)$

$$\log \gamma_i = -Az_i^2\sqrt{I} \tag{6.22}$$

2. The Extended Debye-Huckel model (6.23) which is suitable for an approximate ionic strength $I < 0.1$

$$\log \gamma_i = -Az_i^2 \frac{\sqrt{I}}{1+B\alpha\sqrt{I}} \tag{6.23}$$

3. The Guntelberg model (6.24), which is suitable for an approximate ionic strength of I < 0.1 M and is useful in solutions of several electrolytes.

$$\log \gamma_i = -Az_i^2 \frac{\sqrt{I}}{1+\sqrt{I}} \tag{6.24}$$

4. The Davies model [185], which is suitable for an approximate ionic strength of $I < 0.5$ M [184], see (6.25). The Davies equation typically results in an error of 1.5% at an ionic strength less than 0.1 M and a 5 to 10% error at ionic strength measurements between 0.1 and 0.5 M [186].

$$\log \gamma_i = -Az_i^2 \left(\frac{\sqrt{I}}{1+\sqrt{I}} - 0.3I \right) \tag{6.25}$$

In the preceding equations (6.22) to (6.25) the coefficient A is a function of the dielectric constant $\in$ of the solvent and the temperature and is given by (6.26).

$$A = 1.82\times10^{-6}(\in T)^{-\frac{3}{2}} \tag{6.26}$$

The coefficient B is also a function of the dielectric constant and temperature and can be calculated using (6.27).

$$B = 50.3(\in T)^{-\frac{1}{2}} \tag{6.27}$$

These coefficient values are detailed in [184]. The dielectric constant of water $\in$, which a function of temperature is given by (6.28) [187].

$$\in = 78.54\left[1-(0.004579(T-298))+(11.9\times10^{-6}(T-298)^2)+(28\times10^{-9}(T-298)^3)\right] \tag{6.28}$$

Finally α is a parameter which is dependent on the size of the ion in angstroms.

As outlined, there are several simple activity coefficient calculation models suitable for relatively low ionic strengths. However, before choosing a suitable method to calculate the activity coefficients of an aqueous electrolyte solution, the product streams must first be assessed. An incoming water analysis conducted on behalf of the industry partner was used to determine the ionic strength of the solution and the identity and proportion of the main ionic constituents; these are key elements in determining the choice of suitable activity coefficient calculation method because the accuracy of these methods is dependent on a suitable input. The incoming water analysis is shown in Table 6-1, the water analysis is very detailed and includes many species with a concentration of less than or equal to 1 mg/l, to simplify the identification of the main electrolyte constituents, an assumption is first made that the influence of these minor ionic constituents is negligible.

Table 6-1: Incoming UPW plant water analysis

	Filtered (mg/l)	Total (mg/l)
Cations		
Aluminium (Al)		<0.1
Boron (B)		<0.5
Barium (Ba)		<0.1
Cadmium (Cd)		<0.1
Calcium (Ca)		93
Chromium (Cr)		<0.1
Copper (Cu)		1.7
Iron (Fe)		<0.1
Potassium (K)		1.8
Lithium (Li)		<1
Magnesium (Mg)		6.9
Manganese (Mn)		<0.1
Molybdenum (Mo)		<0.1
Sodium (Na)		10
Nickel (Ni)		<0.1
Lead (Pb)		<0.1
Antimony (Sb)		<0.1
Strontium (Sr)		0.2
Vanadium (V)		<0.1
Zinc (Zn)		<0.1
Anions		
Silicon (Si)		3.2
Fluoride (F)	1	
Chloride (Cl)	20	
Nitrite (NO2)	<0.5	
Nitrate (NO3)	13	
Sulphate (SO4)	46	
Others		**Units**
pH (at 25°C)	7.8	pH units
Conductivity (at 25°C)	580	µS/cm
M-Alkalinity ($CaCO_3$)	210	mg/l
P-Alkalinity ($CaCO_3$)	0	mg/l
Phosphate (PO_4) - Inorganic	<0.1	mg/l
Ammonium (N)	<0.1	mgN/l

The water analysis under consideration does not specify bicarbonate or carbonate ions (major anions typically found in natural waters), however, these can be determined from the M-Alkalinity and P-Alkalinity values given in Table 6-1. Alkalinity can be defined as the ability of water to "*resist changes in pH* [43]". The alkalinity measure of a natural water sample is largely determined by the carbonate system. Two measures of alkalinity are commonly used, P-Alkalinity and M-Alkalinity (the names P and M refer to the method of titration to a pH value) [48]. The ratio of P-Alkalinity to M-Alkalinity in a water sample allows the determination of the type of carbonates present in a water analysis. If the P-Alkalinity is zero, as in this instance, the quantity of bicarbonate ions in terms of calcium carbonate equivalence is given by the M-Alkalinity [48], which according to Table 6-1 is 210 mg/l. Converting from calcium carbonate equivalence in ppm to bicarbonate in ppm uses the relationship in (6.29). The equivalent weight is defined as the molar mass divided by the valence.

$$\text{ppm as } CaCO_3 = \text{ ppm as ion} \times \frac{\text{equivalent weight of } CaCO_3}{\text{equivalent weight of ion}} \qquad (6.29)$$

Conversion factors have been tabulated by Dey and Thomas for common ions, the M-Alkalinity in the incoming plant water analysis value can simply be divided by the factor specific to bicarbonate 0.82 [48]. Using this approach and assuming that at these relatively low concentrations, the ppm is equivalent to mg/l, the bicarbonate ion concentration is calculated to be 256 mg/l. This assumption is shown to be valid at the relevant concentrations and at a temperature of 25°C later in this chapter when molarity is converted to molality for the ionic strength calculations. Including the bicarbonate ion but excluding the ions with a concentration less than or equal to 1 mg/l, the TDS value of the water sample is 448.4 mg/l.

The next step is to carry out a cation/anion balance, which is a useful exercise to determine the validity of water analyses based on the principle of electrical neutrality. In the cation/anion balance the major ion quantities are expressed in terms of electrical equivalent units, termed equivalents or milliequivalents per litre, (eq/l or meq/l respectively). The concentration (mg/l) is divided by the molar mass (g/mol) to determine the molarity (mol/l), then the valence of the specific ion is multiplied by the molarity to calculate the electrical equivalent value (meq/l) [183]. To maintain electrical neutrality, the sum of the cations and the anions should balance; a percentage difference of less than 5% is considered reasonable for routine calculations [183]. The results of the cation/anion balance are shown in Table 6-2, the percentage difference between the cations and the anions is -3.71%, which is within the acceptable error limit cited in [183]. The resulting negative value indicates a surplus of anions, possibly due to the exclusion of the minor cations in Table 6-1 (values < 1 mg/l) in the cation/anion balance. Having calculated the bicarbonate concentration and the general validity of the water analysis, the proportional concentration of cations and anions can now be determined. The proportional concentration of the major cations is shown in Figure 6-3 and the proportional concentration of the major anions in Figure 6-4. As the figures show, the predominant cation is calcium which accounts for 82% of the total of major cations, and the predominant anion is bicarbonate, accounting for 76% of the major anion total.

Table 6-2: Cation/anion balance for water analysis

Main Cations	*Concentration (mg/l)*	*Molar mass (g/mol)*	*Molarity (mol/l)*	*Valence*	*Equivalents*
Calcium (Ca)	93	40.08	2.32	2	4.64
Sodium (Na)	10	23	0.43	1	0.43
Magnesium (Mg)	6.9	24.31	0.28	2	0.57
Potassium (K)	1.8	39.1	0.05	1	0.05
Copper (Cu)	1.7	63.5	0.03	1	0.03
				Sum of cations	**5.72**
Main Anions	*Concentration (mg/l)*	*Molar mass (g/mol)*	*Molarity (mol/l)*	*Valence*	*Equivalents*
Bicarbonate (HCO_3)	256	61	4.20	-1	-4.20
Sulphate (SO_4)	46	96	0.48	-2	-0.96
Chloride (Cl)	20	35.5	0.56	-1	-0.56
Nitrate (NO_3)	13	62	0.21	-1	-0.21
				Sum of anions	**-5.93**
% Difference	**-3.71**				

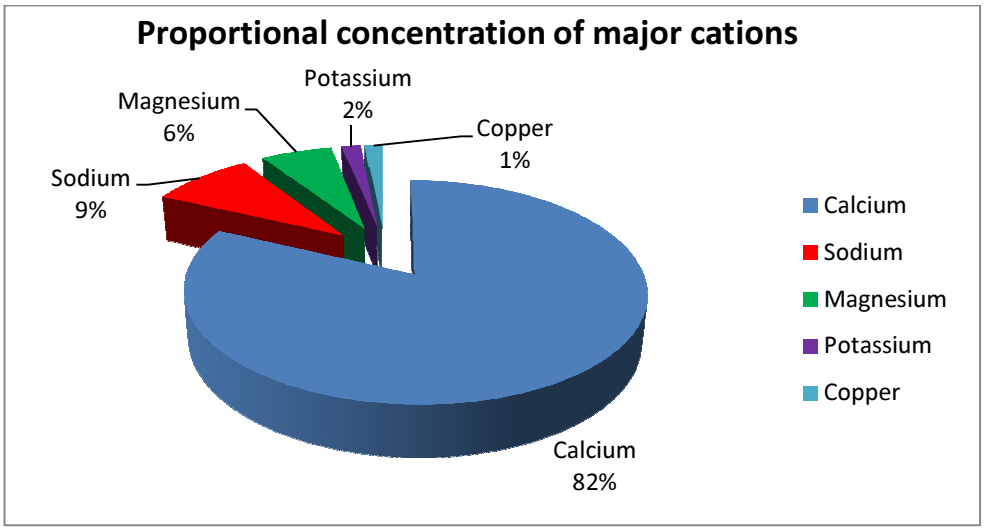

Figure 6-3: Predominant cations in UPW water analysis

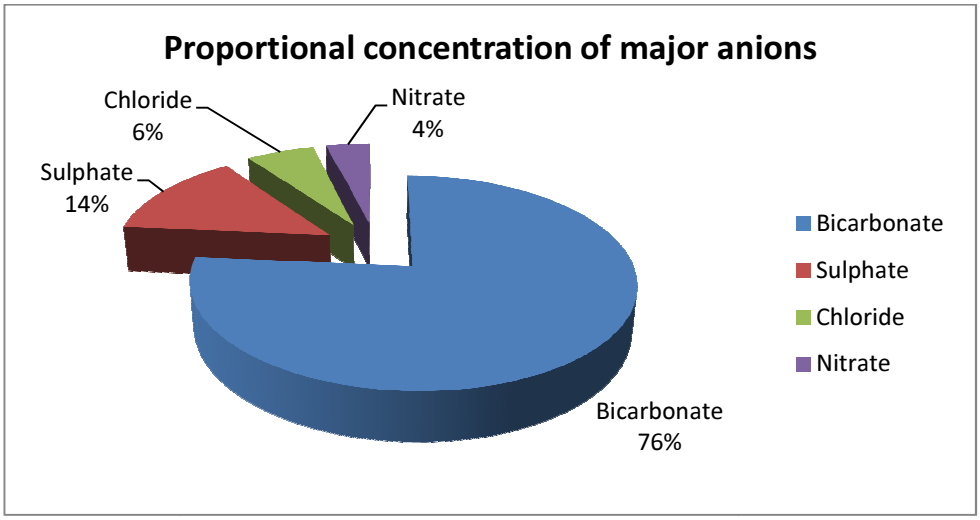

Figure 6-4: Predominant anions in UPW water analysis

Comparing the main constituents of the incoming water analysis with seawater (see Figure 6-5 and Figure 6-6), it is evident that the major constituents in both cases are different. In seawater, sodium and chloride are the most important ions whereas in the incoming water analysis, calcium and bicarbonate are the predominant ions. Based on the seawater ionic composition, it is understandable why seawater has been modelled as an ideal mixture/solution of solid NaCl and water for certain seawater exergy analyses [146, 147]. However, the Model B method of treating water as an ideal mixture of solid salt and water has also been used to perform an exergy analysis for brackish water purification [136, 137, 141]. This leads to two questions; first, is the NaCl and water model appropriate for natural waters other than seawater or should the water model reflect the constituents of the actual aqueous solution under consideration, i.e. where sodium and chloride are not the predominant ionic constituents? Second, is the use of an ideal mixture of solid salt and water appropriate when the behaviour of ideal solutions and electrolytic solutions is very different even at low concentrations [175]?

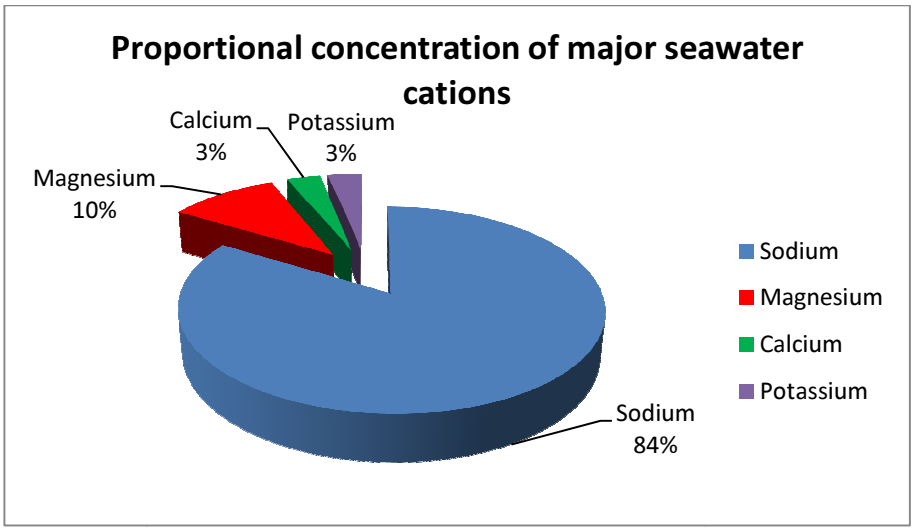

Figure 6-5: Predominant seawater cations, based on data in [170]

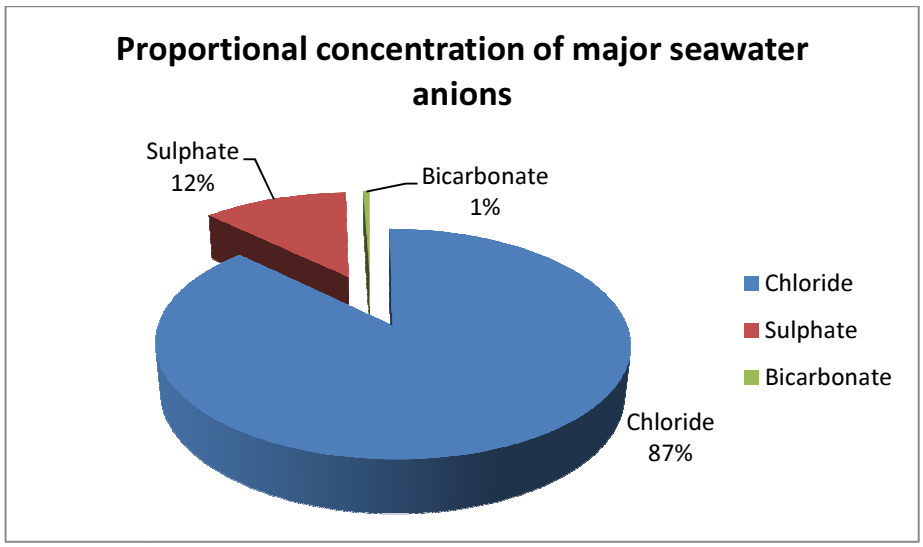

Figure 6-6: Predominant seawater anions, based on data in [170]

The first question in the preceding paragraph is relevant, but should not really be significant if the use of the ideal mixture model of solid salt and water is applicable to water plant analyses. In that event, the specific heat capacity and the molar mass of the solid salt (solid

salts) in question can be used in the model in lieu of the specific heat capacity and molar mass of solid NaCl, see Chapter 3. However, the first question becomes pertinent in light of question 2, i.e. if the ideal mixture model of solid salt and water is not suitable, because then, depending on the choice of aqueous solution model, the activity coefficients of the different constituents are different. For example, the activity coefficient of sodium, a monovalent ion, at a solution ionic strength of 0.01 M, is 0.9, however, at the same ionic strength, the activity coefficient of calcium, a divalent ion, is 0.68 [184]. The rate at which these activities change as a function of changing ionic strength is also different, and therefore, should have an effect on the exergy calculations for UPW plants as the ionic strength of the aqueous electrolyte solution changes with changing purity. These questions are addressed in Chapter 8. According to *Water Treatment: Principles and Design* [43], the activity of the electrolyte species *should* be considered but is generally ignored in water treatment applications.

6.2 Model C physical exergy term

It is expected that the physical exergy of Model C will be calculated using (5.1) based on the incompressible fluid model assumption. First, however, some other relevant assumptions are examined. Due to the fact that these water streams are much lower in salinity than seawater, the density of the streams is treated as the density of pure water. The total salt content of seawater is approximately 35,000 mg/l [5, 170] as opposed to 448.4 mg/l for the incoming UPW plant water analysis (based on the total major ion concentrations in Table 6-2). For each of these salinity values at 25 °C, the densities of the two waters are calculated as 1023.3 kg/m^3 for seawater and 997.4 kg/m^3 for the incoming

UPW plant water, the density of the incoming plant water is closely comparable to reported thermodynamic properties of pure water at the same temperature 997.05 kg/m^3 [188]. The two non-pure water density values were calculated using the density calculation function written in MATLAB, based on the UNESCO International Equation of State for Seawater [172]. Therefore, it is expected that the changing density values at various process stages will not be as relevant to the exergy calculations as in the case of seawater (this expectation is reassessed when the retentate concentrations of the UPW plant are calculated). Several researchers have used the thermodynamic properties of pure water for density and specific heat capacity calculations in river water exergy analysis [178-180].

The incompressible fluid model assumption for pure water can be examined according to the data in Table 6-3, which was adapted from the cited reference [188]. Considering density as a function of both temperature and pressure at the following operating parameters of interest, i.e. 278.15 K to 298.15 K and 1 bar to 25 bar, it is evident that there is little change in density as a function of both pressure and temperature. The percentage differences over the temperature range at constant pressure are shown in the final column of Table 6-3, and over the pressure range at constant temperature in the final row of this table. (This was further checked by estimating the total differential $d\rho(T,P) = \left(\partial\rho/\partial T\right)_P dT + \left(\partial\rho/\partial P\right)_T dP$). Hence, the density of the UPW plant water is treated as a constant, the average density over the temperature range of interest (excluding the relevant temperatures of the heating water in the hot water heat exchanger). The density of the heating water in the hot water heat exchanger is evaluated separately because of its relatively high temperature but is again evaluated as the average density over the

temperature range at 1 bar (i.e. temperatures of the incoming and outgoing heating water). The effect of increased pressure, i.e. 6 bar (typical operating pressure for the UPW plant heat exchanger), on the temperature-density relationship was investigated and was found to be negligible at these higher temperatures.

Table 6-3: Density (kg/m^3) of water as a function of temperature and pressure, adapted from NIST data in [188]

Temperature (K)	***278.15***	***283.15***	***288.15***	***293.15***	***298.15***	***% Diff. (Temperature)***
Pressure (bar)						
1	1000	999.7	999.1	998.2	997.1	0.3%
5	1000.2	999.9	999.3	998.4	997.2	0.3%
10	1000.4	1000.1	999.5	998.6	997.5	0.3%
15	1000.7	1000.4	999.8	998.9	997.7	0.3%
20	1000.9	1000.6	1000	999.1	997.9	0.3%
25	1001.1	1000.8	1000.2	999.3	998.1	0.3%
% Diff. (Pressure)	-0.1%	-0.1%	-0.1%	-0.1%	-0.1%	

The specific heat capacity of water in exergy analysis equations is often assumed to be constant within certain temperature ranges [5, 157, 178, 180], i.e. the average specific heat capacity value of water between the relevant process stream temperatures, see (5.1). This assumption facilitates the approximation of $\int_{T_1}^{T_2} c_v(T)dT$ by $c_v(T_2 - T_1)$ and $\int_{T_1}^{T_2} \frac{c_v(T)}{T}dT$ by $c_v \ln(T_2 / T_1)$. However, many of these previously cited exergy assessments took place at

constant temperature. To assess the accuracy of the constant heat capacity assumption for the UPW plant, the values of the constant volume specific heat capacity at one bar were plotted over the same temperature range as that used previously in the density analysis, see Figure 6-7. This graph shows excellent correlation with the second order polynomial equation displayed on the graph and in (6.30). The coefficient of the squared term is small, however, the values of temperature are in kelvin, and therefore, the squared term is not negligible.

$$c_v(T) = -3\times10^{-5}T^2 + 0.015T + 2.5017 \tag{6.30}$$

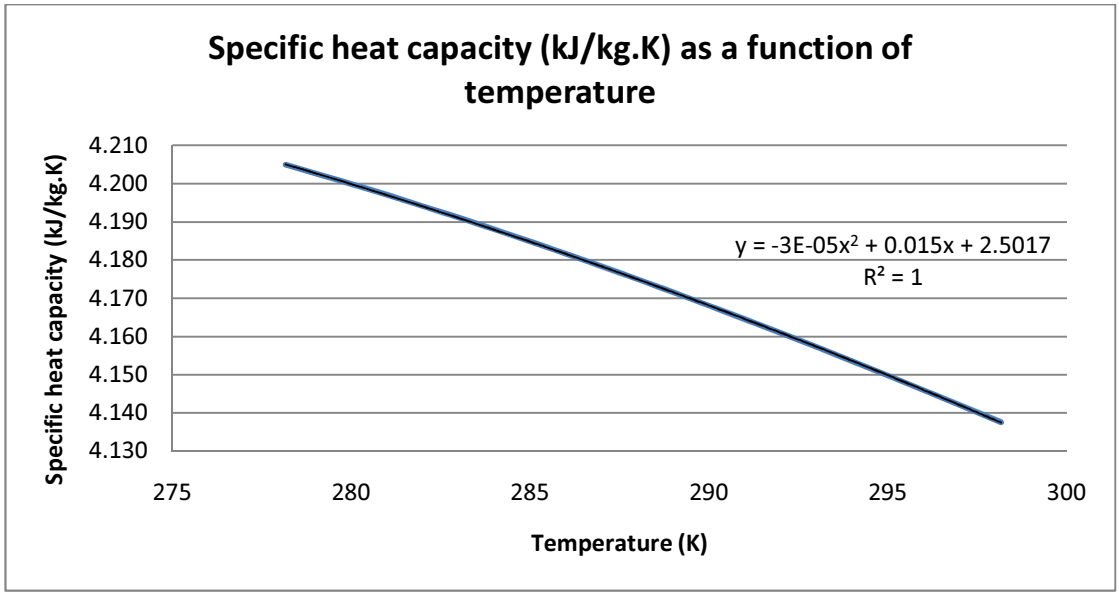

Figure 6-7: Specific heat capacity of pure water as a function of temperature, based on NIST data [188]

Integrating this function between the relevant temperatures 278.15 K and 298.15 K and comparing the results with the product of the average value of the specific heat capacity and the change in temperature, it was found that there was a 3.7% difference (86.64 kJ/kg for the definite integral versus 83.47 kJ/kg for the product average specific heat capacity

and the difference in temperature). A similar analysis was undertaken to assess the change in entropy using average values of the specific heat capacity, i.e. the change in entropy calculated using $c_v \ln(T_2 / T_1)$ versus the integration of the function $\int_{T_1}^{T_2} \frac{c_v(T)}{T} dT$, again resulting in a 3.7% difference between the two approaches. The change in specific entropy varies between 0.2898 kJ/kg.K for the average specific heat capacity and 0.3008 kJ/kg.K for the definite integral. The accuracy of the analytical integration was checked by comparing it with numerical integration programmes written in MATLAB (Simpson's rule). To reduce potential errors, the approach used to determine the relationship between the specific heat capacity and temperature shown in (6.30) is applied when calculating the physical exergy contribution (for the relevant temperatures).

Importantly, there is a possible source of confusion regarding the use of specific heat capacities, for a liquid (modelled as an incompressible substance) it is widely accepted that the specific heat capacity is termed c rather than the c_p and c_v used for gases [109, 128]. However, in thermodynamic tables, values for both c_p and c_v are reported for liquid water at standard temperature and pressure [188]. Based on the thermodynamics facilitating the breakdown of the standard exergy equation $e = h - h_0 - T_0(s - s_0)$ into (2.8), the reported values of c_v in the cited reference [188] are selected in favour of the c_p values.

In reality, the specific heat capacity of water is a function of both temperature and pressure, Figure 6-7 shows how the specific heat capacity changes over the relevant temperature range at one bar. Both temperature and pressure changes are involved in the UPW exergy analysis, for example, the heat exchangers. Variations of the specific heat capacity

(kJ/kg.K) with both temperature and pressure are illustrated in Table 6-4. The final column and row of this table show respectively, (1) the percentage differences between the specific heat capacity at 278.15 K and the specific heat capacity at 298.15 K at constant pressure, and (2) the percentage differences between the specific heat capacity at 1 bar and the specific heat capacity at 25 bar at constant temperature. It is evident that the specific heat capacity varies more significantly with temperature than with pressure. For an incompressible fluid $c_v = c(T)$ [109] and this is largely supported by the data shown in Table 6-4.

Therefore, based on the analysis of the data in Figure 6-7, Table 6-3 and Table 6-4, the assumptions that the UPW plant water can be modelled as an incompressible fluid are valid, two possible exceptions being the heating water in the UPW plant hot water heat exchanger and the density of the RO retentate streams, which are assessed in due course. The effect of the other salinity values on density is not expected to be significant. However, the assumption that the specific heat capacity can be treated as an average value over the temperature range can result in errors. Over the relevant temperature ranges, the specific heat capacity will be treated as a function of temperature and integrated to determine the Model C physical exergy values. Although not considered in great detail in this thesis, ideally, the specific heat capacity of pure water should be compared to the relevant electrolytic solution (at the relevant concentrations of the specific ionic species). This requires further research.

Table 6-4: Specific heat capacity (kJ/kg.K) at constant volume as a function of both temperature and pressure, adapted from data in [188]

Temperature(K)	***278.15***	***283.15***	***288.15***	***293.15***	***298.15***	***% Diff. (Temperature)***
Pressure (bar)						
1	4.205	4.191	4.174	4.157	4.138	1.6%
5	4.203	4.189	4.173	4.155	4.136	1.6%
10	4.201	4.187	4.171	4.154	4.135	1.6%
15	4.199	4.185	4.169	4.152	4.133	1.6%
20	4.197	4.183	4.167	4.150	4.131	1.6%
25	4.195	4.181	4.165	4.148	4.130	1.5%
% Diff. (Pressure)	0.2%	0.2%	0.2%	0.2%	0.2%	

6.3 Model C chemical exergy term

Regarding the Model C chemical exergy equations, for the purposes of practicality, certain assumptions must be made, which in this research are driven primarily by one major constraint, point 1 below and to a lesser extent by point 2;

1. The practical plant measurement limitations;
2. Activity coefficient calculation complexity versus the model accuracy.

First, consider point 1; the main method of measuring the purity of the water in UPW plants is in terms of electrical conductivity measurements. It is not practical to perform detailed water analyses at various process stages.

According to some authors [48, 157], electrical conductivity measurements can be used to estimate the TDS in a water sample using an approximate correlation between conductivity and TDS ($TDS(mg/l) = Conductivity(\mu S/cm) \times 0.64$). However, the relationship between the electrical conductivity at 25 °C reported in Table 6-1 (580 $\mu S/cm$) and the TDS value 448.4 mg/l obtained by summing the ion concentrations in Table 6-2 (including the bicarbonate ion but excluding minor ions) does not obey this relationship. In this specific case, the ratio of the TDS to the electrical conductivity is 0.773. According to Sawyer et al. [189], the ratio linking electrical conductivity and TDS can vary from 0.55 to 0.9. Application of the commonly used 0.64 ratio in this instance results in an under-estimation of the TDS value by 17.2%. The reason for this is that electrical conductivity measurement depends not only on the concentration of the ions (mg/l), but importantly, it depends on the specific ions present (and the relevant temperature) [190]. Thus the blanket application of the 0.64 factor to relate electrical conductivity and TDS without attempting to take account of the specific ionic species present in the water sample may result in significant errors.

To account for the varying contribution of individual ions to the overall electrical conductivity measurement, the major ions in natural water have been ascribed conductivity factors (µS/cm per mg/l) based on their individual abilities to conduct electrical current, these values, obtained from a United Nations Environment Programme (UNEP) manual [190] are listed below;

- Cations
    - Ca^{++} (2.6); Mg^{++}(3.82); K^{+}(1.84); Na^{+}(2.13);
- Anions

- HCO_3^-(0.715); Cl^-(2.14); SO_4^{--}(1.54); NO_3^-(1.15);

The summation of the product of the concentration of each ion (mg/l) and the conductivity factor (μS/cm per mg/l) of the respective ion can be used to approximate the electrical conductivity of the incoming water analysis. When applied to the major ions in Table 6-2 (excluding copper as no value was available in the cited reference [190]), the percentage difference between the measured electrical conductivity value (580 μS/cm at 25°C) and the approximated value using conductivity factors (604.4 μS/cm at 25°C) was calculated to be 4%. Hence, this approach provides a reasonably accurate method of calculating the electrical conductivity from the ions present.

Ionic molar conductivity values at 25 °C ($S.cm^2/mol$) have been published in the literature [186, 189]; these values when multiplied by the molarity of the ions (mol/cm^3) also determine the conductivity contribution of the individual ions (S/cm at 25°C). However, in contrast to the UNEP conductivity factors, ionic molar conductivity values are determined at infinite dilution, i.e. when the current carrying ability of the ions is not affected by other ions in the solution. Infinite conductivity factors (similar to the UNEP conductivity factors) can be developed from molar conductivity values (the molar conductivity divided by the molar mass of the ionic species). The UNEP conductivity factors and the infinite dilution conductivity factors (developed from the molar conductivity values cited in [186, 189]) are compared in Table 6-5. According to Table 6-5, the conductivity factors of calcium, magnesium and sulphate exhibit the greatest change between infinite dilution and the dilution used to determine the UNEP conductivity factors (percentage differences of 11.7%,

12.5% and 7.4% respectively), this is due to their greater likelihood of forming ion pairs, thus reducing electrical conductivity.

Table 6-5: Comparison of conductivity factors

Ionic species	***Molar conductivity (S.cm^2/mol)***[186, 189]	***Conductivity factor at infinite dilution (µS/cm per mg/l)***	***UNEP Conductivity factor (µS/cm per mg/l)***[190]
Ca^{++}	118	2.94	2.6
K^{+}	73.5	1.88	1.84
Mg^{++}	106.1	4.37	3.82
Na^{+}	50.1	2.18	2.13
Cl^{-}	76.3	2.15	2.14
NO_3^{-}	71.4	1.15	1.15
SO_4^{--}	159.6	1.66	1.54
HCO_3^{-}	44.5	0.73	0.716

When the infinite dilution conductivity factors were used to estimate the electrical conductivity of the incoming plant water, the value was calculated to be 650 µS/cm at 25°C, a percentage difference of 10.8% between the summation of the infinite dilution conductivities and the measured electrical conductivity value. The reason for this over-estimation of the electrical conductivity is due to the fact that in real solutions, for certain electrolytes, ion pairing takes place, and consequently, the measured conductivity is less than the theoretical conductivity value determined at infinite dilution. Relevant conductivity factors can aid in assessing the validity of simplifications made to model the UPW plant water streams.

To model an electrolytic solution using an electrical conductivity measurement when one does not have regular, accurate, water analyses requires certain approximations. A full breakdown of ionic species is very difficult to extrapolate from one electrical conductivity measurement. Thus, the author proposes the following method;

- The TDS value is estimated from the electrical conductivity measurement using the 0.773 factor previously determined: without regular water analyses, an assumption is made that the major ionic species in the water do not vary greatly over time;
- Due to the difficulty of extrapolating several electrolytes from one conductivity measurement, a second assumption is made that the sole ionic species is the electrolyte calcium bicarbonate ($Ca(HCO_3)_2$ (the main ionic species in the incoming water analysis were calcium and bicarbonate ions);
- Calcium bicarbonate does not exist as a common electrolyte but only as the dissociated ionic species calcium and bicarbonate ions, consequently, the concentration of the separate ions in the electrolyte is apportioned on the basis that one mole of calcium ions and two moles of bicarbonate ions combine to form one mole of the calcium bicarbonate electrolyte (molar mass 162.1 kg/kmol). Mass is conserved, and therefore, an aqueous solution consisting of 448.4 mg/l of the calcium bicarbonate electrolyte contains 110.9 mg/l of calcium ions (40.1/162.1 multiplied by 448.4 mg/l) and 337.5 mg/l of bicarbonate ions (2(61)/162.1 multiplied by 448.4 mg/l).

The concentrations of calcium and bicarbonate detailed in the last bullet point naturally differ from the measured values in Table 6-1 and Table 6-2. The relationship of interest, however, is that between the concentration (mg/l) of the relevant ions and the electrical

conductivity. This poses an important question which requires investigation: will modelling the consistency of the incoming water solely as calcium and bicarbonate ions result in large errors in electrical conductivity estimations?

When the UNEP conductivity factors of the calcium and bicarbonate ions (2.6 and 0.715 respectively [190]) are multiplied by the proposed ionic concentrations of calcium and bicarbonate ions (110.8 mg/l of calcium ions and 337.6 mg/l of bicarbonate ions), the electrical conductivity is estimated to be 529.6 μS/cm, an absolute percentage difference of 9.5% compared with the measured conductivity value of 580 μS/cm at 25°C in Table 6-1. However, if the contribution of the calcium and bicarbonate ions to the electrical conductivity is calculated using the infinite dilution conductivity factors of Table 6-5, 2.94 and 0.73 respectively, the percentage difference drops to an absolute value of 1.4% (572.2 versus 580 μS/cm at 25°C). This result would imply that the infinite dilution factors are more appropriate than the UNEP conductivity factors in this case. This is reasonable due to the strong dissociation of the calcium and bicarbonate ions in natural waters thus reducing the need for the lower UNEP conductivity factors to estimate electrical conductivity values. Therefore, for this water analysis, it is reasonable to model the TDS as calcium and bicarbonate ions if the infinite dilution conductivity factors are used.

Interestingly, if the TDS value was apportioned between sodium and chloride ions in the same manner and the relevant concentrations were multiplied by the sodium and chloride UNEP conductivity factors the percentage difference between estimated and measured electrical conductivity would be 26.9% (792.9 μS/cm at 25°C versus 580 μS/cm at 25°C).

A relationship linking the electrical conductivity and the concentration of calcium and bicarbonate ions can be developed, based on the infinite dilution conductivity factors, see (6.31), where C is the concentration (mg/l), MW is the molar mass (kg/kmol), CF is the infinite dilution conductivity factor ($\mu S/cm$ per mg/l) (see Table 6-5) and EC is the electrical conductivity ($\mu S/cm$). The factor of two relates to the stoichiometric number of bicarbonate ions, the subscripts refer to the ionic species calcium and bicarbonate and the electrolyte calcium bicarbonate.

$$C_{Ca(HCO_3)_2}\left[\frac{MW_{Ca^{++}}}{MW_{Ca(HCO_3)_2}}(CF_{Ca^{++}})+\frac{2MW_{HCO_3^-}}{MW_{Ca(HCO_3)_2}}(CF_{HCO_3^-})\right]\approx EC\ (\mu S/cm) \quad (6.31)$$

Inserting the relevant values, (6.31) simplifies to (6.32).

$$1.28C_{Ca(HCO_3)_2}\approx EC\ (\mu S/cm) \quad (6.32)$$

In the case of RO membranes the use of the membrane manufacturers' rejection rates can also be considered to estimate TDS at various process stages when available although this tends to be proprietary information (average ionic rejection rates of 99.5% are typically quoted). This rejection rate method was used by Drioli et al. [5] for a seawater desalination process. It was notable in the cited reference, that the potassium ion was neglected in the exergy analysis, possibly due to a lack of membrane rejection rates for potassium. However, there is one key drawback in the use of nominal rejection rates as a sole indicator of TDS; the rejection rates change with respect to changes in key RO operating parameters such as recovery rate, temperature, pressure and feedwater concentration, see Figure 2-9. Rejection rates also vary according to the specific membrane (and tend to be higher for divalent ions than monovalent ions). If detailed RO rejection data and water analyses are

available, then ideally, this approach could be used in tandem with the electrical conductivity measurement (to serve as an accuracy check). In this thesis, the method outlined previously to convert electrical conductivity measurements to TDS is used because it is the most reliable indication of TDS from the UPW plant.

Now consider point 2 (page 159), the choice of aqueous solution model has a significant effect on the activity coefficient calculation complexity; the more complex the modelled electrolyte solution, the more complex the activity coefficient calculation. Several modelling choice examples are listed below and these require the exclusion or inclusion of various terms which are discussed presently;

(1) Various models can be chosen based on the strength of the electrolyte, i.e. the extent of dissociation;
(2) The aqueous electrolytic solution can be modelled as symmetric (e.g. electrolyte pairs with equal valences such as Na^{+} and Cl^{-}, considered 1:1);
(3) The aqueous electrolytic solution can be modelled as asymmetric (e.g. Ca^{++} and HCO_3^{-} (1:2));
(4) The aqueous electrolytic solution can be modelled as pure (only one paired electrolyte, e.g. Na^{+} and Cl^{-} or Ca^{++} and HCO_3^{-});
(5) Multi-component with a shared ion (e.g. Na^{+} and Cl^{-} and Mg^{++} and Cl^{-});
(6) Multi-component with non-shared ion (e.g. Na^{+} and Cl^{-} and Mg^{++} and SO_4^{--});
(7) Multi-component with electrolytes and non-electrolytes. [175, 191-198]

These more complex modelling choices require a Debye-Huckel type term (the first term in (6.22) to (6.25)), which accounts for the long-range ionic interactions, and several virial

coefficient terms, which account for the short-range interactions between ions of opposite sign, like sign and neutral species.

Ideally, industry requires the simplest model which adequately reflects the behaviour of the aqueous solution. To determine this the ionic strength of the solution must be calculated; the ionic strength can be calculated using (6.21). The results are shown in Table 6-6. According to Table 6-6, the ionic strength of the UPW incoming plant water is equal to 0.00893 M. For comparison purposes, the ionic strength was also calculated using molarity instead of molality, and negligible difference was found at the relevant concentration and a temperature of 25°C (0.00893 M using molality to calculate the ionic strength and 0.00891 M using molarity values). When the solution was modelled as a simplified solution consisting of calcium and bicarbonate ions as discussed previously, the ionic strength was calculated to be 0.00832 M. Hence, the simplification of the electrolytic solution does not have any bearing on the selection of activity coefficient calculation model.

The ionic strength of the incoming UPW plant water is 0.00893 M, which is considerably less than the ionic strength of seawater (a TDS of 35,000 mg/l) of approximately 0.7 M [170, 183]. These values of ionic strength are very important because they are used to determine the most appropriate activity coefficient calculation method. Based on the calculated ionic strength value of 0.00893 M, the activity coefficients can be calculated using a selection of equations (6.22) to (6.25).

However, the use of (6.22) requires some further consideration. According to an analysis of the range of validity for Debye-Huckel theory in *Thermodynamics* [175], the limiting values cited in Stumm and Morgan [184] may not be appropriate for ions other than monovalent electrolytes due to ion pairing (the association of polyvalent ions) and the resulting invalidity of Debye-Huckel theory assumptions.

To minimise potential errors (6.22) is not considered further, even though it appears to be relevant at the ionic strength value calculated for the incoming plant water. The model chosen to calculate the activity coefficients for the UPW plant exergy analysis is the Davies model [185] for one main reason; errors in accuracy have been quantified in the literature for the Davies model allowing reasonable confidence in the results (1.5% at < 0.1 M [186]).

Table 6-6: Ionic strength of incoming UPW plant water

Anions/ Cations	*Concentration (mg/l)*	*Molar mass (g/mol)*	*Molarity (mol/l)*	*Density of solution (kg/m^3)*	*Mass fraction of water (kg/kg)*	*Molality (mol/kg)*	*Valence squared (z_i^2)*	*$m_i z_i^2$*
Calcium (Ca)	93	40.08	0.00232	997.4	0.99955	0.00233	4	0.00931
Sodium (Na)	10	23	0.00043	997.4	0.99955	0.00044	1	0.00044
Magnesium (Mg)	6.9	24.31	0.00028	997.4	0.99955	0.00028	4	0.00114
Potassium (K)	1.8	39.1	0.00005	997.4	0.99955	0.00005	1	0.00005
Copper (Cu)	1.7	63.5	0.00003	997.4	0.99955	0.00003	1	0.00003
Bicarbonate (HCO_3)	256	61	0.00420	997.4	0.99955	0.00421	1	0.00421
Sulphate (SO_4)	46	96	0.00048	997.4	0.99955	0.00048	4	0.00192
Chloride (Cl)	20	35.5	0.00056	997.4	0.99955	0.00057	1	0.00057
Nitrate (NO_3)	13	62	0.00021	997.4	0.99955	0.00021	1	0.00021
Total (mg/l)	**448.4**					**Ionic strength**	**$0.5\Sigma m_i z_i^2$**	**0.00893**

In the literature the use of (6.22) has been proposed for determining the activity coefficients in seawater due to the fact that seawater is deemed a good example of a diluted solution [157]. However, according to Stumm and Morgan's [184] analysis of various activity coefficient calculation models, this is not a suitable calculation model based on the ionic strength of seawater (0.7 M). Importantly, based on the ionic strength of seawater, none of the equations (6.22) to (6.25) is suitable. This is further supported by Millero [170] who states that even the extended Debye-Huckel law (i.e. (6.23)) "*serves as a limit in dilute solutions; however it fails at the high ionic strength of seawater…*". Model failure at the ionic strength of seawater is due to deviations that occur from the initial assumptions at higher ionic strength and hydration effects [170]. Values of seawater ionic activity coefficients are compared in Table 6-7, which shows, (1) measured values of activity coefficient [119], (2) values calculated using the extended Debye-Huckel model (6.23) [119], and (3) values calculated using the Pitzer model (discussed in section 6.5) [121]. It is evident that there is good correlation between the measured values and the Pitzer model for most species, the carbonate ion being the major exception, although it is noted that there is a slight difference in the ionic strength values (0.7 M for the measured values versus 0.68 M for the Pitzer model values). The Debye-Huckel extended model differs from the measured values more so for the divalent metal ions than the monovalent metal ions.

Table 6-7: Seawater ionic activity coefficients, based on data in [119, 121]

Ion	*Measured values at I=0.7M*	*Pitzer Model at I=0.68 M*	*Debye-Huckel extended Model at I=0.7 M*
Na^{+}	0.68	0.653	0.71
Mg^{++}	0.23	0.236	0.36
Ca^{++}	0.21	0.211	0.28
K^{+}	0.64	0.614	0.64
Cl^{-}	0.68	0.703	0.64
$SO4^{--}$	0.11	0.128	0.17
$HCO3^{-}$	0.55	0.559	0.68
$CO3^{-}$	0.02	0.045	0.2

It is important to consider the choice of activity coefficient calculation model carefully. More suitable general equations for higher concentrations are detailed in the literature [191-193, 195, 197, 198] and researchers have determined suitable activity coefficients for seawater based on these and other appropriate activity coefficient calculation models [170, 199, 200]. Thus, a different approach for the calculation of activity coefficients should be adopted for seawater exergy analyses than the method that is proposed for UPW plant analysis.

6.4 Proposed Model C approach

For the Model C physical and chemical exergy terms, the methodology, calculation procedure, assumptions and modelling decisions can now be summarised as follows;

1. The incoming UPW plant water analysis is studied to determine the principal ionic species – cations and anions;
2. Specifically, as a result of the incoming water analysis, the UPW plant water is

modelled as an electrolytic solution consisting of calcium and bicarbonate ions, the relationship $TDS = 0.773 \times \mathrm{EC}$ is used to convert electrical conductivity measurements ($\mu S / cm$) to TDS (mg/l) of calcium bicarbonate;

3. The incompressible fluid model is assumed. The density of the plant water is treated as a constant (i.e. the average density over the relevant temperature range) and not a function of salinity for the purposes of calculating the physical exergy and the molalities (and hence the ionic strength). The heating water in the hot water heat exchanger is the only exception due to its relatively high temperature, it too is considered as a function of temperature alone;
4. The specific heat capacity of water is treated as a function of temperature where applicable;
5. Equation (6.19) is used to calculate the molar chemical exergy for the solute (electrolyte) at each relevant process stage;
6. The mole fractions of the electrolytic species and water are calculated using the approach of (6.16) and (6.17), and not that of Model B (refer to Chapter 3, section 3.2.2);
7. The activity coefficient of water is assumed to be unity and the chemical exergy of water at each relevant process stage is calculated using (6.20), thus, the activity of water is assumed to be equivalent to its mole fraction;
8. The choice of activity coefficient calculation model is primarily determined from the ionic strength of the electrolytic solution but also from the specific characteristics of the ions under consideration, e.g. valency and ion association likelihood;

9. Based on point 8, the activity coefficients in this specific case are calculated using the Davies model, see (6.25);
10. The coefficient *A* in the Davies model is acknowledged to be and treated as a function of temperature as it involves both an explicit temperature term and a dielectric constant term which is also a function of temperature, see (6.26) and (6.28). Variations of the coefficient *A* with temperature are tabulated in [175], but can be determined over a more precise temperature range using (6.26) and (6.28).
11. The system is defined as the UPW electrolytic solution stream;
12. The thermo-mechanical dead state is defined as the ambient temperature of the incoming UPW process water and pressure of 1 bar.
13. The salinity dead state is defined as an aqueous solution comprising 135 ppm of calcium bicarbonate (the TDS in river waters varies from 70 to 200 ppm, the average value is selected, calcium and bicarbonate ions are the main ionic species in European rivers [170]);

Regarding the salinity dead state, it was originally planned to use a water analysis from a location near the discharge points of the waste water treatment plant into the River Liffey, contact was made with the Osberstown waste water plant personnel and a water analysis was forwarded to the author. However, unfortunately, the analysis mainly focused on potential organic pollutants and did not contain the necessary ionic breakdown to determine TDS.

6.5 Seawater activity coefficient calculation

The methodology has been outlined for the UPW plant chemical exergy calculations. Due to the higher ionic strength of seawater, the use of the Davies model to calculate the activity coefficients is not appropriate and a different approach is required for seawater.

In the literature, the determination of seawater activity coefficients, activity coefficient calculation methods can be broken down into two main approaches, (1) a specific ion interaction model, and (2) an ion pairing model [170]. The specific interaction models are reliable for calculating the major ionic constituents and the ion pairing method is reliable for calculating the minor ionic components [170]. First, consider an overview of the specific interaction and ion pairing models.

The Pitzer models are specific interaction models and are reliable for the calculation of activity coefficients in various electrolyte solutions including seawater; they are reliable far beyond the ionic strength of seawater. Depending on the model used, the Pitzer equations can be used over the entire concentration range [197, 198]. They are semi-empirical however, and consist of a Debye-Huckel term which accounts for the long-range interionic effects and several virial terms to account for short-range ionic interactions. The calculation of these virial terms involves the use of several parameters including specific ion interaction terms that are fitted to measured values of various electrolyte solutions.

Bromley [201, 202] developed a model to calculate the activity coefficients of strong electrolytes (ions that dissociate fully) to an ionic strength value of 6 M using only one

additional parameter ("*B value*") to the typical Debye-Huckel term. This parameter or "*B value*", specific to various salts and ions, was tabulated in the cited reference (again fitted to data for strongly ionised salts). The model proposed by Bromley is limited and is not suitable for certain electrolytes such as bivalent metal sulphates ($CaSO_4$ and $MgSO_4$), which are common in seawater, due to their incomplete ionisation and thus they cannot be considered strong electrolytes. To treat multi-component solutions, Bromley suggested the use of a single complex salt with a characteristic parameter value, which could be calculated from the specific parameters of the relevant ions in the multi-component solution.

Unfortunately, in order to extend the use of either the Pitzer or Bromley specific interaction models to natural waters, the specific interaction models were limited because suitable parameters for bicarbonate, a major ion in natural waters, were not presented. Specific interaction parameters for this ion are necessary to facilitate calculation of the activity coefficients. Pitzer et al. [203] later addressed the lack of bicarbonate parameter data by determining ion interaction parameters for $Mg(HCO_3)_2$ and $Ca(HCO_3)_2$. The interaction parameters of $Mg(HCO_3)_2$ and $Ca(HCO_3)_2$ were calculated on the basis of mixed solutions dominated by chloride in electrochemical cells, which the authors advocated, were appropriate for seawater due to chloride being the major cation.

Millero [170, 204] used the ion pairing method to calculate the activity coefficients of various solutes in natural waters. The ion pairing method, used typically by marine chemists, calculates the total activity coefficient of an ion in solution as a function of the

product of the activity coefficient of the free ion in the solution and the ratio of the concentration of the free (uncomplexed) ion in the solution to the total concentration of the ion in the solution, see the cited reference [170] for a worked example for the major components of seawater. However, the ion pairing model has limitations and is not reliable at ionic strengths greater than 1 M [170]. The Pitzer equations are suitable for a wide range of ionic strengths and compositions, and in the cited work [170], the use of the Pitzer equations is demonstrated for the calculation of the activity coefficients of a generic cation and anion in a simplified seawater medium (Mg^{++}, Na^{+}, Cl^{-} and SO_4^{--}). Activity coefficients can be calculated based on a full seawater medium or a simplified seawater medium (e.g. Mg^{++}, Na^{+}, Cl^{-} and SO_4^{--}), the activities of the main salts have been tabulated for both in Table 6-8, which is based on data in [170]. As shown in Table 6-8, the use of the simplified medium results in little difference in activity coefficient calculated for the major ions, strongly favouring the use of the simpler model, bicarbonate is the notable exception (a 6.9% difference). This deviation can be explained by the difference in the way bicarbonate interacts with, (1) the many constituents of seawater, and (2) the limited sodium chloride/magnesium sulphate medium. Bicarbonate is not the predominant ion in seawater, however, and thus, this 6.9% deviation can be neglected.

Table 6-8: Activity coefficients of the major ions in seawater calculated for various media, based on data in [170]

Ion	*NaCl and $MgSO_4$*	*Seawater*
Na^+	0.668	0.667
K^+	0.629	0.628
Mg^{++}	0.240	0.240
Ca^{++}	0.215	0.215
Cl^-	0.668	0.667
HCO_3^-	0.597	0.556
SO_4^{--}	0.115	0.113

Based on the non-ideal behaviour of electrolytes, future desalination exergy analyses in seawater applications should consider the use of seawater activity coefficients rather than the traditional ideal mixture approach. In recent years, much work has been carried out in the field of modelling electrolyte solution activities and the application of this research to seawater exergy analyses is strongly recommended.

6.6 Summary

This chapter has investigated the thermodynamics of the chemical exergy term and determined the most appropriate choice for electrolytic solutions. A thorough and accurate approach has been developed for the exergy analysis of the UPW plant using this chemical exergy term (Model C). The Model C exergy calculation terms are separable. The physical exergy definition is similar to the Model A physical exergy term except that the specific heat capacity is not treated as a constant but as a function of temperature over the relevant temperature ranges. However, the chemical exergy term is different to both Model A and

Model B. Importantly, Model C not only determines the exergy calculation terms but how the UPW aqueous streams are modelled.

Following a detailed assessment of the UPW plant incoming water analysis, the system was modelled as an electrolytic solution of calcium and bicarbonate ions. A specific conductivity factor of 0.773 was determined to relate TDS and electrical conductivity for the exergy analysis.

An approach to calculate the activity (incorporating activity coefficients, molality and mole fractions) of the relevant species was outlined. Regarding the solutes, the chemical exergy term uses activity coefficient values calculated using the Davies model. The choice of activity coefficient calculation model was determined by calculating the ionic strength of the solution under consideration 0.00893 M (UPW plant incoming water).

Due to the relatively high ionic strength of seawater (0.7 M), the Davies and the Debye-Huckel models are not suitable for the calculation of seawater activity coefficients. However, this chapter also considered and recommended the application of the more accurate Pitzer models for the calculation of activity coefficients in seawater desalination exergy analyses.

7 Model D

Chapter 7 details the development of Model D, an approach based on the Szargut model to calculate the chemical exergy of electrolytic solutions. The Szargut model is different from Models A, B and C because it takes a global natural capital view and calculates the chemical exergy of each substance with respect to the most likely, final interactions of that substance and the environment. Commonly in exergy analyses, standard chemical exergy values are used, and these values are calculated from a standard dead state reference. However, based on the literature reviewed, no research has investigated whether these standard chemical exergy values are appropriate for the exergy analyses of systems modelled as electrolytic solutions (e.g. water purification processes) at various dead state temperatures and other non-standard states. This chapter, (1) develops a method to calculate the chemical exergy of ions and electrolytes at non-standard dead state temperatures, and (2) investigates the changes in chemical exergy of the ionic/electrolytic species with respect to standard dead state temperatures.

7.1 Reference datum levels for the elements

The Szargut model and its use of reference datum levels and reference species to calculate the chemical exergy of the elements was introduced in Chapter 2. The Szargut model seeks to standardise the calculation of chemical exergy with respect to the reference environment. The rules of standardisation for open systems are reproduced here from the cited reference [116];

- "*If the processes under consideration are chemical, the reference level should be adopted separately for each chemical element taking part in the chemical reactions. If in the process a component is taking part, whose chemical constitution is constant (e.g., a solvent having unchanged chemical constitution), the reference level can be separately adopted for such a component.*
- *As reference species for the calculation of exergy, the common components of the environment should be adopted.*
- *The mean parameters of the conventionally adopted common components of the environment, in the location under consideration (i.e., the ambient temperature, the partial pressure in the air, or the concentration in seawater or in the external layer of the earth's crust) should be taken as the zero level for the calculation of chemical exergy.*
- *If an exact calculation of the chemical exergy is impossible because of the lack of sufficiently exact thermodynamic data, the calculation should be made with currently available data and the result should be accepted as a conventional standard value of the chemical exergy of the element under consideration.*"

Each element or substance is allocated a reference datum level, i.e. the atmosphere, lithosphere or hydrosphere. A reference species is allocated according to Szargut's criterion as discussed previously in the literature review. The chemical exergy of the reference species is calculated independently [93], i.e. it does not depend on the chemical exergy of other substances. The chemical exergy of the element or substance under consideration can then be calculated by formulating a reference reaction (see (2.21)) using only reference

species and the substance in question. As will become apparent, this is strictly only the case for the atmosphere and lithosphere reference datum levels, the hydrosphere requires a different approach, which is discussed later in this chapter. Due to the fact that each new elemental chemical exergy calculation depends on previously calculated reference substance chemical exergy values, there is, by necessity, a 'calculation order'. For example, the chemical exergy of the reference species in the atmosphere should be calculated first: the chemical exergy of species such as water vapour ($H_2O(g)$) and carbon dioxide (CO_2) is determined from their respective partial pressures in the environment. Using reference reactions, these chemical exergy values can in turn be used to calculate the chemical exergy of the elements hydrogen and carbon respectively, which subsequently serve as constituents for the exergy calculation of compounds using (7.1).

$$\overline{e}^{Ch\,\circ}_{Compound} = \Delta_F \overline{g}^{\circ} + \sum_{e} v\overline{e}^{Ch\,\circ} \tag{7.1}$$

In (7.1) $\overline{e}^{Ch\,\circ}_{Compound}$ is the standard molar chemical exergy of the compound under consideration, $\Delta_F \overline{g}^{\circ}$ is the standard Gibbs energy of formation of the compound, v is the stoichiometric coefficient of each element in the compound and $\overline{e}^{Ch\,\circ}$ is the standard molar chemical exergy of each element, the subscript e refers to each of the elements under consideration. Rivero and Garfias [121] mapped the calculation order for the elements and showed the relationships and dependencies of all the elemental chemical exergy calculations on previously calculated values of chemical exergy.

To facilitate the undertaking of exergy balance calculations, Szargut introduced the concept of standard chemical exergy [116]. As a result, the standard chemical exergy values could

be tabulated and used in exergy balances without the need to formulate a reference reaction in order to calculate the chemical exergy of the species of interest. Although the concept of standard chemical exergy and the tabulation of values are of great help for processes which occur at similar temperature and pressure, this is not the case for many other processes. According to some authors [95], slight differences about the standard values can be neglected. The term 'slight differences', however, is ambiguous. When do dead state temperature changes cease to be negligible? Later in this chapter, the chemical exergy of aqueous solutions as a function of changing dead state temperatures is investigated. First, in order to use or amend the standard chemical exergy values, an understanding of the chemical exergy calculation method is necessary.

7.1.1 The atmosphere as a reference datum level

The chemical exergy of reference species of elements such as nitrogen or substances such as carbon dioxide and water vapour, are relatively simple to calculate using the ideal gas model previously discussed in Chapter 6. The standard chemical exergy of these substances is a function of the standard temperature and the conventional mean ideal gas partial pressure in the environment and is calculated using (7.2).

$$\overline{e}_i^{Ch\,\circ} = -RT^{\circ} \ln \frac{P_i^{\circ}}{P^{\circ}} = -RT^{\circ} \ln x_i^{\circ} \qquad (7.2)$$

In (7.2) P° is the standard pressure defined as $1.01325 \times 10^5 Pa$, and P_i° is the conventional mean ideal gas partial pressure in the atmosphere, T° is the standard temperature (298.15 K) and x_i° is defined as the standard conventional mole fraction of i in the atmosphere and R is the universal gas constant (0.0083145 kJ/mol.K).

When the reference species are not elements, for example, in the cases of carbon dioxide or water vapour, the calculated chemical exergy of the reference species can be used to calculate the standard chemical exergy of the element, carbon or hydrogen in this case, using a reference reaction.

To illustrate the method, consider the chemical exergy of hydrogen gas with its reference species water vapour. With standard conventional mean partial pressure in the atmosphere of 0.022 bar [116], the standard chemical exergy of water vapour is calculated to be 9.49 kJ/mol. Then, to calculate the chemical exergy of the element hydrogen, a reference reaction must be formulated, see (7.3) below.

$$H_2 + \frac{1}{2}O_2 \rightarrow H_2O \tag{7.3}$$

The reference reaction by definition contains only the substance under consideration, the specific reference species for that substance, and other reference species, whose chemical exergy has been previously calculated. The general reference reaction equation (2.21) is adapted for this specific reference reaction in (7.4).

$$\overline{e}_{H_2}^{Ch\,\circ} = -\Delta_R \overline{g}^{\circ} + \overline{e}_{H_2O}^{Ch\,\circ} - \frac{1}{2}\overline{e}_{O_2}^{Ch\,\circ} \tag{7.4}$$

The Gibbs energy for the reaction is calculated to be -228.57 kJ/mol, thermodynamic values for the enthalpy of formation and molar entropy were taken from Appendix B of the cited reference [176]. When considering chemical reactions, the molar values of enthalpy and entropy are the standard molar enthalpy of formation $\Delta_F \overline{h}^{\circ}$ and the standard molar entropy $\overline{s}^{\circ}$ for the species under consideration. The Gibbs energy for the reaction can be

calculated using (7.5) which is defined as the difference in the molar Gibbs energy of formation between the products and the reactants of the reference reaction.

$$\Delta_R \bar{g}^\circ = \Delta_R \bar{h}^\circ - T^\circ \Delta_R \bar{s}^\circ = \Delta_F \bar{g}^\circ_{H_2O} - \Delta_F \bar{g}^\circ_{H_2} - \frac{1}{2}\Delta_F \bar{g}^\circ_{O_2} \quad (7.5)$$

The chemical exergy of oxygen (3.97 kJ/mol) is calculated using (7.2) for a conventional mean partial pressure of oxygen 0.2039 bar [116]. Finally, the chemical exergy of hydrogen gas can be calculated by inserting the obtained values into the adapted reference reaction (7.4), see (7.6).

$$\bar{e}^{Ch\,\circ}_{H_2} = -(-228.57) + 9.49 - (0.5)(3.97) = 236.07 \text{ kJ/mol} \quad (7.6)$$

Hence, the standard molar chemical exergy of hydrogen gas is calculated to be 236.07 kJ/mol. This is in agreement with the standard chemical exergy of hydrogen (236.1 kJ/mol) reported in [117].

Note that the conventional mean ideal partial pressures in the atmosphere listed in Table 2 of reference [117] are incorrect, it appears that the wrong units (kPa) have been used in this table, e.g. the conventional mean partial pressure of hydrogen is given as 2.2 kPa in Table 2-4 in [116] and incorrectly as 2.2×10^{-2} kPa in Table 2 of [117].

7.1.2 The hydrosphere as a reference datum level

The approach to calculate the standard molar chemical exergy of species using seawater as a reference datum level is different from the two other reference datum levels. The specific method is based on a model developed by Morris [119] where the standard molar chemical exergy of the species under consideration can be calculated from (7.7).

$$\bar{e}^{Ch\,\circ} = j\left[-\Delta_F \bar{g}^{\circ} + \frac{1}{2} z \bar{e}^{Ch\,\circ}_{H_2} - \sum_e v \bar{e}^{Ch\,\circ} - 2.303 R T^{\circ} z(pH) - R T^{\circ} \ln(M^{\circ}\gamma)\right] \qquad (7.7)$$

In (7.7) j is the number of reference ions or molecules derived from one molecule of the element under consideration, $\Delta_F \bar{g}^{\circ}$ is the Gibbs energy of formation of the reference ion or non-ionised references species, *z* is the valence of the reference ion (positive or negative), *v* is the stoichiometric coefficient of the additional elements *e* in the reference ion. On the right of (7.7) $\bar{e}^{Ch\,\circ}$ is the standard molar chemical exergy of the *n*th element in the reference ion, M° is the standard molality of the reference species in seawater and γ is the activity coefficient of the reference species in seawater. The pH term in (7.7) stems from the definition of pH as the negative logarithm to base 10 of the concentration of the hydrogen ion [116], see (7.8). Thus, the constant value 2.303 is the ratio of the natural logarithm to the base 10 logarithm.

$$pH \approx -\log(M_{H^+}\gamma_{H^+}) \qquad (7.8)$$

The model basis and the associated terms of (7.7) are shown in Figure 7-1, which is adapted from [116]. The model can be described as follows: one mole of the element under consideration and the number of moles of any additional elements in the reference species enters an electrochemical cell with a hydrogen electrode at the standard temperature and pressure; the hydrogen ion in a one molal ideal solution at standard temperature and pressure flows into the cell if the reference ion is positive and leaves the cell if the reference ion is negative; hydrogen gas in the standard state flows away from the cell in the first instance and into the cell in the latter case; the isothermal change in concentration

takes place for the hydrogen ion and the reference species between the standard state one molal solutions and the standard or conventional molalities in seawater [116].

The standard chemical exergy of the element under consideration is the maximum theoretical work that the substance could do if it was allowed to react at standard temperature and pressure with the appropriate reference species. As (7.7) and Figure 7-1 illustrate, the chemical exergy of the element in question is comprised of a number of contributions;

- The Gibbs energy of formation of the reference ion minus the chemical exergy of the other elements which make up the reference ion (the first and third terms on the right of (7.7));
- The redox (oxidation/reduction) reaction involving the transfer of electrons from the hydrogen electrode in the electrochemical cell, i.e. the second term on the right of (7.7). Redox reactions are discussed in greater detail later in this chapter;
- The change in concentration of the hydrogen ion between the 1 M standard state solution in the electrochemical cell and the concentration of the hydrogen ion in seawater (the fourth term on the right of (7.7)); note that the second and fourth terms of this equation are different in sign to account for the positive/negative valence of the reference ion;
- The change in concentration of the reference ion from the 1 M solution in the electrochemical cell to the standard seawater molality (the final term on the right in (7.7)).

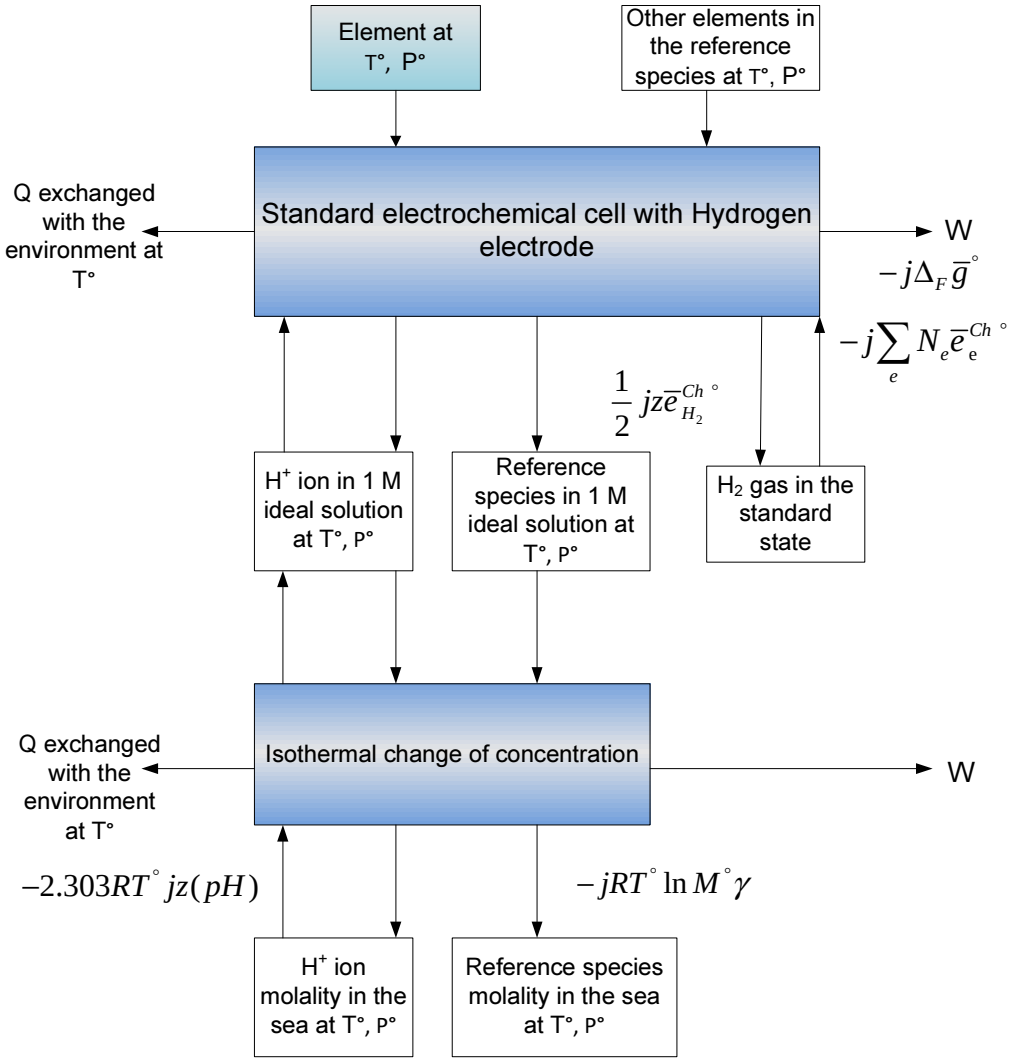

Figure 7-1: Elements with seawater as reference datum level, adapted from [116]

7.1.3 The lithosphere as a reference datum level

For the calculation of the chemical exergy of reference species, with a reference datum level in the lithosphere, the calculation of chemical exergy is relatively straightforward and analogous to the atmospheric reference species. Equation (7.2) is used to calculate the standard chemical exergy of the reference species, in this case however, the value of x_i° is

defined as the standard conventional mole fraction of i in the environment, where *i* is a solid reference species. The determination of the standard conventional mole fraction in the environment for each reference species is an approximation because "*the earth's crust is a very complicated mixture of solid solutions and an exact calculation of its components is impossible* [117]". Szargut [118] developed a method to estimate this value, see (7.9).

$$x_i^\circ = \frac{1}{l_e} n_e^\circ c_e MW^\circ \tag{7.9}$$

In (7.9) n_e° is defined as the mean molal concentration of the element under consideration in the earth's crust (mol/kg), l_e is the number of atoms in the element under consideration in the molecule of the reference species, c_e is the fraction of the element under consideration appearing in the form of reference species, and MW° is the mean molar mass of the upper layer of the continental part of the earth's crust [93]. The chemical exergy of each respective element is again calculated using a reference reaction containing only the specific reference species for that element and other reference species whose chemical exergy is known. The assessment of geological variation in the lithosphere is beyond the scope of this thesis, so the values of standard molar concentration for the reference species are taken without further consideration from [117].

7.1.4 The standard chemical exergy of water

The tabulated standard molar chemical exergy of liquid water is 0.9 kJ/mol [93] in contrast to 9.49 kJ/mol for water vapour calculated earlier. How is the standard chemical exergy of liquid water calculated? Szargut [93] details two methods. First, for areas under

consideration which are remote from the sea, the standard molar chemical exergy of water is calculated as a function of the relative humidity ϕ using (7.10).

$$\overline{e}_w^{Ch\,\circ} = -RT^{\circ} \ln \phi \tag{7.10}$$

The tabulated standard chemical exergy value of water is 0.9 kJ/mol, and therefore, according to (7.10), the standard relative humidity value used to calculate the chemical exergy of water is 0.696. The higher the relative humidity value, the lower the chemical exergy. Thus, the chemical exergy of water is sensitive to changes in location and time, in terms of relative humidity and temperature.

Second, for areas close to the sea, the molar chemical exergy of water can be calculated using a desalination model approach [93], previously discussed in Chapter 5, where the chemical exergy of water can be calculated using (7.11).

$$\overline{e}_w^{Ch\,\circ} = -RT^{\circ} \ln x_w \tag{7.11}$$

Based on an ideal solution, (7.11) is identical to the chemical exergy term of Model A (excluding the N_{sol} and mass flow rate terms of (3.5)). For a typical seawater mass fraction of salt (35,000 ppm or 3.5% mass fraction) and a corresponding mole fraction of water 0.978 using the Model C approach, the molar chemical exergy equates to 0.055 kJ/mol, a factor which is sixteen times lower than the chemical exergy of water reported in the standard chemical exergy tables. There is a significant difference between the values of molar chemical exergy using the two different approaches. Should the two methods result in such different chemical exergy values? Seawater desalination is an energy intensive process, and this low chemical exergy value does not appear to adequately reflect the work input required to purify seawater. This leads back to the discussion of the appropriateness

of the model assumptions underlying Model A in Chapter 5 and whether it is appropriate to model seawater desalination as the extraction of one mole of pure water from an infinitely large ideal mixture of salt and water? Also, it is clear from the discussions in Chapter 6 that electrolytic solutions do not behave as ideal solutions.

The previous sections have outlined the manner in which the standard chemical exergy is calculated. When one considers standard chemical exergy tables retrospectively, it is evident that there is ‘a lot going on in the background’. It may appear superfluous to discuss the calculation of standard chemical exergy in such detail but understanding the calculation of standard chemical exergy is important because the tables are somewhat limited with respect to non-standard reference states. There are limitations to the Szargut model, primarily the complexity of the chemical exergy calculations when states other than the standard state are considered but also potential inaccuracies associated with the lithosphere calculations. On the other hand, the scope of the Szargut model is highly commendable with its consideration of the final, most likely interactions of process wastes with the natural environment.

7.2 Application to water purification exergy analysis

The Szargut model can be applied to mixtures and solutions; the molar chemical exergy of non-ideal solutions is determined from (7.12) where the molar chemical exergy of the solution is the sum of the molar chemical exergy of the individual constituents multiplied by their respective mole fractions, the entropy of mixing term reduces the overall chemical exergy.

$$\overline{e}^{Ch} = \sum_i x_i \overline{e}_i^{Ch} + RT_0 \sum_i x_i \ln a_i \tag{7.12}$$

Equation (7.12) is an elegant expression in that the molar chemical exergy is pre-defined with respect to the global dead state.

The chemical exergy of electrolytic solutions requires further consideration because the chemical exergy of an electrolyte in an aqueous solution is treated differently to the chemical exergy of the solid species in an aqueous solution. According to Szargut et al. [116], the standard molar chemical exergy of an electrolyte i in an aqueous solution can be calculated using (7.13) where the subscript (aq) denotes aqueous.

$$\overline{e}_{i(aq)}^{Ch} = \overline{e}_i^{Ch} + \Delta_F \overline{g}_{i(aq)}^{\circ} - \Delta_F \overline{g}_i^{\circ} \tag{7.13}$$

Thus, the difference between the standard chemical exergy of an electrolyte (where the standard state of the solute is defined as a one molal aqueous solution) and the substance in question is the difference between the standard Gibbs energy of formation of the aqueous species and the standard molar Gibbs energy of formation of substance. For example, consider a one molal solution of sodium chloride. The standard molar chemical exergy value of solid NaCl is reported in the standard chemical exergy tables, i.e. 14.3 kJ/mol [93, 117].

$$\overline{e}_{NaCl(aq)}^{Ch\,\circ} = \overline{e}_{NaCl}^{Ch\,\circ} + \Delta_F \overline{g}_{NaCl(aq)}^{\circ} - \Delta_F \overline{g}_{NaCl}^{\circ} \tag{7.14}$$

The Gibbs energy of formation of the NaCl electrolyte and the Gibbs energy of formation of solid NaCl are reported in the thermodynamic tables, -393.133 kJ/mol and -384.138 kJ/mol respectively [205]. Hence the chemical exergy of aqueous NaCl is calculated to be 5.3 kJ/mol, this is similar to the value of 5.1 kJ/mol reported in [93]. This difference in

results may arise from slightly different values of Gibbs formation energy, the data used here [205] was based on a standard state of 298.15 K and 1 bar. Szargut's values are based on a standard state of 298.15 K but at 1.01325 bar [93]. Standard chemical exergy values for several electrolytes, based on the above approach have been tabulated in the literature [93].

However, based on the incoming UPW plant water analysed in Chapter 6, the calculation of standard chemical exergy using the approach outlined in the previous paragraph is problematic. The main electrolyte in the UPW plant feedwater is calcium bicarbonate $Ca(HCO_3)_2$, and this substance does not exist as a common electrolyte but only as calcium and bicarbonate ions in solution. Data on the Gibbs energy of formation for the electrolyte and the non-ionised substance are very rare (following an extensive search, no data were found). Consequently, the calculation of the chemical exergy must be approached in a different manner.

7.2.1 Determination of the chemical exergy of $Ca(HCO_3)_2$ using individual ionic chemical exergy values

An approach based on the calculation of the standard molar chemical exergy of individual ions rather than the electrolyte is proposed. To use this approach, it is first necessary to investigate whether the sum of the chemical exergy of the individual ions is equivalent to the standard molar chemical exergy of the electrolyte. Consider the electrolyte NaCl and its dissociated ions Na^+ and Cl^-. The chemical exergy of the individual ions is not reported in regular sources of standard chemical exergy data [92, 93, 116, 117, 119, 121]. However, using the same approach as that for the calculation of the chemical exergy of electrolytes,

see (7.13), the chemical exergy of certain individual ions can be calculated. The chemical exergy of the sodium ion can be calculated using (7.15).

$$\overline{e}^{Ch\,\circ}_{Na^+} = \overline{e}^{Ch\,\circ}_{Na} + \Delta_F \overline{g}^{\circ}_{Na^+} - \Delta_F \overline{g}^{\circ}_{Na} \tag{7.15}$$

Based on tabulated standard chemical exergy data in [93] and Gibbs formation data in [205], the chemical exergy of the sodium ion is calculated to be 74.7 kJ/mol according to (7.16).

$$\overline{e}^{Ch\,\circ}_{Na^+} = 336.6 + (-261.9) - 0 = 74.7 \text{ kJ/mol} \tag{7.16}$$

The chemical exergy of chloride ion is now calculated, in this case, the calculation proves to be more ambiguous because the standard chemical exergy tables provide values for both Cl(g) and Cl_2(g). Thus an understanding of the formation reaction of chloride ions is required to determine the correct input data. The formation of an aqueous ion can be modelled as a redox reaction [205, 206]. The redox reaction for the formation of the sodium ion is shown in (7.17).

$$Na + H^+ \rightarrow Na^+ + \frac{1}{2} H_2 \tag{7.17}$$

In general, for a cation M of positive valence *z*, the redox reaction can be written as (7.18) and as (7.19) for an anion X of negative valence *z*.

$$M + zH^+ \rightarrow M^{z+} + \frac{z}{2} H_2 \tag{7.18}$$

$$X + \frac{|z|}{2} H_2 \rightarrow X^{|z|-} + |z| H^+ \tag{7.19}$$

The specific redox reaction is shown for the chloride ion in (7.20); this reaction can be used to determine the values required to calculate the standard molar chemical exergy of the

chloride ion, see (7.21) and (7.22). The standard molar chemical exergy of the chloride ion is calculated to be -69.43 kJ/mol.

$$\frac{1}{2}Cl_2 + \frac{1}{2}H_2 \rightarrow Cl^- + H^+ \tag{7.20}$$

$$\overline{e}^{Ch\,\circ}_{Cl^-} = \frac{1}{2}\overline{e}^{Ch\,\circ}_{Cl_2} + \Delta_F \overline{g}^{\circ}_{Cl^-} - \frac{1}{2}\Delta_F \overline{g}^{\circ}_{Cl_2} \tag{7.21}$$

$$\overline{e}^{Ch\,\circ}_{Cl^-} = \frac{1}{2}(123.6) + (-131.228) - \frac{1}{2}(0) \tag{7.22}$$

Summing the standard molar chemical exergy of the sodium and chloride ions (74.7 kJ/mol and -69.43 kJ/mol) results in the standard molar chemical exergy of the sodium chloride electrolyte 5.27 kJ/mol, this compares well with the standard chemical exergy of the electrolyte calculated earlier, 5.3 kJ/mol. The sum of the chemical exergy values of the cation and anion is approximately equivalent to the standard molar chemical exergy of the electrolyte. The single ion exergy approach was also applied to, and validated for, the electrolyte HCl (with the chemical exergy of the hydrogen ion calculated to be 118.05 kJ/mol using (7.13)) . This approach can be related back to the properties of ions in solution discussed in Wagman et al., where "*the properties of the neutral strong electrolyte in aqueous solution in the standard state are equal to the sum of these values for the appropriate number of ions assumed to constitute the molecule of the given electrolyte* [205]". Therefore, if it is possible to calculate the chemical exergy of the bicarbonate and calcium ions, the chemical exergy of the electrolyte should equate to the sum of the two ionic chemical exergy values.

However, the calculation of the chemical exergy of the bicarbonate ion is also problematic because it exists as an ion and not as a solid or gaseous substance which can be simply modelled as a redox reaction, as was the case for the chloride and sodium ions. Consequently, there are no Gibbs formation data or chemical exergy data for the non-ionised substance HCO_3 to enable the calculation of the chemical exergy of the ion using the same approach as that used previously. This problem can be overcome in a roundabout manner by making use of the reported standard molar chemical exergy of other electrolytes, i.e. data in [93]. There is published standard molar chemical exergy data for sodium bicarbonate, and therefore, the chemical exergy of bicarbonate can be calculated once the chemical exergy of sodium is known. The standard molar chemical exergy of sodium has been previously calculated to be 74.69 kJ/mol. The reported value for the electrolyte sodium bicarbonate is 21.4 kJ/mol [93], and hence, the standard molar chemical exergy of the bicarbonate ion is calculated to be -53.29 kJ/mol. The standard molar chemical exergy of calcium is calculated to be 175.52 kJ/mol using (7.13) with updated calcium exergy data reported in [121] and Gibbs formation energy data in [205]. As discussed in the literature review, the reference datum level for calcium, and other 'column 2' elements, was changed from the hydrosphere reference datum to the lithosphere, and therefore, the more recent data are used. The standard molar chemical exergy of calcium bicarbonate can be calculated as follows.

$$\overline{e}^{Ch\,\circ}_{Ca(HCO_3)_2} = \overline{e}^{Ch\,\circ}_{Ca^{++}} + 2\overline{e}^{Ch\,\circ}_{HCO_3^-} \tag{7.23}$$

Inserting the previously calculated values into (7.24), the molar standard chemical exergy of the electrolyte calcium bicarbonate is calculated to be 68.94 kJ/mol.

$$\overline{e}^{Ch\,\circ}_{Ca(HCO_3)_2} = 175.52 + 2(-53.29) \tag{7.24}$$

There is an alternative approach for the calculation of the bicarbonate ion, and that is to use (7.1). The author was reluctant to use this equation initially because the 'compound' under consideration was an ion, and thus, there was a concern that the equation may not have been valid. However, now having calculated a reasonable value for the chemical exergy of the bicarbonate ion, the results of the two approaches can be compared. The standard molar chemical exergy of the bicarbonate ion can be calculated using the specific version of (7.1) below, see (7.25).

$$\begin{aligned}\overline{e}^{Ch\,\circ}_{HCO_3^-} &= \Delta_F \overline{g}^{\circ}_{HCO_3^-} + \frac{1}{2}\overline{e}^{Ch\,\circ}_{H_2} + \overline{e}^{Ch\,\circ}_{C} + \frac{3}{2}\overline{e}^{Ch\,\circ}_{O_2} \\ &= -586.77 + \frac{1}{2}(236.1) + 410.25 + \frac{3}{2}(3.97)\end{aligned} \tag{7.25}$$

In (7.25) standard molar chemical exergy values were taken from [93, 117] and the Gibbs energy of formation value from [205]. Using this approach the chemical exergy of the bicarbonate ion is calculated to be -52.5 kJ/mol. The two values for bicarbonate show good correlation, however, the new value is chosen over the previously estimated value of -53.29 kJ/mol as it is likely to be the more accurate value, it is certainly a more straightforward and flexible method of calculating the chemical exergy, particularly at non-standard states. The chemical exergy of the calcium bicarbonate electrolyte can now be updated as 70.52 kJ/mol.

7.2.2 Gibbs energy of formation of aqueous ions

Returning to (7.13) now, it is important to consider the Gibbs energy of formation for the aqueous electrolyte. The Gibbs energy of formation for an aqueous species consists of the

enthalpy and entropy of formation of the aqueous species. The standard enthalpy of formation for aqueous species is reported in thermodynamic tables [205]. The entropy of formation for an aqueous ion can be calculated using the general equation (7.26) [205].

$$\Delta_F \overline{s}^{\circ} = \overline{s}^{\circ}_{i(aq)} + \frac{z}{2}\overline{s}^{\circ}_{H_2} - \sum_e v\overline{s}^{\circ} \tag{7.26}$$

In (7.26) $\overline{s}^{\circ}_{i(aq)}$ is the standard absolute molar entropy of the ion in question, *z* is the valence of the ion (positive or negative), $\overline{s}^{\circ}_{H_2}$ is the standard absolute molar entropy of hydrogen gas, *v* and $\overline{s}^{\circ}$ are the stoichiometric coefficients and standard absolute molar entropy of the other elements in the aqueous ion respectively. It is evident that (7.26) is the entropy of reaction ($\Delta_R \overline{s}^{\circ}$) for the redox reactions in (7.17) to (7.20), where the standard molar entropy of the hydrogen ion is zero by convention.

By way of example, consider the Gibbs energy of reaction/formation for the sodium ion using (7.27).

$$\begin{aligned} &\Delta_F \overline{g}^{\circ}_{Na^+(aq)} = \Delta_F \overline{h}^{\circ}_{Na^+(aq)} - T^{\circ}\Delta_F \overline{s}^{\circ}_{Na^+(aq)} \\ &\text{where } \Delta_F \overline{s}^{\circ}_{Na^+(aq)} = \overline{s}^{\circ}_{Na^+(aq)} + \frac{1}{2}\overline{s}^{\circ}_{H_2} - \overline{s}^{\circ}_{Na} \end{aligned} \tag{7.27}$$

Using thermodynamic data from [205], where the enthalpy of formation of the sodium ion is reported as -240.12 kJ/mol, the molar entropy of the sodium ion, hydrogen gas and sodium are reported as 59 J/mol.K, 130.684 J/mol.K and 51.21 J/mol.K respectively, the valence of the sodium ion is one and the standard temperature is 298.15 K, the Gibbs energy of formation is calculated to be -261.92 kJ/mol using (7.27).

7.3 Chemical exergy as a function of the dead state temperature

Standard chemical exergy values are limited to dead states at standard values of temperature, pressure and humidity. In the literature standard chemical exergy values are commonly taken from tables without further consideration [180, 207]. Other researchers [105] have considered chemical exergy changes as a function of dead state temperature variations using the simplified equation developed by Kotas [92].

This section develops an approach to calculate the chemical exergy of ionic species as a function of dead state temperature and seeks to investigate whether changes in chemical exergy as a function of changing dead state temperatures are negligible for aqueous solution applications at relevant dead state temperatures and average local relative humidity values. This work is an extension of others' research, notably the cited references [206, 208]. The change in the chemical exergy of ions and electrolytes as a function of the dead state temperature has not been examined or reported in the literature to date.

Kotas [92] developed a method to correct the chemical exergy for variations about the standard temperature for both ideal gases and real gases (the method serves as a reasonable approximation for real gases). The Kotas method is a function of the enthalpy of combustion and the temperature differences under consideration [92]. Ertesvag [208] investigated the variations in chemical exergy of gaseous fuels and atmospheric gases as a result of changing dead state conditions, i.e. temperatures, pressures and relative humidity. It was found that maintaining a constant mole fraction of water vapour in the air as dead state temperature varies, a typical approach in the literature, led to "*unrealistic, or even*

unphysical, situations when the temperature has more than a small variation [208]". In fact, maintaining a constant mole fraction of water vapour in the air resulted in an increase of chemical exergy with increasing dead state temperature, however, when the mole fraction of water vapour in the air was allowed to vary at constant relative humidity, the chemical exergy of the gases under consideration decreased with increasing dead state temperature.

In current PhD research Brammer [206] has developed a methodology to determine changes in the chemical exergy of various elements and reference species as a function of variations in dead state temperature T_0. The change in chemical exergy of a substance with respect to changes in T_0 depends on how each component of (2.21), (7.1) to (7.5), (7.7), and (7.9) to (7.13) is influenced by changes in temperature. Brammer extended the work of Ertesvag [208] to include the reference species and elements in the hydrosphere and the lithosphere. Brammer found that, (1) changes in atmospheric composition, i.e. changing values of the mean molar fraction of the reference species in the atmosphere as a function of changing values of T_0, see (7.2), and (2) changing values of the Gibbs energy of reaction as a function of T_0, had the greatest overall effect on chemical exergy values. The first point above relates directly to the work carried out by Ertesvag regarding changing values of relative humidity.

For reference species in the lithosphere, Brammer found little data relating changing conventional mean mole fraction values to changes in T_0 (speciation changes as a function

of temperature where x_i° is given by (7.9)). However, based on a hypothetical analysis undertaken, changes in the conventional mean mole fraction of the reference species were deemed negligible in comparison with changes in the Gibbs energy of reaction. For elements with the hydrosphere as a reference datum level (see (7.7)), the effects of dead state temperature variations on molality and activity coefficient values were found to be small in comparison to changes in the Gibbs energy of formation of the reference ion, however, changes in pH with respect to temperature were not negligible and were responsible for a non-linear relationship between temperature and molar chemical exergy.

The application of the Szargut exergy model to UPW plant exergy analyses is considered in terms of the research of Ertesvag [208] and Brammer [206]. The objective is to investigate how the chemical exergy of aqueous ionic solutions changes with respect to changes in the dead state temperature, and importantly, whether these variations are significant for UPW exergy analyses. Their work is extended to account specifically for aqueous ionic streams. Hence, for UPW water streams modelled as electrolytic solutions, the focus is on changes in the chemical exergy of the substances of interest at T_0, and specifically, this includes;

1. Changes in the chemical exergy of water, see (7.10);
2. The change in the chemical exergy of the non-ionised species, the first term on the right of (7.13). This is considered for certain species relevant to typical cations and anions in natural water (i.e. sodium, magnesium, calcium, and chlorine for Na^{+}, Mg^{++}, Ca^{++} and Cl^{-} respectively);
3. Changes in the Gibbs energy of formation of the relevant aqueous ions, i.e. the second term on the right of (7.13);

4. Changes in the Gibbs energy of formation of the non-ionised species, the last term on the right of (7.13); again, this is considered for the aforementioned species and their relevant ions;
5. Changes in the chemical exergy of the bicarbonate ion as a function of temperature;
6. Changes in the activity coefficients as a function of temperature, see (7.12); this issue was previously discussed in Chapter 6;
7. Changes in the chemical exergy of other chemical elements/compounds used in the UPW production process.

7.3.1 Chemical exergy of water as a function of dead state temperature

The chemical exergy of water, which is a function of relative humidity, can be calculated for different values of T_0 using (7.10). A typical relative humidity for Eastern Ireland is 0.77; this value was calculated from climatic data [209] as the average relative humidity recorded for Dublin Airport over a 30 year cycle. Assuming a constant value of relative humidity (0.77), the relationship between the chemical exergy of water and dead state temperature is linear. Table 7-1 shows how the molar chemical exergy of water varies with temperature, increasing from 0.604 kJ/mol to 0.648 kJ/mol as the temperature increases from 278.15 to 298.15 K, an absolute percentage difference of 7.3% over the 20 K temperature difference. The value of water reported in the standard chemical exergy tables is 0.9 kJ/mol, which is based on the standard relative humidity value of 0.696 discussed previously.

Table 7-1: Molar chemical exergy of water at 0.77 relative humidity as a function of T_0

T_0 (K)	$\overline{e}_w^{Ch}$ (kJ/mol)	T_0 (K)	$\overline{e}_w^{Ch}$ (kJ/mol)
278.15	**0.604**	290.15	**0.631**
279.15	**0.607**	291.15	**0.633**
280.15	**0.609**	292.15	**0.635**
281.15	**0.611**	293.15	**0.637**
282.15	**0.613**	294.15	**0.639**
283.15	**0.615**	295.15	**0.641**
284.15	**0.617**	296.15	**0.644**
285.15	**0.620**	297.15	**0.646**
286.15	**0.622**	298.15	**0.648**
287.15	**0.624**	299.15	**0.650**
288.15	**0.626**	300.15	**0.652**
289.15	**0.628**		

7.3.2 The chemical exergy of the non-ionised species as a function of dead state temperature

Considering the aforementioned ions of interest in natural waters, the change in the chemical exergy of the non-ionised species, as a function of dead state temperature, depends on two factors;

1. The change in the Gibbs energy of the reaction between the standard temperature and temperature of interest;
2. The change in the chemical exergy of each of the reference species in the reference reaction.

The Gibbs energy of reaction at the relevant temperature T and the standard pressure of one bar can be calculated using (7.28) where $\Delta_R\overline{h}(T)$ is the molar enthalpy of the reaction at T and $\Delta_R\overline{s}(T)$ is the molar entropy of the reaction at T.

$$\Delta_R\overline{g}(T) = \Delta_R\overline{h}(T) - T\Delta_R\overline{s}(T) \tag{7.28}$$

The change in the Gibbs energy of reaction between the standard state temperature and the temperature of interest at standard pressure can be calculated by subtracting the standard Gibbs energy of reaction equation (7.29) from (7.28).

$$\Delta_R \bar{g}^\circ = \Delta_R \bar{h}^\circ - T^\circ \Delta_R \bar{s}^\circ \tag{7.29}$$

Therefore, the change in the Gibbs energy of reaction between temperature T and the standard temperature T° can be calculated using (7.30).

$$\Delta_R \bar{g}(T) - \Delta_R \bar{g}^\circ = \Delta_R \bar{h}(T) - \Delta_R \bar{h}^\circ - (T\Delta_R \bar{s}(T) - T^\circ \Delta_R \bar{s}^\circ) \tag{7.30}$$

First, consider the change in the enthalpy of reaction between T and the standard temperature T°, i.e. the first two terms on the right of equation (7.30). The enthalpy of reaction at temperature T can be calculated using (7.31), which is a statement of Kirchhoff's Law, where $\Delta_R \bar{c}_P(T)$ is the change in molar heat capacity of the reaction at constant pressure as a function of T. When $\Delta_R \bar{c}_P$ is treated as a constant (7.32) can be used.

$$\Delta_R \bar{h}(T) = \Delta_R \bar{h}^\circ + \int_{T^\circ}^{T} \Delta_R \bar{c}_P(T) dT \tag{7.31}$$

$$\Delta_R \bar{h}(T) = \Delta_R \bar{h}^\circ + \Delta_R \bar{c}_P (T - T^\circ) \tag{7.32}$$

For pure solids, liquids, and gases, values of $\bar{c}_P$ can be calculated as functions of temperature using power series such as the Maier-Kelley or Shomate equations [176]. The Shomate equation is shown in (7.33) where t is defined as $T(K)/1000$ and the coefficients *A* to *E* are defined separately for each pure substance in sources of thermodynamic data, for example, the NIST Chemistry web-Book [210]. The Shomate equation has one important advantage over the Maier Kelley equation; it is relevant for temperatures down to 0 K whereas the Maier-Kelley equation is intended for temperatures above 298.15 K [176].

$$\overline{c}_P^{\circ} = A + Bt + Ct^2 + Dt^3 + \frac{E}{t^2} \tag{7.33}$$

The change in molar heat capacity of the reaction $\Delta_R \overline{c}_p$ for a substance can be calculated by integrating an amended version of (7.33), see (7.34) where the delta values of each of the coefficients are defined as the difference between the sum of the coefficients of the products and sum of the coefficients of the reactants in the relevant reaction, for example, $\Delta_R A = \sum_p A - \sum_r A$ and so forth for each coefficient value.

$$\Delta_R \overline{c}_p^{\circ} = \Delta_R A + \Delta_R Bt + \Delta_R Ct^2 + \Delta_R Dt^3 + \frac{\Delta_R E}{t^2} \tag{7.34}$$

Performing the integration and taking note of the definition of *t* as $T/1000$, the second term on the right of (7.31) can now be calculated from (7.35).

$$\int_{T^{\circ}}^{T} \Delta_R \overline{c}_P dT = \Delta_R A(T - T^{\circ}) + \frac{\Delta_R B(T^2 - T^{\circ 2})}{2(1000)} + \frac{\Delta_R C(T^3 - T^{\circ 3})}{3(1000^2)} + \frac{\Delta_R D(T^4 - T^{\circ 4})}{4(1000^3)} - (1000^2)\Delta_R E\left(\frac{1}{T} - \frac{1}{T^{\circ}}\right) \tag{7.35}$$

When the Shomate coefficients are not tabulated for a substance, e.g. the specific reference species of calcium $CaCO_3$, $\Delta_R \overline{c}_P$ may be treated as a constant over short temperature ranges of approximately 100 K [205]. The values of $\Delta_R \overline{c}_P$ are then simply the sum of the standard molar heat capacity of the reactants minus the sum of the standard molar heat capacity of the products (each multiplied by the stoichiometric coefficients of the relevant reaction), i.e. $\sum_p v\overline{c}_P^{\circ} - \sum_r v\overline{c}_P^{\circ}$, and these molar heat capacity values can be retrieved directly from thermodynamic tables, for example [205].

Now consider the molar entropy of formation terms in (7.30). Combining Kirchhoff's Law and the fact that at constant pressure $d\overline{s} = (\overline{c}_P / T)dT$, the entropy of formation at a temperature T can be calculated using (7.36) when $\Delta_R \overline{c}_P$ is treated as a function of temperature, and by (7.37) when $\Delta_R \overline{c}_P$ is treated as a constant over the temperature range.

$$\Delta_R \overline{s}(T) = \Delta_R \overline{s}^\circ + \int_{T^\circ}^{T} \frac{\Delta_R \overline{c}_P(T)}{T} dT \tag{7.36}$$

$$\Delta_R \overline{s}(T) = \Delta_R \overline{s}^\circ + \Delta_R \overline{c}_P \ln \frac{T}{T^\circ} \tag{7.37}$$

Finally, inserting these values for changes in enthalpy and entropy of the reaction into (7.30), two relations of Gibbs energy of reaction are obtained, (7.38) when $\Delta_R \overline{c}_P$ is treated as a function of temperature and (7.39) when it is treated as a constant.

$$\Delta_R \overline{g}(T) = \Delta_R \overline{g}^\circ + \int_{T^\circ}^{T} \Delta_R \overline{c}_P(T) dT - \Delta_R \overline{s}^\circ (T - T^\circ) - T \int_{T^\circ}^{T} \frac{\Delta_R \overline{c}_P(T)}{T} dT \tag{7.38}$$

$$\Delta_R \overline{g}(T) = \Delta_R \overline{g}^\circ + \Delta_R \overline{c}_P (T - T^\circ) - \Delta_R \overline{s}^\circ (T - T^\circ) - T \Delta_R \overline{c}_P \ln \frac{T}{T^\circ} \tag{7.39}$$

These two equations can be used to calculate the changes in the Gibbs energy of reaction with respect to temperature. Once the chemical exergy values of the other reference species in the reference reaction are known as a function of dead state temperature, the chemical exergy of the element/compound under consideration at the relevant dead state temperature T_0 can be calculated.

Next, changes in the chemical exergy of the reference species in the atmosphere are considered. The mean molar fractions of the atmospheric reference species are a function of the mole fraction of water vapour in the atmosphere, which in turn is a function of the

relative humidity. The mole fraction of water vapour at various values of dead state temperature can be calculated using (7.40) [208] where ϕ is the relative humidity, $P_{sat}(T_0)$ is the saturation pressure of water (bar) at T_0, and P is the atmospheric pressure (bar).

$$x_{H_2O(g)} = \frac{\phi P_{sat}(T_0)}{P} \tag{7.40}$$

Noting that $\phi = P_{H_2O(g)} / P_{sat}(T)$ the mole fraction of water vapour simplifies to $P_{H_2O(g)} / P$, which is valid for ideal gases.

The mole fraction of the atmospheric reference species as a function of the dead state temperature can then be calculated using (7.41) [208] where $x_i^{\text{Dry air}}$ is the mole fraction of the atmospheric reference species i in dry air.

$$x_i = \left(1 - x_{H_2O(g)}\right) x_i^{\text{Dry air}} \tag{7.41}$$

For example, variations in the chemical exergy of oxygen as a function of temperature T_0 at constant relative humidity (0.77) and atmospheric pressure of one bar are shown in Table 7-2. The saturation pressure values at T_0 were obtained using the XSteam function in MATLAB [169] and the mole fraction of oxygen in dry air was obtained in the cited reference [116]. According to Table 7-2, the values of chemical exergy increase monotonically with temperature, an absolute percentage difference of 8.41% in the value of chemical exergy from 278.15 K to 298.15 K. The relationship is not linear due to the non-linear variation of the water vapour mole fraction with the saturation pressure at different values of dead state temperature. Values for the other atmospheric reference species can be calculated in a similar manner.

Table 7-2: Chemical exergy of O_2 at 1 bar and 0.77 relative humidity

T_0(K)	$P_{Sat}(T_0)$ (bar)	x_{O_2} in dry air	x_{O_2} (T_0)	$\overline{e}_{O_2}^{Ch}$ (kJ/mol)
278.15	0.009	0.210	0.208	**3.626**
279.15	0.009	0.210	0.208	**3.640**
280.15	0.010	0.210	0.208	**3.654**
281.15	0.011	0.210	0.208	**3.668**
282.15	0.012	0.210	0.208	**3.683**
283.15	0.012	0.210	0.208	**3.697**
284.15	0.013	0.210	0.208	**3.712**
285.15	0.014	0.210	0.208	**3.727**
286.15	0.015	0.210	0.207	**3.742**
287.15	0.016	0.210	0.207	**3.757**
288.15	0.017	0.210	0.207	**3.772**
289.15	0.018	0.210	0.207	**3.787**
290.15	0.019	0.210	0.207	**3.802**
291.15	0.021	0.210	0.207	**3.818**
292.15	0.022	0.210	0.206	**3.833**
293.15	0.023	0.210	0.206	**3.849**
294.15	0.025	0.210	0.206	**3.865**
295.15	0.027	0.210	0.206	**3.881**
296.15	0.028	0.210	0.205	**3.898**
297.15	0.030	0.210	0.205	**3.914**
298.15	0.032	0.210	0.205	**3.931**
299.15	0.034	0.210	0.204	**3.948**
300.15	0.036	0.210	0.204	**3.965**

The chemical exergy of water vapour as a function of dead state temperature at constant relative humidity (0.77) is shown in Table 7-3.

Table 7-3: Chemical exergy of water vapour as a function of T_0

T (K)	$P_{sat}(T)$ *(bar)*	ϕ	*Std Pressure (bar)*	$x_{H_2O(g)}$	$\overline{e}^{Ch}_{H_2O(g)}$ *(kJ/mol)*	*% Diff. vs.* T°
278.15	0.009	0.77	1	0.007	**11.577**	20.50%
279.15	0.009	0.77	1	0.007	**11.439**	19.54%
280.15	0.010	0.77	1	0.008	**11.336**	18.81%
281.15	0.011	0.77	1	0.008	**11.218**	17.95%
282.15	0.012	0.77	1	0.009	**11.089**	17.00%
283.15	0.012	0.77	1	0.009	**10.970**	16.10%
284.15	0.013	0.77	1	0.010	**10.860**	15.25%
285.15	0.014	0.77	1	0.011	**10.740**	14.30%
286.15	0.015	0.77	1	0.012	**10.614**	13.28%
287.15	0.016	0.77	1	0.012	**10.497**	12.32%
288.15	0.017	0.77	1	0.013	**10.374**	11.28%
289.15	0.018	0.77	1	0.014	**10.260**	10.29%
290.15	0.019	0.77	1	0.015	**10.142**	9.25%
291.15	0.021	0.77	1	0.016	**10.031**	8.25%
292.15	0.022	0.77	1	0.017	**9.906**	7.09%
293.15	0.023	0.77	1	0.018	**9.790**	5.98%
294.15	0.025	0.77	1	0.019	**9.671**	4.83%
295.15	0.027	0.77	1	0.020	**9.551**	3.63%
296.15	0.028	0.77	1	0.022	**9.439**	2.49%
297.15	0.030	0.77	1	0.023	**9.317**	1.22%
298.15	0.032	0.77	1	0.024	**9.204**	0.00%
299.15	0.034	0.77	1	0.026	**9.090**	-1.25%
300.15	0.036	0.77	1	0.027	**8.969**	-2.62%

As Table 7-3 shows, the mole fraction of water vapour in the atmosphere increases with increasing dead state temperature, and consequently, the chemical exergy of water vapour decreases. Although the mole fraction of water vapour in the atmosphere at constant relative humidity is not linear with respect to changes in the dead state temperature, the relationship between the chemical exergy and dead state temperature is linear. However, if the water vapour mole fraction was treated as a constant the chemical exergy of water would increase linearly with increasing dead state temperature. This ‘opposite behaviour’ resulting from the treatment of the mole fraction of water vapour as a constant has been

discussed in the literature [208]. Note also that the standard chemical exergy of water vapour at *standard relative humidity* reported in the literature is 9.5 kJ/mol, which is a 3.2% difference compared with the chemical exergy at 298.15 K reported in Table 7-3 at a relative humidity of 0.77.

Regarding the reference species in the lithosphere it is very difficult to estimate changes in the conventional mean mole fraction of the reference species with respect to changes in T_0, see (7.9) [206]. According to Brammer [206], and based on hypothetical changes of species fraction with temperature, changes in the chemical exergy of the reference species in the lithosphere can be neglected in comparison with the changes in Gibbs energy of the reference reaction. Thus, ignoring possible changes in speciation of reference species as a function of temperature, the chemical exergy of the reference species can be calculated by multiplying the conventional mean mole fraction of the species in the lithosphere by the relevant values of T_0, i.e. according to (7.2). Hence, the chemical exergy of the reference species in the lithosphere increase linearly with increasing dead state temperature. Also examining (7.2), the lower the mole fraction of the reference species in the environment the more sensitive the chemical exergy of the reference species to changes in the dead state temperature.

Having outlined the method, the chemical exergy of the calcium and magnesium (lithosphere as a reference datum level) can now be calculated as a function of changing dead state temperature at constant relative humidity (0.77). First, consider calcium. The standard Gibbs energy of the reaction can be calculated according to the reference reaction

shown in (7.42) using (7.43). The standard Gibbs energy of the reaction was calculated to be -734.43 kJ/mol.

$$Ca + CO_2 + \frac{1}{2}O_2 \rightarrow CaCO_3 \tag{7.42}$$

$$\Delta_R \overline{g}^\circ = \Delta_F \overline{g}^\circ_{CaCO_3} - \Delta_F \overline{g}^\circ_{Ca} - \Delta_F \overline{g}^\circ_{CO_2} - \frac{1}{2}\Delta_F \overline{g}^\circ_{O_2} \tag{7.43}$$

Next, the change in the Gibbs energy of the reaction as a function of temperature can be calculated as a function of temperature using (7.39), the relevant values of $\Delta_R \overline{c}_P$ and $\Delta_R \overline{s}^\circ$ were calculated to be 0.00478 kJ/mol.K and -0.26483 kJ/mol.K respectively for the reference reaction. The values of the change in Gibbs energy of the reaction as a function of temperature are shown in Table 7-4. This table shows that the Gibbs energy of the reaction changes relatively slowly at the relevant temperatures, a percentage difference of 0.72% for a 20 K temperature difference, approximately 0.036% for every degree of temperature change.

Table 7-4 : Change in the Gibbs energy of reaction as a function of T_0 for the formation of $CaCO_3$

Temperature T(K)	$\Delta_R \overline{g}(T)$ *kJ/mol*	$\Delta_R \overline{g}^{\circ}$ *kJ/mol*	*% Diff. vs.* T°
278.15	**-739.73**	-734.43	0.72%
279.15	**-739.46**	-734.43	0.68%
280.15	**-739.20**	-734.43	0.65%
281.15	**-738.93**	-734.43	0.61%
282.15	**-738.67**	-734.43	0.57%
283.15	**-738.40**	-734.43	0.54%
284.15	**-738.14**	-734.43	0.50%
285.15	**-737.87**	-734.43	0.47%
286.15	**-737.61**	-734.43	0.43%
287.15	**-737.34**	-734.43	0.40%
288.15	**-737.08**	-734.43	0.36%
289.15	**-736.81**	-734.43	0.32%
290.15	**-736.55**	-734.43	0.29%
291.15	**-736.28**	-734.43	0.25%
292.15	**-736.02**	-734.43	0.22%
293.15	**-735.75**	-734.43	0.18%
294.15	**-735.49**	-734.43	0.14%
295.15	**-735.22**	-734.43	0.11%
296.15	**-734.96**	-734.43	0.07%
297.15	**-734.69**	-734.43	0.04%
298.15	**-734.43**	-734.43	0.00%
299.15	**-734.17**	-734.43	-0.04%
300.15	**-733.90**	-734.43	-0.07%

The changes in the chemical exergy of each of the reference species as a function of temperature are now considered in addition to the changes in the Gibbs energy of the reference reaction. The specific reference species for calcium is calcite ($CaCO_3$) with additional reference species carbon dioxide and oxygen. According to the method outlined previously to calculate changes in the chemical exergy of reference species as a function of temperature (at constant relative humidity), the values of the molar chemical exergy of calcium as a function of changing T_0 have been calculated and are shown in Figure 7-2 and Table 7-5. Figure 7-2 shows that there is a linear relationship between the molar chemical

exergy of calcium and the dead state temperature T_0, i.e. $\overline{e}_{Ca}^{Ch} = -0.2789T(K) + 814.42$. The value of the molar chemical exergy of calcium decreases with increasing dead state temperature. Over the 20 K temperature range between 278.15 and the standard temperature, there is a 5.57 kJ/mol difference in the magnitude of chemical exergy and a percentage difference of 0.76%.

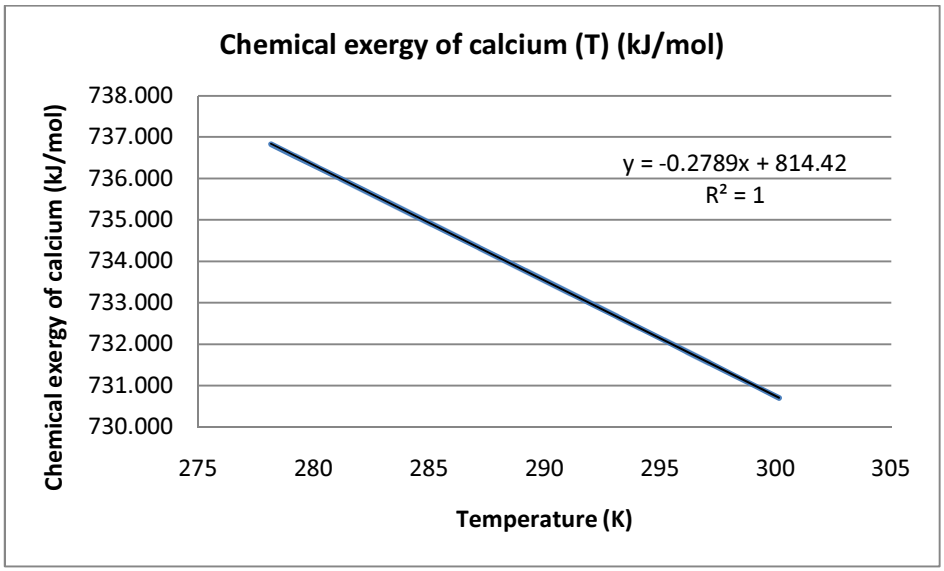

Figure 7-2: Chemical exergy of calcium at constant relative humidity (0.77) as a function of T_0

Table 7-5: Changes in the chemical exergy of calcium at constant relative humidity (0.77) as a function of T_0

T (K)	$\Delta_R \overline{g}(T)$	$\overline{e}^{Ch}_{CaCO_3}$	$\overline{e}^{Ch}_{O_2}$	$\overline{e}^{Ch}_{CO_2}$	$\overline{e}^{Ch}_{Ca}$	% Diff. vs. T°
	kJ/mol	***kJ/mol***	***kJ/mol***	***kJ/mol***	***kJ/mol***	
278.15	-739.73	17.37	3.63	18.45	**736.83**	0.76%
279.15	-739.46	17.43	3.64	18.52	**736.55**	0.72%
280.15	-739.20	17.49	3.65	18.59	**736.28**	0.68%
281.15	-738.93	17.55	3.67	18.65	**736.00**	0.64%
282.15	-738.67	17.62	3.68	18.72	**735.72**	0.61%
283.15	-738.40	17.68	3.70	18.79	**735.44**	0.57%
284.15	-738.14	17.74	3.71	18.86	**735.17**	0.53%
285.15	-737.87	17.80	3.73	18.93	**734.89**	0.49%
286.15	-737.61	17.87	3.74	18.99	**734.61**	0.46%
287.15	-737.34	17.93	3.76	19.06	**734.33**	0.42%
288.15	-737.08	17.99	3.77	19.13	**734.05**	0.38%
289.15	-736.81	18.05	3.79	19.20	**733.78**	0.34%
290.15	-736.55	18.12	3.80	19.27	**733.50**	0.31%
291.15	-736.28	18.18	3.82	19.34	**733.22**	0.27%
292.15	-736.02	18.24	3.83	19.40	**732.94**	0.23%
293.15	-735.75	18.30	3.85	19.47	**732.66**	0.19%
294.15	-735.49	18.37	3.87	19.54	**732.38**	0.15%
295.15	-735.22	18.43	3.88	19.61	**732.10**	0.11%
296.15	-734.96	18.49	3.90	19.68	**731.82**	0.08%
297.15	-734.69	18.55	3.91	19.75	**731.54**	0.04%
298.15	-734.43	18.62	3.93	19.82	**731.26**	0.00%
299.15	-734.17	18.68	3.95	19.89	**730.98**	-0.04%
300.15	-733.90	18.74	3.97	19.96	**730.69**	-0.08%

A similar analysis was carried out for magnesium according to the reference reaction (7.44) with the specific reference species $Mg_3Si_4O_{10}(OH)_2$ (lithosphere), commonly known as talc, and other reference species silicon dioxide (lithosphere), water vapour, and oxygen.

$$3Mg + 4SiO_2 + H_2O(g) + \frac{3}{2}O_2 \rightarrow Mg_3Si_4O_{10}(OH)_2 \qquad (7.44)$$

As was the case for calcite Shomate equation coefficients are not readily available for talc, and consequently, $\Delta_R \overline{c}_P$ was treated as a constant. The Gibbs energy of formation, molar entropy and molar heat capacity of talc were obtained from the cited reference [211]. Values for the conventional mean mole fraction of silicon dioxide and talc in the lithosphere were obtained from [117]. Based on the calculated values of $\Delta_R \overline{c}_P$ (-0.00829 kJ/mol.K) and $\Delta_R \overline{s}^{\circ}$ (-0.501 kJ/mol.K), the results are presented in Table 7-6 and Figure 7-3.

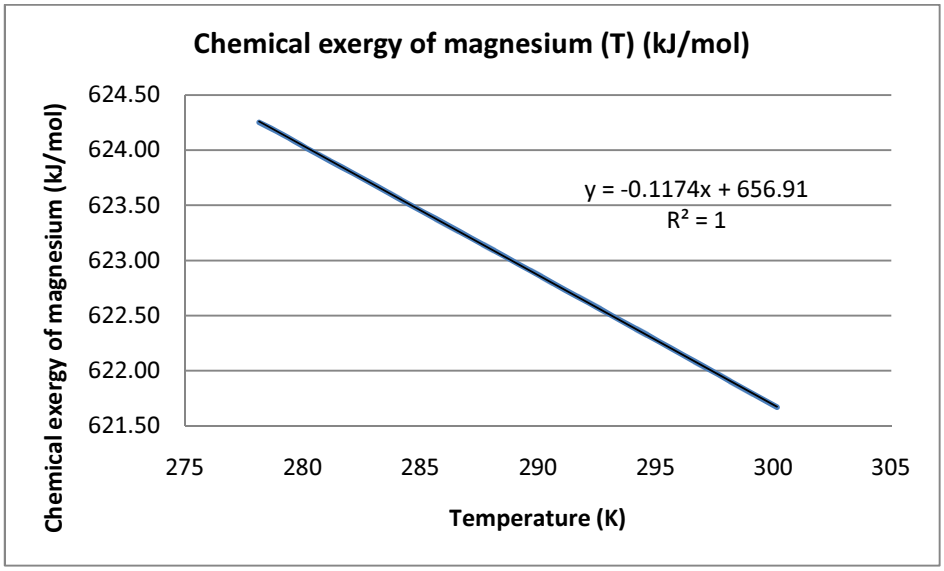

Figure 7-3: Chemical exergy of magnesium at constant relative humidity (0.77) as a function of T_0

Table 7-6: Chemical exergy of magnesium at constant relative humidity (0.77) as a function of T_0

T (K)	$\Delta_R \overline{g}(T)$	$\overline{e}^{Ch}_{Talc}$	$\overline{e}^{Ch}_{SiO_2}$	$\overline{e}^{Ch}_{H_2O(g)}$	$\overline{e}^{Ch}_{O_2}$	$\overline{e}^{Ch}_{Mg}$	*% Diff. vs.* T°
	(kJ/mol)	***(kJ/mol)***	***(kJ/mol)***	***(kJ/mol)***	***(kJ/mol)***	***(kJ/mol)***	
278.15	-1874.88	20.01	1.28	11.58	3.63	**624.25**	0.38%
279.15	-1874.38	20.08	1.28	11.44	3.64	**624.14**	0.36%
280.15	-1873.88	20.15	1.29	11.34	3.65	**624.02**	0.34%
281.15	-1873.38	20.22	1.29	11.22	3.67	**623.90**	0.32%
282.15	-1872.88	20.29	1.30	11.09	3.68	**623.79**	0.30%
283.15	-1872.38	20.37	1.30	10.97	3.70	**623.67**	0.28%
284.15	-1871.88	20.44	1.31	10.86	3.71	**623.55**	0.26%
285.15	-1871.38	20.51	1.31	10.74	3.73	**623.44**	0.25%
286.15	-1870.88	20.58	1.32	10.61	3.74	**623.32**	0.23%
287.15	-1870.38	20.65	1.32	10.50	3.76	**623.21**	0.21%
288.15	-1869.88	20.73	1.33	10.37	3.77	**623.09**	0.19%
289.15	-1869.38	20.80	1.33	10.26	3.79	**622.97**	0.17%
290.15	-1868.88	20.87	1.34	10.14	3.80	**622.85**	0.15%
291.15	-1868.38	20.94	1.34	10.03	3.82	**622.73**	0.13%
292.15	-1867.87	21.01	1.34	9.91	3.83	**622.62**	0.11%
293.15	-1867.37	21.09	1.35	9.79	3.85	**622.50**	0.10%
294.15	-1866.87	21.16	1.35	9.67	3.87	**622.38**	0.08%
295.15	-1866.37	21.23	1.36	9.55	3.88	**622.26**	0.06%
296.15	-1865.87	21.30	1.36	9.44	3.90	**622.14**	0.04%
297.15	-1865.37	21.37	1.37	9.32	3.91	**622.03**	0.02%
298.15	-1864.87	21.44	1.37	9.20	3.93	**621.91**	0.00%
299.15	-1864.37	21.52	1.38	9.09	3.95	**621.79**	-0.02%
300.15	-1863.87	21.59	1.38	8.97	3.97	**621.67**	-0.04%

For magnesium, the difference in the magnitude of molar chemical exergy is 2.34 kJ/mol over the 20 K temperature range, with a percentage difference of 0.38%. The slope displayed in Figure 7-3 is less than that of Figure 7-2 signifying lower sensitivity to changes in dead state temperature than calcium. One reason for this may be the presence of water vapour as a reactant in the reference reaction of magnesium, which was shown to be very sensitive to changes in dead state temperature. Although the change in the Gibbs energy as a function of dead state temperature has an important effect on changes in the chemical exergy of calcium and magnesium, changes in the chemical exergy of the

reference species are also important, some more so than others. An analysis of the chemical exergy of oxygen and carbon dioxide, reference species of calcium, showed that these two species exhibited a percentage difference over a 20 K temperature range (278.15 K to 298.15 K) of -8.42% and -7.43% respectively, whereas the percentage difference for the chemical exergy of water vapour over the same temperature range was 20.5%. Hence, the presence of water vapour as a *reactant* in the reference reaction of magnesium counteracts the reduction in the chemical exergy of magnesium, which occurs as a result of the reduction in Gibbs energy of the reaction. According to the results obtained for calcium and magnesium, the chemical exergy of both elements does not change significantly within the relevant temperature range but this will be considered further in light of the relevant final ionic chemical exergy.

Presently, the chemical exergy of two other elements as a function of dead state temperature are calculated, sodium and chlorine, which form major ionic components of natural waters, the sodium and chloride ions. The reference datum level for these species is the hydrosphere, and thus, they require a different approach, see (7.7). According to Brammer's findings [206], the effect of the last term in (7.7) on chemical exergy, with respect to changes in the dead state temperature, is small in comparison with the other equation terms. Brammer also found that changes in pH with respect to temperature were responsible for a non-linear relationship between the chemical exergy and temperature. The explanation for this is evident when one considers the non-linear relationship between pH at temperature T with respect to pH at standard temperature T° temperature derived by Millero [212], see (7.45).

$$pH(T) = pH^{\circ} + A(T - T^{\circ}) \times 10^{-3} + B(T - T^{\circ})^2 \times 10^{-4}$$

where $A = -9.702 - 2.379x + 3.885x^2$, $B = 1.123 - 0.003x + 0.933x^2$ (7.45)

and $x = pH^{\circ} - 8$

However, before the chemical exergy of sodium and chlorine as a function of dead state temperature can be calculated, there is one further complication to be considered. Based on the model derived by Morris ((7.7) and Figure 7-1), the changes in the chemical exergy of hydrogen as a function of temperature must also be calculated. This requires calculating the Gibbs energy of the reaction not only for the formation of the reference ion (the first term on the right of (7.7)) but also for a second reference reaction, i.e. the formation of water vapour from hydrogen and oxygen. The chemical exergy of hydrogen was calculated and was found to decrease linearly with increasing dead state temperature. Increasing the dead state temperature from 278.15 to 298.15 K resulted in a 1.42% difference in the value of chemical exergy. These results are similar to results obtained in the literature by Ertesvag [208] who found that "*the chemical exergy of hydrogen increased 0.7-0.8% per 10°C of lower ambient temperature*".

Based on the reference reaction for the formation of the chloride ion, see (7.20), and using constant values for the last term of (7.7) according to Brammer's findings, the chemical exergy of chlorine as a function of the dead state temperature was calculated and is shown in Table 7-7 and Figure 7-4.

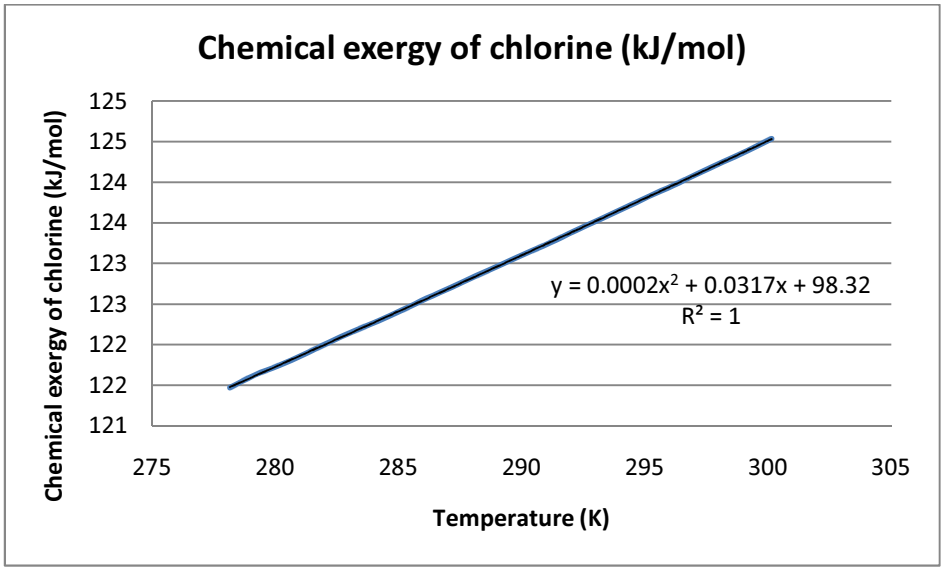

Figure 7-4: Chemical exergy of chlorine at constant relative humidity (0.77) as a function of T_0

Activity coefficient and molality values of $\gamma_{Cl^-} = 0.63$ and $M_{Cl^-} = 0.566$ mol/kg were obtained from the cited reference [117]. The values of the change in the molar heat capacity and the molar entropy of the reaction used to calculate the Gibbs energy of reaction of the chloride ion as a function of T_0 were calculated to be $\Delta_R \overline{c}_P^{\circ}$ (-0.1678 kJ/mol.K) and $\Delta_R \overline{s}^{\circ}$ (-0.1204 kJ/mol.K). The magnitude of $\Delta_R \overline{c}_P^{\circ}$ with respect to the value of $\Delta_R \overline{s}^{\circ}$ is unusual, in the case of calcium and magnesium the value of $\Delta_R \overline{c}_P^{\circ}$ was two orders of magnitude less than the corresponding values of $\Delta_R \overline{s}^{\circ}$. However, for chlorine, the magnitude of $\Delta_R \overline{c}_P^{\circ}$ is greater than $\Delta_R \overline{s}^{\circ}$. These relevant magnitudes are interesting because the molar heat capacity terms in (7.38) and (7.39) have been deemed negligible by Szargut [208]. An analysis of these terms for calcium and magnesium by the author showed that indeed the contribution of the $\Delta_R \overline{c}_P^{\circ}$ terms was very small in comparison to the $\Delta_R \overline{s}^{\circ}$ terms. With regards to magnesium, there was a 0.0003% difference between the change in the Gibbs

energy of the reaction calculated with and without the $\Delta_R \overline{c}_P^{\circ}$ terms at 278.15 K. However, in the case of chlorine, the difference although still very small, i.e. a 0.09% difference in the change of Gibbs energy of the reaction at 278.15 K, is two orders of magnitude greater than the case of magnesium. When the $\Delta_R \overline{c}_P^{\circ}$ values are available, calculating the two extra terms using a spreadsheet is not computationally taxing, and therefore, they have been included for accuracy when available in this thesis.

Table 7-7: Chemical exergy of chlorine at constant relative humidity (0.77) as a function of T_0

T (K)	*j*	*z*	$\overline{e}_{H_2}^{Ch}(T)$ *(kJ/mol)*	$\Delta_R \overline{g}_{Cl^-}(T)$ *(kJ/mol)*	*pH(T)*	$\overline{e}_{Cl_2}^{Ch}(T)$ *(kJ/mol)*	*%Diff. vs.* T°
278.15	2	-1	239.22	-133.520	8.34	**121.47**	-2.29%
279.15	2	-1	239.03	-133.411	8.33	**121.62**	-2.16%
280.15	2	-1	238.87	-133.302	8.31	**121.74**	-2.06%
281.15	2	-1	238.70	-133.191	8.30	**121.88**	-1.94%
282.15	2	-1	238.52	-133.081	8.29	**122.02**	-1.82%
283.15	2	-1	238.35	-132.969	8.27	**122.16**	-1.71%
284.15	2	-1	238.19	-132.857	8.26	**122.29**	-1.60%
285.15	2	-1	238.02	-132.745	8.25	**122.43**	-1.49%
286.15	2	-1	237.84	-132.631	8.24	**122.57**	-1.37%
287.15	2	-1	237.68	-132.518	8.22	**122.71**	-1.25%
288.15	2	-1	237.50	-132.403	8.21	**122.85**	-1.14%
289.15	2	-1	237.34	-132.288	8.20	**122.98**	-1.03%
290.15	2	-1	237.16	-132.173	8.19	**123.12**	-0.91%
291.15	2	-1	237.00	-132.057	8.17	**123.25**	-0.81%
292.15	2	-1	236.83	-131.940	8.16	**123.40**	-0.69%
293.15	2	-1	236.66	-131.823	8.15	**123.54**	-0.57%
294.15	2	-1	236.49	-131.705	8.14	**123.68**	-0.46%
295.15	2	-1	236.31	-131.587	8.13	**123.82**	-0.34%
296.15	2	-1	236.15	-131.468	8.12	**123.96**	-0.23%
297.15	2	-1	235.97	-131.348	8.11	**124.11**	-0.11%
298.15	2	-1	235.81	-131.228	8.10	**124.25**	0.00%
299.15	2	-1	235.64	-131.107	8.09	**124.39**	0.11%
300.15	2	-1	235.47	-130.986	8.08	**124.54**	0.23%

As Table 7-7 shows, the change in the chemical exergy of chlorine as a function of the dead state temperature, in terms of percentage difference, is greater than that of calcium and magnesium. Importantly, the chemical exergy of chlorine increases with temperature as opposed to the chemical exergy of both calcium and magnesium which decreased as the dead state temperature increased. As Figure 7-4 shows, the chemical exergy of chlorine as a function of dead state temperature can be represented by a second order polynomial, i.e. $\overline{e}^{Ch}_{Cl^-} = 0.0002T^2(K) + 0.0317T(K) + 98.32$ in contrast to the linear relationships over the temperature range evident for both calcium and magnesium. For practical purposes the relationship is evidently linear over the temperature range under consideration. The temperature is very unlikely to exceed this range for most applications.

A similar approach was used to calculate the chemical exergy of sodium as a function of dead state temperature, based on the reference reaction for the formation of the sodium ion (7.17). Having calculated values of $\Delta_R\overline{c}^{\circ}_p$ (0.0326 kJ/mol.K) and $\Delta_R\overline{s}^{\circ}$ (0.0731 kJ/mol.K), and using constant values for $\gamma_{Na^+} = 0.65$ and $M_{Na^+} = 0.486$ mol/kg from [117], the chemical exergy of sodium was calculated as a function of dead state temperature. The results are shown in Table 7-8 and Figure 7-5. The chemical exergy of sodium decreases with increasing dead state temperature in the same manner as calcium and magnesium, the magnitude of percentage difference is also similar to the values obtained for these other two elements. However, unlike calcium and magnesium but similar to chlorine, the relationship between chemical exergy and dead state temperature at constant relative humidity is not linear but a polynomial of second order due to the non-linear variation of pH with

temperature, see Figure 7-5. Again, over the temperature range, the relationship is linear for practical purposes.

Table 7-8: Chemical exergy of sodium at constant relative humidity (0.77) as a function of T_0

T (K)	*j*	*z*	$\overline{e}^{Ch}_{H_2}(T)$ *(kJ/mol)*	$\Delta_R\overline{g}_{Na^+}(T)$ *(kJ/mol)*	*pH(T)*	$\overline{e}^{Ch}_{Na}(T)$ *(kJ/mol)*	*%Diff. vs. T°*
278.15	1	1	239.22	-260.46	8.34	**338.30**	0.56%
279.15	1	1	239.03	-260.54	8.33	**338.20**	0.53%
280.15	1	1	238.87	-260.61	8.31	**338.12**	0.50%
281.15	1	1	238.70	-260.68	8.30	**338.03**	0.48%
282.15	1	1	238.52	-260.75	8.29	**337.94**	0.45%
283.15	1	1	238.35	-260.82	8.27	**337.85**	0.42%
284.15	1	1	238.19	-260.89	8.26	**337.76**	0.40%
285.15	1	1	238.02	-260.96	8.25	**337.67**	0.37%
286.15	1	1	237.84	-261.04	8.24	**337.58**	0.34%
287.15	1	1	237.68	-261.11	8.22	**337.48**	0.31%
288.15	1	1	237.50	-261.18	8.21	**337.39**	0.29%
289.15	1	1	237.34	-261.25	8.20	**337.30**	0.26%
290.15	1	1	237.16	-261.32	8.19	**337.20**	0.23%
291.15	1	1	237.00	-261.40	8.17	**337.11**	0.20%
292.15	1	1	236.83	-261.47	8.16	**337.01**	0.17%
293.15	1	1	236.66	-261.54	8.15	**336.92**	0.15%
294.15	1	1	236.49	-261.61	8.14	**336.82**	0.12%
295.15	1	1	236.31	-261.69	8.13	**336.72**	0.09%
296.15	1	1	236.15	-261.76	8.12	**336.62**	0.06%
297.15	1	1	235.97	-261.83	8.11	**336.52**	0.03%
298.15	1	1	235.81	-261.91	8.10	**336.42**	0.00%
299.15	1	1	235.64	-261.98	8.09	**336.32**	-0.03%
300.15	1	1	235.47	-262.05	8.08	**336.22**	-0.06%

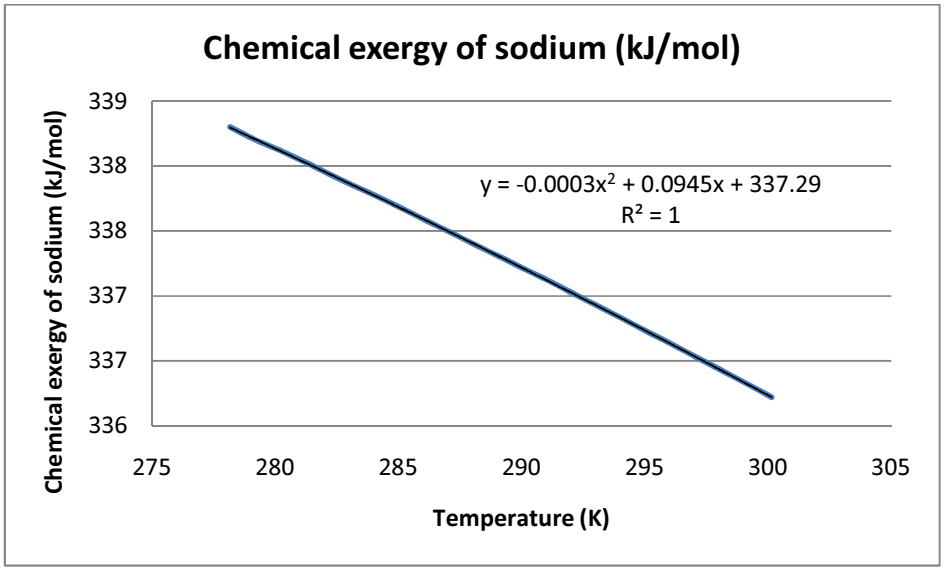

Figure 7-5: Chemical exergy of sodium at constant relative humidity (0.77) as a function of T_0

7.3.3 Change in the Gibbs energy of the reaction for the formation of the aqueous ions as a function of dead state temperature

In this section the second term on the right of (7.13) is calculated for the relevant ions. The change in the Gibbs energy of the reaction for the formation of the aqueous ions chloride and sodium has been calculated in the previous section while calculating the chemical exergy of chlorine and sodium. The change in the Gibbs energy for the formation of the aqueous ions calcium and magnesium are now considered.

The reference reactions of the calcium and magnesium ions are shown in (7.46) and (7.47).

$$Ca + 2H^{+} \rightarrow Ca^{++} + H_2 \qquad (7.46)$$

$$Mg + 2H^{+} \rightarrow Mg^{++} + H_2 \qquad (7.47)$$

Unfortunately, the molar heat capacity of the ions is not available in regular sources of thermodynamic data, e.g. [173, 205, 210]. However, based on the fact that the contribution of the change in the molar heat capacity of the reaction terms in (7.38) and (7.39) was previously found to be small and has been deemed negligible by Szargut [208], the omission of these terms from the relevant Gibbs energy equations should not affect the accuracy of the calculations. The values of $\Delta_R \overline{s}^{\circ}$ calculated for the formation of the ions were 0.036 and -0.04 kJ/mol.K for the calcium and magnesium ions respectively.

The changes in the Gibbs energy of the reaction for the formation of the ions calcium, magnesium, sodium and chlorine, as a function of dead state temperature, are shown in Table 7-9. As the dead state temperature increases, the Gibbs energy of the reaction for the calcium and sodium ions decreases (i.e. become more negative). The opposite is true for the magnesium and chloride ions. The magnitude of the change in Gibbs energy is greater for both the sodium and chloride ions due to the greater values of $\Delta_R \overline{s}^{\circ}$.

Table 7-9: Change in the Gibbs energy of the reaction as a function of T_0 for the ion formation

	$\Delta_R \bar{g}(T)$ *(kJ/mol)*			
T (K)	***Ca^{++}***	***Mg^{++}***	***Na^{+}***	***Cl^{-}***
278.15	-552.86	-455.60	-260.46	-133.52
279.15	-552.89	-455.56	-260.54	-133.41
280.15	-552.93	-455.52	-260.61	-133.30
281.15	-552.97	-455.48	-260.68	-133.19
282.15	-553.00	-455.44	-260.75	-133.08
283.15	-553.04	-455.40	-260.82	-132.97
284.15	-553.07	-455.36	-260.89	-132.86
285.15	-553.11	-455.32	-260.96	-132.74
286.15	-553.15	-455.28	-261.04	-132.63
287.15	-553.18	-455.24	-261.11	-132.52
288.15	-553.22	-455.20	-261.18	-132.40
289.15	-553.25	-455.16	-261.25	-132.29
290.15	-553.29	-455.12	-261.32	-132.17
291.15	-553.33	-455.08	-261.40	-132.06
292.15	-553.36	-455.04	-261.47	-131.94
293.15	-553.40	-455.00	-261.54	-131.82
294.15	-553.44	-454.96	-261.61	-131.70
295.15	-553.47	-454.92	-261.69	-131.59
296.15	-553.51	-454.88	-261.76	-131.47
297.15	-553.54	-454.84	-261.83	-131.35
298.15	-553.58	-454.80	-261.91	-131.23
299.15	-553.62	-454.76	-261.98	-131.11
300.15	-553.65	-454.72	-262.05	-130.99

7.3.4 Change in the Gibbs energy of the reaction for the formation of the non-ionised species

The next step is to assess the change in the Gibbs energy of the non-ionised species, i.e. the last term in (7.13). This section is brief because, by convention, the Gibbs energy of formation of an element at all temperatures is zero [213].

7.3.5 Change in the chemical exergy of the ions as a function of the dead state temperature

Finally, the various terms of (7.13) can be brought together, the results are shown in Table 7-10 and Figure 7-6. The molar chemical exergy of the calcium, magnesium, and sodium ions decreases with increasing dead state temperature, the molar chemical exergy of the chloride ion increases with increasing temperature (or becomes less negative). Over the 20 K temperature range (278.15 to 298.15 K), the change in chemical exergy is significant for the chloride, sodium and calcium ions, percentage differences of 5.06%, 4.26% and 3.42% respectively. Although the change in the chemical exergy for the magnesium ion (0.91%) is not as great as the other ions, it is not negligible. With regards to changes in the magnitude of chemical exergy, the exergy of the calcium ion exhibits the greatest change 6.3 kJ/mol. The chemical exergy of the chloride and sodium ions changes by 3.69 kJ/mol and 3.32 kJ/mol respectively. The relationship between temperature and the chemical exergy of the calcium and magnesium ions is linear. Regarding the sodium and chloride ions the relationship is a second order polynomial, reflecting the results obtained earlier for the chemical exergy of the respective elements. However, as Figure 7-6 shows, over the relevant temperature range, a linear approximation is appropriate.

Table 7-10: Chemical exergy of various ions at constant relative humidity (0.77) as a function of T_0

T (K)	$\overline{e}^{Ch}_{Ca^{++}}$ *(kJ/mol)*	*% Diff. vs. T_0*	$\overline{e}^{Ch}_{Mg^{++}}$ *(kJ/mol)*	*% Diff. vs. T_0*	$\overline{e}^{Ch}_{Na^{+}}$ *(kJ/mol)*	*% Diff. vs. T_0*	$\overline{e}^{Ch}_{Cl^{-}}$ *(kJ/mol)*	*% Diff. vs. T_0*
278.15	183.98	3.42%	168.65	0.91%	77.84	4.26%	-72.79	5.06%
279.15	183.66	3.26%	168.58	0.87%	77.67	4.06%	-72.60	4.81%
280.15	183.35	3.09%	168.50	0.82%	77.52	3.87%	-72.43	4.59%
281.15	183.03	2.93%	168.42	0.78%	77.36	3.67%	-72.25	4.36%
282.15	182.72	2.76%	168.35	0.74%	77.19	3.46%	-72.07	4.11%
283.15	182.41	2.59%	168.27	0.69%	77.03	3.26%	-71.89	3.87%
284.15	182.09	2.43%	168.19	0.64%	76.87	3.06%	-71.71	3.64%
285.15	181.78	2.26%	168.12	0.60%	76.71	2.86%	-71.53	3.39%
286.15	181.46	2.09%	168.04	0.56%	76.54	2.64%	-71.35	3.14%
287.15	181.15	1.92%	167.96	0.51%	76.38	2.44%	-71.16	2.89%
288.15	180.84	1.75%	167.89	0.46%	76.21	2.22%	-70.98	2.64%
289.15	180.52	1.58%	167.81	0.42%	76.05	2.01%	-70.80	2.39%
290.15	180.21	1.40%	167.73	0.37%	75.88	1.80%	-70.61	2.13%
291.15	179.89	1.23%	167.65	0.32%	75.72	1.58%	-70.43	1.88%
292.15	179.57	1.06%	167.58	0.28%	75.54	1.36%	-70.24	1.62%
293.15	179.26	0.88%	167.50	0.23%	75.38	1.14%	-70.05	1.35%
294.15	178.94	0.71%	167.42	0.19%	75.20	0.91%	-69.86	1.09%
295.15	178.63	0.53%	167.34	0.14%	75.03	0.69%	-69.67	0.82%
296.15	178.31	0.36%	167.26	0.09%	74.86	0.46%	-69.49	0.55%
297.15	177.99	0.18%	167.19	0.05%	74.69	0.23%	-69.29	0.27%
298.15	177.68	0.00%	167.11	0.00%	74.52	0.00%	-69.10	0.00%
299.15	177.36	-0.18%	167.03	-0.05%	74.34	-0.23%	-68.91	-0.28%
300.15	177.04	-0.36%	166.95	-0.09%	74.17	-0.47%	-68.72	-0.56%

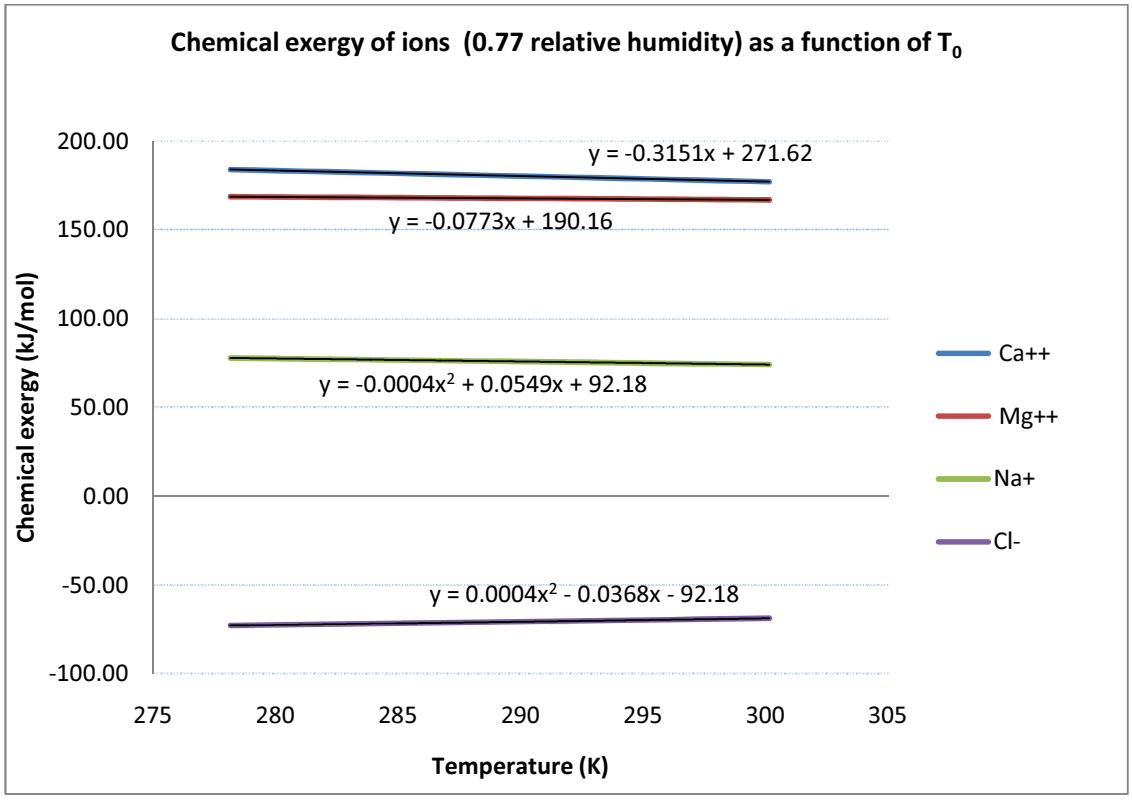

Figure 7-6: Chemical exergy of various ions at constant relative humidity (0.77) as a function of T_0

7.3.6 Chemical exergy of the bicarbonate ion as a function of dead state temperature

The bicarbonate ion is formed in natural waters when calcite, carbon dioxide and water react to form the calcium and bicarbonate ions [184]. The chemical exergy of the bicarbonate ion cannot be calculated in the same manner as the other ions previously considered, i.e. modelled as a simple elemental redox reaction. Resulting from the analysis carried out in section 7.2.1, the molar chemical exergy of the bicarbonate ion can be calculated by considering how each term in (7.25) changes with changing dead state temperature. Changes in the chemical exergy of hydrogen and oxygen as a function of dead

state temperature have previously been calculated, having acted as reference species in previous reference reactions. This leaves for consideration the chemical exergy of carbon and the change in the Gibbs free energy of the formation of the bicarbonate ion as functions of dead state temperature.

The molar chemical exergy of carbon as a function of dead state temperature was calculated by;

1. Calculating the change in the Gibbs energy of formation as a function of dead state temperature according to the reference reaction (7.25); a value of -0.2876 kJ/mol.K was calculated for $\Delta_R \overline{s}^{\circ}$;
2. Calculating the change in the chemical exergy of the reference species in (7.48), i.e. CO_2 (O_2 was previously calculated).

$$C + O_2 \rightarrow CO_2 \qquad (7.48)$$

Values for the molar heat capacity of the bicarbonate ion are not available in common sources of thermodynamic data [173, 205, 210], and therefore, the molar heat capacity terms have been neglected. The value for $\Delta_R \overline{s}^{\circ}$ was calculated to be -0.2876 kJ/mol.K.

Based on (7.25) and (7.48), the chemical exergy of the bicarbonate ion was calculated over the relevant temperature range and the results are shown in Table 7-11. According to these results, the chemical exergy of the bicarbonate ion shows significant sensitivity to changes in the dead state temperature, a 9.65% difference and a change in the magnitude of chemical exergy of 5.63 kJ/mol over the temperature range (278.15 to 298.15 K). The change in the Gibbs energy of formation is the main contributing factor for the significant

change in the chemical exergy of the bicarbonate ion, caused by the relatively high value calculated for $\Delta_R \overline{s}^{\circ}$. The chemical exergy changes undergone by the elements practically cancel each other over the temperature range, i.e. the decrease in the chemical exergy of hydrogen (multiplied by its stoichiometric coefficient 0.5) is counteracted by the increase in the chemical exergy of carbon and oxygen (multiplied by the relevant stoichiometric coefficient 1.5), see (7.25).

Table 7-11: Chemical exergy of the bicarbonate ion at constant relative humidity (0.77) as a function of T_0

T (K)	$\Delta_R \overline{g}(T)$ *(kJ/mol)*	$\overline{e}^{Ch}_{H_2}$ *(kJ/mol)*	$\overline{e}^{Ch}_{C}$ *(kJ/mol)*	$\overline{e}^{Ch}_{O_2}$ *(kJ/mol)*	$\overline{e}^{Ch}_{HCO_3^-}$ *(kJ/mol)*	*% Diff. vs. T0*
278.15	-592.52	239.22	409.13	3.63	**-58.35**	9.65%
279.15	-592.23	239.03	409.18	3.64	**-58.08**	9.23%
280.15	-591.95	238.87	409.24	3.65	**-57.79**	8.78%
281.15	-591.66	238.70	409.30	3.67	**-57.51**	8.33%
282.15	-591.37	238.52	409.35	3.68	**-57.23**	7.89%
283.15	-591.08	238.35	409.41	3.70	**-56.95**	7.43%
284.15	-590.80	238.19	409.46	3.71	**-56.67**	6.97%
285.15	-590.51	238.02	409.52	3.73	**-56.39**	6.51%
286.15	-590.22	237.84	409.58	3.74	**-56.11**	6.04%
287.15	-589.93	237.68	409.63	3.76	**-55.83**	5.57%
288.15	-589.65	237.50	409.69	3.77	**-55.55**	5.10%
289.15	-589.36	237.34	409.75	3.79	**-55.26**	4.61%
290.15	-589.07	237.16	409.80	3.80	**-54.98**	4.12%
291.15	-588.78	237.00	409.86	3.82	**-54.70**	3.62%
292.15	-588.50	236.83	409.91	3.83	**-54.42**	3.13%
293.15	-588.21	236.66	409.97	3.85	**-54.14**	2.62%
294.15	-587.92	236.49	410.03	3.87	**-53.85**	2.11%
295.15	-587.63	236.31	410.08	3.88	**-53.57**	1.59%
296.15	-587.35	236.15	410.14	3.90	**-53.28**	1.06%
297.15	-587.06	235.97	410.20	3.91	**-53.00**	0.54%
298.15	-586.77	235.81	410.25	3.93	**-52.72**	0.00%
299.15	-586.48	235.64	410.31	3.95	**-52.43**	-0.54%
300.15	-586.19	235.47	410.36	3.97	**-52.15**	-1.09%

7.4 Summary

The Szargut model has been examined in detail and its application to UPW exergy analyses has been considered. One important limitation of Szargut standard chemical exergy values is that the chemical exergy of the relevant species is referenced to a standard dead state. This chapter, (1) developed a methodology to calculate the chemical exergy of electrolytic solutions at various dead state temperatures and relative humidity values, and (2) specifically investigated the chemical exergy changes in relevant ionic species and found that the chemical exergy of the ions was generally sensitive to changes in the dead state temperature. The developments of this chapter are termed Model D.

The ions under consideration included sodium, chloride, calcium, magnesium and bicarbonate. It was found that the chemical exergy of the majority of the ionic species investigated changed significantly with changing values of dead state temperature, particularly the bicarbonate ion, which exhibited a 9.65% difference change and a decrease in the magnitude of chemical exergy of 5.63 kJ/mol over the relevant temperature range. In terms of magnitude, the chemical exergy of the calcium ion exhibited the greatest change in molar chemical exergy, decreasing by 6.3 kJ/mol over the temperature range under consideration with a percentage difference change of 3.42%.

8 UPW plant analysis

In this chapter Model B, Model C and Model D are used to undertake an exergy analysis of a semiconductor UPW plant. The objectives of this analysis are to compare the exergy models and to characterise the plant. The UPW plant under consideration is several years old. The plant layout and the data used to conduct this exergy analysis, along with all relevant assumptions, are considered in detail in Appendix B. The inlets and outlets to all process stages are numbered. Certain processes contain several modules; the modules in each process are designated by lower case letters. For example, the inlet to the second module of the ion exchange process is termed 1b. Principal technologies in the make-up and primary loops include first and second pass (two-stage) RO, ion exchange, electro-deionisation and various levels of filtration from multi-media filtration to one micron filtration.

The boundary of each of the processes has been dictated by the presence of suitable measurement equipment. For example, consider the two make-up loop heat exchangers, due to the necessary assumptions resulting from absent or non-functioning measurement gauges (detailed in Appendix B), certain pressures at the inlet of one heat exchanger were equated to the outlet of the process immediately upstream. Unfortunately, assumptions such as these may have the effect of attributing exergy destruction to the heat exchanger, when in fact, some of the exergy destruction results from the pipe-work between the two processes. These assumptions have been unavoidable within the project constraints, illustrating the importance of installing and maintaining suitable measurement equipment in an effort to accurately characterise and manage plant energy consumption.

Due to the lack of instrumentation in certain processes in the polishing loop, only the make-up and primary loops were evaluated. The greatest change in the concentration of the UPW plant water occurs during these first two process loops, so from the perspective of the exergy model comparison, the omission of the polishing loop is not important. Based on the data in Appendix B, the resistivity of the product water at the end of the primary loop was 17.8 MΩ.cm at 25 °C, the typical resistivity of the UPW factory supply is 18.2 MΩ.cm at 25 °C. The resistivity of the incoming UPW plant water is approximately 0.0024 MΩ.cm at 25 °C. Therefore, the change undergone in the product water from the start of the make-up loop to the end of the primary loop, in terms of resistivity, can be described by a factor of over 7000. Regarding the polishing loop, the factor of increased resistivity is approximately unity.

The UPW plant exergy analysis did not consider the exergy of organic compounds for one main reason, i.e. the instrumentation in the first two loops of the UPW plant measures the concentration of species in terms of conductivity or resistivity solely. Several researchers [179, 180] have considered the chemical exergy of organic matter in natural waters based on measurements such as Total Organic Carbon (TOC), Chemical Oxygen Demand (COD) and Biological Oxygen Demand (BOD); however, this information was not available at the various process stages in the make-up and primary loops.

8.1 Exergy analysis of the plant processes

The exergy analysis of the UPW plant is broken down into two focus areas, (1) the model comparison, and (2) the characterisation of the plant. Both the exergy rates and the rates of

exergy destruction at the various process stages have been calculated using the three models.

The system was defined in Chapter 6 section 6.4 as the stream of the UPW product water in the plant. The thermo-mechanical dead state was defined as the ambient temperature of the incoming UPW water (16 °C), pressure of 1 bar, and relative humidity of 0.77. The same thermo-mechanical dead state was adopted for all three models. For Models B and C an average ionic concentration (135 ppm), typical of European river water [170], was defined as the chemical (or ionic concentration) dead state. As discussed in Chapter 7, regarding Model D, the intrinsic chemical exergy values are somewhat pre-defined with respect to the Szargut reference environment. Importantly however, Model D considers changes in intrinsic chemical exergy resulting from non-standard dead state temperatures and relative humidity values.

Based on the assessment of the incoming UPW plant water, a factor of 0.773 was used to relate electrical conductivity and TDS (see Chapter 6 section 6.3). Regarding Model B, to maintain the approach of Cerci [136], the aqueous solution was defined as an ideal mixture of solid NaCl and water. The Model B approach equates salinity or total TDS to a mass fraction of NaCl [171], apparently, irrespective of the ionic aqueous solution. Consequently, the NaCl mass and mole fractions at the various process stages were determined from the TDS values, which in turn were determined from the conductivity measurements using the 0.773 factor. The Model B equations are discussed in detail in Chapter 3 section 3.2.2.

Regarding Models C and D, the aqueous solution was defined as an electrolytic solution of calcium and bicarbonate ions. The approach used to, (1) calculate the physical exergy, (2) define the electrolytic solution, and (3) calculate the activity of the electrolytic species and water was essentially identical for both Model C and Model D (see Chapter 6 section 6.4). The key difference between Model C and Model D was the calculation of the chemical exergy term. The Model C chemical exergy was calculated according to (8.1).

$$\dot{E}^{Ch} = RT_0 \left[\dot{N}_w \ln \frac{x_w^{RDS}}{x_w^{DS}} + \dot{N}_{Ca^{++}} \ln \frac{(M\gamma)_{Ca^{++}}^{RDS}}{(M\gamma)_{Ca^{++}}^{DS}} + \dot{N}_{HCO_3^-} \ln \frac{(M\gamma)_{HCO_3^-}^{RDS}}{(M\gamma)_{HCO_3^-}^{DS}} \right] \tag{8.1}$$

The Model D chemical exergy was calculated according to (8.2).

$$\begin{aligned} \dot{E}^{Ch} &= \dot{N}_w \overline{e}_w^{Ch} + \dot{N}_{Ca^{++}} \overline{e}_{Ca^{++}}^{Ch} + \dot{N}_{HCO_3^-} \overline{e}_{HCO_3^-}^{Ch} \\ &+ RT_0 \left[\dot{N}_w \ln x_w^{RDS} + \dot{N}_{Ca^{++}} \ln (M\gamma)_{Ca^{++}}^{RDS} + \dot{N}_{HCO_3^-} \ln (M\gamma)_{HCO_3^-}^{RDS} \right] \end{aligned} \tag{8.2}$$

The superscripts RDS and DS in (8.1) and (8.2) refer to the restricted dead state under consideration and the dead state. For both Model C and Model D, the molar flow rates were calculated from the mass flow rates of the relevant species (based mainly on SCADA volumetric flow rates), which in turn were based on apportioning the TDS between the relevant species according to the method outlined in Chapter 6 section 6.3. The activity coefficients were calculated using (6.25), the molalities of the electrolytic species and the mole fraction of water were calculated according to the methods discussed in Chapter 6 section 6.1.

Now consider the characterisation of the UPW plant, exergy destruction at the relevant process stages was calculated using the exergy balance equation for steady state operation, see (2.5). For the processes under consideration in the UPW plant, the equation simplifies

to the sum of exergy rates and any electrical work inputs entering each process minus the sum of the exergy rates leaving each process. The exergetic efficiency of the important process stages was also calculated and was based on the rational exergetic efficiency, which considers the specific function of the process under consideration.

8.1.1 Examination of assumptions for UPW exergy analysis

Before the results are presented some model assumptions, which were discussed previously in Chapter 6, are re-examined briefly. In general, it was found that the use of the average specific heat capacity (c_v) resulted in minor errors when compared with the integration of c_v as a function of temperature (less than 0.25% for the majority of process stages). The relevant functions were fitted according to NIST data [188]. There were two exceptions, however, the hot water heat exchanger heating water stream (process stages 5 and 6), which resulted in absolute percentage differences of approximately 3.7% for the incoming heating water and 10.5% for the outgoing heating water. Having integrated all the specific heat capacity values as a function of temperature for the comparison, they were subsequently used to calculate the physical exergy values.

Density values were treated as a constant with the exception of the heating water stream in the hot water heat exchanger. As proposed in Chapter 6 section 6.2, the density of the system was calculated at the first pass RO retentate concentrations to investigate possible changes in density due to increased concentration. Negligible difference was found between the average density value calculated over the temperature range for pure water and the average density calculated over the temperature range for the RO retentate concentrations, a percentage difference of 0.09% (998.2 kg/m^3 versus 999.07 kg/m^3 using the density

calculation model written in MATLAB). Thus, the same density value of pure water (998.2 kg/m^3) was used for the retentate streams.

8.2 UPW exergy analysis results

The results are broken down into two main sections;

1. The model comparison, which is a general analysis of the exergy rates and exergy destruction rates calculated using each of the models at the various process stages;
2. The plant characterisation which consists of;
    a. An analysis of the exergy destruction results to identify the principal sources of thermodynamic irreversibilities in the UPW plant make-up and primary loops;
    b. An analysis of the rational exergetic efficiency of processes and process modules.

8.2.1 Model comparison – exergy rates and exergy destruction rates

The exergy rates and exergy destruction rates calculated using the three models can now be compared.

8.2.1.1 Exergy rates – model comparison

The total, physical and chemical exergy rates calculated at each process stage using Model B, Model C and Model D are shown in Table 8-1.

Table 8-1: Comparison of exergy rates calculated using Model B, Model C and Model D

Process	*Process stage*	*Total exergy rates (kW)*			*Physical exergy rates (kW)*		*Chemical exergy rates (kW)*		
		Model B	***Model C***	***Model D***	***Model B***	***Model C & Model D***	***Model B***	***Model C***	***Model D***
Multi-media filters	1b	10.1	11.8	799.2	11.8	11.8	-1.63	0.074	787.4
	1c	9.7	11.4	767.8	11.3	11.3	-1.57	0.071	756.5
	1d	9.3	10.8	732.4	10.8	10.8	-1.49	0.067	721.7
	2b	9.7	11.4	798.7	11.3	11.3	-1.64	0.074	787.4
	2c	9.3	10.9	767.3	10.9	10.9	-1.57	0.071	756.5
	2d	8.9	10.4	732	10.4	10.4	-1.5	0.067	721.7
Pre-heat heat exchangers	3 (Product)	27.8	32.7	2298.1	32.5	32.5	-4.69	0.212	2265.6
	3 (Heating)	109	119.5	5027.7	119.2	119	-10.16	0.455	4908.7
	4 (Product)	32.2	37.1	2302.5	36.9	36.9	-4.68	0.210	2265.6
	4 (Heating)	73.6	84.2	4992.3	83.7	83.7	-10.16	0.455	4908.7
Hot water heat exchangers	5 (Product)	32.2	37.1	2302.5	36.9	36.9	-4.68	0.211	2265.6
	5 (Heating)	689.1	686.1	1417.8	690.7	686	-1.59	0.068	731.8
	6 (Product)	53.7	58.4	2323.7	58.4	58.2	-4.69	0.210	2265.6
	6 (Heating)	490.4	524.2	1255.9	**492**	**524.1**	-1.59	0.069	731.8
Biocide/anti-scalant treatment	7	53.7	58.4	2323.7	58.4	58.2	-4.69	0.209	2265.6
	8	53.7	58.4	2323.7	58.4	58.2	-4.69	0.209	2265.6
RO pre-filters	9	53.7	58.4	2323.7	58.4	58.2	-4.69	0.209	2265.6
	10	51.1	55.8	2321.1	55.8	55.6	-4.68	0.209	2265.6
Sodium bisulphite treatment	11	51.1	55.8	2321.1	55.8	55.6	-4.68	0.209	2265.6
	12	51.1	55.8	2321.1	55.8	55.6	-4.68	0.209	2265.6

Table 8-1: Comparison of exergy rates calculated using Model B, Model C and Model D

Process	*Process stage*	*Total exergy rates (kW)*			*Physical exergy rates (kW)*		*Chemical exergy rates (kW)*		
		Model B	***Model C***	***Model D***	***Model B***	***Model C & Model D***	***Model B***	***Model C***	***Model D***
First pass RO high pressure pumps/RO inlet	13a	27.5	29.9	1296	29.9	29.8	-2.4	0.098	1266.2
	13c	27.7	30.1	1303	30.1	30	-2.41	0.099	1273
	14a	58	60.5	1326.6	60.4	60.4	-2.39	0.098	1266.2
	14c	47	49.5	1322.3	49.5	49.4	-2.41	0.099	1273
First pass RO	15a	16.8	15.3	941.2	15.3	15.2	1.54	0.133	926
	15c	17.1	15.6	958.8	15.6	15.5	1.54	0.128	943.4
	16a	10	13.9	354.1	13.3	13.4	-3.38	0.510	340.8
	16c	6.2	10.1	339.7	9.5	9.5	-3.37	0.521	330.2
	17a	2	5.9	346.1	5.4	5.4	-3.38	0.510	340.8
	17c	1.8	5.7	335.4	5.2	5.2	-3.38	0.521	330.2
RO tank inlet	18	41.3	37.5	2384.9	37.4	37.1	3.89	0.329	2347.8
RO tank outlet/Primary distribution pumps inlet	19	41.3	37.5	2384.9	37.4	37.1	3.89	0.329	2347.8
Primary pumps outlet/Caustic treatment inlet	20	56.8	53	2400.4	52.9	52.6	3.89	0.329	2347.8
Caustic treatment outlet	21	56.2	52.9	2400.4	52.9	52.6	3.31	0.217	2347.8
First pass RO high pressure pumps/RO inlet	22b	18.8	17.6	800.5	17.7	17.6	1.11	0.072	782.9
	22c	18.4	17.3	784.7	17.3	17.2	1.08	0.071	767.5
	22d	19.1	18	815.3	18	17.9	1.13	0.074	797.4
	23b	56.1	55	837.8	55	54.9	1.1	0.072	782.9
	23c	57.1	56.1	823.5	56	56	1.08	0.071	767.5
	23d	56.9	55.8	853.1	55.8	55.7	1.13	0.074	797.4

Table 8-1: Comparison of exergy rates calculated using Model B, Model C and Model D

Process	*Process stage*	*Total exergy rates (kW)*			*Physical exergy rates (kW)*		*Chemical exergy rates (kW)*		
		Model B	***Model C***	***Model D***	***Model B***	***Model C & Model D***	***Model B***	***Model C***	***Model D***
Second pass RO	24b	19.5	18.4	702.6	18.3	18.3	1.18	0.112	684.3
	24c	20.2	19.2	682.1	19.1	19.1	1.15	0.108	663.1
	24d	21	19.9	707	19.8	19.8	1.19	0.112	687.2
	25b	6.2	6.3	104.9	6.2	6.3	-0.04	0.000	98.6
	25c	6.9	6.9	111.4	6.9	6.9	-0.03	0.000	104.4
	25d	6.8	6.7	116.9	6.8	6.7	-0.03	0.000	110.2
	26b	1.5	1.6	100.2	1.6	1.6	-0.04	0.000	98.6
	26c	1.6	1.7	106.1	1.7	1.7	-0.03	0.000	104.4
	26d	1.7	1.7	112	1.8	1.7	-0.03	0.000	110.2
Electro-deionisation process	27b	20.9	19.7	723.3	19.7	19.6	1.23	0.115	703.7
	27c	19.9	18.8	696.3	18.7	18.7	1.17	0.111	677.6
	27d	20.1	19	695.5	18.9	18.9	1.18	0.110	676.6
	28b	14.8	13.7	642.8	13.7	13.6	1.11	0.108	629.2
	28c	14.8	13.7	643.8	13.7	13.6	1.11	0.108	630.2
	28d	14.7	13.6	639.9	13.6	13.5	1.1	0.108	626.3
	29b	1.3	1.2	75.6	1.2	1.2	0.12	0.009	74.4
	29c	0.9	0.8	48.1	0.8	0.7	0.07	0.005	47.4
	29d	0.9	0.8	51.1	0.8	0.8	0.07	0.005	50.3

Table 8-1: Comparison of exergy rates calculated using Model B, Model C and Model D

Process	*Process stage*	*Total exergy rates (kW)*			*Physical exergy rates (kW)*		*Chemical exergy rates (kW)*		
		Model B	***Model C***	***Model D***	***Model B***	***Model C & Model D***	***Model B***	***Model C***	***Model D***
Primary mixed bed ion exchange	30b	14.3	13.2	653.9	13.2	13.1	1.13	0.110	640.8
	30c	13.7	12.6	625.3	12.6	12.5	1.08	0.105	612.8
	30d	14	12.9	639.1	12.9	12.8	1.1	0.108	626.3
	31b	13.2	12.1	652.8	12.1	12	1.13	0.110	640.8
	31c	12.6	11.6	624.3	11.5	11.5	1.08	0.105	612.8
	31d	12.9	11.8	638.1	11.8	11.7	1.1	0.108	626.3
One micron cartridge filters	32	38.1	34.9	1914.6	34.8	34.6	3.31	0.323	1880
	33	37.5	34.4	1914.1	34.2	34	3.31	0.323	1880
UPW tank inlet	34	31.4	28.8	1602.1	28.6	28.5	2.77	0.270	1573.6
Diverted flow to RO tanks	35	6.1	5.6	312	5.6	5.5	0.54	0.053	306.4

First, the total exergy rate (kW) is considered. The total exergy rates calculated using Model B and Model C are similar in terms of magnitude at each process stage. However, the Model D exergy rates are much greater in magnitude than the other two models. The total exergy rate does not facilitate ready comparison between the models. Therefore, the next step is to assess the models in terms of de-coupled physical and chemical exergy. One disadvantage of Model B is its integrated chemical and physical exergy calculation approach, leading to an aggregate exergy value. A method of decoupling the Model B physical and chemical exergy was presented in Chapter 5 and this approach is used again to break down Model B into physical and chemical exergy.

Looking at the physical exergy results, it is evident that, for the majority of process stages, the physical exergy values are similar. There is one notable exception, the outgoing heating water stream in the hot water heat exchanger (process stage 6). The physical exergy calculated according to Model B is 492 kW and this compares with a value of 524.1 kW calculated using the Model C/Model D approach, an absolute percentage difference of 6.5% which is now assessed.

The presence of salt in the Model B physical exergy calculations (in contrast to the pure water of the Model C/Model D approach) was investigated and ruled out as the cause of the differences in the following manner. The Model B physical exergy for the heating water at process stage 6 was calculated for pure water and compared with the physical exergy calculated for the ideal mixture at the relevant salt mass fractions. There was negligible difference between the physical exergy values, 492 kW including the relevant salt mass

fractions and 492.1 kW for pure water. Next, the physical exergy was broken down into its thermal and pressure terms and assessed, the main cause of the difference was found to be the manner in which the change in the specific internal energy $(u-u_0)$ was calculated. In an effort to compare and determine the most appropriate value of $(u-u_0)$ the change in specific internal energy was calculated in four ways, (1) using the XSteam function in MATLAB [169] at the relevant temperatures and pressures (250.8 kJ/kg), (2) the product of the average c_v (over the temperature interval) and the temperature difference (242.5 kJ/kg), (3) using NIST values of internal energy at the relevant temperatures and pressures (250.5 kg/mol [188]), and finally (4) rechecking, refitting and re-integrating the NIST c_v data (the same value as previously calculated as part of the overall physical exergy calculation, i.e. 268.8 kJ/kg).

The change in internal energy values calculated using the MATLAB XSteam function and the NIST internal energy data are very similar. When compared with the XSteam and NIST values, the use of average c_v values resulted in a percentage difference of 3.3%. It was expected that the average values would result in some error due to the fact that the heat capacity is not constant over the temperature range under consideration. The main issue, however, lies with the 6.5% difference between the fitted data and the tabulated NIST data/XSteam values. Theoretically $u(T)-u(T_0)=\int_{T_0}^{T} c_v(T)dT$ and therefore fitting $c_v(T)$ data and integrating seems like a reasonable approach. The deviation is due to the difference between the manner in which the relevant property tables are constructed from fundamental relations (i.e. the Helmholtz function for steam tables according to the cited

reference [109]) and the fitting of c_v data to a very specific temperature interval using Excel™, see Figure 8-1. This is an interesting finding that requires further research.

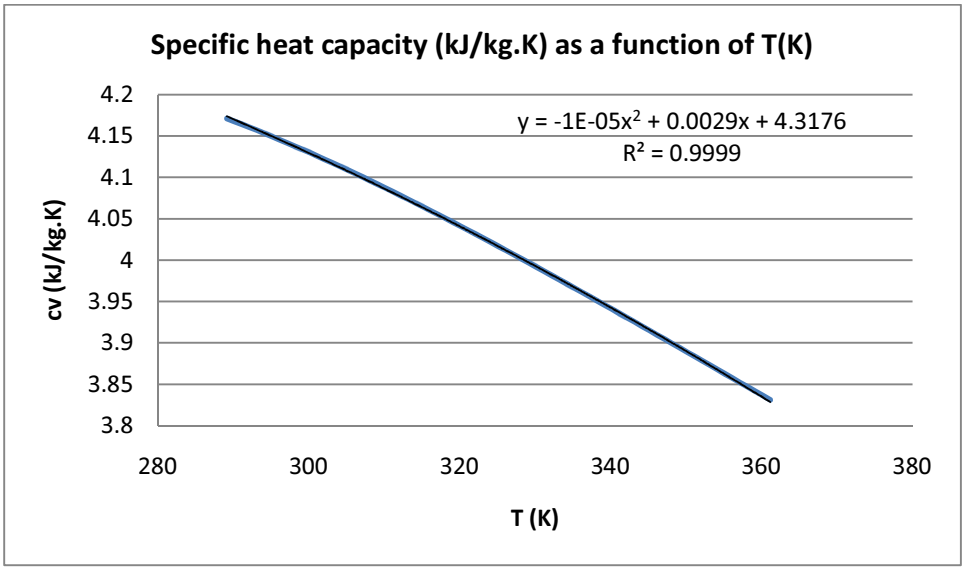

Figure 8-1: Specific heat capacity (c_v) as a function of temperature over the specific temperature range (289.15 to 361.15 K)

The physical exergy calculated using Model B was shown to be almost identical at process stage 6 for both pure water and the ideal mixture. Treating the stream as pure water simplifies the MATLAB programmes required to calculate physical exergy. The most concentrated process stage 16c can now be considered, if it can be shown that the physical exergy of the most concentrated stream in the UPW plant can be treated as pure water, it is evident that all less concentrated streams can be simplified to pure water. The physical exergy for the ideal mixture was calculated to be 9.53 kW while the physical exergy of pure water was calculated to be 9.54 kW. Therefore, according to the approach developed to break down Model B total exergy into physical and chemical exergy contributions, and at

the relevant mass fraction values of NaCl, there is negligible difference between the physical exergy of pure water and the physical exergy of the ideal mixture. In general, there are very minor differences between the physical exergy calculated using the de-coupled Model B and the Model C/Model D approaches, the hot water heat exchanger being the main exception.

According to Table 8-1, the three sets of chemical exergy rates are dissimilar. The Model B and Model C chemical exergy rates differ in general by one order of magnitude. The Model D chemical exergy rates include an intrinsic chemical exergy term, and thus, they are significantly greater in magnitude than the other two models. Model B chemical exergy rates are both positive and negative. The chemical exergy rates calculated using Model C and Model D are positive at all process stages. Regarding Model B, the greatest chemical exergy rate value -10.16 kW occurs at process stages 3 and 4 for the pre-heat heat exchanger heating water stream. It is however significant that this is also the largest volumetric flow rate in the UPW plant (507 m^3/h calculated from the heat exchanger mass energy balance), chemical exergy rates being a product of the mass or molar flow rates and the specific or molar chemical exergy respectively. This Model B finding coincides with the largest chemical exergy rate calculated using Model D, 4908.65 kW for the heating water at process stages 3 and 4. The chemical exergy rates calculated using Model C are generally small. The largest chemical exergy rate values occur at process stages 16a and 17a (0.51 kW), and 16c and 17c (0.52 kW), i.e. the first pass RO retentate streams and post throttling valve streams. It is interesting that these retentate streams are the most concentrated process stages in the UPW plant. Contrary to the Model B and the Model D

chemical exergy rates, which coincided with the high volumetric flow rates, the first pass RO retentate volumetric flow rates are relatively small in comparison with other make-up loop flow rates. Thus, one would expect the molar chemical exergy values to be significant. With respect to analysing the plant, the chemical exergy rates offer greater insight, however, in order to compare the manner in which chemical exergy is calculated using the three models, the molar chemical exergy approach used for the model comparison in Chapter 5 facilitates a clearer view.

8.2.1.2 Exergy destruction rates - model comparison

The exergy destruction rates arising due to irreversibilities in the UPW plant processes are now assessed in terms of the model comparison. Exergy destruction rates calculated using the three models are presented in Table 8-2. At first glance the key source of exergy destruction in the UPW plant make-up and primary loops is the hot water heat exchanger, and this finding pertains to all three models. The exergy destruction rates calculated using Model C and Model D are identical for the vast majority of processes. Consequently, only one percentage difference value is reported, i.e. the percentage difference between the exergy destruction rates calculated using Model B and Model D, shown in the final column of Table 8-2. The reason that, on the whole, the exergy destruction rates are identical for Model C and Model D is due to the cancellation of the intrinsic chemical exergy in the process exergy balance when no chemical reaction takes place. Intrinsic chemical exergy cancellations have been noted several times in the literature [105, 120].

Looking at the results in Table 8-2, it is evident that the exergy destruction rates calculated using the three models are very similar. There are two exceptions in terms of percentage

difference values; the caustic treatment (sodium hydroxide) (49.2%) and the hot water heat exchanger (20.6 %).

The caustic treatment is considered first, although it is acknowledged that the exergy destruction rates under consideration are not significant (1.2, 0.7 and 0.6 kW for Model B, Model C and Model D respectively). It is an interesting process stage, however, because it is the only stage where the Model C and the Model D exergy destruction rates are not identical. During the caustic treatment, according to the data in Appendix B Table 1, no changes in temperature or pressure occur. There is, however, a work input from the chemical metering pumps, which is identical for all models. The important change taking place is the increase in ionic concentration caused by the caustic injection treatment. The chemical reaction occurring between the system and the sodium hydroxide is not considered in detail due to the reasons relating to dosage rates outlined in Appendix B (page B3). However, the results of the chemical reaction are manifest in the increase in ionic conductivity from the RO tank (process stages 18 and 19) to the second pass RO, where a conductivity measurement is in situ. The ionic concentration changes from 6.3 ppm at process stage 20 to 23.2 ppm at process stage 21, see Appendix B Table 1. Thus, the differences in the exergy destruction rates relate solely to differences in the chemical exergy values calculated by each of the models.

Table 8-2: Comparison of exergy destruction rates calculated using Model B, Model C and Model D

Process	*Process module*	*Exergy destruction (kW)*			*% Diff.*
		Model B	*Model C*	*Model D*	
Multi-media filters	b	0.5	0.5	0.5	0
	c	0.4	0.4	0.4	0
	d	0.4	0.4	0.4	0
Pre-heat heat exchangers		31	30.9	30.9	0.3
Hot water heat exchangers		177.2	140.7	140.7	**20.6**
Biocide/anti-scalant treatment		0.6	0.6	0.6	0
RO pre-filters		2.6	2.6	2.6	-0.4
Sodium bisulphite treatment		0.6	0.6	0.6	0
First pass RO high pressure pumps	a	55.5	55.5	55.5	0
	c	55.7	55.6	55.6	0
First Pass RO	a	31.3	31.3	31.3	-0.1
	c	23.8	23.8	23.8	0
Throttling valves	a	8	8	8	0
	c	4.3	4.3	4.3	0
Exergy losses	**a**	**2**	**5.9**	**346.1**	
	c	**1.8**	**5.7**	**335.4**	
RO tank		1.8	1.8	1.8	0
Primary distribution pumps		20.2	20.2	20.2	0

Table 8-2: Comparison of exergy destruction rates calculated using Model B, Model C and Model D

Process	*Process module*	*Exergy destruction (kW)*			*% Diff.*
		Model B	*Model C*	*Model D*	
Caustic treatment		1.2	0.7	0.6	**49.2**
Second pass RO high pressure pumps	b	34.7	34.7	34.7	0
	c	38.3	38.2	38.2	0.3
	d	35.2	35.2	35.2	0
Second pass RO	b	30.5	30.3	30.3	0.5
	c	29.9	30	30	-0.3
	d	29.1	29.2	29.2	-0.2
Throttling valves	b	4.7	4.7	4.7	0
	c	5.3	5.3	5.3	0
	d	5	5	5	0
Electro-deionisation process	b	38.8	38.8	38.8	0
	c	31.9	31.9	31.9	0
	d	30.9	30.9	30.9	0
Primary mixed bed ion exchange	b	1.1	1.1	1.1	0
	c	1.1	1.1	1.1	0
	d	1.1	1.1	1.1	0
One micron cartridge filters		0.5	0.5	0.5	0

The hot water heat exchanger has previously been discussed with regards to physical exergy. Presently, the 20.6 % difference in the exergy destruction rates is considered in terms of total exergy. It is evident that this difference does not relate to chemical exergy because the concentration of the system remains constant during the process. (This statement requires justification: there are very minor differences in chemical exergy which have been attributed to round off errors, see Table 8-1 columns 8 and 9.) Therefore, the differences in exergy destruction calculated by the models are caused by the differences in physical exergy calculated using Model B and Model C/Model D, already discussed.

One very important set of values shown in Table 8-2 relates to the UPW plant exergy losses (shown in bold type), sometimes termed external exergy losses in the literature. The aggregate values for Model B, Model C and Model D are 3.8 kW, 11.6 kW and 681.5 kW respectively. The three values vary in magnitude, the Model B exergy losses are approximately one third the value of the Model C exergy losses. The Model D values are much greater in magnitude than the other two models.

The significance of these exergy losses is now considered. Theoretically, with respect to Model B and Model C, if the exergy loss streams were allowed to mix with water at the dead state, the exergy loss values signify the maximum work obtainable, i.e. the sum of thermal work, pressure work and chemical (in this case concentration) work. Regarding Model D, the exergy loss value again represents the theoretical maximum amount of thermal and pressure work that could be obtained. However, it also considers and quantifies, (1) the exergetic value of water (which is becoming an increasingly valuable

natural resource), and (2) the chemical exergy of the electrolyte, which is a function of the chemical exergy of the relevant elements and the Gibbs energy of formation of the ions.

In the literature the exergy losses have been thought of in different ways, (1) the impact of the process waste on the environment [111], or (2) the work input required to bring the more concentrated stream to the dead state concentration [136]. Exergy losses, however, should also always be thought of as a potential work source, for example, a difference in temperature can pre-heat the incoming UPW plant stream, a difference in pressure can drive a turbine, and a difference in chemical potential can perform chemical work.

The key advantage of Model D (and the entire Szargut model approach) is that it not only quantifies the overall possibilities of the work that may be developed from exergy losses, it appropriates a *value* to natural resources such as water in terms of their availability in the natural environment, unlike the other two models which only consider changes in concentration. The technologies to harness the potentially available work may not be available or feasible at present but this approach does provide a theoretical framework of possibility with respect to the natural capital of the earth.

8.2.2 UPW plant characterisation

In the previous section the exergy destruction rates of the plant were assessed in terms of the model comparison and it was found that the exergy destruction rates calculated using the three models were similar for the majority of processes. The notable exception was the hot water heat exchanger. Here, the plant exergy destruction is considered in terms of the

processes responsible for the majority of exergy destruction. The Model D exergy destruction rate values are used for this analysis.

8.2.2.1 Exergy destruction rates

Exergy is delivered to the UPW plant in the form of the incoming UPW feedwater at a certain temperature, pressure, concentration, and mass flow. Subsequently, exergy is added at various process stages, e.g. by combining mass flows and electrical work inputs to the pumps and the electro-deionisation process. Then, due to thermodynamic irreversibilities such as heat transfer across a finite temperature difference, throttling and mixing/separation, exergy is destroyed. The further downstream in the plant the exergy destruction takes place, the more costly the exergy destruction in terms of cumulative exergy inputs.

The exergy destruction rates, calculated using Model D, are shown in Table 8-3. The top ten processes in terms of exergy destruction, which contribute 98.4% of total exergy destruction for the make-up and primary loops, are shown in Figure 8-2, where an aggregate value has been calculated for processes with several modules, such as the RO and EDI processes.

Table 8-3: UPW plant exergy destruction rates calculated using Model D

Process	***Process module***	***Model D (kW)***
Multi-media filters	b	0.5
	c	0.4
	d	0.4
Pre-heat heat exchangers		30.9
Hot water heat exchangers		**140.7**
Biocide/anti-scalant treatment		0.6
RO pre-filters		2.6
Sodium bisulphite treatment		0.6
First pass RO high pressure pumps	a	55.5
	c	55.6
First Pass RO	a	31.3
	c	23.8
Throttling valves	a	8.0
	c	4.3
RO tank		1.8
Primary distribution pumps		20.2
Caustic treatment		0.6
Second pass RO high pressure pumps	b	34.7
	c	38.2
	d	35.2
Second pass RO	b	30.3
	c	30.0
	d	29.2
Throttling valves	b	4.7
	c	5.3
	d	5.0
Electro-deionisation process	b	38.8
	c	31.9
	d	30.9
Primary mixed bed ion exchange	b	1.1
	c	1.1
	d	1.1
One micron cartridge filters		0.5

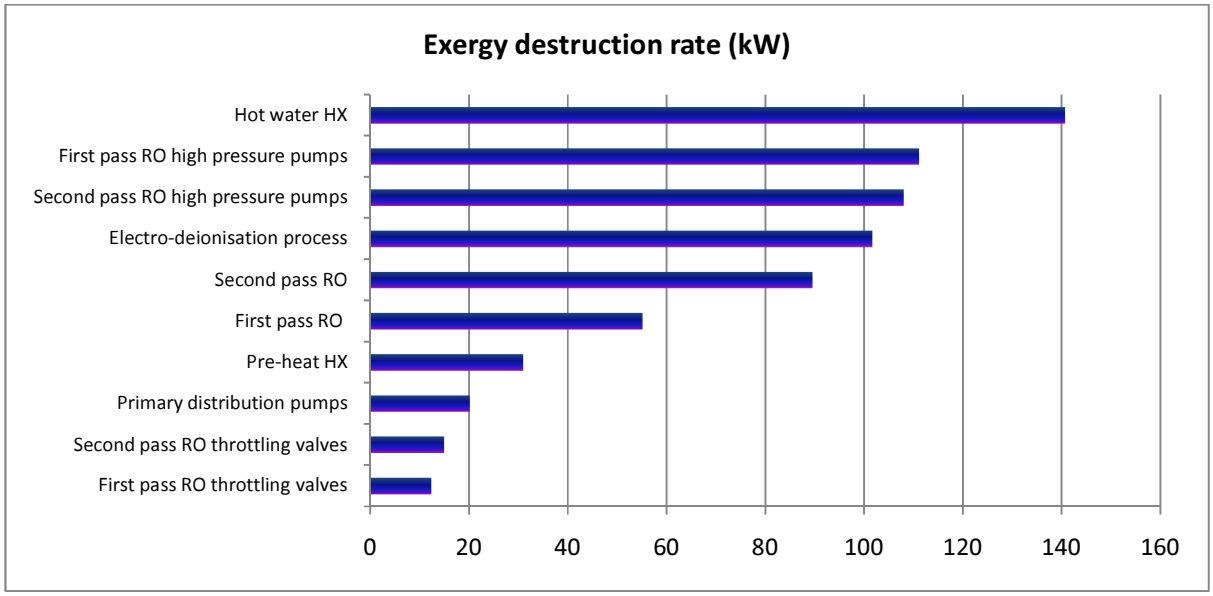

Figure 8-2: Top ten sources of exergy destruction in the UPW plant make-up and primary loops

According to Figure 8-2, and based on the available plant measurement data, the main source of exergy destruction in the UPW plant make-up and primary loops is the hot water heat exchanger (HX). Other major contributors of exergy destruction, in order of importance, are the first and second pass RO high pressure pumps, the electro-deionisation process and the second and first pass RO processes.

In the case of the hot water heat exchanger, heat transfer takes place over a relatively large temperature difference. The incoming heating water is at a temperature of 361 K and incoming product water at a temperature of 294 K. Naturally there is always a trade-off between a large temperature difference and excessive heat transfer area. However, these losses should be accounted for with a sound economic rationale.

The magnitude of the exergy destruction in the RO high pressure pumps is interesting: the UPW plant pumps are fitted with either VSDs or motor managers, typically viewed as potential options to improve pump energy efficiency. Nevertheless, the aggregate exergy destruction in the first pass RO pumps was calculated to be 111 kW and 108 kW for the second pass RO pumps. Typically, there are two first pass RO pumps in operation at any one time, increasing the pressure of an average feedwater flow rate of 130 m^3/hr from 4.7 bar to between 10 and 13 bar. The electrical work input was measured as 75 and 86 kW for each of the two pumps. Regarding the second pass RO pumps, there are typically three in service. The pressure of an average flow rate of 81 m^3/hr is increased from 4.2 bar to approximately 21 bar, with an electrical work input of approximately 75 kW.

According to Figure 8-2, the next most important sources of exergy destruction are the electro-deionisation process and the second pass RO process. These processes occur in the primary loop and are thus located relatively far downstream in the process sequence. RO process improvements can potentially be sought through the use of low pressure membranes which reduce the operating pressures required to achieve similar permeate fluxes. Software packages such as ROSA [163] facilitate the swapping of membranes to determine different pressure requirements. However, due to the criticality of the water purity, all potential process changes should be carefully assessed.

8.2.2.2 Exergetic efficiency

The exergetic efficiency of the processes responsible for the top ten sites of exergy destruction is now considered. Each module in the relevant processes is compared where applicable, potentially highlighting poor performance in similar equipment. In addition to

individual modules, like processes are also compared. According to the rational exergetic efficiency approach discussed in the literature review, the exergetic efficiency should be defined according to the function of the process.

The function of the heat exchanger is to heat or cool the product stream. According to the literature review, the rational exergetic efficiency for heating purposes is commonly defined as the increase in exergy of the cold stream divided by the decrease in exergy of the hot stream [95, 109]. The rational exergetic efficiency of the heat exchangers was calculated using (2.9).

The rational exergetic efficiency of the RO high pressure pumps can be defined as the increase in exergy of the product stream divided by the total electrical work input, which is identical in structure to the pump energy efficiency equation discussed in the cited reference [214], signifying that mechanical energy is equivalent to exergy. (When the process is isothermal, the results obtained using (8.3) are identical to the results obtained using the Kotas approach.)

$$\text{Exergetic efficiency of the pumps} = \frac{\Delta \dot{E}}{\dot{W}} \tag{8.3}$$

The rational exergetic efficiency of the electro-deionisation modules relates to the change in the chemical exergy of the incoming product water, thus increasing its purity. The rational exergetic efficiency for the EDI can be calculated according to the approach of Kotas [92] using (8.4), (8.5) and (8.6), where $\dot{E}^{Ch}$ is the chemical exergy rate, $\dot{E}^{Ph}$ is the

physical exergy rate, and the numerical subscripts refer to the relevant process stages discussed in Appendix B.

$$\dot{E}_{Desired\ output} = \left|\dot{E}_{27}^{Ch} - (\dot{E}_{28}^{Ch} + \dot{E}_{29}^{Ch})\right| \tag{8.4}$$

$$\dot{E}_{Used} = \dot{E}_{27}^{Ph} - (\dot{E}_{28}^{Ph} + \dot{E}_{29}^{Ph}) + \dot{W}_{29} \tag{8.5}$$

$$\text{Exergetic efficiency of the EDI} = \frac{\left|\dot{E}_{27}^{Ch} - (\dot{E}_{28}^{Ch} + \dot{E}_{29}^{Ch})\right|}{\dot{E}_{27}^{Ph} - (\dot{E}_{28}^{Ph} + \dot{E}_{29}^{Ph}) + \dot{W}_{29}} \tag{8.6}$$

The rational exergetic efficiency of the RO modules is defined in the same manner except that the electrical work input is zero in (8.6) because the electrical work in the RO process has already been included in the RO pump calculations, see (2.19).

The function of the throttling valves (often termed concentrate valves for RO) is difficult to define; the valves reduce the pressure exergy of the RO retentate streams. In seawater RO desalination processes, this pressure exergy is often used to perform useful work, for example, to pressurise a second stream using pressure exchangers or to drive a Pelton turbine. The throttling process is a source of exergy destruction. It seems counter-intuitive to define the exergetic efficiency of a largely wasteful process. According to Cornelissen, the rational efficiency cannot be applied to "*purely dissipative systems, because no desired product can be defined in this case* [110]". The rational efficiency of the throttling valves is therefore undefined.

The rational exergetic efficiencies of the relevant processes are reported in Table 8-4. It is acknowledged that the exergetic efficiencies are calculated in different ways for certain processes, depending on the function of the system, but the rational exergetic efficiency

does facilitate direct comparison between different modules in the same process and between like processes.

Table 8-4: Rational exergetic efficiencies of the process stages and modules responsible for the majority of the exergy destruction

Process	***Module***	***Rational exergetic efficiency (%)***
Hot water heat exchanger		12.5
Pre-heat heat exchanger		13.1
Second pass RO pumps	b	51.9
	c	50.4
	d	51.8
First pass RO pumps	a	35.5
	c	25.8
Primary distribution pumps		43.5
EDI	b	0.006
	c	0.008
	d	0.008
Second pass RO	b	0.13
	c	0.124
	d	0.131
First pass RO	a	1.7
	c	2.3
Second pass RO throttling valves	b	Undefined
	c	Undefined
	d	Undefined
First pass RO throttling valves	a	Undefined
	c	Undefined

For example, according to Table 8-4, the second pass high pressure RO pumps have a higher rational exergetic efficiency value than the first pass RO pumps. The rational exergetic efficiency of the primary distribution pumps falls somewhere between the two. Looking at the individual modules now, the efficiencies of each of the second pass RO

pumps are similar. However, the efficiencies of the two first pass RO pumps vary between 35.5 and 25.8%, highlighting the poorer performance of module **c**. Assessing the data relating to module **c** in Appendix B Table 1, it is evident that the pressure of the product water is increased from 4.7 bar to 10 bar using 75 kW of power. In contrast, module **a** increases the pressure from 4.7 bar to 13.1 bar using 86 kW of power.

The rational exergetic efficiency of the EDI process is very low in comparison to the RO process. However, there is a mitigating factor, which should be highlighted. The EDI efficiencies include the electrical work of the rectifiers and brine recycling pumps whereas the electrical work of the RO process is included in the RO pump calculations. The inclusion of the electrical work input lowers the rational exergetic efficiency of the EDI process. It should also be stated, that when the electrical work is excluded, the efficiencies are still very low, 0.048%, 0.062% and 0.057% for modules **b**, **c** and **d** respectively. At the EDI module level, the efficiency of module **b** is approximately 40% lower than modules **c** and **d**. This is a consequence of the higher electrical power drawn by the module **b** rectifiers (based on the electrical measurement data obtained, see Appendix B Table 1).

The first pass RO process has an exergetic efficiency value greater than ten times that of the second pass RO process. At the module level, the second pass RO modules are all similar in terms of efficiency. In contrast, regarding the first pass RO modules, the efficiency of module **c** is approximately 26% higher than module **a**, possibly due to the higher pressure drop or different concentration values for the two modules, see Appendix B Table 1. The significantly lower exergetic efficiency values of the second pass RO process (and the EDI

process) are very interesting. As the purity of the product stream increases, the exergetic efficiency of the RO and EDI processes get progressively lower. Based on (8.6), the rational exergetic efficiency reduces if, (1) the change in chemical exergy decreases, (2) the exergy used increases, or (3) a combination of the two. As the purity of the water increases further downstream in the process sequence the change in the chemical exergy can only get smaller, so unless the exergy used to purify the water reduces in tandem with the changing chemical exergy, the purer the water the lower the exergetic efficiency.

There is one important issue with respect to the results in Table 8-4, which requires further consideration, and this pertains to the exergetic efficiencies of the heat exchangers. According to the reported exergetic efficiencies in Table 8-4, there is very little difference between the exergetic efficiency of the hot water heat exchanger and the pre-heat heat exchanger, with exergetic efficiency values of 12.5% and 13.1% respectively. Yet, the exergy destruction rates calculated for the hot water heat exchanger far exceeded that of the pre-heat heat exchanger, 140.7 kW and 30.9 kW respectively, see Table 8-3. The difference in exergetic efficiencies calculated using (2.9) does not appear to adequately represent the hot water heat exchanger exergy destruction footprint. The heat exchanger efficiencies were calculated again using the Kotas rational efficiency approach, see (2.12).

A comparison of the heat exchanger rational exergetic efficiencies is shown in Table 8-5. There is a significant change in the exergetic efficiency of the pre-heat heat exchanger using the Kotas rational efficiency, increasing from 13.1% to 22.5%. The exergetic efficiency of the hot water heat exchanger also increases, from 12.5% to 13.8%. The Kotas

rational efficiency results better reflect the differences in the exergy destruction rates of the two processes.

Table 8-5: Comparison of rational exergetic efficiency for heat exchangers

Process	*Common rational exergetic efficiency (%)*	*Kotas rational exergetic efficiency (%)*
Hot water heat exchanger	12.5	13.8
Pre-heat heat exchanger	13.1	22.5

8.3 Assessment of the results in light of other research objectives

In this section the UPW exergy analysis results are considered in light of other research objectives, which have been discussed in the introduction and the literature review but also as other questions have arisen throughout this research. These issues are addressed under separate headings and include the following considerations;

1. For UPW applications, which model is the most appropriate or do the models give similar results?
2. Does the use of the ideal mixture model in lieu of the electrolytic solution model result in different chemical exergy values at relevant UPW concentrations?
3. Does the approach developed in Chapter 7 to calculate the chemical exergy of electrolytic solutions affect the UPW plant chemical exergy rates in comparison to standard chemical exergy values?
4. Is chemical exergy important for UPW applications or can it be ignored, thus simplifying the approach?

5. Finally, regarding Model D and the Szargut model, can the UPW flow streams be treated as the chemical exergy of pure water, i.e. can the ionic species be neglected in the analysis, thus simplifying the approach?

8.3.1 Which model is the most appropriate or do the models give similar results

Starting with the second part of the question regarding the similarity of model results, this depends on which results are being considered. The exergy rates look dissimilar, which is largely due to the inclusion of the Model D intrinsic chemical exergy, see Table 8-1. The physical exergy rates calculated using the Model B and the Model C/Model D approach are relatively similar except for the hot water heat exchanger, and the chemical exergy rates are dissimilar for all three models. However, when these different exergy rates were used to calculate the UPW exergy destruction rates, the results proved to be very similar, see Table 8-2. There were, however, two notable exceptions, the caustic (sodium hydroxide) treatment and the hot water heat exchanger. The reason for the hot water heat exchanger differences was due to the different ways in which the change in internal energy was calculated. It is difficult to say which value is the more correct. Intuitively though, fitting and integrating the specific heat capacity as a function of absolute temperature to the data over the *specific temperature range* is the better approach (Model C/Model D). However, it was not really the choice of model which caused the 20.6% difference in the exergy destruction rates obtained for hot water heat exchanger but how the changes in the internal energy were calculated.

Differences in the exergy destruction rates calculated for the caustic treatment process resulted essentially from a chemical reaction, which although could not be formally included in the exergy balance, manifested itself in increased electrical conductivity at the relevant process stage. For a separation or mixing process, where no change in chemical composition (no chemical reaction) takes place, changes in concentration are governed by mass concentration balance laws, thus the intrinsic chemical exergy terms cancel. This is the reason why the Model C and the Model D exergy destruction rates were identical for all processes except the caustic treatment process. In effect, the chemical exergy destruction rates were determined by each of the $RT_0 \ln a_i$ terms at the inlets and outlets of the process stages. When changes in chemical composition occur, neither Model B nor Model C is suitable as they only consider changes in concentration. However, even if chemical reactions are not an important consideration for a specific plant analysis, Model D has an important advantage over Model B and Model C, and that is the representation of chemical exergy losses.

8.3.2 Ideal mixture model versus the electrolytic solution model (calcium bicarbonate versus sodium chloride)

This issue was originally considered in Chapter 6. The intention initially was to break the issue into two parts: the first part would have considered whether the use of calcium bicarbonate salt in lieu of the sodium chloride salt in Model B affected the chemical exergy calculation results. However, calcium bicarbonate does not exist as a solid salt crystal, and therefore, no value of specific heat capacity for the solid salt was available in the regular

thermodynamic data sources. Thus, the analysis was not possible. Nevertheless, the issue heading this section is more interesting than the aforementioned one.

Rather than carry out an analysis of the entire two loops, only the first pass RO process was considered, mainly because this particular process encapsulated the greatest concentration differences of any process in the UPW plant, facilitating chemical exergy assessment at three different concentrations (302 ppm for the RO feedwater, 5.5 to 7.7 ppm for the RO permeate and 1111.3 to 1147 ppm for the RO retentate). For the purposes of this assessment, the chemical exergy rates were calculated for NaCl using the Model C approach, primarily because this section focuses on how concentration changes are modelled.

The main changes in setting up the calculation model using NaCl in lieu of $Ca(HCO_3)_2$ occurred as a result of, (1) apportioning the TDS between the sodium and chloride ions, and (2) the calculation of the ionic strength and activity coefficients (the valence of both ions is one in the case of sodium and chloride ions). First, the difference in chemical exergy was considered for calcium bicarbonate when the ideal mixture model was used instead of the electrolytic solution model; the results are shown in Table 8-6. The chemical exergy rates in Table 8-6 admittedly are small with respect to UPW plant exergy rates. Nonetheless, there is a notable difference between the use of the electrolytic model and the ideal solution model to calculate chemical exergy, particularly for the RO feedwater (25.1%) and the RO retentate (16.1%). The difference between the modelling approaches is negligible at the RO permeate purity levels. At high purity, the models are almost identical,

this occurs because the ideal mixture model and the electrolytic model are identical at infinite dilution (returning to Raoult's and Henry's laws). As the concentration increases to the RO feedwater levels, the chemical exergy rates calculated by the models diverge. As concentration increases further still to the RO retentate levels, the models appear to begin converging again.

Table 8-6: Comparison of chemical exergy rates calculated using the electrolytic solution model and the ideal mixture model for aqueous solution (calcium bicarbonate)

Process stage	*Ideal mixture $Ca(HCO_3)_2$ (kW)*	*Electrolytic solution $Ca(HCO_3)_2$ (kW)*	*% Diff. Electrolytic vs. Ideal mixture $Ca(HCO_3)_2$*
14a	0.123	0.098	**25.1**
14c	0.124	0.099	**25.1**
15a	0.132	0.133	**0.4**
15c	0.127	0.128	**0.6**
16a	0.592	0.510	**16.1**
16c	0.605	0.521	**16.1**

Next, the same analysis is carried out for the electrolytic solution modelled as an aqueous solution of sodium and chloride ions, see Table 8-7. As the results show, the percentage difference in chemical exergy rates is lower than for the calcium bicarbonate analysis, a maximum percentage difference of 10.7% between the ideal mixture and electrolytic models in comparison with 25.1% for the calcium bicarbonate electrolyte. The same pattern is repeated as the concentrations change, however, the percentage difference values are less than half the values reported in Table 8-6.

Table 8-7: Comparison of chemical exergy rates calculated using the electrolytic solution model and the ideal mixture model for aqueous solution (sodium chloride)

Process stage	*Ideal mixture NaCl (kW)*	*Electrolytic solution NaCl (kW)*	*% Diff. Electrolytic vs. Ideal mixture (NaCl)*
14a	0.228	0.205	**10.7**
14c	0.229	0.207	**10.7**
15a	0.245	0.245	**0.2**
15c	0.235	0.235	**0.3**
16a	1.095	1.021	**7.2**
16c	1.119	1.044	**7.2**

Finally, the chemical exergy rates calculated using the electrolytic solution model are compared for both calcium bicarbonate and sodium chloride, see Table 8-8. The chemical exergy rates of the aqueous solution, modelled as an electrolytic solution of sodium and chloride ions, are approximately twice that of the calcium and bicarbonate ions.

Table 8-8: Comparison of chemical exergy rates calculated using calcium bicarbonate versus sodium chloride

Process stage	*Electrolytic solution $Ca(HCO_3)_2$ (kW)*	*Electrolytic solution NaCl (kW)*
14a	0.098	0.205
14c	0.099	0.207
15a	0.133	0.245
15c	0.128	0.235
16a	0.510	1.021
16c	0.521	1.044

The latter comparison is somewhat disingenuous in that the same TDS values were apportioned between both electrolytic solution models. If the UPW plant incoming water could be appropriately modelled as sodium and chloride ions, the factor relating TDS and electrical conductivity would be different from the factor derived in this thesis (0.773). However, it does serve to illustrate an important point and that is the chemical exergy values obtained depend on how the relevant solution is modelled.

8.3.3 Model D versus the Szargut model standard chemical exergy values

The chemical exergy rates calculated using *standard* chemical exergy values were compared with the chemical exergy rates obtained using the Model D chemical exergy values derived in Chapter 7. The standard chemical exergy value for water is 0.9 kJ/mol [93, 116] and the standard chemical exergy values for the calcium and bicarbonate ions were calculated to be 175.52 kJ/mol and -52.5 kJ/mol respectively in Chapter 7. In contrast, the Model D chemical exergy values were calculated to be 0.628 kJ/mol, 180.52 kJ/mol and -55.26 kJ/mol for water, the calcium ion and the bicarbonate ion respectively.

The results are presented in Table 8-9 which only shows the first pass RO process because the difference in values was found to be systematic. According to the results in Table 8-9, there are significant differences between the chemical exergy rate values calculated using the two approaches, an absolute percentage difference of 43%. As found previously, the increase in the magnitude of the chemical exergy results should not impact on the exergy destruction rates due to the cancellation of the intrinsic chemical exergy terms. However, with respect to any UPW plant exergy losses, the 43% difference is important. Using

standard chemical exergy values in this case resulted in the significant over-estimation of the theoretical potential of the exergy losses to perform useful chemical work. This finding is based on a dead state temperature of 289.15 K. However, according to the results obtained in Chapter 7, greater differences in the chemical exergy values were obtained as the difference between the dead state temperature and standard temperature increased. Thus, it is expected that the difference in results between the two approaches would increase in magnitude as the dead state temperature decreased.

Table 8-9: Comparison of chemical exergy rates calculated using standard chemical exergy values and the Model D chemical exergy values

Process stage	***Std chemical exergy (kW)***	***Model D (T_0, φ) (kW)***	***Absolute % Diff.***
14a	1814.1	1266.2	43
14c	1823.8	1273	43
15a	1327	926	43
15c	1352	943.4	43
16a	487.6	340.8	43
16c	472.4	330.2	43

8.3.4 Is chemical exergy important for UPW applications or can it be ignored thus simplifying the approach

This question is similar to that of Section 8.3.1, however, it is now considered specifically in terms of the most important objectives of an exergy analysis;

1. To determine the most important exergy destruction sites;
2. To determine the exergetic efficiency of plant process and modules;
3. To determine exergy losses.

In essence, the question is whether or not the exclusion of chemical exergy affects the results obtained for the objectives listed above?

First point 1 is considered. For the assessment, the exergy destruction rates obtained using both total exergy and physical exergy were compared. There were two distinct considerations, (1) does the sole use of the physical exergy rates affect the percentage difference in exergy destruction between the models, and (2) does the sole use of physical exergy rates affect the magnitude and hierarchy of the exergy destruction rates?

It was found that the use of physical exergy in lieu of total exergy did not affect the percentage differences between the exergy destruction rates calculated using the three models. (The total exergy destruction rates calculated using the various models were previously shown in Table 8-2.) According to the key results of this investigation, which are shown in Table 8-10, there was one major exception, the caustic treatment, previously addressed in detail. The magnitudes and hierarchy of the exergy destruction rates, calculated using Model D, are shown in Figure 8-3. According to these results, neither the

hierarchy of exergy destruction rates nor the magnitude of exergy destruction rates is affected by the choice of physical exergy in lieu of total exergy rates. Therefore, to characterise the significant exergy destruction rates of the UPW plant, it was found that chemical exergy could be ignored.

Table 8-10: Comparison of total exergy destruction rates versus physical exergy destruction rates, effect on model comparison

Process	***Process module***	***Total exergy % Diff. between the models***	***Physical exergy % Diff. between the models***
Hot water heat exchangers		20.6	20.6
Caustic treatment		**49.2**	**0.0**

Next, the exergetic efficiency values are considered. For the heat exchangers and pumps, no change of chemical exergy takes place, and thus, when the chemical exergy terms are included, they cancel, leaving only the physical exergy terms for consideration. In contrast, however, regarding the RO and EDI processes, the rational exergetic efficiency is a function of the change in chemical exergy. Consequently, for these two processes, chemical exergy is necessary to ascertain the rational exergetic efficiency.

Finally, the exergy losses are considered, a comparison of total, physical and chemical exergy losses for the three models is reported in Table 8-11. According to these results, exergy losses do significantly differ depending on whether chemical exergy is included or

not, particularly with regards to Model B and Model D, where the chemical losses are significant contributors to total exergy losses.

Table 8-11: Comparison of exergy losses - total, physical and chemical exergy losses

Aggregate exergy losses	*Total exergy losses (kW)*	*Physical exergy losses (kW)*	*Chemical exergy losses (kW)*
Model B	3.8	10.6	-6.8
Model C	11.6	10.6	1
Model D	681.5	10.6	670.9

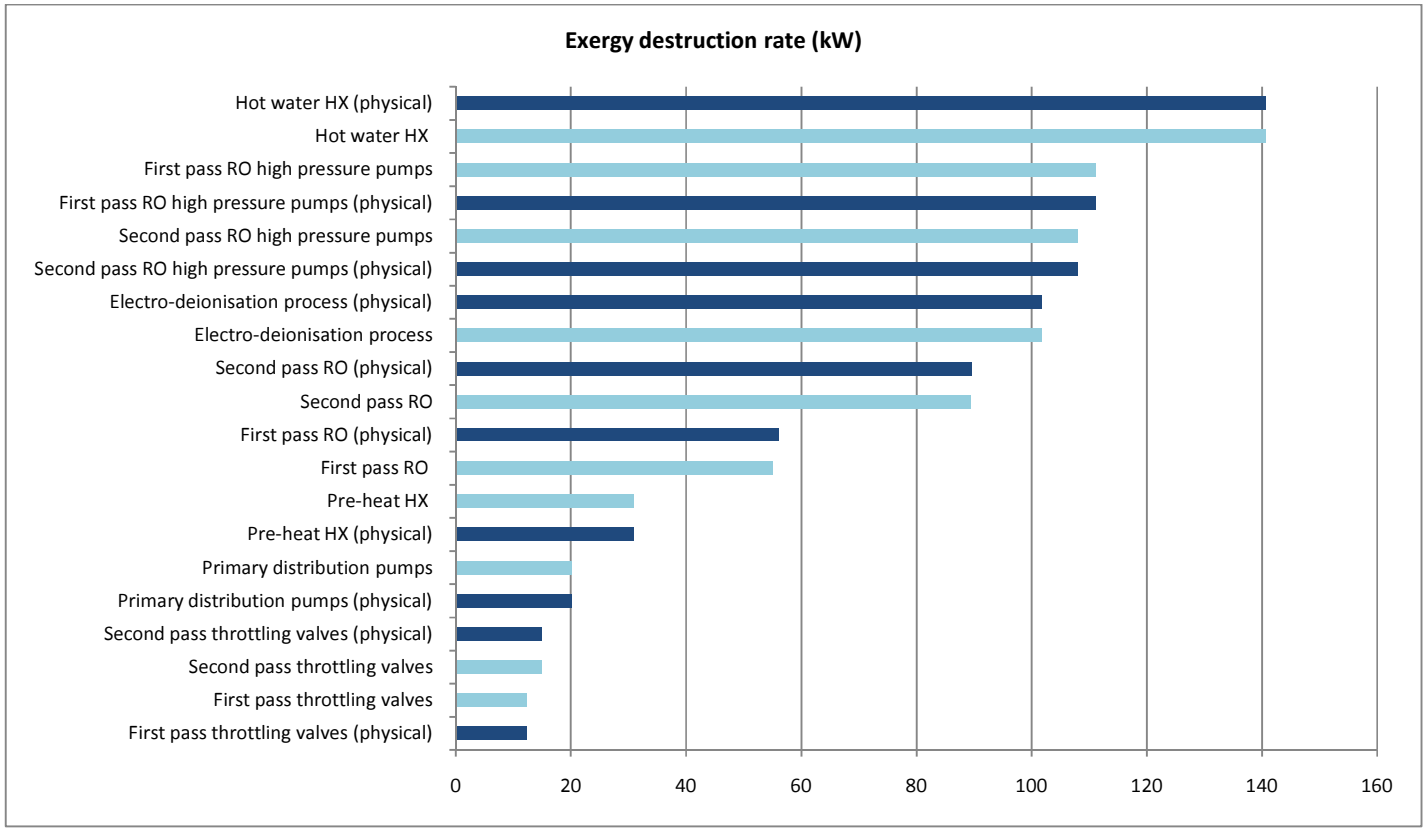

Figure 8-3: Comparison of exergy destruction rates and hierarchy of exergy destruction rates – physical versus total exergy

8.3.5 Can the UPW flow streams be modelled as the chemical exergy of pure water thus simplifying the approach (Model D/Szargut model)

This question is important because the use of the chemical exergy of pure water greatly simplifies the approach. To address this question, the chemical exergy rate of pure water was calculated at the relevant mass and molar flow rates using (8.7).

$$\dot{E}_w^{Ch} = \dot{N}_w \overline{e}_w^{Ch} \tag{8.7}$$

For similar reasons to the electrolytic solution/ideal mixture model comparison earlier in Section 8.3.2, the results were only considered for the first pass RO process. The chemical exergy rates of both pure water and the electrolytic solution are shown in Table 8-12. The percentage difference values between the two modelling choices are shown in the final column. According to these results, it is evident that there is very little difference between the two approaches. At the most concentrated flow in the UPW plant, i.e. the first pass RO retentate (process stages 16a and 16c), the absolute percentage difference is less than 0.5%. Therefore, it would appear that the UPW plant flow streams could be modelled as pure water. However, there is one other important consideration, the rational exergetic efficiency calculations.

The rational exergetic efficiency of the RO and the EDI processes is defined according to their function, and that is to change the chemical exergy of the incoming feedwater. When the chemical exergy of pure water is used in the rational exergetic efficiency calculations, the efficiency is zero because no change in chemical exergy is inferred. Regarding the

exergy losses, however, it is evident from this analysis that less than 0.5% of the total exergy losses relate to the electrolytic species.

Table 8-12: Comparison of chemical exergy rates calculated for the UPW streams modelled as an electrolytic solution and pure water

Process stage	*Electrolytic solution Chemical exergy rate (kW)*	*Pure water Chemical exergy rate (kW)*	*% Diff. Electrolytic solution vs. pure water*
14a	1265.3	1266.2	-0.1
14c	1272	1273	-0.1
15a	926	926	0
15c	943.4	943.4	0
16a	339.3	340.8	-0.4
16c	328.6	330.2	-0.5

8.4 Summary

An exergy analysis of the UPW plant make-up and primary loops was undertaken. Although the exergy rates calculated using the three models were different, in general, the exergy destruction rates calculated using each of the models were very similar. This finding is contrary to the findings of Chapter 3, when the exergy destruction rates of Model B and Model A were compared. The caustic treatment, due to the implicit chemical reaction, and the hot water heat exchanger, due to differences in the calculation of the change in specific internal energy, were key exceptions indicating that the choice of model still has a bearing on exergy destruction rate calculations for certain processes.

The make-up and primary loops of the UPW plant were characterised in terms of both exergy destruction rates and rational exergetic efficiency. The hot water heat exchanger was found to be responsible for the highest rate of exergy destruction, followed by the RO high pressure pumps and the EDI process. Regarding rational exergetic efficiency (considering only changes in chemical exergy), the EDI process had the lowest value, followed by the second pass RO process (excluding the second pass RO pumps). The fact that these two processes, (1) have the lowest exergetic efficiency values, (2) are relatively high in terms of exergy destruction rates, and (3) are located downstream in the process sequence indicates to the author that they should be priorities in terms of exergy performance mitigation. However, it was also noted that, (and this is largely a consequence of the UPW plant objective), the purer the product water requiring further purification the lower the exergetic efficiency will generally be. In terms of rational exergetic efficiency (considering only changes in physical exergy), the throttling processes were undefined. The exergetic efficiency of other relevant processes in order of ascending rational efficiency were the hot water heat exchanger (using the Kotas rational efficiency approach); the pre-heat heat exchanger (Kotas approach); the first pass RO high pressure pumps; the primary distribution pumps; and the second pass RO high pressure pumps. Following an extensive literature search, there are *no exergy analysis results for UPW plants* with which to compare these results.

Several desalination exergy analyses found that the majority of exergy destruction occurred in the RO core processes. If the RO pumps were not considered separately to the RO

process in this research, the results of this analysis would concur with the desalination findings (based on the aggregate RO pump and RO process exergy losses, see Figure 8-3).

For the most part, as already stated, the models give similar results, however, Model D is the most appropriate for UPW applications for several reasons;

1. The quantification of the exergy losses, particularly regarding the exergetic value of water;
2. The flexibility of the approach to consider chemical reactions typical of many water purification plants.

The chemical exergy values depend on the modelling approach. The percentage differences between the electrolytic solution model and the ideal mixture model are more significant for the ionic solution modelled as calcium and bicarbonate ions than that of sodium and chloride ions. More than likely, this is due to the fact that the calcium ion has a valence of two, and thus, the activity of the ion differs more significantly from the mole fraction than, for example, monovalent ions like sodium. Importantly, the chemical exergy values depend on how the incoming plant water is modelled. Applying an inappropriate conversion factor to relate electrical conductivity and TDS and hence modelling the stream inappropriately can lead to significant errors in chemical exergy calculation.

The chemical exergy rates of aqueous solutions, calculated using Model D, were compared with the chemical exergy of aqueous solutions using the Szargut standard chemical exergy values. A significant difference was found between the two approaches, an absolute

percentage difference of 43% at each of the UPW plant process stages. The findings of Section 8.3.5 would suggest that this 43% difference is predominantly due to differences in the chemical exergy value of water. This is interesting because during the reference environment comparison of Munoz and Michaelides [120], discussed previously in the literature review, the high chemical exergy of water in the Szargut reference environment was commented upon in comparison with the chemical exergy of water in other reference environments. The Szargut chemical exergy of water is highly sensitive to changes in the relative humidity, and therefore, the use of standard values of relative humidity can result in significant differences in chemical exergy values. This should be an important consideration for water purification processes.

The importance of chemical exergy in the exergy analysis of UPW plants was assessed, i.e. whether chemical exergy could be ignored in UPW applications and whether chemical exergy could be modelled as pure water rather than an electrolytic solution. In general, it was found that the use of only physical exergy resulted in negligible difference for the calculation of the UPW exergy destruction rates or the hierarchy of processes responsible for the main sites of exergy destruction. However, with respect to the determination and understanding of plant exergy losses, chemical exergy was found to be important. Regarding the exergetic efficiency calculations of the key separation processes, modelling the flows as an electrolytic solution was necessary to obtain non-zero values of rational exergetic efficiency.

8.4.1 Overview of research

Following a detailed assessment of both semiconductor and desalination industry energy mitigation approaches, the focus of this research thesis was determined to be the exergy analysis of a semiconductor UPW plant. However, one significant challenge became evident following an extensive literature review of desalination industry exergy analyses: of the several exergy models detailed in the literature, which is the most appropriate exergy model to use? Various desalination exergy analyses appeared to have been conducted in a vacuum and didn't seem to consider the similarity or differences between the various approaches (or indeed the validity of different approaches). Also, it was unclear, whether chemical exergy would be important in the UPW plant exergy analysis at the relatively low ionic concentrations typical of UPW plants in contrast to other more concentrated applications such as brackish water or seawater desalination.

Model A and Model B, two prevalent desalination exergy models, were compared using a dataset in the literature and it was found that the exergy destruction rates calculated using each model differed significantly. Further research, which involved de-coupling the physical and chemical exergy terms of Model B and an in-depth analysis of the two modelling approaches, determined that Model A was not suitable for plant exergy analyses due to inappropriate underlying model assumptions relating to the definition of the chemical exergy term.

Research, which focused on the electrolytic solution literature, determined that electrolytic solutions behave quite differently to ideal mixtures, even at relatively low concentrations.

The next objective, then, was to determine a more suitable chemical exergy model, which did consider electrolytic solution behaviour. Two potentially suitable models were identified, (1) a model solely concerned with concentration differences based on the thermodynamics of electrolytic solutions, and (2) a model suitable for electrolytic solutions based on the Szargut reference environment. An accurate approach was developed to ensure correct the application of these electrolytic solution models (Model C). The incoming UPW plant water was carefully assessed to determine the suitability of the factor relating the TDS and electrical conductivity measurements; the suitability of the activity coefficient calculation model was matched with the ionic strength and valence of the relevant ions; and the specific heat capacity and density data were carefully assessed at the relevant UPW plant parameters. (The same accurate approach was used for the subsequently developed Model D.) Model D was developed which enabled the calculation of the intrinsic chemical exergy of electrolytic solutions and ionic species at non-standard dead state temperatures and relative humidity. It was found that the chemical exergy of ionic species was generally sensitive to changes in dead state temperature. For example, the chemical exergy of the bicarbonate ion changed by 9.65% as the dead state temperature changed from standard temperature to a dead state temperature of 278.15 K, at a relative humidity of 0.77.

Finally, Model B, Model C, and Model D were applied to the UPW plant make-up and primary loops in an effort to compare the models and characterise the plant in terms of exergy flows, exergy destruction, exergy losses and rational exergetic efficiency. The results of the UPW plant exergy analysis have been discussed in detail in this chapter.

9 Conclusions and recommendations

The conclusions and recommendations of this research thesis are now presented.

9.1 Conclusions

- Exergy analysis is a powerful tool to characterise UPW plants.
- The results of exergy analyses depend on the exergy model used and how the aqueous solution under consideration is modelled.
- To undertake a water purification plant exergy analysis, the exergy model should reflect the electrolytic behaviour of the relevant streams and consider an appropriate separation model. On this basis, the current, predominant exergy models are not appropriate;
    - The Drioli ideal mixture model (Model A) is unsuitable due to underlying chemical exergy model assumptions – separation and ideal mixture assumptions;
    - The Cerci aqueous solution model (Model B) is unsuitable because it models an aqueous ionic solution as an ideal mixture of solid salt (cr) and water; the integrated nature of the model does not facilitate clear understanding of physical and chemical exergy rate flows.
- At the typical UPW plant concentrations the use of the ideal mixture model resulted in significant differences in the calculation of chemical exergy when compared with the electrolytic solution approach. Differences between the ideal mixture and

electrolytic solution approaches were greater when the solution was modelled as calcium and bicarbonate ions as opposed to sodium and chloride ions.

- Although the total exergy rates calculated using the three models were different, the exergy destruction rates for each of the models were similar in magnitude. There were two exceptions, the hot water heat exchanger and the caustic treatment process. Regarding the hot water heat exchanger, it was found that the physical exergy value depends on how the change in internal energy is calculated, and this varies between the typical values in thermodynamic data tables and the integration of a suitable polynomial relating the specific heat capacity to absolute temperature over the specific temperature range. The caustic treatment differences were caused by an implicit chemical reaction and served to illustrate model differences in the calculation of chemical exergy.
- Although chemical exergy proved to be negligible in identifying the processes responsible for the majority of exergy destruction in the UPW plant, chemical exergy is important to ascertain exergy losses and the rational exergetic efficiency values of several UPW plant processes, and thus, should not be neglected.
- The processes most responsible for exergy destruction in the UPW plant were the hot water heat exchanger; first and second pass RO high pressure pumps; and the electro-deionisation process. When the second pass RO process was considered in total (pumps, RO module and throttling valve), it was the site of greatest exergy destruction.

- The processes with the lowest exergetic efficiency values (based on changes in chemical exergy) were the electro-deionisation process; the second pass RO process; and the first pass RO process.
- The processes with the lowest exergetic efficiency (based on changes in physical exergy) were the hot water heat exchanger; the pre-heat heat exchanger; the first pass RO pumps; the primary distribution pumps; and the second pass RO high pressure pumps.
- The Kotas rational efficiency definition resulted in more appropriate results for the heat exchangers and is recommended over the common heat exchanger rational exergetic efficiency.
- The intrinsic chemical exergy values of aqueous ionic solutions were found to be very sensitive to changes in the dead state temperature and relative humidity.
- The use of Model D had a significant impact on the exergy loss rates calculated for the UPW plant, a percentage difference of 43% in comparison with the Szargut model standard chemical exergy rates.
- Model D is the most appropriate model for the exergy analysis of UPW and other water purification plants for several reasons, (1) it facilitates the assessment of chemical reactions in the plant, (2) it offers a more appropriate interpretation of exergy losses, and (3) it considers the exergetic value of one of the earth's most prized resources, water.

9.2 Thesis contribution

This research thesis has made a novel contribution to knowledge on several levels;

- The research undertaken in this thesis has compared the merits and limitations of current desalination exergy models and has attempted to bridge the existing gap between the desalination exergy approach and the approach of other key exergy researchers;
- An accurate approach has been developed for the application of exergy analyses to UPW plants and other water purification processes - Model C and Model D;
- A novel method to calculate the chemical exergy of electrolytic solutions as a function of dead state temperature and relative humidity (i.e. non-standard states) has been developed - Model D;
- The developed models (Model C and Model D) have been used to undertake the exergy analysis of a semiconductor UPW plant and compared with the current, predominant desalination exergy model;
- This is a first presentation of a UPW plant exergy analysis in the literature.

9.3 Recommendations for further research

Further research is required to determine whether such high UPW purity standards are really necessary.

It was not feasible to consider the exergy analysis of the UPW plant polishing loop due to the lack of necessary measurement equipment. Therefore, if measurement data were to

become available, the polishing loop should be assessed. The assessment should also be extended to consider the exergy flows and exergy losses in fab UPW demand loops.

Further research is required to determine the feasibility of exergy destruction mitigation, which was based on the hierarchy of processes identified as responsible for both high exergy destruction rates and low rational exergetic efficiency. This however, would require close consultation with the industry partner.

Further research could also consider an economic analysis. Certain processes are not adequately characterised by exergy analyses. For example, the exergy destruction of the mixed bed ion exchange was found to be negligible in this research. However, although the exergy destruction rates were insignificant, the ion exchange resins require intermittent regeneration and thus may require additional consideration in economic terms.

Further research is required to assess the differences between the electrolytic solution and ideal mixture models at seawater salinity levels. The Model C and Model D approaches developed here should be applied to a seawater desalination plant facilitating comparison with Model B at the relevant salinity values. The proposed research would use the more accurate Pitzer models to estimate the activity coefficients at the relevant ionic strengths, instead of the Debye-Huckel model or other less accurate models.

REFERENCES

[1] Williams, E.D., Ayres, R.U. and Heller, M., (2002), "The 1.7 kilogram microchip: Energy and material use in the production of semiconductor devices", *Environmental Science and Technology,* Vol.36 (24), pp. 5504-5510.

[2] Roche, T.S. and Peterson, T.W., (1996), "Reducing DI water use", *Solid State Technol.,* Vol.39 (12), pp. 5.

[3] Peters, L., (1998), "Ultrapure water: Rewards of recycling", *Semicond Int,* Vol.21 (2), pp. 71-72.

[4] Topical Reports - Energy and Water Efficiency for Semiconductor Manufacturing, [online], http://www.p2pays.org/ref%5C04/03271/. (Accessed 12/03/08)

[5] Drioli, E., Curcio, E., Di Profio, G., Macedonio, F. and Criscuoli, A., (2006), "Integrating membrane contactors technology and pressure-driven membrane operations for seawater desalination: Energy, exergy and costs analysis", *Chem.Eng.Res.Design,* Vol.84 (3), pp. 209-220.

[6] Shannon, M.A., Bohn, P.W., Elimelech, M., Georgiadis, J.G., Marinas, B.J. and Mayes, A.M., (2008), "Science and technology for water purification in the coming decades", *Nature,* Vol.452 (7185), pp. 301-310.

[7] Mehdizadeh, H., (2006), "Membrane desalination plants from an energy-exergy viewpoint", *Desalination,* Vol.191 (1-3), pp. 200-209.

[8] International Technology Roadmap for Semiconductors, Executive Summary, [online], http://www.itrs.net/Links/2007ITRS/Home2007.htm (Accessed 10/2/08)

[9] Porter, M.E. and van der Linde, C., (1995), "Green and Competitive: Ending the Stalemate", *Harv.Bus.Rev.,* Vol.73 (5), pp. 120-134.

[10] Klassen, R.D. and Whybark, D.C., (1999), "The Impact of Environmental Technologies on Manufacturing Performance", *Academy of Management Journal,* Vol.42 (6), pp. 599-615.

[11] CNN Money website, [online], http://money.cnn.com/magazines/fortune/fortune500/2009/index.html. (Accessed 15/04/10)

[12] Bakshi, B.R. and Fiksel, J., (2003), "The quest for sustainability: Challenges for process systems engineering", *AICHE J.,* Vol.49 (6), pp. 1350-1358.

[13] Lovins, A.B., Lovins, L.H. and Hawken, P., (1999), "Road map for natural capitalism", *Harv.Bus.Rev.,* Vol.77 (3), pp. 145-158.

[14] Branham, M., Gutowski, T. G., Jones, A. and Sekulic, D. P., (2008), "A thermodynamic framework for analyzing and improving manufacturing processes", *Electronics and the Environment, 2008. ISEE 2008. IEEE International Symposium,* 1-6.

[15] Georgescu-Roegen, N., (1971), *The Entropy Law and the Economic Process,* Harvard University Press, Massachussets, United States.

[16] International Database World Population, [online], http://www.census.gov/ipc/www/idb/worldpopgraph.php. (Accessed 19/04/10)

[17] Gutowski, T., Dahmus, J., Thiriez, A., Branham, M. and Jones, A., (2007), "A Thermodynamic Characterization of Manufacturing Processes", *Electronics & the Environment, Proceedings of the 2007 IEEE International Symposium,* 137-142.

[18] Rocky Mountain Institute, "Negawatts for fabs, Advanced Energy productivity for Fun and Profit", [online], http://www.rmi.org/images/PDFs/Energy/E98-03_NegawattsForFabs.pdf. (Accessed 10/03/08)

[19] Geng, H., ed., (2005), *Semiconductor Manufacturing Handbook,* McGraw-Hill, United States.

[20] Meltzer, T.H., (1993), *High-Purity Water Preparation,* Tall Oaks Publishing, Colorado, United States.

[21] Hu, S., Wu, J., Chan, D.Y., Hsu, R.T. and Lee, J.C., (2008), "Power consumption benchmark for a semiconductor cleanroom facility system", *Energy Build.,* Vol.40 (9), pp. 1765-1770.

[22] SEMI S23-0705, Guide for Conservation of Energy, Utilities and Materials used by Semiconductor Manufacturing Equipment.

[23] Veltri, A., DeGenova, J. and O'Hara, P., (2000), "Recycling spent ultrapure rinse water - a case control study in the use of a financial analysis tool", *J.Environ.Health,* Vol.63 (4), pp. 17-22.

[24] Parekh, B., (2008), "Emerging Applications of High Purity Water: Meeting Challenges of Advanced Semiconductor Manfacturing", *Ultrapure Water Journal,* Vol. May .

[25] Krishnan, N., Williams, E.D. and Boyd, S.B., (2008), "Case studies in energy use to realize ultra-high purities in semiconductor manufacturing", *16th IEEE International Symposium on Electronics and the Environment, ISEE, May 19 - 22,* Institute of Electrical and Electronics Engineers Inc San Francisco, CA, United states.

[26] Energy Efficient Cleanrooms Information Site, [online], http://ateam.lbl.gov/cleanroom/technical.html. (Accessed 20/05/09)

[27] International Technology Roadmap for Semiconductors 2007 Edition, Environment, Safety and Health, [online], http://www.itrs.net/Links/2007ITRS/2007_Chapters/2007_ESH.pdf. (Accessed 31/08/09)

[28] Cohen, R.M., (2003), "Energy efficiency for semiconductor manufacturing facilities", *ASHRAE J.*, Vol.45 (8), pp. 28-34.

[29] Dubov, I., (2005), "Heat recovery, energy savings for semiconductor plant", *ASHRAE J.*, Vol.47 (12), pp. 56-58.

[30] Dubov, I., (2003), "Chilled water plant efficiency", *ASHRAE J.*, Vol.45 (6), pp. 37-40.

[31] Fiorino, D.P., (2000), "Reducing steam costs: Six conservation and efficiency measures", *ASHRAE J.*, Vol.42 (2), pp. 31-39.

[32] Fiorino, D.P., (2000), "Cost-effective industrial boiler plant efficiency advancements", *Energy Eng*, Vol.97 (3), pp. 7-26.

[33] Hu, S. and Chuah, Y.K., (2003), "Power consumption of semiconductor fabs in Taiwan", *Energy*, Vol.28 (8), pp. 895-907.

[34] Schrecengost, R. and Naughton, P., (2004), "Cleanroom Energy Optimization Methods", [online], http://repository.tamu.edu/bitstream/handle/1969.1/4617/ESL-HH-04-05-18.pdf?sequence=4 (Accessed 10/2/08)

[35] Texas Instruments, Sustainability at Texas Instruments, [online], http://www.ti.com/corp/docs/rennerroadfab/rfab_tour.pdf. (Accessed 02/03/08)

[36] Fitzsimons, L., Corcoran, B. and Young, P., (2009), "Review of Strategic Semiconductor Cleanroom Energy Reduction Efforts", *IMC 26, International Manufacturing Conference 2009, 2-4th September 2009*, Dublin.

[37] Masuda, T., Samata, S. and Mikata, Y., (2005), "Virtual fab technology utility simulation and its application to 300 mm CR facility design and energy reduction", ISSM 2005, *13-15 Sept, 2005*: IEEE San Jose, CA, USA 17-20.

[38] Tschudi, W., Mills, E., Xu, T. and Rumsey, P., (2005), "Measuring and Managing Cleanroom Energy Use", *HPAC Engineering*, December: 29-35.

[39] Tschudi, W., (2005), "Rediscovering green design", *HPAC Heating, Piping, AirConditioning Engineering*, Vol.77 (9), pp. 11-12.

[40] Naughton, P., (2005), "Measurement of conservation of energy by semiconductor manufacturing equipment and setting of targets for improvements", *IEEE International Symposium on Semiconductor Manufacturing, Sep 13-15 2005*: Institute of Electrical and Electronics Engineers Inc., Piscataway, NJ 08855-1331, United States San Jose, CA,

United States 7-16.

[41] Naughton, P., (2006), "New tool for targeting energy improvements in semiconductor manufacturing equipment", *17th Annual SEMI/IEEE Advanced Semiconductor Manufacturing Conference, ASMC 2006, May 22-24, 2006*: Institute of Electrical and Electronics Engineers Inc., Piscataway, NJ 08855-1331, United States Boston, MA, United States 428-432.

[42] Jensen, J.N., (2003), *A Problem-Solving Approach to Aquatic Chemistry*, John Wiley and Sons, United States.

[43] MWH., (2005), *Water Treatment: Principles and Design*, (2nd ed.), John Wiley & Sons, New Jersey, United States.

[44] Hussey, D.F., Foutch, G.L. and Ward, M.A., (2000), "Water, Ultrapure", *in Ullmann's Encylcopedia of Industrial Chemistry*, Wiley-VCH.

[45] Willis, S., (2007), "Pure water technology", *Pharmaceutical Technology Europe*, Vol.19 (7), pp. 32-37.

[46] Meltzer, T.H., (1997), *Pharmaceutical Water Systems*, Tall Oaks publishing INC., Littleton, Colorado, United States.

[47] Ohmi, T., (1993), *Ultraclean Technology Handbook: Ultrapure water*, CRC Press.

[48] Dey, A. and Thomas, G., (2003), *Electronics Grade Water Preparation*, Tall Oaks Publishing, Colorado, United States.

[49] DeGenova, J. and Shadman, F., (1997), "Recovery, reuse, and recycle, of water in semiconductor wafer fabrication facilities", *Proceeding of the Symposium on Environmental Aspects of Electrochemical Technology: Applications in Electronics, 7-8 Oct. 1996*: Electrochem. Soc Pennington, NJ, USA 3-15.

[50] Klusewitz, G. and McViegh, J., (2002), "Water usage reduction in a semiconductor fabricator", *ASMC 2002, 30 April-2 May 2002*: IEEE Boston, MA, USA 340-6.

[51] Paul, D., (2009), "Microelectronics Water Treatment System Overview", *Ultrapure Water Journal*, Vol. May.

[52] FILMTEC Membranes, Basics of RO and NF, [online], http://www.dow.com/PublishedLiterature/dh_003b/0901b8038003b454.pdf?filepath=liquidseps/pdfs/noreg/609-02003.pdf&fromPage=GetDoc. (Accessed 22/08/09)

[53] Hager + Elsasser Website, Reverse Osmosis for semiconductor plant in Singapore, [online], http://www.hager-elsaesser.com/en/solutions-services/industry-specific-solutions/semiconductors-electronics.html. (Accessed 05/10/10)

[54] Vertex Hydropore website, [online], http://www.reverseosmosis.com.au/reverse_osmosis_definition.htm. (Accessed 14/04/09)

[55] Sourirajan, S., (1970), *Reverse Osmosis*, Logos Press Ltd. in association with Elek Books Ltd., London, U.K.

[56] Lacey, R.E. and Loeb, S., (1979), *Industrial Processing with Membranes*, Robert E. Krieger, New York, United States.

[57] Terms and Equations of Reverse Osmosis, [online], http://www.membranes.com/docs/trc/termsequ.pdf. (Accessed 22/08/09)

[58] Criscuoli, A.and Drioli, E., (1999), "Energetic and exergetic analysis of an integrated membrane desalination system", *Desalination*, Vol.124 (1-3), pp. 243-249.

[59] Semiat, R., (2008), "Energy issues in desalination processes", *Environmental Science and Technology*, Vol.42 (22), pp. 8193-8201.

[60] Blank, J.E., Tusel, G.F. and Nisanc, S., (2007), "The real cost of desalted water and how to reduce it further", *Desalination*, Vol.205 (1-3), pp. 298-311.

[61] Darwish, M.A. (2007), "Desalting fuel energy cost in Kuwait in view of $75/barrel oil price", *Desalination*, Vol.208 (1-3), pp. 306-320.

[62] Darwish, M.A., Alotaibi, S. and Alfahad, S., (2008), "On the reduction of desalting energy and its cost in Kuwait", *Desalination*, Vol.220 (1-3), pp. 483-495.

[63] Fundamentals of RO-NF Technology, Hydranautics website, [online], http://www.membranes.com/index.php?pagename=tech_papers.(Accessed 22/08/09)

[64] Fritzmann, C., Lowenberg, J., Wintgens, T. and Melin, T., (2007), "State-of-the-art of reverse osmosis desalination", *Desalination*, Vol.216 (1-3), pp. 1-76.

[65] MacHarg, J. and Truby, R., (2004), "West Coast Researchers Seek to Demonstrate SWRO Affordability", *The International Desalination and Water Reuse Quarterly*, Vol.14 (3).

[66] Hydranautics website, Effect of New generation of Low Pressure, High Salt Rejection Membranes on Power Consumption of RO Systems, [online], http://www.membranes.com/index.php?pagename=tech_papers. (Accessed 22/08/09)

[67] Wilf, M. and Klinko, K., (2001), "Optimization of seawater RO systems design", *Desalination*, Vol.138 (1-3), pp. 299-306.

[68] Voros, N., Maroulis, Z.B. and Marinos-Kouris, D., (1996), "Optimization of reverse osmosis networks for seawater desalination", *Computers and Chemical Engineering*,

Vol.20 pp. S345-S350.

[69] Voros, N.G., Maroulis, Z.B. and Marinos-Kouris, D., (1996), "Salt and water permeability in reverse osmosis membranes", *Desalination,* Vol.104 (3), pp. 141-154.

[70] Marcovecchio, M.G., Aguirre, P.A. and Scenna, N.J., (2005), "Global optimal design of reverse osmosis networks for seawater desalination: modeling and algorithm", *Desalination,* Vol.184 (1-3), pp. 259-271.

[71] Avlonitis, S.A., (2005), "Optimization of the design and operation of seawater RO desalination plants", *Sep.Sci.Technol.,* Vol.40 (13), pp. 2663-2678.

[72] Lu, Y., Hu, Y., Zhang, X., Wu, L. and Liu, Q., (2007), "Optimum design of reverse osmosis system under different feed concentration and product specification", *J.Membr.Sci.,* Vol.287 (2), pp. 219-229.

[73] Vince, F., Marechal, F., Aoustin, E. and Breant, P., (2008), "Multi-objective optimization of RO desalination plants", *Desalination,* Vol.222 (1-3), pp. 96-118.

[74] Kim, S.J., Lee, Y.G., Oh, S., Lee, Y.S., Kim, Y.M., Jeon, M.G., Lee, S., Kim, I.S. and Kim, J.H., (2009), "Energy saving methodology for the SWRO desalination process: control of operating temperature and pressure", *Desalination,* Vol.247 (1-3), pp. 260-270.

[75] Geisler, P., Krumm, W. and Peters, T.A., (2001), "Reduction of the energy demand for seawater RO with the pressure exchange system PES", *Desalination,* Vol.135 (1-3), pp. 205-210.

[76] Moftah, K., (2008), "Is There a Place for Energy Recovery in Brackish Water RO Applications?", *Ultrapure Water Journal,* Vol. June/July, pp.13.

[77] Macedonio, F., Curcio, E. and Drioli, E., (2007), "Integrated membrane systems for seawater desalination: energetic and exergetic analysis, economic evaluation, experimental study", *Desalination,* Vol.203 (1-3), pp. 260-276.

[78] Al-Obaidani, S., Curcio, E., Macedonio, F., Di Profio, G., Al-Hinai, H. and Drioli, E., (2008), "Potential of membrane distillation in seawater desalination: Thermal efficiency, sensitivity study and cost estimation", *J.Membr.Sci.,* Vol.323 (1), pp. 85-98.

[79] Koutsakos, E. and Moxey, D., (2007), "Membrane Management System", *Desalination,* Vol.203 (1-3), pp. 307-311.

[80] Romero-Ternero, V., Garcia-Rodriguez, L. and Gomez-Camacho, C., (2005), "Thermoeconomic analysis of wind powered seawater reverse osmosis desalination in the Canary Islands", *Desalination,* Vol.186 (1-3), pp. 291-298.

[81] Folley, M., Peñate Suarez, B. and Whittaker, T., (2008), "An autonomous wave-

powered desalination system", *Desalination*, Vol.220 (1-3), pp. 412-421.

[82] Bermudez-Contreras, A., Thomson, M. and Infield, D.G., (2008), "Renewable energy powered desalination in Baja California Sur, Mexico", *Desalination*, Vol.220 (1-3), pp. 431-440.

[83] Miranda, M.S. and Infield, D., (2003), "A wind-powered seawater reverse-osmosis system without batteries", *Desalination*, Vol.153 (1-3), pp. 9-16.

[84] Thomson, M., Miranda, M.S. and Infield, D., (2003), "A small-scale seawater reverse-osmosis system with excellent energy efficiency over a wide operating range", *Desalination*, Vol.153 (1-3), pp. 229-236.

[85] Gilau, A.M. and Small, M.J., (2008), "Designing cost-effective seawater reverse osmosis system under optimal energy options", *Renewable Energy*, Vol.33 (4), pp. 617-30.

[86] Hoek, E.M., Allred, J., Knoell, T. and Jeong, B., (2008), "Modeling the effects of fouling on full-scale reverse osmosis processes", *Journal of Membrane Science*, Vol.314 (1-2), pp. 33-49.

[87] Raluy, R.G., Serra, L., Uche, J. and Valero, A., (2004), "Life-cycle assessment of desalination technologies integrated with energy production systems", *Desalination*, Vol.167 (1-3), pp. 445-458.

[88] Raluy, R.G., Serra, L. and Uche, J., (2005), "Life cycle assessment of desalination technologies integrated with renewable energies", *Desalination*, Vol.183 (1-3), pp. 81-93.

[89] Raluy, G., Serra, L. and Uche, J., (2006), "Life cycle assessment of MSF, MED and RO desalination technologies", *Energy*, Vol.31 (13), pp. 2025-2036.

[90] Vince, F., Aoustin, E., Bréant, P. and Marechal, F., (2008), "LCA tool for the environmental evaluation of potable water production", *Desalination*, Vol.220 (1-3), pp. 37-56.

[91] Ahern, J.E., (1980), *The Exergy Method of Energy Systems Analysis*, John Wiley & Sons, Canada.

[92] Kotas, T.J., (1995), *The Exergy Method of Thermal Plant Analysis*, (2nd ed.), Krieger Publishing Company, Florida, United States.

[93] Szargut, J., (2005), *Exergy Method - Technological and Ecological Applications*, WIT Press, Southampton, U.K.

[94] Bejan, A., (2006), *Advanced Engineering Thermodynamics*, (3rd ed.), John Wiley & Sons, New Jersey and Canada.

[95] Bejan, A., Tsatsaronis, G. and Moran, M., (1996), *Thermal Design and Optimization*, John Wiley & Sons, Canada.

[96] Dincer, I., (2002), "The role of exergy in energy policy making", *Energy Policy,* Vol.30 (2), pp. 137-149.

[97] Sciubba, E. and Wall, G., (2007), "A brief commented history of exergy from the beginnings to 2004", *International Journal of Thermodynamics,* Vol.10 (1), pp. 1-26.

[98] Tsatsaronis, G., (2007), "Comments on the paper 'a brief commented history of exergy from the beginnings to 2004'", *International Journal of Thermodynamics,* Vol.10 (4), pp. 187-190.

[99] Yantovski, E., (2007), "Comments on the table of exergy flows in the paper 'a brief commented history of exergy from the beginnings to 2004'", *International Journal of Thermodynamics,* Vol.10 (4), pp. 193-194.

[100] Sciubba, E. and Wall, G., (2007), "Authors' reply to E. Yantovski's comments", *International Journal of Thermodynamics,* Vol.10 (4), pp. 194-194.

[101] Sciubba, E. and Wall, G., (2007), "Authors' reply to G. Tsatsaronis' comments", *International Journal of Thermodynamics,* Vol.10 (4), pp. 191-192.

[102] Hepbasli, A., (2008), "A key review on exergetic analysis and assessment of renewable energy resources for a sustainable future", *Renewable and Sustainable Energy Reviews,* Vol.12 (3), pp. 593-661.

[103] van Gool, W., (1998), "Thermodynamics of chemical references for exergy analysis", *Energy Conversion and Management,* Vol.39 (16-18), pp. 1719-1728.

[104] Dincer, I., Hussain, M.M. and Al-Zaharnah, I., (2004), "Energy and exergy use in the utility sector of Saudi Arabia", *Desalination,* Vol.169 (3), pp. 245-255.

[105] O'Toole, F., (1992), "A New Approach to Flow Constraints in Exergy Analysis", PhD, Trinity College, Dublin.

[106] Gaggioli, R.A. and Petit, P.J., (1976), "SECOND LAW ANALYSIS, FOR PINPOINTING THE TRUE INEFFICIENCIES IN FUEL CONVERSION SYSTEMS", *Preprints of Papers - American Chemical Society, Division of Fuel Chemistry,* Vol.21 (2), pp. 56-75.

[107] Tsatsaronis, G., (2008), "Recent developments in exergy analysis and exergoeconomics", *International Journal of Exergy,* Vol.5 (5-6), pp. 489-499.

[108] Bisio, G. and Rubatto, G., (2000), "Thermodynamic analysis of chemically reacting systems; choice of a reference state for exergy", *Proceedings of 35th Intersociety Energy*

*Conversion Engineering Conference,*Vol.2, *24-28 July 2000*: American Inst. Aeronaut. & Astronautics Reston, VA, USA 890-9.

[109] Moran, M.J. and Shapiro, H.N., (2006), *Fundamentals of Engineering Thermodynamics*, (5th ed.), Wiley, England.

[110] Cornelissen, R.L., (1997), "Thermodynamics and Sustainable Development", PhD, University of Twente.

[111] Romero-Ternero, V., Garcia-Rodriguez, L. and Gomez-Camacho, C., (2005), "Exergy analysis of a seawater reverse osmosis plant", *Desalination*, Vol.175 (2), pp. 197-207.

[112] Marin, J.M. and Turegano, J.A., (1986), "CONTRIBUTION TO THE CALCULATION OF CHEMICAL EXERGY IN INDUSTRIAL PROCESSES (ELECTROLYE SOLUTIONS)", *Energy*, Vol.11 (3), pp. 231-236.

[113] Tsatsaronis, G., (2007), "Definitions and nomenclature in exergy analysis and exergoeconomics", *Energy*, Vol.32 (4), pp. 249-53.

[114] Hermann, W.A., (2006), "Quantifying global exergy resources", *Energy*, Vol.31 (12), pp. 1349-66.

[115] Sato, N., (2004), *Chemical Energy and Exergy-An Introduction to Chemical Thermodynamics for Engineers*, Elsevier, Amsterdam, The Netherlands.

[116] Szargut, J., Morris, D.R. and Steward, F.R., (1988), *Exergy Analysis of Thermal, Chemical and Metallurgical Processes*, Hemisphere, New York, United States.

[117] Szargut, J., Valero, A., Stanek, W. and Valero, A., (2005), "Towards an International Legal Reference Environment", *Proceedings of ECOS 2005, Trondheim, Norway, pages 409-420*.

[118] Szargut, J., (1989), "Chemical exergies of the elements", *Appl.Energy*, Vol.32 (4), pp. 269-286.

[119] Szargut, J. and Morris, D.R., (1985), "CALCULATION OF THE STANDARD CHEMICAL EXERGY OF SOME ELEMENTS AND THEIR COMPOUNDS, BASED UPON SEA WATER AS THE DATUM LEVEL SUBSTANCE", *Bulletin of the Polish Academy of Sciences: Technical Sciences*, Vol.33 (5-6), pp. 293-305.

[120] Munoz, J.R. and Michaelides, E.E., (1999), "The impact of the model of the environment in exergy analyses [of power plants]", *Transactions of the ASME.Journal of Energy Resources Technology*, Vol.121 (4), pp. 268-76.

[121] Rivero, R. and Garfias, M., (2006), "Standard chemical exergy of elements updated",

Energy, Vol.31 (15), pp. 3310-3326.

[122] Ahrendts, J., (1977), "Thermodynamics of Chemical Reactive Systems; DIE EXERGIE CHEMISCH REAKTIONSFAEHIGER SYSTEME", *VDI Forschungsheft,* (579).

[123] Kameyama, H., Yoshida, K., Yamauchi, S. and Fueki, K., (1982), "EVALUATION OF REFERENCE EXERGIES FOR THE ELEMENTS", *Appl.Energy,* Vol.11 (1), pp. 69-83.

[124] Sussman, M., Choosing a reference environment-state for available-energy computations. 72nd Annual Meeting of the American Institute of Chemical Engineers, San Francisco, U.S. 1979.

[125] Kestin, J., (1980), "Availability: The concept and associated terminology", *Energy,* Vol.5 (8-9), pp. 679-692.

[126] Ranz, L., (1999), "Analisis de los costes exergeticos de la Riqueza Mineral Terreste. Su aplicacion para la gestion de la sosteniblidad", PhD, Universidad de Zaragoza.

[127] Dincer, I. and Rosen, M.A., (2007), *Exergy: energy, environment and sustainable development,* Elsevier, United States.

[128] Cengel, Y.A. and Boles, M.A., (2007), *Thermodynamics An Engineering Approach,* (6th ed.), McGraw-Hill, New York, United States.

[129] Smyth, B.P., (1997), "Exergy Analysis of a Multi-Effect Evaporation Unit for Seawater Desalination", Research M.Sc., Trinity College Dublin.

[130] El-Nashar, A., (1999), "Cost allocation in a cogeneration plant for the production of power and desalted water - comparison of the exergy cost accounting method with the WEA method", *Desalination,* Vol.122 (1), pp. 15-34.

[131] Spiegler, K.S.and El-Sayed, Y., (2001), "The energetics of desalination processes", *Desalination,* Vol.134 (1-3), pp. 109-128.

[132] El-Sayed, Y., (2001), "Designing desalination systems for higher productivity", *Desalination,* Vol.134 (1-3), pp. 129-158.

[133] Cerci, Y., Cengel, Y.A. and Wood, B., (1999), "Minimum separation work for desalination processes", *American Society of Mechanical Engineers, Advanced Energy Systems Division (Publication) AES,* Vol.39 pp. 545-552.

[134] Cerci, Y., (2003), "Improving the Thermodynamic and Economic Efficiencies of Desalination Plants: Minimum Work Required and Case Studies of Four Working Plants", PhD, University of Nevada, United States.

[135] Cerci, Y., (2002), "The minimum work requirement for distillation processes", *Exergy, An International Journal*, Vol.2 (1), pp. 15-23.

[136] Cerci, Y. (2002), "Exergy analysis of a reverse osmosis desalination plant in California", *Desalination*, Vol.142 (3), pp. 257-266.

[137] Kahraman, N., Cengel, Y.A., Wood, B. and Cerci, Y., (2005), "Exergy analysis of a combined RO, NF, and EDR desalination plant", *Desalination*, Vol.171 (3), pp. 217-232.

[138] Kahraman, N. and Cengel, Y.A., (2005), "Exergy analysis of a MSF distillation plant", *Energy Conversion and Management*, Vol.46 (15-16), pp. 2625-2636.

[139] Romero-Ternero, V., Garcia-Rodriguez, L. and Gomez-Camacho, C., (2005), "Thermoeconomic analysis of a seawater reverse osmosis plant", *Desalination*, Vol.181 (1-3), pp. 43-59.

[140] Romero-Ternero, V., (2003), "Analisis Termoeconomico de la Desalacion de Aqua de Mar Mediante Osmosis Inversa con Aplicaion de Energia Eolica", PhD, University of La Laguna.

[141] Aljundi, I.H., (2009), "Second-law analysis of a reverse osmosis plant in Jordan", *Desalination*, Vol.238 (1-3), pp. 207-215.

[142] Uche, J., Serra, L. and Valero, A., (2001), "Thermoeconomic optimization of a dual-purpose power and desalination plant", *Desalination*, Vol.136 (1-3), pp. 147-158.

[143] Uche, J., Serra, L. and Valero, A., (2006), "Exergy costs and inefficiency diagnosis of a dual-purpose power and desalination plant", *Journal of Energy Resources Technology, Transactions of the ASME*, Vol.128 (3), pp. 186-192.

[144] Sorin, M., Jedrzejak, S. and Bouchard, C., (2006), "On maximum power of reverse osmosis separation processes", *Desalination*, Vol.190 (1-3), pp. 212-220.

[145] Fiorini, P. and Sciubba, E., (2005), "Thermoeconomic analysis of a MSF desalination plant", *Desalination*, Vol.182 (1-3), pp. 39-51.

[146] Bouzayani, N., Galanis, N. and Orfi, J., (2007), "Comparative study of power and water cogeneration systems", *Desalination*, Vol.205 (1-3), pp. 243-253.

[147] Bouzayani, N., Galanis, N. and Orfi, J., (2009), "Thermodynamic analysis of combined electric power generation and water desalination plants", *Appl.Therm.Eng.*, Vol.29 (4), pp. 624-633.

[148] Mabrouk, A.A., Nafey, A.S. and Fath, H.E., (2007), "Thermoeconomic analysis of some existing desalination processes", *Desalination*, Vol.205 (1-3), pp. 354-373.

[149] Banat, F. and Jwaied, N., (2008), "Exergy analysis of desalination by solar-powered membrane distillation units", *Desalination*, Vol.230 (1-3), pp. 27-40.

[150] Sayyaadi, H. and Saffari, A., (2010), "Thermoeconomic optimization of multi effect distillation desalination systems", *Appl.Energy*, Vol.87 (4), pp. 1122-1133.

[151] Mistry, K.H., Lienhard, J.H. and Zubair, S.M., (2010), "Effect of entropy generation on the performance of humidification- dehumidification desalination cycles", *International Journal of Thermal Sciences*, Vol.49 (9), pp. 1837-1847.

[152] Uche, J., Serra, L., Herrero, L.A., Valero, A., Turegano, J.A. and Torres, C., (2003), "Software for the anlaysis of water and energy systems", *Desalination*, Vol.156 (1-3), pp. 367-378.

[153] Nafey, A.S., Fath, H.E. and Mabrouk, A.A., (2006), "A new visual package for design and simulation of desalination processes", *Desalination*, Vol.194 (1-3), pp. 281-296.

[154] Nafey, A.S., Fath, H.E.S. and Mabrouk, A.A., (2006), "Exergy and thermoeconomic evaluation of MSF process using a new visual package", *Desalination*, Vol.201 (1-3), pp. 224-240.

[155] Khoshgoftar Manesh, M.H., Amidpour, M. and Hamedi, M.H., (2009), "Optimization of the coupling of pressurized water nuclear reactors and multistage flash desalination plant by evolutionary algorithms and thermoeconomic method", *Int.J.Energy Res.*, Vol.33 (1), pp. 77-99.

[156] Khoshgoftar Manesh, M.H. and Amidpour, M., (2009), "Multi-objective thermoeconomic optimization of coupling MSF desalination with PWR nuclear power plant through evolutionary algorithms", *Desalination*, Vol.249 (3), pp. 1332-1344.

[157] Uche, J., (2000), "Themoeconomic Analysis and Simulation of a Combined Power and Desalination Plant", PhD, Universidad de Zaragoza.

[158] Abdulrahim, H.K. and Alasfour, F.N., (2010), "Multi-Objective Optimisation of hybrid MSF-RO desalination system using Genetic Algorithm", *International Journal of Exergy*, Vol.7 (3), pp. 387-424.

[159] Tchanche, B.F., Lambrinos, G., Frangoudakis, A. and Papadakis, G., (2010), "Exergy analysis of micro-organic Rankine power cycles for a small scale solar driven reverse osmosis desalination system", *Appl.Energy*, Vol.87 (4), pp. 1295-1306.

[160] Nafey, A.S. and Sharaf, M.A., (2010), "Combined solar organic Rankine cycle with reverse osmosis desalination process: Energy, exergy, and cost evaluations", *Renewable Energy*, Vol.35 (11), pp. 2571-2580.

[161] Gasmi, A., Belgaieb, J. and Hajji, N., (2010), "Technico-economic study of an

industrial reverse osmosis desalination unit", *Desalination*, Vol.261 (1-2), pp. 175-180.

[162] Rensonnet, T., Uche, J. and Serra, L., (2007), "Simulation and thermoeconomic analysis of different configurations of gas turbine (GT)-based dual-purpose power and desalination plants (DPPDP) and hybrid plants (HP)", *Energy*, Vol.32 (6), pp. 1012-1023.

[163] ROSA software download, DOW Website, [online], http://www.dow.com/liquidseps/design/rosa.htm. (Accessed 03/03/10)

[164] IMS Design, Hydranautics membranes website, [online], http://www.membranes.com/index.php?pagename=design. (Accessed 13/02/10)

[165] Fitzsimons, L., Corcoran, B., Young, P. and Foley, G., (2010), "A Comparison of Prevalent Desalination Exergy Models", *7th International Conference on Heat Transfer, Fluid Mechanics and Thermodynamics (HEFAT 2010), 19-21 July*, Antalya, Turkey.

[166] Spiegler, K.S. and Laird, A.D., eds., (1980), *Principles of Desalination, Part A*, 2nd ed., Academic Press, New York, United States.

[167] Molinari, R., Gagliardi, R. and Drioli, E., (1996), "Methodology for estimating saving of primary energy with membrane operations in industrial processes", *Desalination*, Vol.100 (1-3), pp. 125-137.

[168] Macedonio, F. and Drioli, E., (2010), "An exergetic analysis of a membrane desalination system", *Desalination*, Vol.261 (3), pp. 293-299.

[169] X-Steam function, [online], http://www.mathworks.com/matlabcentral/fileexchange/9817. (Accessed 2009/2010)

[170] Millero, F.J., (2005), *Chemical Oceanography*, (3rd ed.), CRC Press, Florida, United States.

[171] Cerci, Y., Personal communication via email (10/09/10).

[172] International Equation of State of Seawater, 1980, [online], http://unesdoc.unesco.org.remote.library.dcu.ie/Ulis/cgi-bin/ulis.pl?catno=47363&set=4ADEF8FB_3_167&gp=0&lin=1&ll=1. (Accessed 22/10/09)

[173] Perry, R.H. and Green, D.W., (1997), *Perry's Chemical Engineers' Handbook*, (7th ed.), McGraw-Hill, New York, United States.

[174] Fitzsimons, L., Corcoran, B., Young, P. and Foley, G., (2010), "Desalination Exergy Models: Mathematical and Seawater Model Comparison", *Fifth International Ege Energy Symposium and Exhibition (IEESE-05), 27-30 June*, Denizli, Turkey.

[175] Lewis, G.N. and Randall, M., (1961), *Thermodynamics*, (2nd ed.), Revised by Pitzer, K.S. and Brewer, L., McGraw-Hill, United States.

[176] Anderson, G., (2005), *Thermodynamics of Natural Systems*, (2nd ed.), Cambridge University Press, New York, United States.

[177] Pitzer, K.S., (1980), "Electrolytes. From dilute solutions to fused salts", *J.Am.Chem.Soc.*, Vol.102 (9), pp. 2902-2906.

[178] Zaleta-Aguilar, A., Ranz, L. and Valero, A., (1998), "Towards a unified measure of renewable resources availability: the exergy method applied to the water of a river", *Energy Conversion and Management*, Vol.39 (16-18), pp. 1911-1917.

[179] Armando, G., Alejandro, Z., Barbara, G. and Hugo, R.V., (2003), "On an Exergy Efficiency Definition of a Wastewater Treatment Plant", *International Journal of Thermodynamics*, Vol.6 (4), pp. 169-176.

[180] Martínez, A. and Uche, J., (2010), "Chemical exergy assessment of organic matter in a water flow", *Energy*, Vol.35 (1), pp. 77-84.

[181] Debye, P. and Huckel, E., (1923), *Physik. Z.*, Vol.24 pp. 185-334.

[182] Debye, P. and Huckel, E., (1924), *Physik. Z.*, Vol.25 pp. 97.

[183] Deutsch, W.J., (1997), *Groundwater Geochemistry*, CRC Press, United States.

[184] Stumm, W. and Morgan, J.J., (1996), *Aquatic Chemistry*, (3rd ed.), John Wiley & Sons Inc., New York, United States.

[185] Davies, C.W., (1962), *Ion Association*, Butterworths, London.

[186] Levine, I.N., (2002), *Physical Chemistry*, (5th ed.), McGraw-Hill, New York, United States.

[187] Harned, H. and Owen, B., (1958), *The Physical Chemistry of the Electrolyte Solution*, (3rd ed.), Reinhold, New York, United States.

[188] Lemmon, E.W., McLinden, M.O. and Friend, D.G., (2010), "Thermophysical Properties of Fluid Systems", in *P.J. Linstrom and W.G. Mallard, eds., NIST Chemistry WebBook*, (NIST Standard Reference Database Number 69 ed.), National Institute of Standards and Technology, Gaithersburg MD, United States.

[189] Sawyer, C.N., McCarty, P.L. and Parkin, G.F., (1994), *Chemistry for Environmental Engineering*, (4th ed.), McGraw-Hill, Singapore.

[190] Electrical Conductivity; United Nations Environment Programme Manual, Chapter

12, [online], http://www.rrcap.unep.org/male/manual/national/12Chapter12.pdf. (Accessed 06/12/10)

[191] Pitzer, K.S. and Mayorga, G., (1973), "Thermodynamics of electrolytes. II. Activity and osmotic coefficients for strong electrolytes with one or both ions univalent", *J.Phys.Chem.*, Vol.77 (19), pp. 2300-2308.

[192] Pitzer, K.S., (1973), "Thermodynamics of electrolytes. I. Theoretical basis and general equations", *J.Phys.Chem.*, Vol.77 (2), pp. 268-77.

[193] Pitzer, K.S. and Kim, J.J., (1974), "Thermodynamics of electrolytes. IV. Activity and osmotic coefficients for mixed electrolytes", *J.Am.Chem.Soc.*, Vol.96 (18), pp. 5701-5707.

[194] Pitzer, K.S., (1977), "Electrolyte theory - improvements since Debye and Hueckel", *Acc.Chem.Res.*, Vol.10 (10), pp. 371-377.

[195] Pitzer, K.S. and Simonson, J.M., (1986), "Thermodynamics of multicomponent, miscible, ionic systems: theory and equations", *J.Phys.Chem.*, Vol.90 (13), pp. 3005-9.

[196] PITZER, K.S., (1980), "Thermodynamics of Aqueous Electrolytes at Various Temperatures, Pressures, and Compositions", *in Thermodynamics of Aqueous Systems with Industrial Applications*, AMERICAN CHEMICAL SOCIETY, WASHINGTON, D. C., pp. 451-466.

[197] Clegg, S.L. and Pitzer, K.S., (1992), "Thermodynamics of multicomponent, miscible, ionic solutions: generalized equations for symmetrical electrolytes", *J.Phys.Chem.*, Vol.96 (8), pp. 3513-3520.

[198] Clegg, S.L., Pitzer, K.S. and Brimblecombe, P., (1992), "Thermodynamics of multicomponent, miscible, ionic solutions. Mixtures including unsymmetrical electrolytes", *J.Phys.Chem.*, Vol.96 (23), pp. 9470-9479.

[199] Millero, F.J., (1974), "The Physical Chemistry of Seawater", *Annual Review of Earth and Planetary Sciences*, Vol.2 pp. 101-150.

[200] Harvie, C.E.and Weare, J.H., (1980), "The prediction of mineral solubilities in natural waters: the Na-K-Mg-Ca-Cl-SO_4-H_2O system from zero to high concentration at 25° C", *Geochim.Cosmochim.Acta*, Vol.44 (7), pp. 981-997.

[201] Bromley, L.A., (1973), "Thermodynamic properties of strong electrolytes in aqueous solutions", *AICHE J.*, Vol.19 (2), pp. 313-320.

[202] Bromley, L.A., Singh, D., Ray, P., Sridhar, S. and Read, S.M., (1974), "THERMODYNAMIC PROPERTIES OF SEA SALT SOLUTIONS", *AICHE J.*, Vol.20 (2), pp. 326-335.

[203] Pitzer, K.S., Olsen, J., Simonson, J.M., Roy, R.N., Gibbons, J.J. and Rowe, L., (1985), "Thermodynamics of aqueous magnesium and calcium bicarbonates and mixtures with chloride", *Journal of Chemical & Engineering Data*, Vol.30 (1), pp. 14-17.

[204] Millero, F.J. and Schreiber, D.R., (1982), "USE OF THE ION PAIRING MODEL TO ESTIMATE ACTIVITY COEFFICIENTS OF THE IONIC COMPONENTS OF NATURAL WATERS", *Am.J.Sci.*, Vol.282 (9), pp. 1508-1540.

[205] Wagman, D.D., Evans, W.H. and Parker, V.B., (1982), *NBS Tables of Chemical Thermodynamic Properties: Selected values for inorganic and C1 and C2 organic substances in SI units*, American Chemical Society and the American Instituite of Physics for the National Bureau of Standards, Washington D.C., United States.

[206] Brammer, N., Personal communication via email (August/Sept 2010).

[207] Kazim, A., (2004), "Exergy analysis of a PEM fuel cell at variable operating conditions", *Energy Conversion and Management*, Vol.45 (11-12), pp. 1949-1961.

[208] Ertesvåg, I.S., (2007), "Sensitivity of chemical exergy for atmospheric gases and gaseous fuels to variations in ambient conditions", *Energy Conversion and Management*, Vol.48 (7), pp. 1983-1995.

[209] Met Eireann website, Climate for Dublin Airport, [online], http://www.met.ie/climate/dublinairport.asp. (Accessed 18/11/10)

[210] Linstrom, P.J. and Mallard, W.G., eds., *NIST Chemistry WebBook, NIST Standard Reference Database Number 69*, National Institute of Standards and Technology, Maryland, United States, http://webbook.nist.gov, (Accessed 10/11/10).

[211] Hemingway, B.S., (1991), "Thermodynamic properties of anthophyllite and talc: Corrections and discussion of calorimetric data", *American Mineralogist*, Vol.76 (9/10), pp. 1589-1596.

[212] Millero, F.J., (1979), "The thermodynamics of the carbonate system in seawater", *Geochim.Cosmochim.Acta*, Vol.43 (10), pp. 1651-1661.

[213] Housecroft, C.E. and Sharpe, A.G., (2007), *Inorganic Chemistry*, (3rd ed.), Pearson Education Ltd., England.

[214] Cengel, Y.A. and Turner, R.H., (2001), *Fundamentals of Thermal-Fluid Sciences*, (International ed.), McGraw-Hill, New York, United States.

APPENDICES

Appendix A

Appendix B

Appendix C

Appendix A

Review of Cleanroom Energy Reduction Efforts

Abstract

Semiconductor manufacturing takes place in a tightly controlled cleanroom environment. Maintaining this environment at the required specification, and the supply of utilities to semiconductor tools, is generally viewed in terms of facilities service provision. Traditionally, utilities supplied to semiconductor tools were seen as being 'on tap' and little regard was given to their conservation. As semiconductor fabs age, in conjunction with their respective product technologies, product profit margins decrease. Combining this typical pattern of reducing profit margins with current increasing energy costs, the conservation of energy becomes an important factor in the control of operating costs. Energy and resource reduction, and the improved thermal management of cleanrooms in semiconductor manufacturing have been highlighted as difficult challenges by the International Technology Roadmap for Semiconductors (ITRS) 2007 Executive Summary.

This paper is a review of energy reduction efforts carried out in the semiconductor manufacturing industry. The main focus is to highlight opportunities for energy conservation by assessing various energy reduction measures reported in the literature and to evaluate them in conjunction with a cleanroom design guide, the reported economic benefits are collated and tabulated.

Introduction

Energy efficiency, and the ability to deploy energy saving technologies, is a source of competitive advantage in today's semiconductor manufacturing environment. Traditionally, utilities supplied to semiconductor tools and energy use in general were seen as being 'on tap' and little regard was given to their conservation [1]. Energy and resource reduction, and the improved thermal management of cleanrooms in semiconductor manufacturing have been highlighted as difficult challenges by the International Technology Roadmap for Semiconductors (ITRS) 2007 Executive Summary [2]. The objective of this paper is to review some of the efforts that have been, and are being, carried out to reduce energy consumption in semiconductor fabs. First some industry characteristics are discussed.

Semiconductor Industry Economic Characteristics

Rapidly changing semiconductor technology, driven by Moore's Law, results in compressed product life cycles. Speed to market becomes an important source of competitive advantage where timely new product introduction can result in very large profit margins. Fabs are built quickly and energy efficiency generally plays a small role in overall construction considerations [3]. For the newly introduced product, the focus is on ramping up to production quickly and maximising early product yields and revenue. Product output

and quality are the key drivers initially, however, as fabs and their related technologies age, product profit margins diminish. This change from high margin new product to commodity requires greater operating flexibility and cost management. Combining this typical pattern of reducing profit margins with current increasing energy costs, the conservation of energy becomes an important factor in the control of operating costs.

Energy use within Fabs

According to ISMI [1] [4],

> "*The global semiconductor industry could save nearly $500 million per year in energy costs—or enough electricity to power a small city—by making modest improvements to its tools and facility support systems…*"

There are various complimentary approaches to reducing energy consumption, or indeed its environmental impact, in existing fabs. There is a process optimisation view, i.e. by making processes as efficient as possible greater product output is achievable for the same energy input [1, 5], this fits in with the Lean Manufacturing philosophy. A second approach, relating to supply chain management, is to investigate whether more cost effective or energy-efficient energy suppliers exist, or perhaps whether energy can be obtained from a sustainable source, thus lowering carbon footprint. A third approach is to measure and try to understand the main drivers of fab energy consumption and how they are interrelated. Once understood, reduction efforts are targeted appropriately. There is a both a push and a pull element to consumption, understanding and questioning both better directs reduction efforts. Ideally, all three elements should be addressed; however this paper primarily reviews energy reduction efforts from the latter perspective.

Semiconductor manufacturing takes place in a tightly controlled ultra-clean environment, to put the environment into context, a class 1 cleanroom is 10,000 times cleaner than a hospital operating theatre [6]. Maintaining this cleanroom standard is generally the remit of the facilities group and is viewed in terms of service provision. The facilities group supplies utilities required for both the cleanroom and the operation of the semiconductor manufacturing equipment (SME). Utilities include process cooling water (PCW), ultrapure water (UPW), bulk gases, make-up air (MUA) and re-circulated air for the HVAC system. The semiconductor manufacturing process is highly complex, and product quality is dependent on both the environmental quality of the cleanroom, and the quality of supplied utilities. A detailed description of the manufacturing process is beyond the scope of this paper, but simply put, the process consists of a silicon wafer undergoing hundreds of processing steps as layer upon layer of integrated electronic circuitry is built, despite the number of processing steps tolerance dimensions at the angstrom (10^{-10}m) level are common.

Review of Facilities Reduction Efforts

The literature reviewed can be broken down into two general areas, the first addresses the supply side of energy and reviews papers describing and quantifying facilities improvements at existing and new fabs. Improvement efforts are reviewed under various

[1] ISMI: International SEMATECH Manufacturing Initiative

utilities headings. These improvements are assessed in light of a guide for energy efficient cleanroom design [3]. This Lawrence Berkeley National Laboratory guide aims to make energy saving recommendations, while at the same time acknowledging that efficiency has often taken a back seat to other cleanroom considerations such as cleanliness, temperature and humidity control. Although primarily a cleanroom design guide, the document offers relevant case studies and challenges some industry norms. The second area, the focus of a second paper, relates to energy demand and reviews the relatively new concept of SME energy management. It should be stated that the majority of the literature on fab energy reduction found, consisted of various project reports on energy reduction efforts and the associated monetary savings.

Heat Recovery

The use of heat recovery is a highly effective and economical source of relatively low temperature thermal energy. Substantial economic benefits have been reported in several case studies.

Fabs generate thermal energy, heat generated by the manufacturing equipment, lighting, and people in the cleanroom (‘q’ in Figure 1) must be removed to meet the tight temperature control requirements. Heat in the cleanroom is removed via PCW, exhaust systems and re-circulated air cooling, Figure 1. Heat recovery from the re-circulating air path was used by a fab in Taiwan [7] to reduce the energy used by the MUA handler heating coils and the re-circulation cooling coils. The MUA system was further improved by implementing heat recovery between the pre-heating and pre-cooling coils of the MUA handlers, Figure 2. The pre-cooling coil doubles up as a pre-heating coil after dehumidification, this approach was also used in a semiconductor fab in the United States [8]. This fab also used refrigerant heat of condensation to pre-heat incoming city water prior to de-ionisation (UPW), the reduced steam consumption resulted in annual savings of over $1,000,000. A Tokyo fab construction project [9] used return PCW loop heat recovery to pre-heat MUA air before conditioning and pre-heat industrial water prior to purification.

Similarly, the pre-heating of industrial water and the use of heat recovery for heating loads were utilised by a large semiconductor manufacturer in the United States. To supplement the use of heat recovery, variable volume pumping and VSDs (variable speed drives) for fans were used to increase heat recovery loop energy efficiency. This heat recovery loop was predicted to result in an 85% reduction in natural gas during full production as boiler heating requirements drop. [10]

The construction of a new Texas Instruments fab [11] used a holistic approach to design for sustainability and energy efficiency. Heat recovery was used for MUA pre-heating, the pre-heating of industrial water, and general exhaust heat recovery was used for space heating.

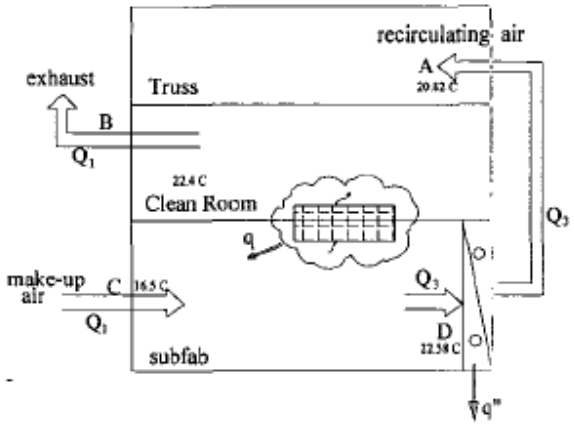

Figure 1: Simplified Model of a Cleanroom [7]

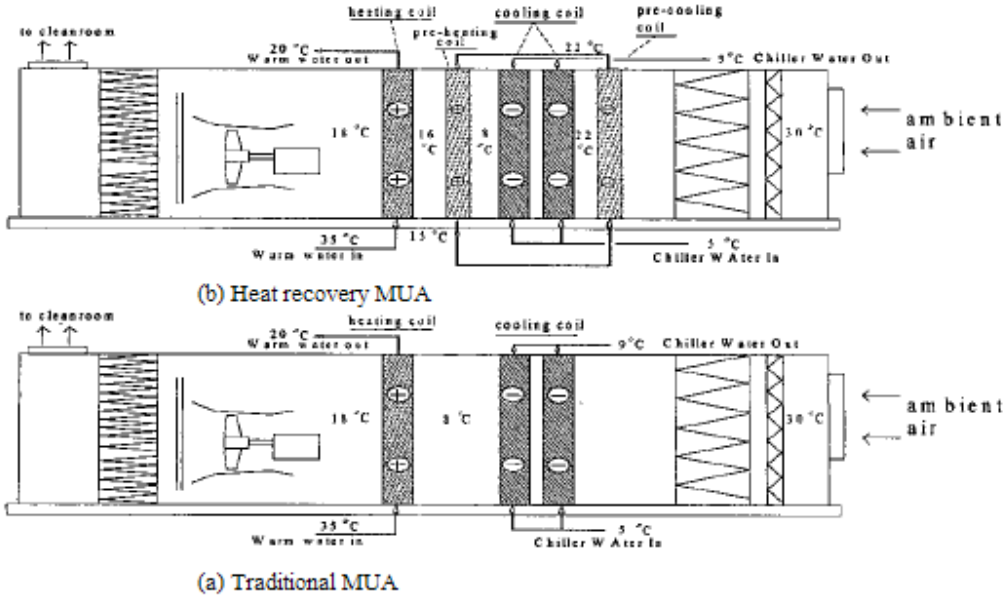

Figure 2: Traditional Versus Heat Recovery MUA handlers (adapted [7]

Exhaust

Exhaust is replaced by MUA to maintain the positive pressurisation of the cleanroom, the MUA handlers take in outside air, dehumidify/humidify the air as appropriate, the air is then reheated to the required temperature and supplied to the cleanroom. Various exhaust types generated by SME include general fab exhaust, VOC exhaust and acid exhaust. General exhaust is essentially warm air, contains no hazardous chemicals, and is usually exhausted to atmosphere. It was stated in the previous paragraph that general exhaust was

used for space heating in the holistic design approach of Texas Instruments. VOC and acid exhaust must undergo specific treatments before going to atmosphere.

Exhaust efficiency is addressed in the guide for energy efficient cleanroom design. The results of an International SEMATECH study in 2001 found that exhaust specifications were greater than necessary in several pieces of cleanroom equipment - wet benches, ion implanters, vertical furnaces and gas cabinets. Optimised exhaust flow resulted in some significant flow reductions including a 56% reduction in wet bench exhaust and a 62% reduction in ion implant tool "right cabinet". Exhaust flow reductions for similar tool types in a semiconductor manufacturing plant are predicted to result in annual savings of $33,000; this is based on $4 per cubic feet per meter of exhaust. [3]

General exhaust was returned to the re-circulating air path in the Tokyo fab [9], this type of heat recovery was not reported in the other fab energy reduction reports. According to the authors, the cost of cooling the 30°C exhaust air, using the re-circulated air cooling coils, was less than the cost of de-humidifying the MUA. Other exhaust types such as solvent and acid exhaust were benchmarked against similar tools and re-set accordingly; the authors discovered that certain tools requiring exhaust ducts purely for maintenance reasons had been left open inadvertently. In the Tokyo fab, addressing exhaust issues resulted in MUA reduction of 20,000m^3/hour. [9]

Chilled Water Loops and Free Cooling

The energy efficient cleanroom design guide advocates the use of a dual temperature chiller loop. Typically, there are two different temperature requirements for the chilled water plant; first, the lower temperature requirement provides chilled water for MUA de-humidification (25-30% of chiller load). Second, the medium temperature requirement provides PCW and re-circulation air cooling (60-70%). There are two approaches taken, in the first approach a single low temperature chiller plant is used, this satisfies the MUA dehumidification requirements. In this case, the medium temperature requirements are met using heat exchangers and a mixing loop. The second approach is to have a dual temperature chilled water plant loop. A case study presented in the design guide illustrates the savings potential of the dual temperature chiller loop: a cleanroom campus requiring 2,370 tons of MUA cooling and 1,530 tons of re-circulation air and PCW cooling used a dual temperature chilled water system of 42°F for the low temperature, and 55°F for the medium temperature loop. Annual savings were approximately $1,000,000; the initial investment for the system was $2,000,000 resulting in a simple payback of 2 years. [3]

The use of cooling tower 'free cooling' (cooling tower systems typically have an efficiency of 0.05-0.15 kW/ton of refrigeration versus chiller efficiency of 0.5-0.7 kW/ton of refrigeration) provides an efficient alternative to chilled water cooling, cooling tower applicability depends on wet bulb temperature and is shown in Table 1.

Table 1: Free cooling application (adapted [3]**)**

At least 3000 hours/year where wet bulb temperature is below: (°F)	*Applicability*
55	PCW
45	PCW and Re-circulated air cooling
35	All chilled water use

Two of the fab energy reduction [10, 11] publications adopt different views on the issue of dual temperature chiller loops. One manufacturer uses a single temperature loop although it has a higher energy cost, referring to the decision as a "*win-lose*" strategy, i.e. those with lower capital but higher energy costs [10]. It should be noted that the manufacturer's decision to opt for a single temperature loop was based on a simple payback model, it was reported that a study was again underway at the semiconductor manufacturer to assess another system configuration again with a split loop. The Texas Instruments fab construction has a dual plant to "*match needs to capacity*", a 40°F loop meets dehumidification needs and other needs are met by the 54°F loop [11].

In the case of a fab in Israel [12, 13], efficiencies were generated in the heat recovery chilled water system by integrating two separate control systems for water temperature leaving the cooling tower and water temperature exiting the condenser into a single control system that optimises energy use under various "*ambient conditions and chiller thermal load variations*". Savings of approximately $198,000 were calculated from the inception of the optimal control system in 2004 to previous 2001 figures.

Air Change Rates, Demand Controlled Filtration, FFUs, and Minimum Pressure Drop

According to the cleanroom design guidelines, "*…the pressure drop of an air delivery system is the design parameter with the largest impact on the power required by the system* [3]." Of the three commonly used airflow system designs, pressurised plenum, ducted high Efficiency Particulate Arresting (HEPA), and Fan Filter Units (FFUs) there are significant energy efficiency variations. Figure 3 shows the results of a benchmarking exercise, the average efficiency (cfm/kW) of re-circulation systems are shown for class 10 and class 100 cleanrooms. The best in class re-circulation system used the pressurised plenum design and had an efficiency rating of 10,140 cfm/kW. The schematic of the best in class system is shown in Figure 4. Design efficiency is due to low pressure drop, VSD controlled axial fans, and the fact that there is no restrictive ducting in the air path. [3]

FFUs and ducted HEPA systems have similar average measured energy efficiency, see Figure 3. FFUs do have certain advantages in that they are easy to install, portable, easy to control, they do have significant unit energy-efficiency variations across their operating range however. Tests carried out by the Lawrence Berkley National Laboratory revealed efficiency variations of a factor of three or more over typical operating conditions. If FFUs are required, the guide advocates the selection of the most efficient unit and the

optimisation of operating parameters. Essentially, whatever airflow system is chosen the key is to reduce the pressure drop where possible, this is achieved by lowering the face velocity in air handlers, choosing low pressure drop filters, and optimising the airflow design path including the size of ducting diameter. [3]

While design of air handling systems plays an important role in design for energy-efficiency, it is only applicable to new cleanroom construction. For existing cleanrooms a major energy consideration is the selection of air change rates (ACR). ACR, according to the guide, are based on outdated and often non-scientific evidence, the rates do not take account of increased filtration efficiency since the 1990s. In reality, a number of semiconductors operate at lower ACR than recommended without increasing particle counts. Larger ACR result in over-sizing of re-circulation fans and hence, increased energy use. In contrast, lower ACR has a large impact on fan energy (Fan Law). As people are the largest contamination source in cleanrooms, lowering ACR may be possible when the cleanroom is unoccupied. [3]

Research has been carried on demand controlled filtration, two studies have attempted to control airflow based on cleanliness monitoring using particle counters. Results showed that greater airflow is not always cleaner due to the effects of turbulence and optimisation is possible. A control system was developed linking fan speed (VSD), room cooling and particle count information, although still at the "*measurement and verification phase*", annual energy savings are predicted to be $51,000 based on an initial investment of $167,000. [14]

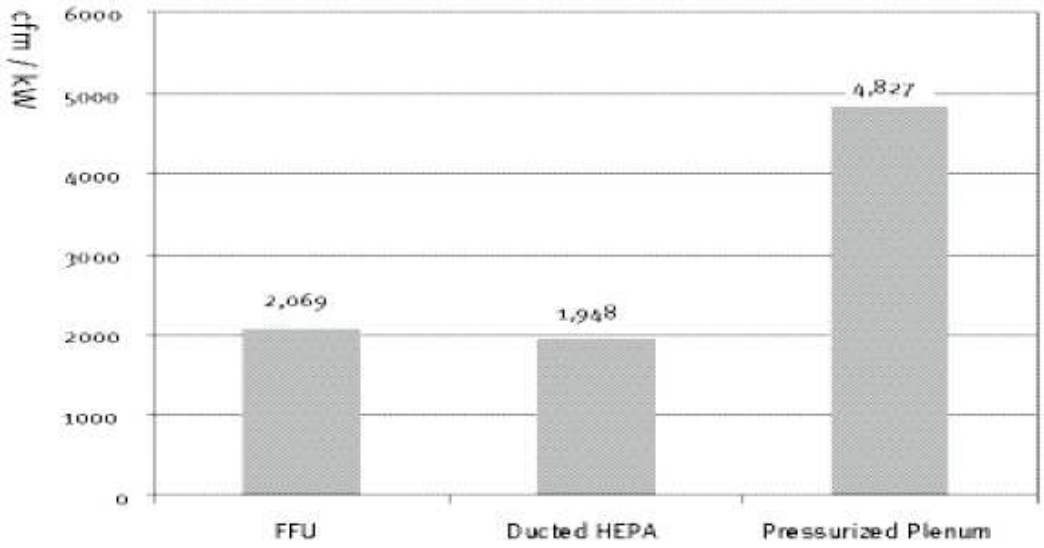

Figure 3: Average Measured Efficiency of re-circulation system types [3]

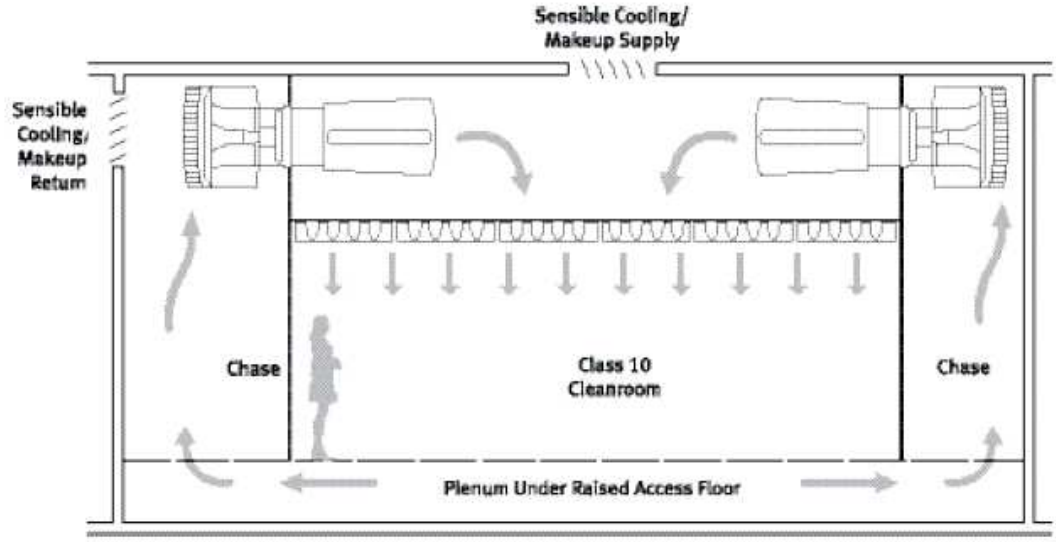

Figure 4: Re-circulation air handling systems design schematic at facility C [3]

The large semiconductor manufacturer [10] reduced cleanroom bay airflow from 0.46 m/s (90 fpm) to 0.37 m/s (72 fpm) and reduced cleanroom filter coverage from 50% overall coverage to 33%. Duct diameters were reduced to HEPA (High Efficiency Particulate Arresting) filters to take advantage of capital cost savings. Again this is one of the organisations "*win-lose strategies*". For the Texas Instruments fab [11], specific airflow energy-saving ideas include the optimal use of FFU (Fan Filter Units) and HEPA filters, again HVAC face velocity was reduced to reduce fan energy. Pressure losses in the HVAC were reduced by using the "big duct, small fan principle"; this is contrary to the HEPA duct size reduction in the previous study, where capital cost savings were deemed more favourable than the potential energy savings.

Boiler efficiency

The implementation of boiler efficiency measures at a semiconductor manufacturing plant in the United States resulted in annual energy savings of $293,500. The primary efficiency outcomes reported, were the pre-heating of combustion air using the hot flue gases prior to exhaust, and the pre-heating of boiler feedwater using a feedwater economiser to again make use of the hot flue gases. These two measures served a dual-reduction purpose, the boiler fuel was reduced due to the increase in the enthalpy of the feedwater, and the fan energy was also reduced as a result of the reduced combustion airflow. Other savings were obtained from variable speed feedwater pumping and reducing fan power costs by reducing excess air in the combustion furnace. [8]

Vacuum Pump Optimisation

The use of vacuum pumps in the semiconductor industry typically accounts for 5-20% of total cleanroom electrical consumption. There are ways of significantly reducing vacuum pump energy consumption. The selection of an efficient pump, combined potentially with the use of an idling protocol integrated with the SME, and measures such as optimum pump location beside SME could result in 50-90% vacuum pump energy reduction. [3]

Miscellaneous

Other energy reduction efforts include, the use of a high pressure atomising humidifier (in lieu of air atomising humidification) [10, 11], the optimisation of air compressor effectiveness by successfully sequencing the different operating characteristics of one rotary screw and several centrifugal compressors [10]. The use of co-generation was adopted in the Tokyo plant [9], but after investigation by the large semiconductor manufacturer [10], was deemed too expensive, "*…would have created its own NO_x problem, and could not pay back on life-cycle costs at current energy rates*". Other energy efficiency measures in the Texas fab [11] include the use of demand controlled ventilation, natural and/or highly efficient lighting and, importantly, ensuring quality insulation and infiltration installation. It is estimated that when the Texas plant is up to full production operating cost savings of $4 million per year will be achieved. Energy cost reduction is estimated at 20% and water use reduction at 35%.

A summary of the various projects is given in Table 2. For the purposes of the table the following abbreviations are used;

- Fab A: NEC Corp. Semiconductor plant, Tokyo, 1997, new plant construction [9]
- Fab B: United Microelectronics Corporation, Taiwan, 2002, 200mm existing plant [7]
- Fab C: Large U.S. Semiconductor, 2003, United States, new and existing plants at various U.S. sites [10]
- Fab D: Tower Semiconductor, Israel, 2003-2005 [12, 13]
- Fab E: Texas Instruments, existing fab Dallas Texas , 2000 [8]
- Fab F: Texas Instruments, Texas fab - 220,000 square feet cleanroom, 2007, holistic approach to new fab construction [11]

Table 2: Summary of energy reduction efforts

Fab	*Main Energy Reduction Efforts*	*Total Savings/Benefits*
A	Co-generation, Heat recovery, Optimise refrigeration efficiency, Cooling tower, Increase PCW delta T.	Overall 18% reduction of energy, 28% reduction for HVAC systems
B	MUA handler heat recovery, General Exhaust heat recovery, Cleanroom pressure reduction, Exhaust benchmarking.	$686,300 (converted from Taiwanese dollars)
C	Heat recovery, HEPA filter coverage reduction and reduced airflow velocity, Variable volume pumping and VSDs, Optimisation of operating characteristics of 1 rotary and 4 centrifugal compressors, High pressure atomising humidifier.	Small heat recovery program - $207,000 annual savings High Pressure Humidification - 700,000kWh/year energy savings
D	Increase in chiller water setpoint, most efficient chillers as lead chillers, cleaning of chiller condensers, Optimising cooling load distribution between chillers, Integrating of heat recovery chiller and cooling tower control systems.	Capital investment of $20,000 resulted in overall project annual savings (2 phases) of $198,000
E	MUA heat recovery, pre-cooling heat used for reheating MUA, Pre-heating of incoming city water prior to purification, Preheating of boiler feedwater, Boiler Combustion air preheating.	$1,369,000 annual savings 1.1.year composite simple payback
F	Holistic approach - Heat recovery, Big duct - small fan, VSDs, Dual Temperature chilled water loop, Vacuum pump efficiency - idle signal protocol, High pressure MUA humidification, Attention to detail on insulation and infiltration, Solar water heating.	$1 million in operating costs in 1st year On completion $4 million annual savings

Discussion

Energy efficiency efforts can be applied to both new and existing fabs. New fab and facilities design offers scope for innovative energy-saving ideas, however, there can be

reluctance in the industry to adopt a new potentially riskier design over the safety of the 'tried and tested' approach. Considering the investment required to construct a new fab, this attitude is understandable, the cost for fab facilities was reported as exceeding $500 million in 2003 [10]. Building in energy efficiency at the design stage offers high leverage, the holistic approach adopted by Texas Instrument for the Texas fab results in potentially large operating savings, $4 million in predicted annual energy savings [11]. Large savings are also evident in the adoption of the dual-temperature chilled water loop, $1,000,000 operating energy savings and 2 year simple payback [3], and in the use of heat recovery to reduce steam costs [8], over $1,000,000 and 0.8 year simple payback. However, smaller scale investments can also be fruitful; the $20,000 retro-fit capital investment by Tower Semiconductor resulted in annual energy savings of $198,000 [12, 13].

The literature shows that various economic methods are used to evaluate energy reduction efforts; these vary from simple payback to a 10 year Net Present Value model. Cohen argues that a simple payback analysis for energy savings evaluation is not an effective method to evaluate potential energy reduction projects, and that the "*life-cycle/net present cost*" model is more appropriate for long production 'ramp-ups' [10]. Simple payback analysis resulted in the choice of a single temperature chiller loop; according to the paper this choice was now being re-visited. These variations in assessment methods highlight the conflict that exists between short payback expectations and valid energy saving initiatives with longer term benefits. This is particularly true as energy costs continue to fluctuate. Naugthon makes a valid point,

> "*While many environmental initiatives are driven by regulatory forces, energy conservation is driven by paybacks and return on investment (ROI). Demands on available capital have prevented many energy conservation projects from being implemented, and SME suppliers driven by equipment performance have little incentive to improve the energy performance of their products* [15]."

The Texas Instruments report quantifies the potential savings available when design for sustainability is integrated into construction plans; no mention however is made of how the facilities were sized. The over-sizing of facilities driven by peak demand predictions, and the addition of various capacity safety margins at design, is potentially one of the main causes of energy waste. Below are some points to consider in the management of energy resources.

For new fabs

- Ensure management commitment to energy efficiency
- Adopt a holistic approach to design for sustainability and energy efficiency
- Size facilities as accurately as possible considering realistic expansion margins, use an accurate simulation or suitable model
- Optimise total cleanroom heat dissipation systems
- Choose optimal cleanroom design to minimise pressure drops, optimise the interaction of high efficiency components within cleanroom systems
- Although the economic pressure exists to construct fabs quickly, consider the longer term energy and cost savings of design for sustainability and energy efficiency

- Use the highest efficiency utility generation systems
- Educate workforce on the energy impact of process choices, product choices, behaviour etc.

Although not ideal, retro-fit projects offer significant potential for energy saving improvements, the supply and the demand side of energy has been addressed, below are some recommendations for existing fabs.

For existing fabs

- Ensure management commitment to energy conservation
- Use reasonable economic tools for evaluating energy efficient projects
- Manage cleanroom heat dissipation effectively
- Educate workforce on the energy impact of process choices, behaviour etc.
- Understand main drivers of energy consumption and their interaction within cleanroom and facilities systems – educate, measure, return to/challenge specification, benchmark, monitor and control
- Use the highest efficiency utility generation systems, retro-fit for efficiency where possible.

Conclusions

This research has reviewed semiconductor manufacturing energy reduction projects available in the literature. Energy efficient semiconductor manufacturing is a relatively new goal; the review shows that a large quantity of the literature on the topic consists of facilities based reduction projects for new and existing fabs. The literature primarily discusses project reports outlining and quantifying improvements, several of these have been tabulated, see Table 2. Significant energy savings are possible and have been demonstrated through successful case studies, e.g. dual temperature chilled water loop. One key point of note is that energy project assessment methods that expect rapid return on investment, such as simple payback, hinder potential energy efficiency efforts.

References

[1] Naughton, P. 2005, "Measurement of conservation of energy by semiconductor manufacturing equipment and setting of targets for improvements", *IEEE International Symposium on Semiconductor Manufacturing, Conference Proceedings, Sep 13-15 2005,*: Institute of Electrical and Electronics Engineers Inc., Piscataway, NJ 08855-1331, United States San Jose, CA, United States, 7-16.

[2] International Technology Roadmap for Semiconductors, Executive Summary, [online], http://www.itrs.net/Links/2007ITRS/Home2007.htm (Accessed 10/2/08).

[3] High Performance Cleanrooms, A Design Guidelines Sourcebook. 2006, [on-line], http://hightech.lbl.gov/documents/CLEANROOMS/Cleanroom_Air_Design.pdf (Accessed 07/03/08)

[4] SEMATECH News, ISMI Study Finds Significant Cost Savings, [online], http://www.sematech.org/corporate/news/releases/20051222a.htm. (Accessed 02/02/08)

[5] Seryak, J., Epstein, G.and and D'Antonio, M., (2006), "Lost Opportunities in Industrial Energy Efficiency: New Production, Lean Manufacturing and Lean Energy", pp. 12/3/08, [online], http://txspace.tamu.edu/bitstream/handle/1969.1/5653/ESL-IE-06-05-36.pdf?sequence=1. (Accessed 12/03/08)

[6] Intel, Inside the Intel Manufacturing Process, What is a Cleanroom?, [online], http://www.intel.com/education/cleanroom/. (Accessed 26/03/08)

[7] Chun-Hung Tsai1, et al., 2002, "Strategies of energy saving in a wafer fab", *2002 Semiconductor Manufacturing Technology Workshop, 10-11 Dec. 2002,* Taiwan Semicond. Ind. Assoc Hsinchu, China, 85-9.

[8] Fiorino, D.P. (2000), "Reducing steam costs: Six conservation and efficiency measures", *ASHRAE J.*, Vol.42 (2), pp. 31-39.

[9] Wakuda, T., Kenji Nagata and Motozou Kojima 1997, "Construction of an energy-saving semiconductor plant", *Proceedings of the 1997 IEEE International Symposium on Semiconductor Manufacturing Conference, Oct 6-8 1997,*: IEEE, Piscataway, NJ, USA San Francisco, CA, USA, 57-60.

[10] Cohen, R.M. (2003), "Energy efficiency for semiconductor manufacturing facilities", *ASHRAE J.*, Vol.45 (8), pp. 28-34.

[11] Texas Instruments, Sustainability at Texas Instruments, [online], http://www.ti.com/corp/docs/rennerroadfab/rfab_tour.pdf. (Accessed 02/03/08)

[12] Dubov, I. (2003), "Chilled water plant efficiency", *ASHRAE J.*, Vol.45 (6), pp. 37-40.

[13] Dubov, I. (2005), "Heat recovery, energy savings for semiconductor plant", *ASHRAE J.*, Vol.47 (12), pp. 56-58.

[14] Tschudi, W., David Faulkner and Allen Hebert 2005, "Energy efficiency strategies for cleanrooms without compromising environmental conditions", *American Society of Heating, Refrigerating and Air-Conditioning Engineers, ASHRAE 2005 Annual Meeting,*Vol.111 PART 2, *Jun 25-29 2005,*: Amer. Soc. Heating, Ref. Air-Conditoning Eng. Inc., Atlanta, GA 30329, United States Denver, CO, United States, 637-645.

[15] Naughton, P. 2006, "New tool for targeting energy improvements in semiconductor manufacturing equipment", *17th Annual SEMI/IEEE Advanced Semiconductor Manufacturing Conference, ASMC 2006,* Vol.2006, *May 22-24 2006,* Institute of Electrical and Electronics Engineers Inc., Piscataway, NJ 08855-1331, United States Boston, MA, United States, 428-432.

Appendix B

UPW Plant measurement data

1. Introduction

Information is provided here regarding the sources of measurement data used in the F24 UPW exergy analysis, e.g. flow rates, temperatures, pressures and changes in chemical composition. The measurement data were obtained from a combination of two sources. The most important source of data was the factory SCADA system Cimplicity, any SCADA data obtained from Cimplicity are denoted by (S). Other measurement data, not available on Cimplicity, were obtained from on-line instrumentation and are denoted by (O). There are reservations about the accuracy of the measurement data obtained from the on-line instrumentation due to irregular calibration; in contrast, the SCADA instrumentation is regularly calibrated. The SCADA data form the basis of various process control loops throughout the UPW plant and are considered accurate. Where there has been a choice of data source, the SCADA data have been used.

When any required measurement instrumentation was not available at a particular process stage, certain assumptions were made and data were taken (with or without modifications) from the most suitable locations either upstream or downstream of the process stage in question (as deemed most appropriate by the author). Decisions made regarding the choice of the most appropriate location depended on factors such as distance between processes, changes in elevation, insulation etc., these assumptions, alongside any modifications, are reported in the next section. The on-line instrumentation in some sections of the plant left something to be desired. For example, consider the primary mixed bed ion exchange: of the four modules, only one module had two working pressure gauges (inlet and outlet pressure). Pressure gauges on the heat exchangers were scarce; the hot water heat exchanger had only one pressure gauge. Another difficulty was encountered when trying to discern the incoming water temperature: on one occasion, the industrial city water inlet temperature gauge displayed a temperature of 61 °F (approximately 16 °C) while the incoming product water temperature gauge of the pre-heat heat exchanger displayed a

temperature of 3.5 °C (although no heating or cooling of the water occurred between the two measurement locations). However, based on several visits to the plant and monitoring changes in the measurements, the author chose the most likely measurement values. Again, this is not ideal, but unfortunately it was the case.

The exergy rates were calculated at the locations shown in Figures 1 and 2, flows of the product water, including any recycled streams, are shown in Figure 3. The ionic concentration of the UPW plant water was calculated from conductivity measurements using the relationship developed in Chapter 6. When conductivity measurements were not available at process stages, the ionic concentration was inferred using mass balance equations for the electrolyte. The ionic constituency of the plant water was based on the UPW incoming plant water analysis, discussed in detail in Chapter 6. Changes in the chemical concentration of the product water, when they occurred, are detailed in Section 2.

Flow rates, including recycled flows, were checked to insure that flow rates in one plant location agreed with other expected aggregate flow rates in another location. Due to the fact that this measurement data collection was a snapshot of different plant flows taken over a period of approximately fifteen minutes, the summation of flow rates from different locations, which were expected to be identical, often differed slightly. However, the data were checked to ensure that there was a reasonable match between flow rates in different plant locations. Although an assumption was made that the plant operates at steady state, the regular sampling frequency (approximately every 5 seconds) indicated that the plant flow rates were dynamic (although they did not change greatly in magnitude). For example, consider the second pass RO retentate flow rates, which are recycled to the first pass RO inlet (see Figure 3). The summation of the second pass RO retentate flow rates did not tally exactly with the difference between the summation of the RO feedwater flow and the summation of the MMF flow rates (i.e. $\sum Q_{25} \neq \sum Q_{13} - \sum Q_{1}$), there was a difference of approximately 4 m^3/hr. So, which flow rate data should be used, (1) hypothetical second pass retentate flow rates which balance the first pass RO flow rates, or (2) the second pass RO retentate data (at a different sampling time-stamp)? In this particular case, the flow rate difference is problematic because the flow rate and the conductivity of the second pass RO

reject help to determine the conductivity of the incoming plant water (see Figure 3). This issue was resolved in the following manner;

1. The flow rate and concentration data obtained from the second pass RO retenate stream were used to determine the average conductivity of the RO reject stream;
2. The difference between the RO feedwater flow rates and the combined MMF and second pass RO retentate flow rates was used as the second pass retentate flow rate (solely in order to determine the concentration of the incoming UPW plant water);
3. The hypothetical flow rate of the second pass RO retentate stream and the actual concentration data from the second pass RO retentate stream were combined, and hence used to determine the conductivity of the incoming feedwater.

A less complicated example was observed with respect to the electro-deionisation process outlet and the primary mixed bed ion-exchange inlet, where there was a flow rate difference of 0.6 m^3/hr, in this case the actual values were used.

Chemical dosing processes such as anti-scalant/biocide and sodium bisulphite were neglected in the overall exergy analysis for two reasons. First, dosage rates are controlled using analytical chemical detection equipment, e.g. the amount of chlorine/chloramines in the RO feedwater is monitored as it causes degradation of the RO membranes, when the concentration of chlorine exceeds a certain threshold, sodium bisulphite is injected into the system. Therefore, the flow rates of these chemicals cannot be modelled as steady state operations. Second, the chemical composition of the anti-scalant and biocide and the chemistry involved in the dosing processes is beyond the scope of this thesis. Neglecting the chemical exergy of these additives should not result in significant errors, for example, sodium bisulphite, an organic compound, is not an electrolyte, and therefore, it should not affect the conductivity reading downstream in the first pass RO modules. Sodium hydroxide, added prior to the second pass RO process, is used to regulate pH. In this case, sodium hydroxide is a strong electrolyte, and thus the change in concentration due its addition is assumed to manifest itself as the change in concentration between the RO tanks inlet (process stage 18) and the concentration at the RO feed pumps inlet (process stage 22). The electrical work used by the metering pumps is included in the exergy analysis, however.

The data for the electrical work (kW) inputs to the main pumps were provided by the electrical technician and was obtained from either the variable speed drives or the pump motor managers. The electrical work inputs to the electro-deionisation process comprised of the relatively small electrical work input to the brine recycle and metering pumps and the main input to the EDI rectifiers. The electrical work to the rectifiers was calculated according to the following equation, $W = V \times I \times \sqrt{3}$ where V and I are the voltage (V) and current (A) and $\sqrt{3}$ relates to the three-phase power factor.

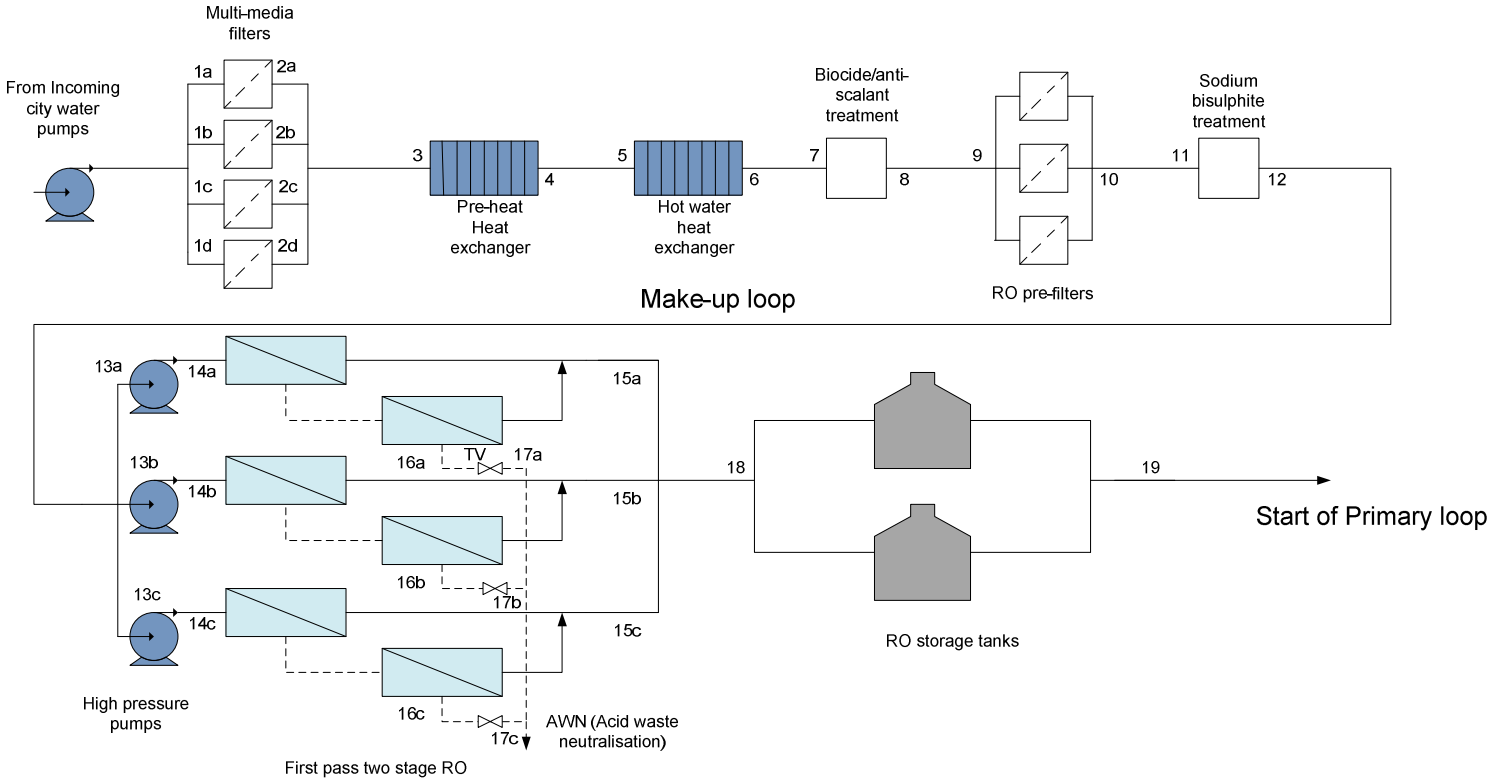

Figure 1: UPW exergy calculation locations, make-up loop

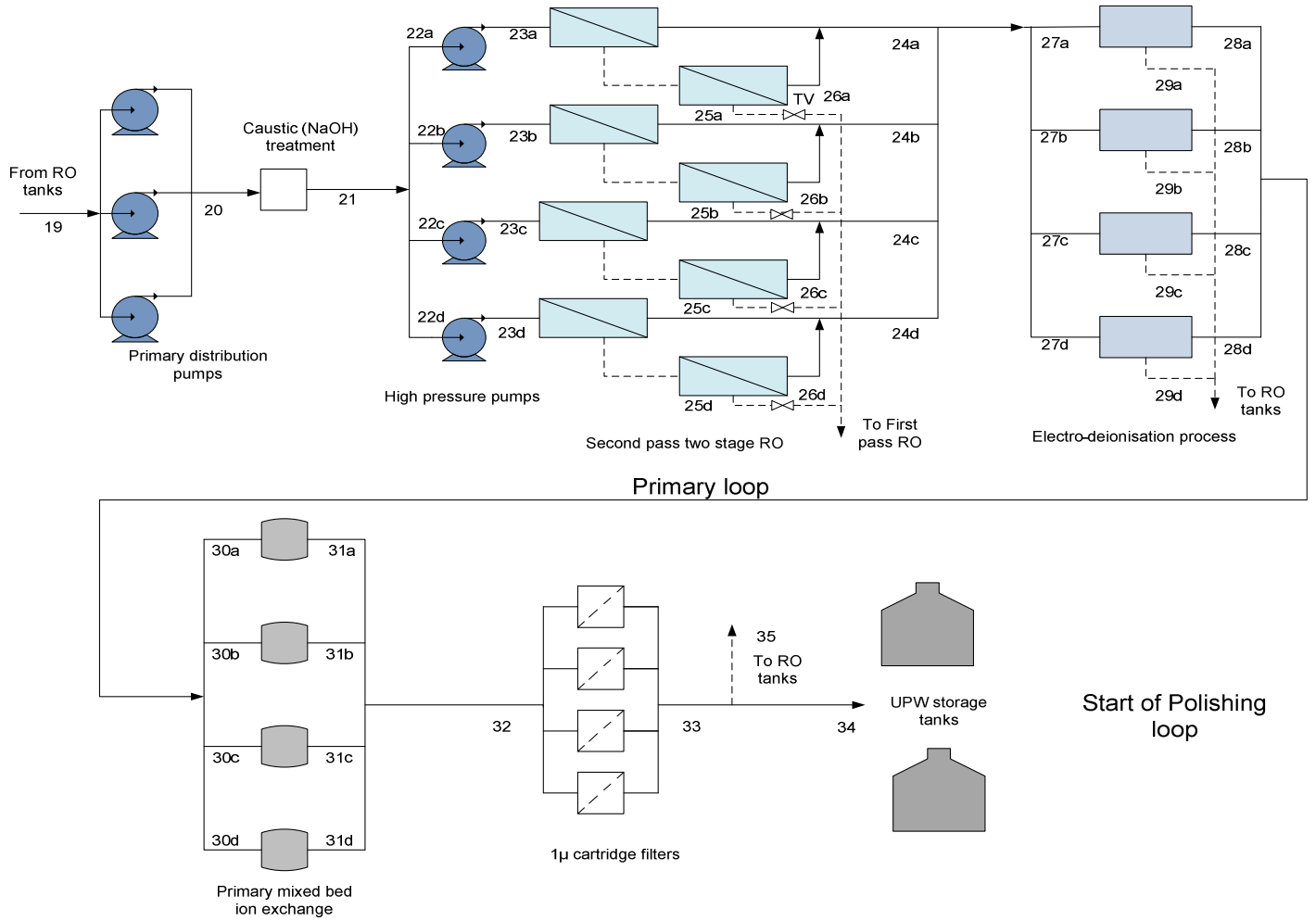

Figure 2: UPW exergy calculation locations, primary loop

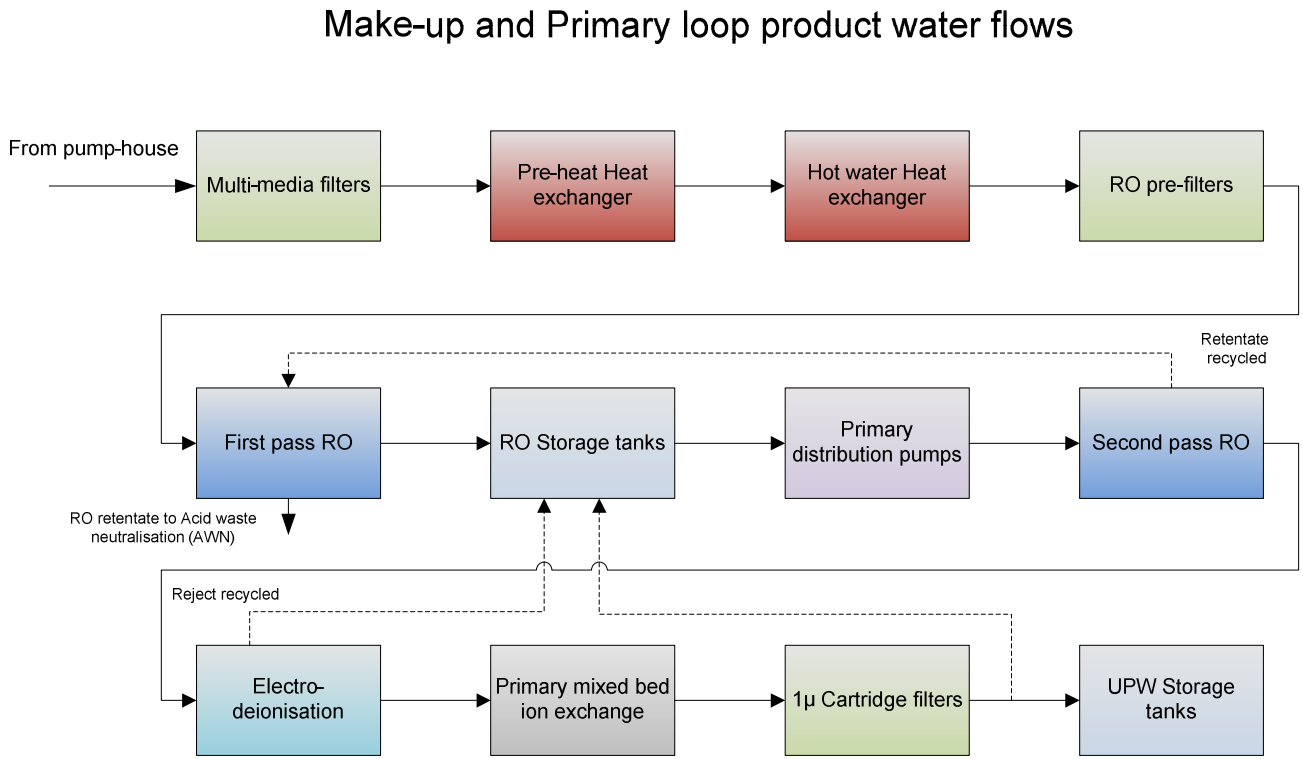

Figure 3: Make-up and primary loop product water flows

2. Process Stages

1. **Multi-media filters (MMF) inlet - each filter is designated by the letters a, b, c and d:**
   i. Measured flow rates (S) in situ, assumed to be a steady flow device;
   ii. Pressure gauges (O) in situ;
   iii. Temperature (O) taken from the industrial city water inlet immediately upstream of the process;
   iv. The concentration of the incoming water was a little complex to calculate. The first conductivity measurement (S) available in the plant was located at the first pass RO process; however, that value included a contribution from the second pass RO recycled retentate stream (see Figure 3). The concentration of the incoming plant water C_3 (mg/l) can be calculated using the following equation $\sum Q_1 \times C_1 = \sum Q_{13} C_{13} - \sum Q_{25} C_{25}$ (mass balance for the electrolyte). However, due to the dynamic nature of the data sampling, the summation of the second pass RO retentate flow rates was not equivalent to the difference between the summation of the first pass RO feedwater flow rates and the summation of the MMF flow rates, i.e. $\sum Q_{13} \neq \sum Q_1 + \sum Q_{25}$. As outlined previously in Section 1, the concentration of the second pass RO retentate C_{25} was calculated using the actual second pass RO retentate flow rates, i.e. $C_{25} = \frac{\sum Q_{25} C_{25}}{\sum Q_{25}}$. The hypothetical flow rate of the second pass RO retentate $\sum Q_{25'}$ was calculated as according to the following equation $\sum Q_{25'} = \sum Q_{13} - \sum Q_1$. Then finally the concentration of the incoming water was calculated as follows; $C_1 = \frac{\sum Q_{13} C_{13} - \sum Q_{25'} \times C_{25}}{\sum Q_1}$ where Q and C refer to the volumetric flow rate (kg/m^3) of the aqueous solution and the concentration (mg/l) of the calcium bicarbonate electrolyte in the aqueous

solution respectively, and the numerical subscripts refer to the process stages shown in Figures 1 and 2;

2. **Multi-media filters (MMF) outlet:**
    i. Measured flow rates (S) in situ;
    ii. Pressure gauges (O) in situ, however, two out of the three outlet pressure gauges on the three in-service MMFs appeared not to be working as the pressure gauges displayed equivalent incoming and outgoing pressures (where one would expect to see a pressure drop in a filtration process). The other gauge showed the expected pressure drop, on this basis, the same pressure drop was attributed to all three MMF modules;
    iii. Temperature (O) taken from the industrial city water inlet upstream of the process; assumed to be an isothermal process;
    iv. Concentration, see point 1.

3. **Pre-heat heat exchanger inlet – product water and heating water:**
    i. Flow rate (S) of the product water was taken as the summation of the MMF flow rates upstream of this process stage, assumed to be a steady flow device;
    ii. Flow rate of the heating water not available, calculated by means of a mass energy balance using thermodynamic properties determined from the XSteam function in MATLAB {{689 MATLAB Central website}}, i.e. $\dot{m}_{Hot} = \frac{\dot{m}_{Cold}(h_{Cold\ \text{in}} - h_{Cold\ \text{out}})}{(h_{Hot\ \text{out}} - h_{Hot\ \text{in}})}$;
    iii. Pressure (O) of the incoming product water was estimated as the MMF outlet pressure upstream of the process;
    iv. Pressure (a combination of (S) and (O)) of the incoming heating water can be calculated by subtracting a delta P value (S) (i.e. a pressure difference between the incoming and outgoing heating water) from the outgoing heating water pressure (O) measurement in situ;
    v. Temperature (O) of the incoming product water in situ;

vi. Temperature of the incoming heating water taken from the condenser water supply temperature (S) in another part of the plant with the assumption of negligible heat loss due to excellent insulation;
vii. Concentration of the product water, see point 1;
viii. Concentration of the heating water, see point 1.

4. Pre-heat heat exchanger outlet – product water and heating water:

i. Flow rate (S) of the product water was taken as the summation of the MMF flow rates upstream of this process stage, assumed to be a steady flow device;
ii. Flow rate of the heating water not available, calculated by means of a mass energy balance, see point 3;
iii. Pressure (O) of the outgoing product water in situ;
iv. Pressure (O) of the outgoing heating water in situ;
v. Temperature (S) of the outgoing product water in situ;
vi. Temperature (O) of the outgoing heating water in situ;
vii. Concentration of the product water, see point 1;
viii. Concentration of the heating water, see point 1.

5. Hot water heat exchanger inlet – product water and heating water:

i. Flow rate (S) of the product water was taken as the summation of the MMF flow rates upstream of this process stage, assumed to be a steady flow device;
ii. Flow rate of the heating water was not available, but was calculated by means of a mass energy balance, see point 3;
iii. Pressure of the incoming product water, estimated from the pre-heat heat exchanger outgoing pressure (O) directly upstream;
iv. Pressure of the incoming heating water, not available, pressure drop was assumed to be similar to the pressure drop of the pre-heat heat exchanger, thus the incoming heating water pressure was calculated as the sum of the delta P value in the pre-heat heat exchanger and the pressure of the outgoing heating water;

v. Temperature (O) of the incoming product water in situ;
vi. Temperature (O) of the incoming heating water in situ;
vii. Concentration of the product water, see point 1;
viii. Concentration of the heating water is assumed to be the same as the UPW incoming plant water, see point 1.

6. Hot water heat exchanger outlet – product water and heating water:

i. Flow rate (S) of the product water was taken as the summation of the MMF flow rates upstream of this process stage, assumed to be a steady flow device;
ii. Flow rate of the heating water not available, but calculated by means of a mass energy balance, see point 3;
iii. Pressure (O) of the outgoing product water, assumed to be identical to the RO pre-filters downstream of this process stage;
iv. Pressure (O) of the outgoing heating water in situ;
v. Temperature (S) of the outgoing product water in situ;
vi. Temperature (O) of the outgoing heating water in situ;
vii. Concentration of the product water, see point 1;
viii. Concentration of the heating water, see point 1.

7. Chemical feed (biocide/anti-scalant) treatment inlet:

i. Flow rate (S) of the product water was taken as the summation of the MMF flow rates upstream of this process stage, assumed to be a steady flow device;
ii. Pressure (O) of the product water taken from the RO pre-filters inlet directly downstream of the process;
iii. Temperature (S) of the outgoing product water taken from hot water heat exchanger product water outlet directly upstream of this process, assuming that there was negligible heat loss due to excellent insulation;
iv. Concentration, see point 1; in this thesis the additional chemical exergy of the chemical treatments has been neglected for two reasons, i.e. the dosage

is intermittent and cannot be treated as steady state and the author is unsure of the exact chemical make-up of the various treatments.

v. Electrical work input to the metering pumps was provided by the electrical technician.

8. Chemical feed (biocide/anti-scalant) treatment outlet:

i. Flow rate (S) of the product water was taken as the summation of the MMF flow rates upstream of this process stage, assumed to be a steady flow device;

ii. Pressure (O) of the product water taken from the RO pre-filters inlet directly downstream of the process;

iii. Temperature (S) of the outgoing product water taken from hot water heat exchanger product water outlet directly upstream, assuming that there was negligible heat loss due to excellent insulation;

iv. Concentration, see point 1.

9. RO pre-filters inlet:

i. Flow rate (S) of the product water was taken as the summation of the MMF flow rates upstream of this process stage, assumed to be a steady flow device;

ii. Pressure (O) of incoming product water in situ;

iii. Temperature (S) of incoming product water taken from hot water heat exchanger product water outlet upstream of this process, assuming that there was negligible heat loss due to excellent insulation;

iv. Concentration, see point 1.

10. RO pre-filters outlet:

i. Flow rate (S) of the product water was taken as the summation of the MMF flow rates upstream of this process stage, assumed to be a steady flow device;

ii. Pressure (O) of outgoing product water in situ;

iii. Temperature (S) of the outgoing product water taken from hot water heat exchanger product water outlet upstream of the process, assuming that there was negligible heat loss due to excellent insulation;
iv. Concentration, see point 1.

11. Chemical feed (sodium bisulphite) treatment inlet:

i. Flow rate (S) of the product water was taken as the summation of the MMF flow rates upstream of this process stage, assumed to be a steady flow device;
ii. Pressure (S) of the product water taken from the RO pre-filters outlet directly upstream of the process;
iii. Temperature (S) of the outgoing product water taken from hot water heat exchanger product water outlet, assuming that there was negligible heat loss due to excellent insulation;
iv. Concentration, see point 1;
v. Electrical work input to the metering pumps was provided by the electrical technician.

12. Chemical feed (sodium bisulphite) treatment outlet:

i. Flow rate (S) of the product water was taken as the summation of the MMF flow rates upstream of this process stage, assumed to be a steady flow device;
ii. Pressure (S) of the product water taken from the RO pre-filters outlet directly upstream of the process;
iii. Temperature (S) of the outgoing product water taken from the hot water heat exchanger product water outlet, assuming that there was negligible heat loss due to excellent insulation;
iv. Concentration, see point 1.

13. First pass high pressure pumps inlet – each RO module is designated by letters a, b and c:

i. Flow rate for each pump was equal to the RO inlet flow rate for the associated RO module, calculated from either $Q_F = Q_P + Q_R$ or the % Recovery value (S), i.e. % Recovery= $\frac{Q_P}{Q_F}$, where Q_F is the volumetric flow rate of the feedwater, Q_P is the volumetric flow rate of the permeate (S) and Q_R is the volumetric flow rate of the retentate (S). Note here that the total feedwater flow rate for the RO modules is greater than the summation of MMF flows due to second pass RO retentate flow recycle; assumed to be a steady flow device;

ii. Pressure (O) – pump suction pressure taken from the RO pre-filters outlet directly upstream of the process, (pump suction pressures (O) were available on the two in-service RO modules, however, the two values differed greatly despite having the same water supply, thus the RO pre-filter values were selected instead) ;

iii. Temperature (S) of incoming product water (pump suction temperature) taken from the associated RO module downstream of this process, assumed to be an isothermal process;

iv. Concentration of the product water calculated from the first pass RO inlet conductivity measurement (S);

v. Electrical work W inputs to the pumps were provided by the electrical technician:

14. First pass high pressure pumps outlet was assumed to be identical to first pass RO inlet:

i. RO inlet flow rate, see point 13, assumed to be a steady flow device;

ii. Pressure (S), i.e. the pump discharge pressure, was in situ;

iii. Temperature (S) of the pump discharge stream taken from the associated RO module;

iv. Concentration of the product water calculated from the first pass RO inlet conductivity measurement (S).

15. First pass RO permeate water:

i. Flow rate (S) of the permeate water in situ;
ii. Pressure (O) of the permeate water gauges in situ but two of the three gauges were broken. Based on a discussion with the UPW technician the permeate pressure and the reading on of the pressure gauges, the pressure of the permeate stream was assumed to be 1.2 bar (gauge pressure);
iii. Temperature (S) of the permeate water in situ, process assumed isothermal;
iv. Concentration of the permeate water was calculated from the permeate conductivity measurement (S) in situ.

16. First pass RO retentate water:

i. Flow rate (S) of the retentate water in situ;
ii. Pressure (S) of the retentate was in situ;
iii. Temperature (O) of the retentate in situ, process was assumed isothermal;
iv. Concentration of the retentate stream was calculated from the following equation $Q_F C_F = Q_P C_P + Q_R C_R$ (mass balance for the electrolyte), where Q_F is the volumetric flow rate of the feedwater, see point 13, Q_P is the flow rate of the permeate (S) and Q_R is the flow rate of the retentate (S), and the incoming feed water C_F and permeate C_P concentrations were calculated from the conductivity measurements (S) in situ.

17. Retentate water post throttling valve:

i. Flow rate (S) of the retentate water in situ;
ii. Pressure (S) of the retentate post throttling valve pressure was assumed to be 1 bar (gauge pressure), based on discussion with the UPW technician;
iii. Temperature (O) of the retentate in situ, process was assumed isothermal;
iv. Concentration, see point 16 above.

18. RO tanks inlet:

i. The potential flow rates into and out of the RO tanks are manifold, see Figure 4. There is a possible recirculation flow from the primary distribution pumps downstream, which cannot be quantified in detail; there is also the potential to divert flows from primary and polish loop processes downstream. To simplify the problem, assumptions were made that, (1) the RO tanks are steady flow devices, (2) flow is only rarely recycled from the primary distribution pumps, and cleaning and regeneration flows are seldom used, and consequently, these flow rates are treated as zero for this exergy analysis, and (3) the difference between the flow rates into and out of the RO tanks is solely provided by the one micron cartridge filters downstream of the process. The final assumption was made after checking the flow control valve of the primary mixed bed ion exchange (fully closed), no valve showing a diverted flow from the polish mixed bed ion exchange was evident on Cimplicity. Thus the flow rate into the RO tanks can be calculated as follows, $Q_{18} = \sum Q_{15} + \sum Q_{29} + \sum Q_{35}$, and $Q_{35} = \sum Q_{22} - (\sum Q_{15} + \sum Q_{29})$, where Q is the volumetric flow rate and the numerical subscripts refer to the process stages in Figures 1 and 2;

ii. Pressure (O) was assumed to be 1 bar (gauge pressure);

iii. Temperature (O) taken from the first pass RO upstream (the temperature at all three sources of RO tank inlet flow was identical) ;

iv. Concentration at the RO tanks inlet includes a contribution from the RO permeate concentration streams upstream, the EDI reject and the one micron cartridge filter outlet streams downstream in the process; it can be calculated using the following relationship,

$$C_{18} = \frac{\sum Q_{15}C_{15} + \sum Q_{29}C_{29} + \sum Q_{35}C_{35}}{\sum Q_{15} + \sum Q_{29} + \sum Q_{35}}$$

where Q and C refer to the volumetric flow rates (kg/m^3) and the concentration of the electrolyte (mg/l) respectively and the numerical subscripts refer to the process stages shown in Figures 1 and 2.

19. RO tanks outlet assumed to be identical to Primary distribution pumps inlet:

i. Flow rate was taken as the summation of the total second pass RO feedwater flow rates downstream of this process stage, which in turn were calculated according to point 13;

ii. Pressure was estimated to be the 1 bar (gauge pressure), which in turn was based on an estimation of the height of water in the RO tank using the following equation $P = \rho g h$, where P is the gauge pressure (Pa), ρ is the density of the aqueous solution (kg/m^3), g is gravitational acceleration (m/s^2) and h is the height of the aqueous solution in the tank (m), based on conversation with UPW technician the height of the water was assumed to be 10.2 m approximately;

iii. Temperature (S) was taken from the RO modules downstream of this process;

iv. Concentration taken from the RO tanks inlet, see point 18;

v. Electrical work W inputs to the pumps were provided by the electrical technician.

20. Primary distribution pumps outlet assumed to be identical to sodium hydroxide treatment inlet:

i. Flow rate was taken as the summation of the total second pass RO feedwater flow rates downstream of this process stage, see point 13;

ii. Pump discharge pressure (S) in situ;

iii. Pump discharge temperature (S) was taken from the RO modules directly downstream of this process;

iv. Concentration taken from the RO tanks inlet, see point 18;

v. Electrical work W inputs to the caustic metering pumps were provided by the electrical technician.

21. Sodium hydroxide treatment outlet:

i. Flow rate (S) was taken as the summation of the total second pass RO feedwater flow rates downstream of this process stage, see point 13;

ii. Pressure was taken from the primary distribution pumps outlet (S) directly upstream of this process;
iii. Temperature (S) was taken from the RO modules directly downstream of this process;
iv. Concentration (O) was calculated from the RO tanks outlet conductivity directly upstream of process.

22. Second pass high pressure pumps inlet assumed to be identical to sodium hydroxide treatment outlet – each RO module is designated by letters a, b, c and d:

i. Flow rate for each pump was calculated according to point 13, assumed to be a steady flow device;
ii. Pressure - the pump suction pressure was taken from the primary distribution pumps outlet (S) upstream of this process;
iii. Temperature (S) was taken from the associated RO module directly downstream of this process, assumed to be an isothermal process;
iv. Concentration (S) of the product water calculated from the conductivity measurement in situ (any change in concentration between the RO outlet and this stage is assumed to result from the NaOH treatment);
v. Electrical work W inputs to the pumps were provided by the electrical technician.

23. Second pass high pressure pumps outlet was assumed to be identical to the second pass RO inlet:

i. Flow rate of the RO feedwater was calculated according to point 13;
ii. Pump discharge pressure (S) in situ;
iii. Temperature (S) of the pump discharge stream taken from the associated RO module in situ, assumed to be an isothermal process;
iv. Concentration (S) of the product water calculated from the RO conductivity measurement in situ.

24. Second pass RO permeate water:

i. Flow rate (S) of the permeate water in situ;
ii. Pressure (O) of the permeate water in situ;
iii. Temperature (S) of the permeate water in situ, the process was assumed to be isothermal;
iv. Concentration of the permeate stream was calculated from the permeate conductivity measurement (S) in situ.

25. Second pass RO retentate water:

i. Flow rate (S) of the retentate water in situ;
ii. Pressure (S) of the retentate was in situ;
iii. Temperature (S) of the retentate water in situ, the process was assumed isothermal;
iv. Concentration of the retentate stream was calculated using the following equation, $Q_F C_F = Q_P C_P + Q_R C_R$, where Q and C are the volumetric flow rate (m^3/hr) and concentration of the electrolyte (mg/l) respectively, and the subscripts F, P and R refer to the feedwater, the permeate and the retentate respectively. Concentrations (mg/l) of the feedwater and permeate were calculated from the conductivity measurements (S) in situ.

26. Retentate water post throttling valves:

i. Flow rate (S) of the retentate water in situ;
ii. Pressure (S) of the retentate post throttling valve was assumed to be 1 bar (gauge pressure), based on a discussion with UPW technician;
iii. Temperature (S) of the retentate water in situ, the process was assumed isothermal;
iv. Concentration, identical to point 25.

27. Electro-deionisation (EDI) inlet – product water:

i. Flow rate (S) of the product water was in situ, the flow of the product water was modelled as steady flow;
ii. The pressure (S) of the incoming product water was in situ;

iii. The temperature (O) of the product water was in situ;

iv. The concentration of the product water was calculated using resistivity measurements (S) in situ at the inlet of each EDI module;

v. Electrical work W of the EDI, calculated using data (S) on VA rectifier in situ, a second electrical work input due to the metering and brine recirculation pumps was provided by the electrical technician.

28. Electro-deionisation (EDI) outlet - product water:

i. Flow rate (S) of the product water was in situ;

ii. The pressure (S) of the outgoing product water was in situ;

iii. The temperature (O) of the product water in situ, assumed to be an isothermal process;

iv. The concentration of the product water was calculated using resistivity measurements (S) in situ at the outlet of each EDI module.

29. Electro-deionisation (EDI) outlet - reject water:

i. Flow rate (S) of the reject water was calculated as the difference between the volumetric flow rates of the incoming product water and the outgoing product water $Q_F = Q_P + Q_R$ where Q is the volumetric flow rate (m^3/hr) and the subscripts *F*, *P* and *R* refer to the feedwater, the product water and the reject water respectively;

ii. The pressure of the outgoing reject water was not available, this water is recycled to the RO tanks, pressure was assumed to be 1 bar (gauge pressure);

iii. The temperature (O) of the reject water in situ, assumed to be an isothermal process;

iv. The concentration of the reject water was calculated using the following equation $Q_F C_F = Q_P C_P + Q_R C_R$ (mass balance for the electrolyte), where Q_F is the volumetric flow rate of the feedwater (S), Q_P is the flow rate of the product water (S), and Q_R is the flow rate of the reject (see point 29i

above), and the incoming feed water C_F and outgoing product water C_P concentrations were calculated from the resistivity measurements (S) in situ;

30. Primary mixed bed ion exchange (IX) inlet:

i. Flow rate (S) of the product water was in situ, assumed to be a steady flow device;

ii. The pressure (O) of the incoming product water was in situ (however, only one set of incoming and outgoing pressure gauges appeared to be working, thus these two pressure values were attributed to the other two in-service IX modules);

iii. The temperature (O) of the product water was in situ;

iv. The concentration of the incoming product water can be calculated from the EDI outlet concentrations upstream, calculated as an average from resistivity measurements (S), i.e. $C_{30} = \frac{\sum Q_{28} C_{28}}{\sum Q_{28}}$ where Q and C refer to the volumetric flow rates (m^3/hr) and concentrations (mg/l), and the numerical subscripts refer to the process stages in Figure 2.

31. Primary mixed bed ion exchange (IX) outlet:

i. Flow rate (S) of the product water was in situ;

ii. The pressure (O) of the outgoing product water in situ;

iii. The temperature (O) of the product water in situ;

iv. The concentration of the outgoing product water was in situ, again this can be calculated using resistivity measurements (S);

v. Chemical work of the primary mixed bed IX (cannot be estimated using exergy analysis but can be considered by cost of regeneration chemicals).

32. One micron cartridge filters inlet:

i. Flow rate (S) of the product water was taken from the primary mixed bed IX upstream, assumed to be a steady flow device;

ii. The pressure (O) of the incoming product water in situ;

iii. The temperature (O) of the product water taken from the primary mixed bed IX directly upstream of this process, with the assumption of negligible heat loss due to excellent insulation, assumed to be an isothermal process;

iv. The concentration of the incoming product water was taken from the primary mixed bed IX outlet upstream, calculated using resistivity measurements (S).

33. One micron cartridge filters outlet:

i. Flow rate (S) of the product water was taken from the primary mixed bed IX upstream, the aggregate flow;

ii. The pressure (O) of the outgoing product water was in situ;

iii. The temperature (O) of the product water was taken from the primary mixed bed IX upstream of this process;

iv. The concentration of the incoming product water was taken from the IX outlet upstream; this was calculated using resistivity measurements (S).

34. UPW tank inlet:

i. Flow rate (S) of the product water was calculated as the difference between the aggregated flow of the primary mixed bed IX upstream and the flow rate into the RO tanks attributed to point 35 upstream (see point 18);

ii. The pressure (O) of the product water was taken as the pressure at the outlet of the one micron cartridge filters directly upstream;

iii. The temperature (O) of the product water was taken from the primary mixed bed IX upstream of this process;

iv. The concentration of the incoming product water was taken from the IX outlet upstream; this was calculated using resistivity measurements (S).

35. Post one micron cartridge filter stream (diverted to the RO tanks):

i. Flow rate (S) of the product water was taken as the difference between the flow rate into the RO tanks, i.e. $\sum Q_{15} + \sum Q_{29}$ and out of the RO tanks, i.e. $\sum Q_{22}$, see point 18;

ii. The pressure (O) of the outgoing product water was in situ;

iii. The temperature (O) of the product water was taken from the primary mixed bed IX upstream of this process;

iv. The concentration of the incoming product water was taken from the IX outlet upstream; this was calculated using resistivity measurements (S).

Finally, the data obtained from the SCADA system Cimplicity and the on-line instrumentation (based on all the preceding assumptions in Section 2), are shown in Table1. Only the process equipment in service on the day of the data collection is shown in the table (e.g. 1a (MMF (a)) was not in service on the day in question). Also note that the previously discussed gauge pressure values have been converted to absolute pressure values.

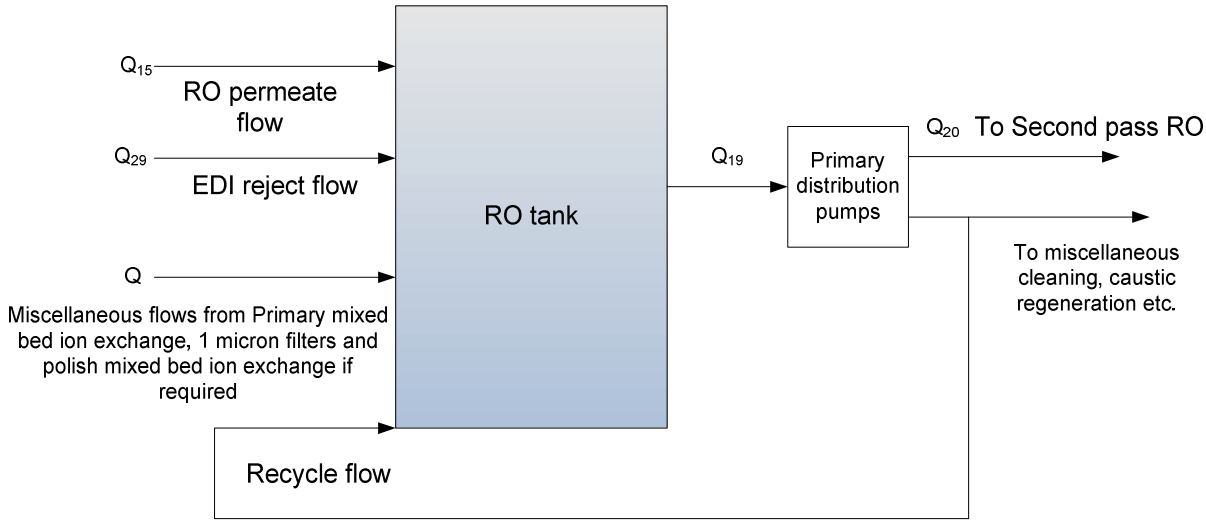

Figure 4: Possible flow configurations for the RO tanks

Table 1: Process data from UPW plant

Process	*Process stage*	*Q (m^3/h)*	*T (K)*	*P (bar)*	*Conductivity (uS/cm @ 25°C)*	*W (kW)*
Multi-media filters	1b	81.4	289	6.2	411.4	
	1c	78.2	289	6.2	411.4	
	1d	74.6	289	6.2	411.4	
	2b	81.4	289	6.0	411.4	
	2c	78.2	289	6.0	411.4	
	2d	74.6	289	6.0	411.4	
Pre-heat heat exchangers	3 (Product water)	234.2	289	6.0	411.4	
	3 (Heating water)	507	295	6.9	411.4	
	4 (Product water)	234.2	294	5.3	411.4	
	4 (Heating water)	507	293	5.8	411.4	
Hot water heat exchangers	5 (Product water)	234.2	294	5.3	411.4	
	5 (Heating water)	78	361	7.3	411.4	
	6 (Product water)	234.2	297	5.1	411.4	
	6 (Heating water)	78	349	6.2	411.4	
Biocide/anti-scalant treatment	7	234.2	297	5.1	411.4	0.6
	8	234.2	297	5.1	411.4	
RO pre-filters	9	234.2	297	5.1	411.4	
	10	234.2	297	4.7	411.4	
Sodium bisulphite treatment	11	234.2	297	4.7	411.4	0.6
	12	234.2	297	4.7	411.4	

Table 1: Process data from UPW plant

Process	***Process stage***	***Q (m^3/h)***	***T (K)***	***P (bar)***	***Conductivity (uS/cm @ 25°C)***	***W (kW)***
First pass RO high pressure pumps /RO inlet	13a	130.9	297	4.7	390	86
	13c	131.6	297	4.7	390	75
	14a	130.9	297	13.1	390	
	14c	131.6	297	10.0	390	
First pass RO	15a	95.8	297	2.2	7.1	
	15c	97.6	297	2.2	9.9	
	16a	35.1	297	10.2	1435.1	
	16c	34	297	6.6	1481.1	
	17a	35.1	297	2.0	1435.1	
	17c	34	297	2.0	1481.1	
RO tank inlet	18	242.9	297	2.0	8.2	
RO tank outlet (Pumps inlet)	19	242.9	297	2.0	8.2	35.7
Primary pumps out (Caustic inlet)	20	242.9	297	4.3	8.2	0.6
Caustic treatment outlet	21	242.9	297	4.3	29.9	
First pass RO high pressure pumps /RO inlet	22b	81	297	4.3	29.9	72
	22c	79.4	297	4.3	29.9	77
	22d	82.5	297	4.3	29.9	73
	23b	81	297	20.9	29.9	
	23c	79.4	297	21.9	29.9	
	23d	82.5	297	20.8	29.9	

Table 1: Process data from UPW plant

Process	*Process stage*	*Q (m^3/h)*	*T (K)*	*P (bar)*	*Conductivity (uS/cm @ 25°C)*	*W (kW)*
Second pass RO	24b	70.8	297	5.8	1.7	
	24c	68.6	297	6.5	1.7	
	24d	71.1	297	6.5	1.7	
	25b	10.2	297	18.6	225.6	
	25c	10.8	297	19.6	209.0	
	25d	11.4	297	17.7	205.8	
	26b	10.2	297	2.0	225.6	
	26c	10.8	297	2.0	209.0	
	26d	11.4	297	2.0	205.8	
Electro-deionisation process	27b	72.8	297	6.2	1.7	33.9
	27c	70.1	297	6.1	1.7	27.6
	27d	70	297	6.2	1.7	26.3
	28b	65.1	297	4.0	0.06	
	28c	65.2	297	4.0	0.06	
	28d	64.8	297	4.0	0.06	
	29b	7.7	297	2.0	15.2	
	29c	4.9	297	2.0	23.1	
	29d	5.2	297	2.0	21.7	

Table 1: Process data from UPW plant

Process	***Process stage***	***Q (m^3/h)***	***T (K)***	***P (bar)***	***Conductivity (uS/cm @ 25°C)***	***W (kW)***
Primary mixed bed ion exchange	30b	66.3	297	3.6	0.06	
	30c	63.4	297	3.6	0.06	
	30d	64.8	297	3.6	0.06	
	31b	66.3	297	3.0	0.055	
	31c	63.4	297	3.0	0.056	
	31d	64.8	297	3.0	0.056	
One micron cartridge filters	32	194.5	297	2.9	0.056	
	33	194.5	297	2.8	0.056	
UPW tank inlet	34	162.8	297	2.8	0.056	
Diverted flow to RO tanks	35	31.7	297	2.8	0.056	

Appendix C

The Model A equation for the molar chemical exergy of water can be considered as a special case for the separation of one mole of a mixture component from a two component mixture, this analysis is reproduced (although adapted slightly) from Cengel and Boles [1]. Consider the extraction of pure water from a large two component ideal mixture of water and salt. The entropy of mixing is therefore the minimum amount of work required to completely separate the mixture into its constituents, and thus, the minimum separation work per mole is given by (1).

$$\bar{w}_{\min} = -RT_0(x_w \ln x_w + x_s \ln x_s) \tag{1}$$

If the total work is considered, the minimum work of separation is given by (2).

$$W_{\min} = -RT_0(N_w \ln x_w + N_s \ln x_s) \tag{2}$$

Now consider the work to separate one mole of water from a large ideal mixture of water and salt, i.e. $N_w \gg 1$. This can be calculated by subtracting the work required to separate the remaining mixture when one mole of water is extracted, i.e. $-RT_0[(N_w - 1)\ln x_w + N_s \ln x_s]$ from the original minimum work of separation, see (2). Subtracting the two leads to (3), which is the Model A molar chemical exergy term.

$$\bar{w}_{\min} = -RT_0 \ln x_w \tag{3}$$

REFERENCES

[1] Cengel, Y.A. and Boles, M.A., (2007), *Thermodynamics: An Engineering Approach*, (6^{th} ed.), McGraw-Hill, New York.